EJA
European Journal of Anatomy
Volume 25 - Number 4 July 2021

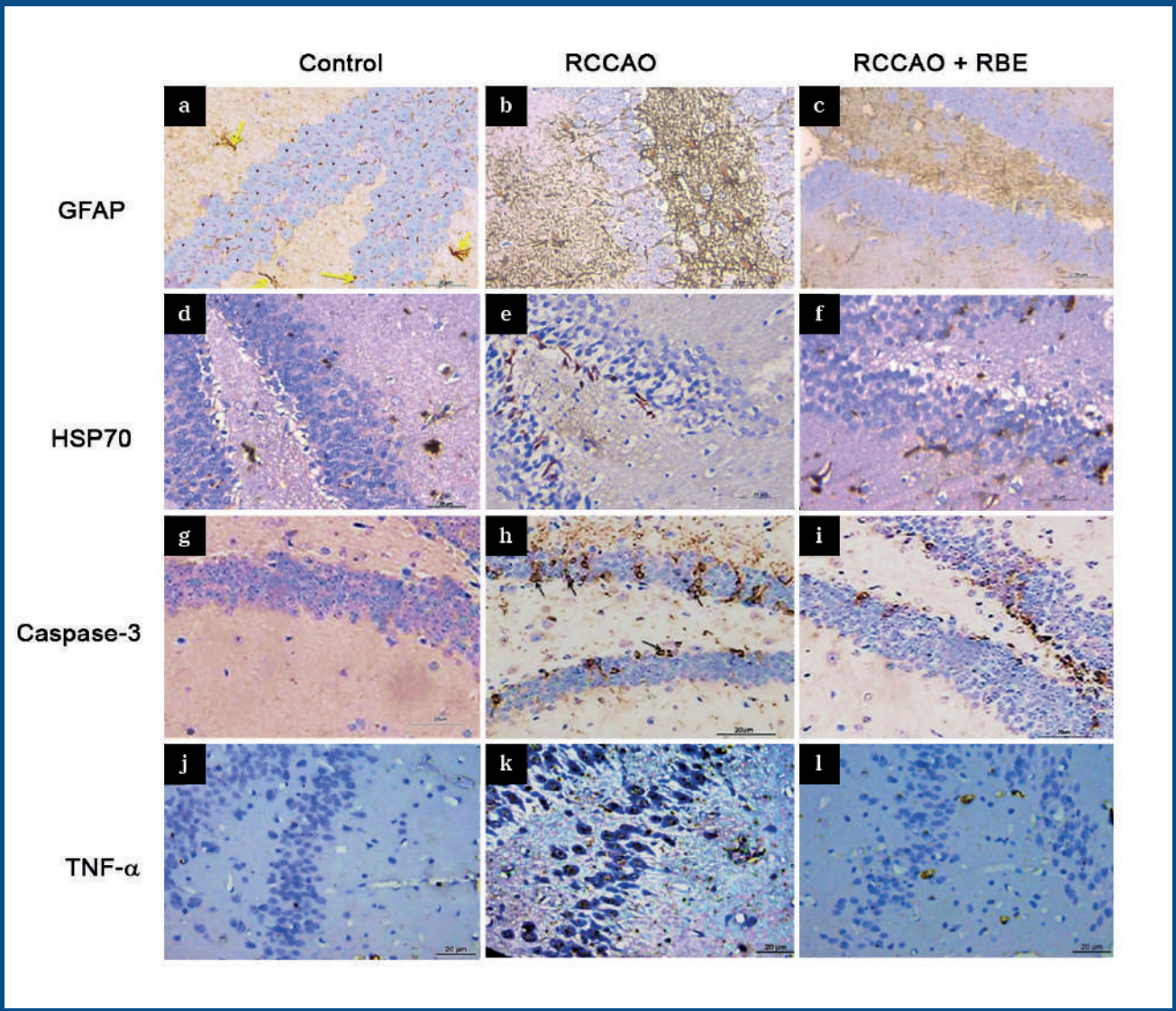

Indexed in:

CLARIVATE
- JCR:2020
- Q4 (21/23)
- I.F. J.C.I.: 0.19

DIALNET
EMBASE / Excerpta Medica

SCOPUS
- SJCR: 2020
- Q4 (31/39)
- I.F.: 0.162

Emerging Sources Citation Index
LATINDEX. Catálogo v1.0 (2002-2017)

Official Journal of the Spanish Society of Anatomy

www.eurjanat.com

EJA
European Journal of Anatomy

Volume 25 - Number 4 July 2021

CONTENTS

Original Articles

Case Reports

Descriptive Article

Ameliorating effect of N-acetylcysteine on iron toxicity of the liver and pancreas in albino rats: histochemical and ultrastructural study

Hany M.A. Sonpol[1,2], Medhat Taha[1,3], Raouf F. Bedeer[1], Lashin S. Ali[4,5], Turki A.S. Baokbah[6], Amira E. Farage[7], Rasha A. Elsisy[7], Mona A. Abdelkareem[7]

[1] Department of Anatomy and Embryology, Faculty of Medicine, Mansoura University, Egypt

[2] Basic medical sciences, College of Medicine, University of Bisha, Saudi Arabia

[3] Anatomy Department, Al- Qunfudah Medical College, University of Umm AL-Qura, Makka, Saudi Arabia

[4] Physiology Department, Faculty of Medicine, Mansoura University, Egypt

[5] Physiology Department, Faculty of Medicine, Horus University, Egypt

[6] Department of Medical Emergency Service, Al- Qunfudah Health Sciences College, University of Umm AL-Qura, Makka, Saudi Arabia

[7] Department of Anatomy and Embryology, Faculty of Medicine, Kafrelsheikh University, Egypt

SUMMARY

Iron overload is common with chronic liver disease. Iron supplementation in diabetes mellitus patients causes severe pancreatic damage. In our study we aimed to test the possible protective effects of N-acetylcysteine (NAC) on the iron toxicity of rat liver and pancreas. We divided thirty-two male albino rats into four groups, eight animals each. For four weeks the experimental animals were treated as follows: Group I (control group): rats received daily single intra-peritoneal injection of NaCl solution in equal volume to same amount of the iron injection; Group II (NAC-treated group): a dose of 300mg/kg of NAC was given to the rats of this group by oral gavage once daily; Group III (Iron-treated group): the rats of this group received intraperitoneal injection of iron in a dose of 100mg/kg, three times per week; Group IV (NAC and iron-treated group): the rats were treated daily with oral NAC administration in a dose of 300 mg/kg and intraperitoneal injection with iron in a dose of 100 mg/kg, three times per week. After four weeks of treatment, the experimental rats were anaesthetized and sacrificed, the blood was collected for biochemical analysis and the liver and pancreas organs were dissected for histopathological investigations and electron microscopic examination.

Iron overload caused marked centrolobular hepatic vacuolization, impacted sinusoids with brownish hemosiderin pigment associated with single cell necrosis, and apoptosis in hepatic cells together with pancreatic acinar degeneration associated with marked interstitial hemosiderin deposition. Biochemical assay revealed elevated levels of serum iron, ferritin and iron binding

Corresponding author:
Hany M.A. Sonpol. Department of Anatomy and Embryology, Faculty of Medicine, Mansoura University, Egypt. Mob.: 00966565922847.
E-mail: Hany_sonpol@live.com

Submitted: December 10, 2020. **Accepted:** January 2, 2021
Not final proof's revision by the authors

capacity in the iron-treated rat group due to the resulting oxidative stress. The use of NAC plus iron reduced the iron toxicity on hepatic and pancreatic tissues, with marked decrease of hepatic vacuolization and decrease of hemosiderin sedimentation in the hepatic sinusoids with decreased pancreatic acinar degeneration and necrosis. The application of NAC in the protocol of therapy improved the serum iron, ferritin and total iron binding capacity levels in the experimental rats.

Key words: N-Acetylcysteine – Iron overload – Liver – Pancreas – Ferroptosis

INTRODUCTION

Iron is an essential metal whose deficiency or excess in the organism is associated with pathologic situations. Iron is clearly hermetic (dose-response relationship), as a small dose of iron is required for human body, the recommended daily intake is 10-15 mg iron/day. Iron is essential in oxygen transport and plays fundamental roles in the oxidative phosphorylation process and other enzymatic functions. Large doses of iron (more than 30 mg/day) produce toxic effects on the liver and brain (Anderson and Shah, 2013; Musacco-Sebio et al., 2014). Systemic iron level depends mainly on iron absorption, storage, and recycling. About 80% of the iron stored in the human body is bound to hemoglobin, with the average of the stored amount in the human body equal to 2–4 gm of iron. In case of iron deficiency, the hemoglobin production decreases leading to anemia, while iron overload causes cell damage (Fung and Nemeth 2013).

The liver has a significant and important role in the metabolic regulation of the iron by production of hepcidin (a key regulating hormone of the entry of iron into the circulation in mammals). Chronic liver diseases affect iron metabolism and result in iron overload. This effect is partially due to low levels of hepcidin. In addition, the accumulated iron causes more damage to the liver by imposing more oxidative stress on hepatocytes (Milic et al., 2016). On the other hand, iron is deposited in acinar cells of the pancreas and in the islets of Langerhans, which in turn may lead to fibrosis and damage of the beta cells resulting in diabetes mellitus (Whittaker et al., 1996). Moreover, Sampaio et al. (2014) stated that iron supplementation in diabetic patients leads to a more oxidative stress that severely affects the pancreatic and the cardiac tissues, denoting that rapid iron supply could produce morphological changes in a relatively short period of time.

NAC is a safe and affordable medication. It is not present in natural sources, although cysteine is present in many food sources like turkey meat, chicken, eggs, yogurt, and garlic (Larsson et al., 2015). NAC is a mucolytic drug which is well tolerated; it modifies the grasping mucous secretions and amplifies glutathione S-transferase activity. The main role of NAC as antioxidant is the stimulation of glutathione (GSH) synthesis, enhancing the detoxification process and acting directly to scavenge the oxygen free radicals (Shahin et al., 2009).

NAC is formed of a small molecule which includes the precursor of reduced GSH and a thiol group. Its clinical efficacy in the treatment of acute heavy metal poisoning had been approved through its protective effect on liver and kidney. It processes antioxidative properties and acts as a chelating agent to eliminate the heavy metals due to its thiol group (Kaplan et al., 2008).

The main target of our study was to investigate the protective role of NAC as a potent antioxidant against the iron toxicity and the resulting induced ferroptosis in the hepatic and pancreatic tissues of male albino rats.

MATERIALS AND METHODS

Experimental animals

Thirty-two male albino rats, weighing 200-250 gm, were used in the present study. Rats were housed in metal cages at room temperature and good ventilation. Rats were fed with standard food-pellets that contained all necessary nutritive elements. They were provided a free access to tap water and were acclimatized for one week prior to the treatment.

Experimental design

Experimental rats were randomly divided into four groups, eight animals each group. For four weeks, the duration of the experiment, the rat groups received treatment as follows: Group I (control group) received a daily single intra-peritoneal injection of 0.9% NaCl (normal saline) (pH: 7.4) in equal volume to iron injection; in Group II (NAC treated group), the rats received NAC (Fluimucil) in a dose of 300 mg/kg by oral gavage according to (Galicia-Moreno et al., 2009); in Group III (iron-treated group), the rats received intraperitoneal injection of iron in a dose of 100 mg/kg (Zhoa et al., 2005), three times per week; in Group IV (NAC and iron-treated group), the rats received NAC in a dose 300 mg/kg by oral gavage daily and intraperitoneal injection of iron in a dose of 100 mg/kg three times per week.

Drugs

- ***Haemojet*** (Iron): Haemojet ampoules were purchased from a local pharmacy; the drug is produced by Pharco B International Pharmaceutical Company for the European Egyptian Pharmaceutical Industrial Company, Alexandria, Egypt. A pack of three ampoules, each ampoule containing two ml solution with equivalent elemental iron (100mg) as ferric hydroxide polymaltose complex.
- ***Fluimucil*** (N-Acetylcysteine): Fluimucil tablets (Zambon Switzerland Ltd, 6814 Cadempino, - Switzerland, imported by: Pharma Con Company) were purchased from a local pharmacy, with active constituent is NAC 600 mg. Tablets were dissolved in deionized distilled water, and given to the rats by oral gavage in a dose of 300 mg/kg daily.

Tissue collection

After four weeks, the experimental rats were anaesthetized by isoflurane inhalation and sacrificed. To separate the serum, we collected blood slowly by cardiac puncture, allowing it to clot for 30 min, at least, at room temperature, followed by centrifugation at 2500 rpm for 15 min at 4 °C. The liver and pancreas organs were dissected out and tissues were sampled and processed for different histopathological procedures.

Histopathological procedures

Specimens from liver and pancreas were taken and emerged in 10% buffered formaldehyde solution for at least 24 h for fixation. The specimens were embedded in paraffin wax and 5-µm sections were prepared for histological staining (Slaoui and Fiette, 2011). Prepared slides were stained with hematoxylin and eosin (H&E) stain for an assessment of morphology of the hepatic and pancreatic tissues and observation of the presence, distribution and invasion of the inflammatory cells. Prussian blue (Pb) staining was done for detection of iron deposition in the hepatic and pancreatic tissues (Muñoz et al., 2009). Stained tissue sections slides were examined under a light microscope at 40X magnification.

Electron Microscopic Study

The ultrastructure of the hepatic and pancreatic cells was examined by the use of transmission electron microscopy. To prepare the hepatic and pancreatic tissues, fixation with 2.5% glutaraldehyde in 0.1M phosphate buffer (pH 7.4) overnight at 4 °C was done, with subsequent post-fixation processing in 2% phosphate-buffered osmium tetroxide. The tissues were dehydrated through a serial of graded ethanol, washed in propylene oxide, and embedded in epon resin using EMbed-812 embedding kit. Ultra-thin sections (60–80 nm thick) were done and mounted on copper grids then stained with uranyl acetate and lead citrate (Peerapanyasut et al., 2014, Peerapanyasut et al., 2019). Examination of the ultrastructure of the prepared specimens was done using JEM-2200 FS transmission electron microscope (JEOL- JEM -100 SX electron microscope, Japan, at the electron microscope unit, Mansoura Faculty of Medicine).

Biochemical analysis

Blood samples were collected and serum was separated for biochemical analysis. Quantitative measurements of serum iron level and serum total iron binding capacity were identified using quantitative diagnostic kits, while measuring of the level of serum ferritin was done using enzyme immune assay ELISA kit (Hosseini et al., 2018).

Statistical analysis

Data collected were represented as means ± SEM. Statistical analysis was done by using GraphPad Prism -6, GraphPad Software, San Diego, California. Test used for multiple comparisons between the different groups was One-way ANOVA test. In all tests P value set as <0.05 or less was considered to be statistically significant.

RESULTS

H&E histopathological findings

Histopathological examination with light microscope of liver sections from the control rats stained with H&E showed normal architecture of the hepatic lobules with the hepatocytes arranged as cords radiating from the central vein. The hepatocytes cytoplasm appeared strongly granulated, eosinophilic, and with distinct central nuclei**.** The hepatocytes in the sections from liver of rats treated with NAC showed a mild degree of vacuolization, while sections from the liver of rats of the iron-treated group showed marked hepatic vacuolization mainly with centrolobular distribution, and impacted sinusoids with brownish haemosiderin pigments. Also, there were many hepatocytes revealed, single cell necrosis and apoptosis in this group. Meanwhile, sections from the rats of the last group (NAC + Iron-treated group) showed a marked decrease the hepatic vacuolization, decreased apoptosis, and an obvious clear decrease of the haemosiderin pigments impaction within the blood sinusoids (Fig. 1).

Pancreatic sections from the rats of both control group and NAC treated group showed normal pancreatic architecture composed of serous acini with apical acidophilia and basal basophilia. The nuclei were basal in position, rounded in shape and

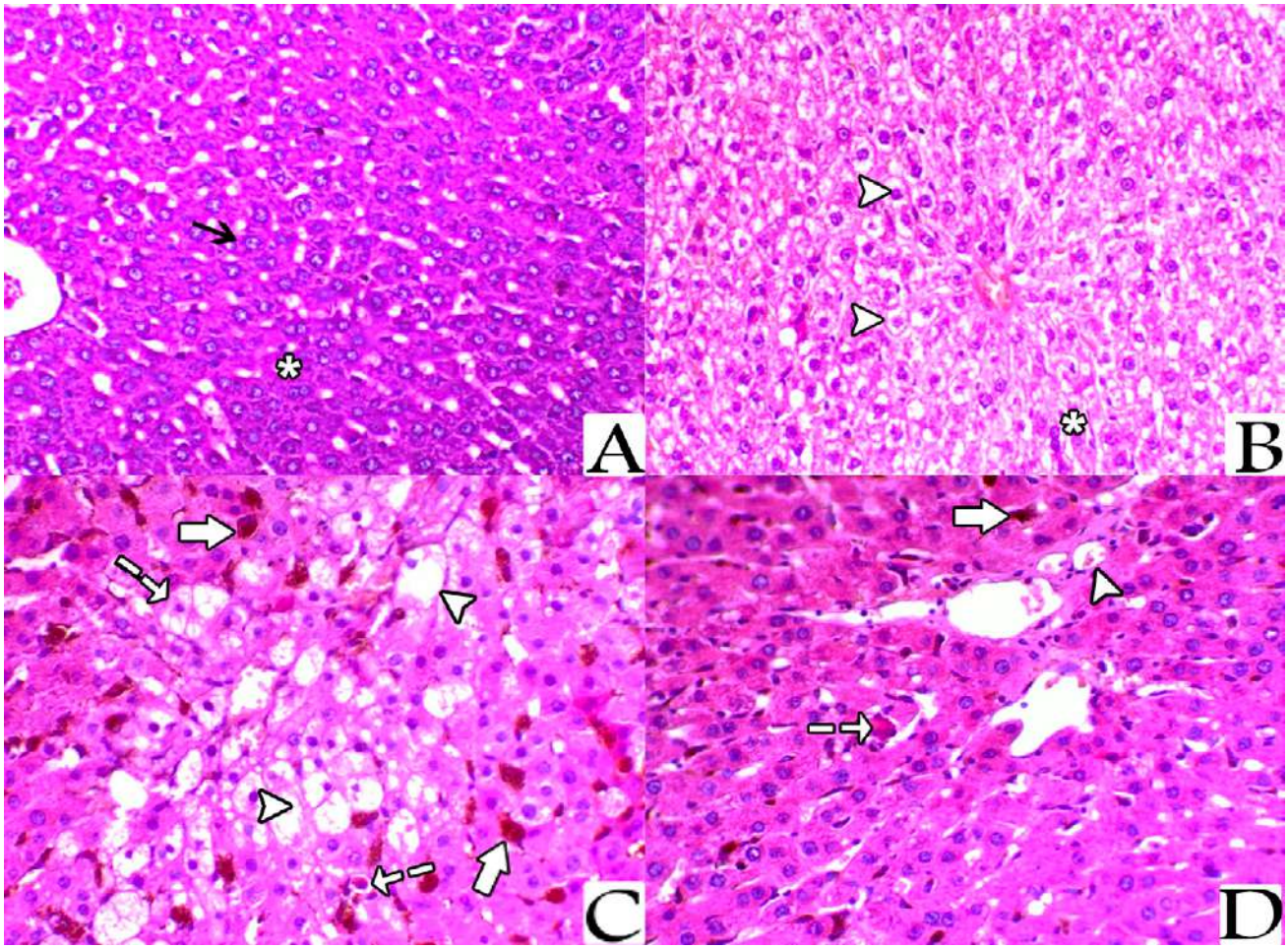

Fig. 1.- (A) Control rat liver, showing normal shaped hepatocytes arranged in cords with basophilic nuclei and acidophilic cytoplasm (thin arrow), some hepatocytes were binucleated (asterisk). **(B)** NAC-treated rat liver showing hepatocytes with mild vacuolization (arrowhead) and binucleated hepatocytes (asterisk). **(C)** Iron-treated rat liver showing centrolobular hepatocytes with marked vacuolization (arrowhead), haemosiderosis within the hepatic sinudoids (thick arrow), and some hepatocytes revealed single cell necrosis and apoptosis (dotted arrow). **(D)** NAC + iron-treated rat liver showing mild degree of hemosiderin deposition in hepatic sinusoids (thick arrow), and mild hepatocytes vacuolization (arrowhead) and few hepatocytes showing single cell necrosis (dotted arrow). H&E staining, x200.

surrounded by basal basophilic cytoplasm**.** While sections from the pancreas of the iron-treated rats revealed marked pancreatic acinar degeneration, necrosis, and associated with marked interstitial hemosiderin deposition. However, sections from the pancreas of the rats treated with both NAC and iron at same time showed a mild degree of acinar degeneration and decreased hemosiderin pigments deposition (Fig. 2).

Electron microscopic study

Examination by TEM of sections prepared from the liver of both control group and NAC-treated group showed hepatocytes with their nuclei exhibited regular outlines, prominent peripheral heterochromatin and prominent nucleolus. The cytoplasm showed regular rough endoplasmic reticulum (rER) surrounding the nucleus and many scattered mitochondria with apparent cristae. Multiple glycogen rosettes and few well circumscribed lipid globules were also seen**.** Sections from the liver of iron-treated rats showed hepatic steatosis associated with deposition of iron particles. On the other hand, ultrastructural examination of hepatocytes from rats treated with both of NAC and iron showed marked decrease of hepatic steatosis associated with decreased iron particles deposition (Fig. 3).

By electron microscope, examination of the prepared pancreatic sections of both control group and NAC-treated rats revealed the well-known normal picture of the exocrine cells of the pancreas. The exocrine acinar cells contained spherical electron dense secretory granules of variable sizes and shape, which were aggregated in the apical cytoplasm called zymogen granules. The acinar cells had large basal nuclei with prominent central nucleoli and dispersed

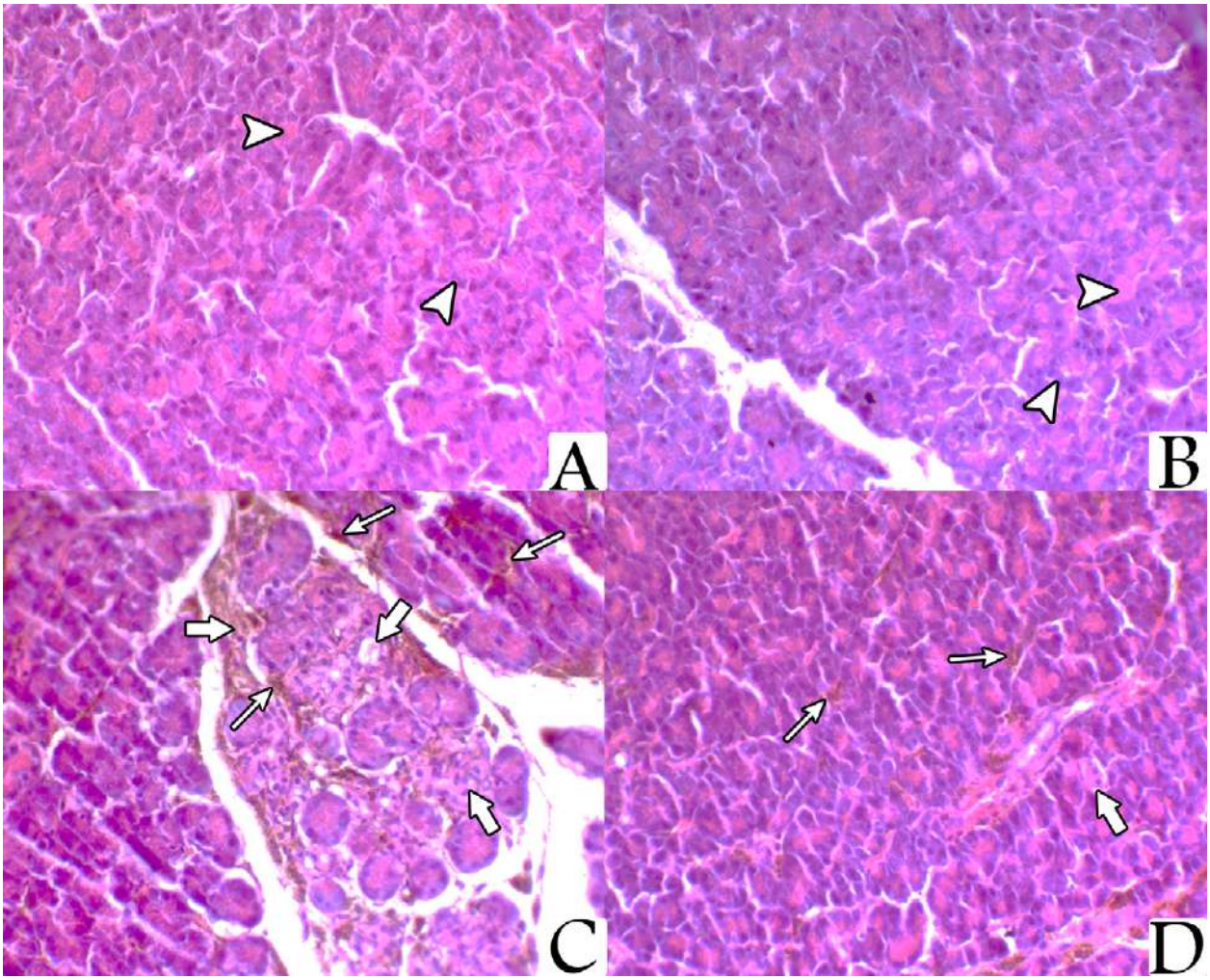

Fig. 2.- (A) Control rat pancreas, showing normal shaped pancreatic acini revealing apical acidophilic and basal basophilic appearance (arrowhead). **(B)** NAC-treated rat pancreas, revealing normally appearing pancreatic acini (arrowhead). **(C)** Iron-treated rat pancreas showing marked acinar degeneration (broad arrow) associated with excessive vascular and interstitial haemosiderosis (thin arrow). **(D)** NAC + iron-treated rat pancreas showing mild degree of acinar degeneration (broad arrow) and mild haemosiderosis (thin arrow). H&E staining, x200.

chromatin. Their cytoplasm was characterized by extensive perinuclear rough endoplasmic reticulum arranged in parallel strands and abundant rounded mitochondria, which had regular cristea**.** Most of the acinar cells from the iron-treated rats' specimens revealed marked degenerative changes manifested by multiple vacuoles, dilated rER, and the nuclei were small, irregular with condensed chromatin (pyknotic). For the rats that were treated with both NAC and iron, most of the ultrastructural examined sections showed that the pancreatic acinar cells were completely normal and arranged around central lumen making the normal architecture of the pancreatic acini. Each cell had basally located nuclei and apical zymogen granules. The cytoplasm had normal mitochondria and normal rough endoplasmic reticulum. The nuclei were rounded, with central nucleoli, basally located and heterochromatic (Fig. 4).

Prussian blue stain

Prussian blue stain was used for the identification of iron in tissues. It is an extremely sensitive stain, and can even detect single granule of iron in cells. On examination of sections from the liver of control rat group and NAC-treated rat group stained with Pb, it showed a mild reactive Pb staining mostly within blood sinusoids**.** Sections from the liver of iron-treated rats revealed an extensive centrolobular staining with Pb stain, whereas sections of the liver of rats that were treated with bath NAC and iron showed marked decrease of sinusoidal staining with Pb denoting decreased hemosiderin deposition (Fig. 5).

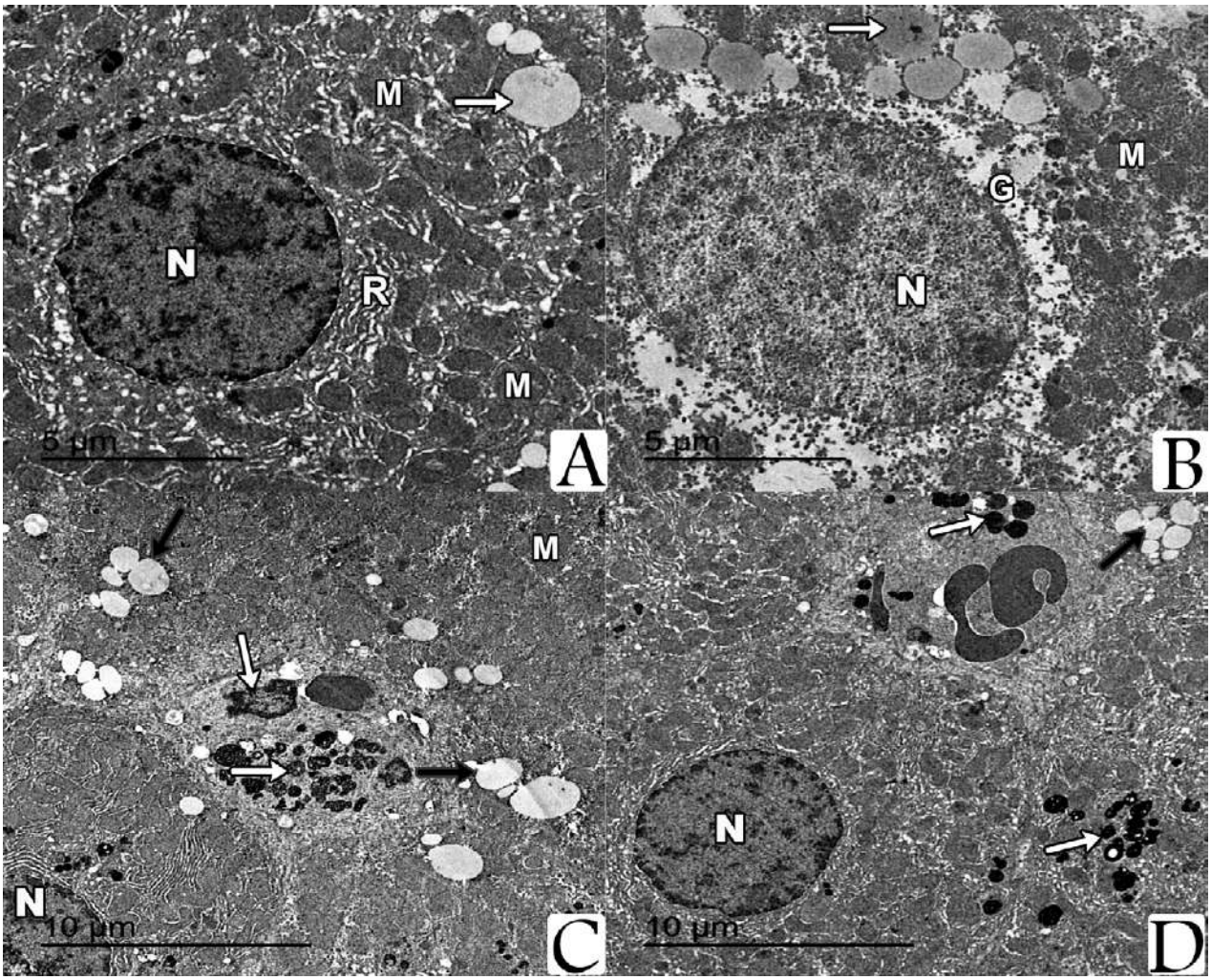

Fig. 3.- (A) Ultramicrograph revealing the ultrastructure of the hepatocyte of control group rat with the nucleus (N) surrounded by rough endoplasmic reticulum (R), mitochondria of normal appearance (M) and appearance of few fat droplets (thin arrow). **(B)** Ultrastructure of the hepatocyte of NAC-treated rat showing normal appearance of the nucleus (N), normally appearing mitochondria (M), with the presence of few fat droplets (thin arrow, and glycogen granules (G). **(C)** Ultrastructure of the hepatocyte of iron-treated rat showing hepatic steatosis (black arrow) associated with deposition of iron particles (white arrow), normal nucleus (N), and mitochondria (M). **(D)** Ultrastructure of the hepatocyte of the NAC + iron-treated rat showing marked decrease of hepatic steatosis (black arrow) associated with decreased deposition of the iron particles (white arrow), normal nucleus (N), and mitochondria (M). Scale bars: A, B = 5 µm, C, D =10 µm.

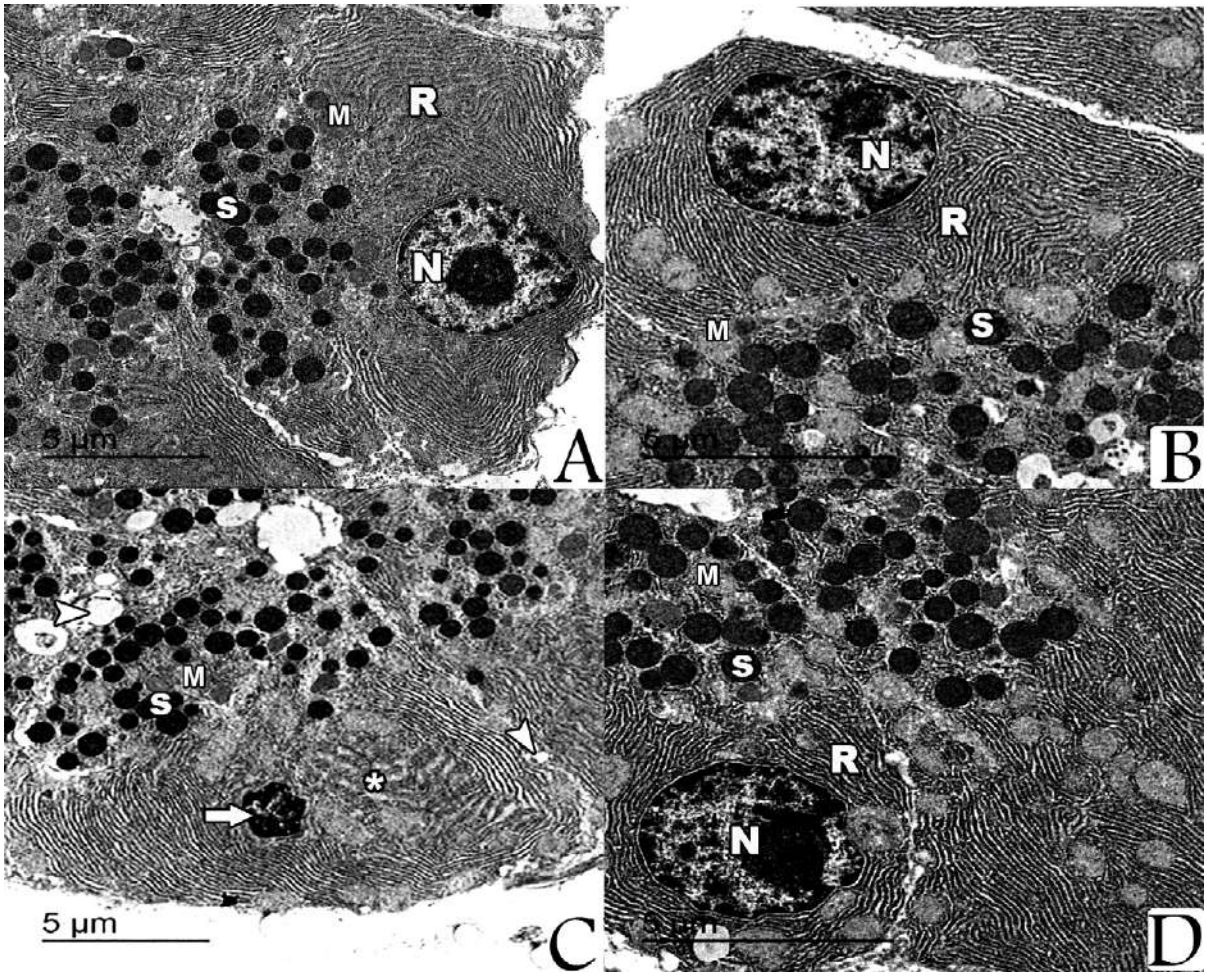

Fig. 4.- (A) Ultrastructure of control group rat pancreatic acinar cell revealing normal nucleus with normal nucleolus (N), normal appearance of secretory granules (S), and rough endoplasmic reticulum (R). **(B)** Ultrastructure of the pancreatic acinar cell of NAC-treated rat with normal nucleus (N), rough endoplasmic reticulum (R), cytoplasmic secretory granules (S), and normally appearing mitochondria (M). **(C)** Ultrastructure of the pancreatic acinar cell of iron-treated rat revealing nuclear pyknosis (thick arrow), associated vacuolation of intercellular junction (arrowhead), dilated rER (asterisk), decreased number and size of mitochondria (M), and few cytoplasmic secretory granules (S). **(D)** Ultrastructure of the pancreatic acinar cell of NAC + iron-treated rat revealing normal shaped nucleus (N) and normal secretory granules (S). Scale bars A-D = 5 µm.

Sections from the pancreas of the control rat group and NAC-treated rat group stained with PB revealed a mild interstitial haemosiderin deposition, while sections from the pancreas of iron-treated rats stained with PB showed marked interstitial haemosiderin deposition. Sections from the pancreas of rat group treated with both NAC plus iron showed a marked decrease Pb-stained area denoting decreased interstitial haemosiderin deposition (Fig. 6).

Biochemical analysis (Table 1, Fig. 7)

As regards to the levels of serum iron, in NAC-treated group, there was no significant (p value < 0.001) increase in the levels of serum iron as compared with control group, in iron-treated group there was a highly significant increase in the levels of serum iron as compared with control group (p value < 0.001). In the rats that were treated with combined NAC and iron, there was significant (P value < 0.05) decrease in serum iron level as compared with iron-treated group, but it is still highly significantly increased as compared with the control group (p value < 0.001).

In serum ferritin levels, in NAC-treated group, there was no significant (p value < 0.001) increase in the level of serum ferritin as compared with control group, while the iron-treated group had a highly significant (P value < 0.001) increase in the level of serum ferritin as compared with control group. In the combined NAC and iron-treated group, there was significant (P value < 0.05) decrease in serum ferritin level as compared with the iron-treated group, but still significantly higher than control group too (p value < 0.001).

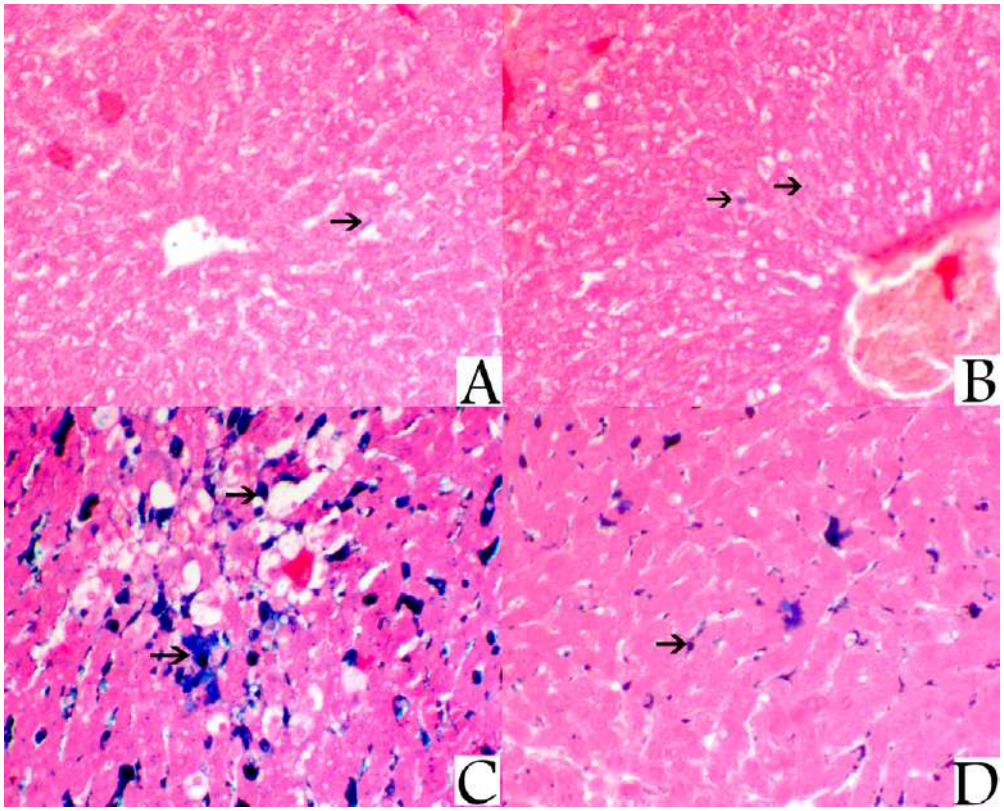

Fig. 5.- (A) Control rat liver showing mild Prussian blue reaction within blood sinusoids (thin arrow). **(B)** NAC-treated rat liver showing mild sinusoidal Prussian blue reaction (thin arrow). **(C)** Iron-treated rat liver showing extensive centrolobular reaction with Prussian blue staining indicating marked sinusoidal haemosiderin deposition (thin arrow). **(D)** NAC + iron-treated rat liver showing marked decrease of sinusoidal haemosiderin staining (thin arrow). Prussian blue stain, x200.

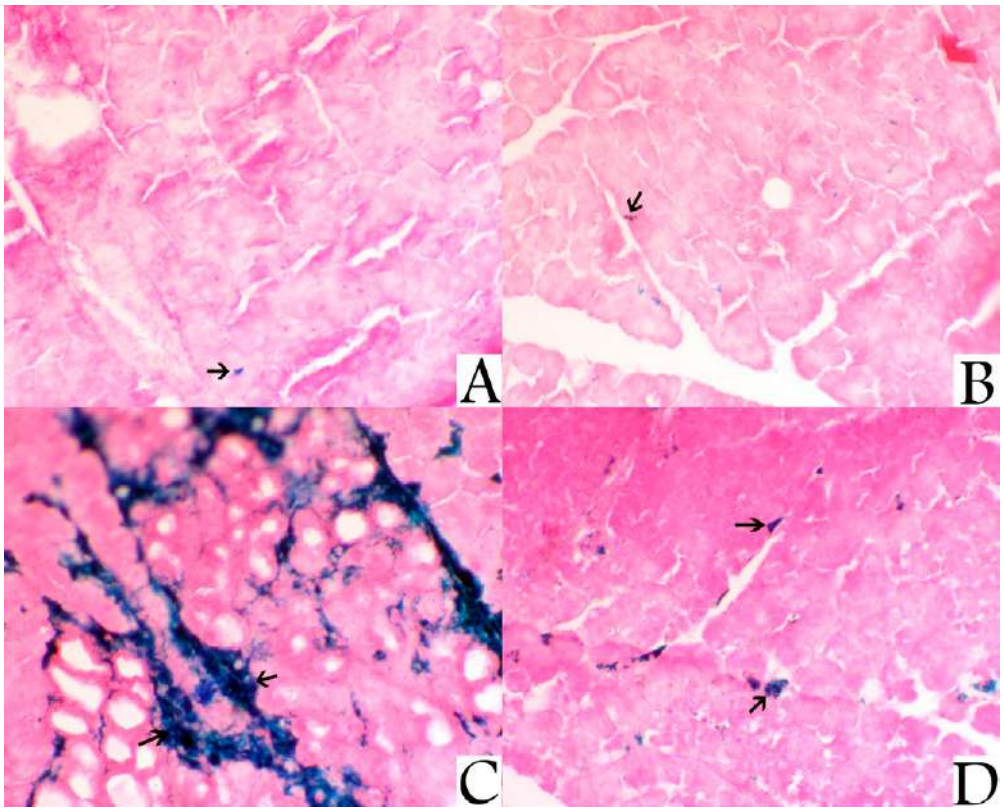

Fig. 6.- (A) Control rat pancreas showing mild interstitial haemosiderin deposition (thin arrow). **(B)** NAC-treated rat pancreas showing mild interstitial Prussian blue reaction (thin arrow). **(C)** Iron-treated rat pancreas showing extensive interstitial haemosiderin deposition (thin arrow). **(D)** NAC + iron-treated rat pancreas showing marked decrease of interstitial haemosiderin staining (thin arrow). Prussian blue stain, x200.

Table 1. Biochemical analysis in serum in all groups of study.

Mean+SEM	Control	NAC-treated	Iron-treated	NAC+iron treated
Serum Iron level mg/dl	133.2 ± 2.151	148.7 ± 2.108	627.7 ± 2.060	381.8 ±2.227
Serum ferritin level ng/dl	0.568± 0.017	0.648 ± 0.015	2.867 ± 0.023	1.138 ±0.007
Serum TIBC ng/dl	298.3± 1.892	305.7 ± 2.275	789.8± 1.740	348.8±2.496

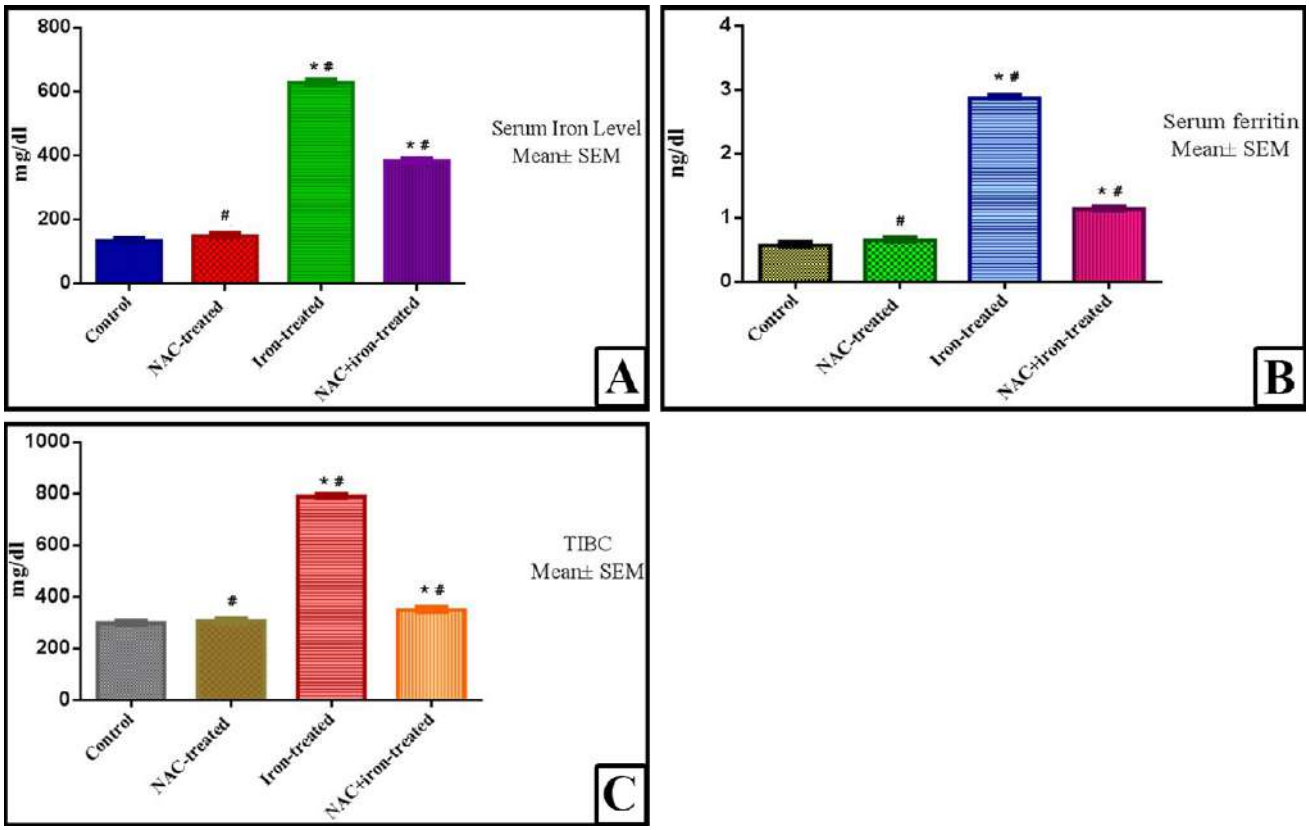

Fig. 7.- (A) Histogram of the serum iron levels (mean±SEM) in the different experimental groups. **(B)** Histogram of the serum ferritin levels (mean±SEM) in the different experimental groups. **(C)** Histogram of the total iron binding capacity (TIBC) levels (mean±SEM) of the different experimental groups. (*) indicates the significant difference from the control group, p value < 0.001 and (#) indicates significant difference from other groups, p value < 0.05.

Regarding the serum total iron binding capacity (TIBC) levels, in the NAC-treated group there was no significant increase in the level of (TIBC) as compared with control group (p value < 0.001). In the iron-treated group there was a highly significant increase in the level of (TIBC) as compared with control group (p value < 0.001). Addition of NAC to iron treatment of the rats, there was a significant (p value < 0.05) decrease in serum (TIBC) level as compared with iron-treated group but it is still highly significant increased as compared with the control group (p value < 0.001).

DISCUSSION

Iron is considered an essential element for many cellular processes in living bodies. Elevated iron in tissue results in several pathological conditions, especially in hepatic function (Fraga and Oteizab, 2002).

Iron overload is usually associated with oxidative stress. Oxidative stress results from excess release of oxygen free radicals, exceeding the antioxidant mechanism capacity. Therefore, current studies should be directed towards establishing novel means to make limitation and decrease the

potential iron-dependent damage through decrease and elimination of the formation and release of these free radicals (Puntarulo, 2005).

Excess and acute iron administration is associated with reduction and consumption of the reduced GSH system in hepatocytes and changes in the GSH system enzymes (Abu-Kishk., 2010). GSH plays a key role in regulating numerous cellular activities and helps to keep the immune system. As an antioxidant, it helps to neutralize free radicals that damage cells and tissues at the molecular level. GSH is a powerful antioxidant, is created by binding of amino acid cysteine with two other amino acids glycine and glutamine. NAC form the medical supplement of the amino acid cysteine (Cathy and Richard, 2020).

Ferroptosis is a form of nonapoptotic cell death for which key regulators remain unknown. Depletion of GSH causes inactivation of glutathione peroxidases (GPXs), which is an essential regulator of ferroptotic cell death (Yang et al., 2013). In their study on Sertoli cells and testicular ischeama and reperfusion, Li et al. (2018), reported that ferroptosis is a pervasive and dynamic type of cell death; they interestingly find that depletion of GSH is accompanied with accumulation of iron, and lipid reactive oxygen species (ROS) in addition to blockage of GSH dependent (GPX4) due to GSH depletion. Activation of the GPX4 with availability of GSH blocked the induced ferroptosis by reducing lipid ROS levels and the resulting cell death due to ischeamia that was inhibited by the ROS inhibitor NAC.

In this study, intake of excess iron led to accumulation of granular iron deposits in pancreatic and liver tissues. It was observed that there was a significant difference between iron-treated group and combined NAC and iron-treated group regarding serum iron level, TIBC, and serum ferritin levels, denoting that the addition of NAC had no additional effect on increasing iron absorption from gastrointestinal tract. This is in contrast to Abu-Kishk et al. (2010), who stated that the oral administration of NAC after acute iron toxicity increases the iron absorption from the gastrointestinal tract, leading to higher serum iron levels and hence more liver damage and mortality. Breitbart et al. (2011) and Boveris et al. (2012) discussed that hepatotoxicity induced by acute iron toxicity is caused mostly due to free radical generation and the subsequent lipid peroxidation, as iron helps to induce the creation and liberation of hydroxyl radical, one of the most potent free radicals, which in turn triggers the lipid peroxidation.

Due to high reactivity of the free oxygen radicals, they produce damage to the cells they originate, and their elimination leads to reduced GSH depletion. Due to this affection of GSH system by acute iron toxicity, NAC is suggested as adjuvant treatment. NAC is a well-established potent antioxidant and GSH substitute, which is widely used as an antidote for various intoxications reducing the lipid peroxidation and enhancing the endogenous antioxidant system (Hundekari et al., 2013).

The major findings of this study are as follows: 1) administration of iron for four weeks led to developing of iron overload condition in the rats, shown by an increase in the following: serum iron, TIBC, and serum ferritin, concurrent treatment of the rats with NAC and Iron led to significant decrease in serum iron, TIBC, and serum ferritin compared to iron overloaded groups. 2) NAC treatment with iron overloading exposure significantly improved hepatocytes mitochondrial condition, with decline of the vacuolization process, decreased of both degeneration of acinar cells and vascular and interstitial haemosiderosis. The same results were obtained by Wongjaikam et al. (2016), who reported that NAC provided enhancing effects in reduction of systemic and cardiac iron overload plus decreasing the plasma and cardiac oxidative stress. In turn, administration of NAC resulted in improvement of the cardiac mitochondrial function, cardiac sympathovagal balance and left-ventricular function.

The liver coordinates the balance of the body iron levels by releasing hepcidin, “the iron hormone”. During different physiological conditions, the production of hepcidin is decreased or induced by iron deficiency or by iron loading respectively. Hepcidin stimulates the breakdown of the iron exporter “ferroportin” to decrease the entry of iron into the bloodstream from dietary sources, iron

recycling macrophages, and from the different body stores (Wang and Babitt, 2019). There are no known mechanisms to control the excretion of excess iron, hence regulation of the body iron homeostasis takes place at the sites of absorption, utilisation and recycling (Wallace, 2016). Increased TIBC and accumulation of the free iron leads to an increase in the entry of free iron into hepatic cells and beta cells of the pancreas: this is in agreement with study of Wongjaikam et al. (2017), who reported that excess of iron accumulated in cardiac tissue with entry of the free iron into cardiac cells causes increased oxidative stress via Haber-Weiss and Fenton's reactions. Induction of acute iron overload in rats by a single intraperitoneal injection of iron-dextran (300 mg/kg) or chronic iron overload by injection of 30 mg/kg/daily for 9 weeks led to oxidative damage of heart and liver which was partly attenuated by subcutaneous injection of NAC (150 mg/kg once), in which the ratio of iron dextran to NAC content was 2:1 (Lou et al., 2009).

Our study showed that increased serum iron and ferritin levels resulted in increased hepatic vacuolization, which affected the function and number of the mitochondria, pancreatic nuclear pyknosis and interstitial haemosiderin deposition. This is in agreement with Gao et al. (2010), who reported in his work a mitochondrial swelling in the iron-overloaded rats with mitochondrial depolarization and damage by increased oxidative stress. Also, Avila et al. (2016) discussed the mitochondrial injury and dysfunction within the cardiac cells resulted from increased oxidative stress in iron-overloaded rats.

In the present study, hepatic steatosis was induced by or associated with increased iron and ferritin levels. This was significantly decreased with adjuvant treatment with NAC. As a general role, exogenous iron overloading resulted in hepatic fibrosis. A proof had been reported in a bunch of studies that hepatic iron overload fails to initiate the expected a fibrogenic response. The results of Park et al. (1987), after he had used iron overloading protocol for 12-months through "3% dietary carbonyl iron" administration led to increase in the hepatic iron concentration more than 50 folds only initiate a mild-to-moderate hepatic fibrosis in rats, mild hepatocyte necrosis and leukocyte infiltration. These results were difficult to reconcile with another experiment that was by the same group of investigators using a 14-month iron loading protocol with no significant fibrosis after (Brown et al., 1997).

Another exception for the golden rule of iron overload and fibrogenic response was reported by induction of hepatic overload in C57Bl/6 mice group fed on a diet containing ferrocene throughout 4 months, which led to a 15 folds increase in hepatic iron levels. This regimen resulted in iron deposition in hepatocytes and sinusoidal lining cells, together with appearance of large siderotic nodules in centrilobular region of the liver. The only fibrogenic response histologically proved was predominantly localized to the siderotic nodules. This pattern of fibrosis had been seen also with long-term carbonyl iron feeding (Valerio and Petersen, 2000). Other experiments had identified the newly appeared collagen fibrils in the liver after iron overload via electron microscopy. However, the use of electron microscopy for identification of the collagen fibrils revealed the minimal extent of fibrosis in these studies (Roberts et al., 1993). Das et al. (2016), after the induction of the hepatic iron overload in C57BL/6 mice, reported increases in histological fibrosis accompanied by significant inflammation, an evident that the induction of inflammation may be important in potentiating hepatic fibrosis in iron overloading model.

CONCLUSION

In our study, iron-overload led to a centrilobular interstitial haemosiderin deposition, hepatic steatosis, sinusoidal impaction of iron particles, mitochondrial dysfunction, nuclear pyknosis, and hepatic and pancreatic increased vacuolization. All these histopathological changes markedly decreased with concomitant treatment with N-Acetyl cysteine to the iron overloaded rats. With the limitation in our study that antioxidant markers should be assessed although we search for the histopathological changes. Further investigations for the detailed mechanism are required.

REFERENCES

ABU-KISHK I, KOZER E, GOLDSTEIN LH, WEINBAUM S, BAR-HAIM A, ALKAN Y, PETROV I, EVANS S, SIMAN-TOV Y, BERKOVITCH M (2010) Oral N-acetylcysteine has a deleterious effect in acute iron intoxication in rats. *Am J Emerg Med*, 28(1): 8-12.

ANDERSON ER, SHAH YM (2013) Iron homeostasis in the liver. *Comp Physiol*, 3(1): 315-330.

ÁVILA RA, SILVA M, PEIXOTO JV, KASSOUF-SILVA I, FOGAÇA R, DOS SANTOS L (2016) Mechanisms involved in the in vitro contractile dysfunction induced by different concentrations of ferrous iron in the rat myocardium. *Toxicol In Vitro*, 36: 38-45.

BOVERIS A, MUSACCO-SEBIO R, FERRAROTTI N, SAPORITO-MAGRIÑÁ C, TORTI H, MASSOT F, REPETTO MG (2012) The acute toxicity of iron and copper: biomolecule oxidation and oxidative damage in rat liver. *J Inorg Biochem*, 116: 63-69.

BROWN KE, POULOS JE, LI L, SOWEID AM, RAMM GA, O'NEILL R, BRITTON RS, BACON BR (1997) Effect of vitamin E supplementation on hepatic fibrogenesis in chronic dietary iron overload. *Am J Physiol Gastrointest Liver Physiol*, 272: 116-123.

DAS S, DESAULNIERS J, DYCK J, KASSIRI Z, OUDIT G (2016) Resveratrol mediates therapeutic hepatic effects in acquired and genetic murine models of iron-overload. *Liver Int*, 36: 246-257.

FRAGA CG, OTEIZAB PI (2002) Iron toxicity and antioxidant nutrients. *Toxicology*, 180(1): 23-32.

FUNG E, NEMETH E (2013) Manipulation of the hepcidin pathway for therapeutic purposes. *Haematologica*, 98(11): 1667-1676.

GALICIA-MORENO M, RODRIGUEZ-RIVERA A, REYES-GORDILLO K, SEGOVIA J, SHIBAYAMA M, TSUTSUMI V, VERGARA P, MORENO MG, MURIEL P (2009) N-acetylcystein prevents carbon tetrachloride induced liver cirrhosis: Role of liver transforming growth factor –beta and oxidative stress. *Eur J Gastroenterol Hepatol*, 21(8): 908-914.

GAO X, QIAN M, CAMPIAN JL, MARSHALL J, ZHOU Z, ROBERTS AM, KANG YJ, PRABHU SD, SUN XF, EATON JW (2010) Mitochondrial dysfunction may explain the cardiomyopathy of chronic iron overload. *Free Radic Biol Med*, 49(3): 401-407.

HOSSEINI M, DURDI-QUJEQ D, AHMAD TA, RANAEE M, HAJIAN-TILAKI K (2018) The efficacy of the aqueous extracts of Anethum graveolens, Urtica dioica, and Silybum marianum on the liver function in iron overloaded rats. *Iran J Ped Hematol Oncol*, 8(4): 213-220.

KAPLAN M, ATAKAN IH, AYDOGDU N, AKTOZ T, OZPUYAN F, SEREN G, TOKUÇ B, INCI O (2008) Influence of N-acetylcysteine on renal toxicity of cadmium in rats. *Pediatr Nephrol*, 23: 233-241.

KERKSICK C, WILLOUGHBY D (2005) The antioxidant role of glutathione and N-acetyl-cysteine supplements and exercise-induced oxidative stress. *J Int Soc Sports Nutr*, 2(2): 38-44.

LARSSON SC, HÅKANSSON N, WOLK A (2015) Dietary cysteine and other amino acids and stroke incidence in women. *Stroke*, 46(4): 922-926.

LI L, HAO Y, ZHAO Y, WANG H, ZHAO X, JIANG Y, GAO F (2018) Ferroptosis is associated with oxygen-glucose deprivation/reoxygenation-induced Sertoli cell death. *Int J Mol Med*, 41: 3051-3062.

LOU LX, GENG B, CHEN Y, YU F, ZHAO J, TANG C-S (2009) Endoplasmic reticulum stress involved in heart and liver injury in iron-loaded rats. *Clin Exp Pharmacol Physiol*, 36(7): 612-618.

MILIC S, MIKOLASEVIC I, ORLIC L, DEVCIC E, NADA STARCEVIC-CIZMAREVIC E, STIMAC D, KAPOVIC M, RISTIC S (2016) The role of iron and iron overload in chronic liver disease. *Med Sci Monit*, 22: 2144-2151.

MUÑOZ M, VILLAR I, GARCÍA-ERCE JA (2009) An update on iron physiology. *World J Gastroenterol*, 15: 4617-4626.

MUSACCO-SEBIO R, FERRAROTTI N, SAPORITO-MAGRIÑA C, SEMPRINE J, FUDA J, TORTI H, BOVERIS A, REPETTO MG (2014) Rat brain oxidative damage in iron and copper overloads. *Metallomics*, 6: 1410-1416.

PARK C, BACON B, BRITTENHAM G, TAVILL A (1987) Pathology of dietary carbonyl iron overload in rats. *Lab Investig*, 57: 555-563.

PEERAPANYASUT W, THAMPRASERT K, WONGMEKIAT O (2014) Ubiquinol supplementation protects against renal ischemia and reperfusion injury in rats. *Free Radic Res*, 48: 180-189.

PEERAPANYASUT W, KOBROOB A, PALEE S, CHATTIPAKORN N, WONGMEKIAT O (2019) N-acetylcysteine attenuates the increasing severity of distant organ liver dysfunction after acute kidney injury in rats exposed to bisphenol A. *Antioxidants J*, 8: 497.

PUNTARULO S (2005) Iron, oxidative stress and human health. *Mol Aspects Med*, 26(4-5): 299-312.

REBECCA LG, ROBERT P (2019) Impact of supplementary amino acids, micronutrients, and overall diet on glutathione homeostasis. *Nutrients*, 11(5): 1056.

ROBERTS FD, CHARALAMBOUS P, FLETCHER L, POWELL LW, HALLIDAY JW (1993) Effect of chronic iron overload on procollagen gene expression. *Hepatology*, 18: 590-595.

SAMPAIO AS, SILVA M, DORNAS WC, COSTA DC, SILVA ME, DOS SANTOS RC, DE LIMA WG, PEDROSA ML (2014) Iron toxicity mediated by oxidative stress enhances tissue damage in an animal model of diabetes. *Biometals*, 27: 349-361.

SHAHIN AY, HASSANIN IM, ISMAIL AM, KRUESSEL JS, HIRCHENHAIN J (2009) Effect of oral N-acetyl cysteine on recurrent preterm labor following treatment for bacterial vaginosis. *Int J Gynecol Obstet*, 104: 44-48.

SLAOUI M, FIETTE L (2011) Histopathology procedures: from tissue sampling to histopathological evaluation methods. *Mol Biol*, 691: 69-82.

VALERIO LG, PETERSEN DR (2000) Characterization of hepatic iron overload following dietary administration of dicyclopentadienyl iron (Ferrocene) to mice: Cellular, biochemical, and molecular aspects. *Exp Mol Pathol*, 68: 1-12.

WALLACE DF (2016) The regulation of iron absorption and homeostasis. *Clin Biochem Rev*, 37(2): 51-62.

WANG CY, BABITT J (2019) Liver iron sensing and body iron homeostasis. *Blood*, 133(1): 18-29.

WHITTAKER P, HINES FA, ROBL MG, DUNKEL VC (1996) Histopathological evaluation of liver, pancreas, spleen, and heart from iron-overloaded Sprague-Dawley rats. *Toxicol Pathol*, 24: 558-563.

WONGJAIKAM S, KUMFU S, KHAMSEEKAEW J, SRIPETCHWANDEE J, SRICHAIRATANAKOOL S, FUCHAROEN S, CHATTIPAKORN SC, CHATTIPAKORN N (2016) Combined iron chelator and antioxidant exerted greater efficacy on cardioprotection than monotherapy in iron-overloaded rats. *PLoS One*, 11(7): e0159414.

WONGJAIKAM S, KUMFU S, KHAMSEEKAEW J, CHATTIPAKORN SC, CHATTIPAKORN N (2017) Restoring the impaired cardiac calcium homeostasis and cardiac function in iron overload rats by the combined deferiprone and N-acetyl cysteine. *Sci Rep*, 7: 44460.

YANG WS, SRIRAMARATNAM R, WELSCH ME, SHIMADA K, SKOUTA R, VISWANATHAN VS, CHEAH JH, CLEMONS PA, SHAMJI AF, CLISH CB, BROWN LM, GIROTTI AW, CORNISH VW, SCHREIBER SL, STOCKWELL BR (2014) Regulation of ferroptotic cancer cell death by GPX4. *Cell*, 156(1-2): 317-331.

ZHAO Y, LI H, GAO Z, XU H (2005) Effects of dietary baicalin supplementation on iron overload-induced mouse liver oxidative injury. *Eur J Pharmacol*, 509(2-3): 195-200.

Physical and ultrasonographic examination of palmaris longus tendon in the Arabian Gulf Region

Bhagath K. Potu[1], Ahmad A. Alnaggar[2, 3], Ayesha Fatima[1], Abdel H. Salem[1], Raouf A. Fadel[1]

[1] Department of Anatomy, College of Medicine & Medical Sciences, Arabian Gulf University, Kingdom of Bahrain
[2]Consultant in Radiology, Zagazig University, Egypt & [3]Royal Bahrain Hospital, Kingdom of Bahrain

SUMMARY

Most of the studies published on the palmaris longus (PL) prevalence are by physical examination methods. None of the reported prevalence studies in Arab populations are based on ultrasonography; hence we have undertaken this study. Our study was performed on 79 (34 male and 45 female) young/adult Arabs. The occurrence of PL tendon was recorded by a physical examination method (Schaeffer's test), followed by ultrasound measurement of the thickness, width and circumference of the PL tendon at the wrist and the distance between the PL tendon and the median nerve at the wrist, bilaterally. Of 158 wrists examined, the physical examination method revealed the presence of PL tendon in 138 (87.3%) subjects, whereas the ultrasound method revealed 149 (94.3%). Schaeffer's test gave a false-negative result for 11 cases. The thickness, width and circumference of the PL tendon at the wrist were: 1.14±0.44 mm (right side) & 1.19±0.41 mm (left side); 4.08±1.34 mm (right side) & 4.36±1.26 mm (left side); 8.98±2.94 mm (right side) & 9.45±2.67 mm (left side), respectively. Gender differences in the thickness, width and circumference of the PL tendon at the wrist were: 1.31±0.42 mm (male) and 1.06±0.40 mm (female); 4.61±1.23 mm (male) and 3.93±1.29 mm (female); 10.04±2.59 mm (male) and 8.60±2.82 mm (female), respectively. The distance of the PL tendon from the median nerve (measured 2 cm proximal to distal wrist crease) were: 1.30±0.63 mm & 1.24±0.61 mm on right & left sides; 1.40±0.60 mm & 1.17±0.62 mm in male and females, respectively. The ultrasonographic measurements were statistically significant among genders, while no such significance was detected between the sides. This study has documented both topographic and ultrasonographic description of the PL tendon in a Gulf Arab population; ultrasonography is more reliable for detecting the PL tendon than Schaeffer's test.

Key words: Palmaris longus – Schaeffer's test – Ultrasound examination – Morphometric data – Arabs

INTRODUCTION

The palmaris longus (PL) is a slender, elongated muscle located medial to the flexor carpi radialis (FCR). It originates from the medial epicondyle,

Corresponding author:
Dr. Bhagath Kumar Potu. Department of Anatomy, College of Medicine and Medical Sciences, Arabian Gulf University, Kingdom of Bahrain, Arabian Gulf. E-mail: potubk@agu.edu.bh

Dissemination history:
This research was presented at "Anatomical Society Winter Meeting (2019)" held from 18th – 20th December in Lancaster University, UK. Presentation number # 1

Submitted: December 8, 2020. **Accepted:** January 13, 2021

the epicondylar ridge of the humerus, from the adjacent intermuscular septa and the antebrachial fascia. It terminates as a long-slender flattened tendon, which passes over the flexor retinaculum and inserts on the central part of the flexor retinaculum and palmar aponeurosis. The morphology of PL is extremely variable (Clemente, 1985). Reports have shown that the PL may be absent, duplicated, triplicated, reversed or presented as a digastric muscle with various insertions. It has been observed from various studies that the PL is inserted into the fascia of the forearm, the hypothenar eminence, the tendon of the flexor carpi ulnaris muscle, the abductor pollicis brevis, into the carpal tunnel or Guyon's canal, the pisiform bone and the scaphoid bone (Lalit et al., 2014). The presence of the PL can be assessed by various physical examination methods (Schaeffer, 1909) such as Schaeffer's test, Pushpakumar's test, Thomson's test, Mishra's test, Reimann test, Gangata test, Hiz test, Bhattacharya test, Lotus sign and four finger sign test. These have been used to confirm the presence of PL in various populations (Pushpakumar et al., 2004; Thompson et al., 1921; Mishra, 2001; Reimann et al., 1994; Gangata, 2009; Hiz et al., 2011). Since there are many other bulky muscles in the forearm to flex the wrist, its absence does not seem to have any functional loss on the biomechanical functions of the wrist region. Moreover, PL is dispensable, so it is the best choice for grafts in tendon reconstruction (Ozasa et al., 2018), lip augmentation (Trussler et al., 2008) and penile reconstruction surgeries (Garaffa et al., 2013). The extent of absence of PL reported in humans varies in different populations. Its absence was reported for the first time by Columbus in *De Re Anatomica*, cited by Schaeffer (Schaeffer, 1909). PL has been studied extensively using various examination methods, and prevalence of its agenesis varies significantly across the different population from 0.6% to 64% (0.6% in Koreans, 1.02% in Ugandans, 2.9% in Asians, 3-4.3% in Japanese, 3.3-17.2% in Brazilian, 4.5-22.5% in African Americans, 4.5-50.8% in Egyptians, 2.1-4.6% in Chinese, 4.4-32.2% in Hungarians, 5.8-15.2% in Canadians, 6.7-25% in Nigerians, 9.3-11.7% in Malaysians, 11.6% in Czechs, 13.2-33.7% in Iranians, 18.3% in Iraqis, 20.2-37% in Indians, 24% in North American Caucasians, 25% in Irish, 16.7-40.5% in Saudi and Bahraini population of Arabian Gulf region, and highest reported is 15-64% in Turkish population) as mentioned in a meta-analysis (Pekala et al., 2017). A recent meta-analysis based on 19 cadaveric studies revealed that the overall absence of the PL is about 10.3%. With regards to gender, females have been reported to have higher absence, 14.5%, as compared to 6.0% in males. 49 studies in which the function of PL was assessed, the overall absence of PL was 15.6%: males had a pooled absence of PL in 15.1% and17.6% in females (Pekala et al., 2017).

It is important to note that the PL tendon lies immediately superficial to the median nerve at the level of the wrist. When a variant PL is present, its proximity to the median nerve places the latter at risk during tendon harvesting procedures. The median nerve is also more vulnerable to misidentification in patients with congenital absence of the PL tendon. Therefore, safe harvesting of the PL requires a thorough understanding of the relevant anatomy, particularly the relevant anatomical distances, as well as distinguishing the nerve from tendon. There are reports of surgical errors while harvesting the median nerve instead of the PL tendon (Choo et al., 2017; Vastamaki, 1987; Weber and Mackinnon, 2007; Leslie et al., 2017), suggesting that the accurate preoperative assessment of the tendon-nerve relationship is crucial to minimize the risk of such devastating complications. A recent report revealed that the preoperative clinical examination to document the presence of PL did not prevent the accidental erroneous excisions of the median nerve during PL harvest. Hence, more effective methods of estimating graft dimensions must be explored in patients requiring PL tendon grafting (Leslie et al., 2017). A reliable preoperative assessment is only possible through the imaging techniques. The efficacy and reliability of ultrasound measurements to predict PL graft dimensions, however, has not been evaluated comprehensively.

Although few studies (Sater et al., 2010; Raouf et al., 2013; Alzahrani et al., 2017; Alkhamis et al., 2017) were done in the past using physical examination methods on Arab populations, none of these have studied the prevalence

and morphological features of PL using the ultrasonography. The objectives of our study were to: (1) determine the presence of PL in Gulf Arabs with physical and ultrasound examination, and (2) perform the morphometry of the PL tendon (thickness, width, and circumference) at the wrist and measure its distance from the median nerve using ultrasonography technique.

MATERIALS AND METHODS

Sample

This study was carried out from February 2019 to March 2020 at Anatomy-Pathology Learning Resource Center (APLRC), Arabian Gulf University, Kingdom of Bahrain. The study subjects were medical students (n= 79, Male: 34; Female: 45) of age between 19-24 years, from the Gulf Co-operative Council (GCC) countries. The number of subjects from different Gulf Arab nations is listed in Table 1. The sample excluded the subjects who had a history of hand surgery or abnormality of the upper limbs. This study was approved by Institutional Research & Ethics Committee (Project number G-E011-PI-11/18). The participation in the study was voluntary, and written informed consent was obtained from all the subjects before performing the procedures.

Physical examination

For examining the PL tendon, a standard testing method "Schaeffer's test" was used. Subjects were asked to place their thumb against their little finger while flexing the wrist (Fig. 1A). With this test, presence or absence of the PL tendon on both right and left sides were registered.

Ultrasound evaluation

Irrespective of the PL tendon finding on physical examination, all subjects underwent ultrasonographic evaluation on "SIEMENS ACUSON P 500 Ultrasound System" located in anatomy lab, College of Medicine & Medical Sciences, Arabian Gulf University. Ultrasonography was performed to indicate the presence of PL tendon and to measure its thickness, width and circumference at the wrist. In addition to the above parameters, the distance of the PL tendon from the median nerve at the wrist (2 cm proximal to distal wrist crease) was also measured. This protocol was adopted from Ertem et al. (2010) (Fig. 1B). Ultrasonography was performed by an experienced radiologist with an array probe with the frequency of 6-15 MHz, which is appropriate for the superficial structures.

Table 1. Sample and number of cases of PL tendon identified by clinical test method and ultrasonographic examination.

Population	Sample Size (No of Wrists)	Presence of PL tendon			
		Schaeffer's test		Ultrasound Examination	
		Right	Left	Right	Left
Bahrain	Male (n=30) Female (n=36) Total = 66	12 15 27	14 17 31	13 17 30	15 18 33
Saudi Arabia	Male (n=22) Female (n=04) Total = 26	11 01 12	11 02 13	11 01 12	11 02 13
Kuwait	Male (n=10) Female (n=14) Total=24	03 06 09	04 05 09	05 06 11	05 05 10
Oman	Male (n=06) Female (n=36) Total=42	03 15 18	02 17 19	03 17 20	03 17 20
Overall	Male (n=68) Female (n=90)	29 37	31 41	32 41	34 42
	Total = 158	**138 (87.3%)**		**149 (94.3%)**	

*Overall, PL tendon absent for 12.7% by Schaeffer's test and 5.7% by ultrasound examination; PL: palmaris longus.

Fig. 1A.- Physical examination method: Schaeffer test. The subjects were asked to place their thumb against their little finger while flexing the wrist. Arrow shows the PL-Palmaris longus tendon.

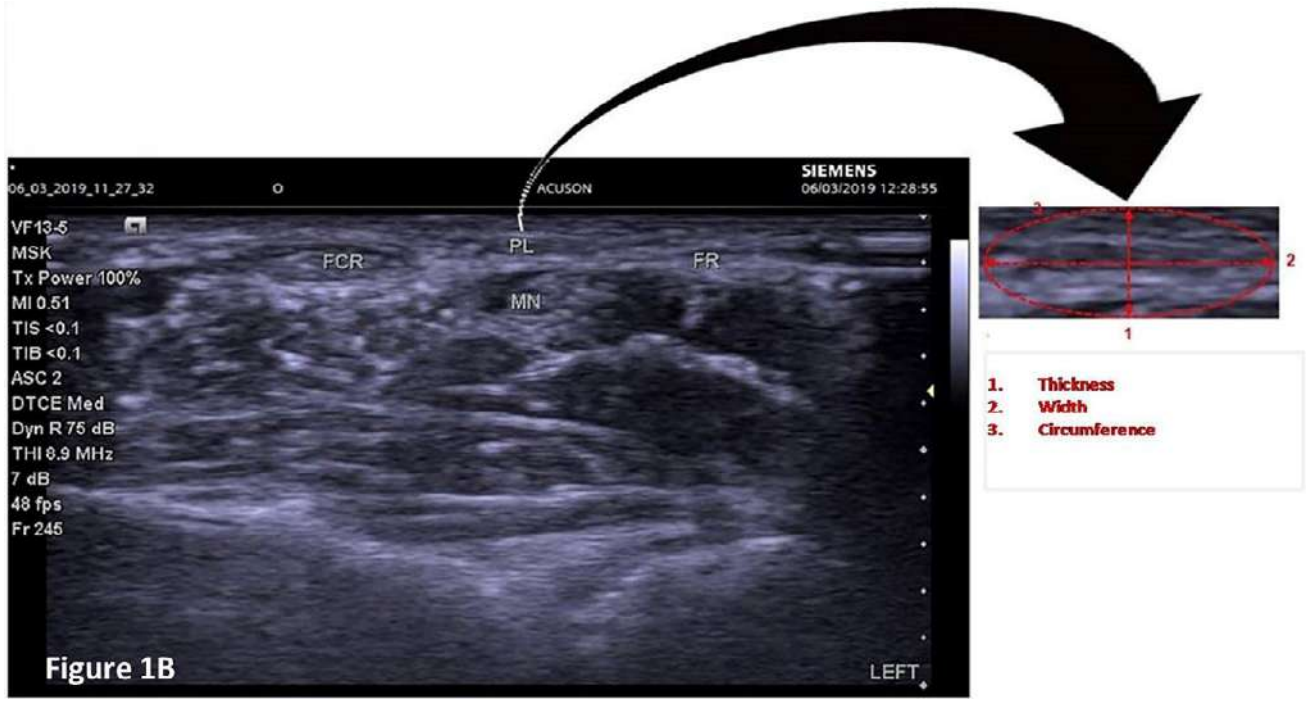

Fig. 1B.- Ultrasonographic image of the wrist with palmaris longus tendon (PL tendon) and the measurements conducted on it. FCR-Flexor carpi radialis; MN: Median nerve; FR: Flexor retinaculum.

Statistical analysis

All statistical analyses were performed using SPSS version 23 (SPSS Inc., USA). Measurements are presented as mean and SD. *Chi-square* test was performed to see whether any significant differences between the outcomes of physical examination and ultrasonography findings. To examine the gender differences in means of the parameters studied, we have used two sample independent *t-test*.

RESULTS

Prevalence (Physical and Ultrasound examination)

In our study of 158 wrists, 138 wrists revealed the presence of the PL tendon by physical examination method (87.3%) whereas absent in 20 wrists (12.7%).

Of 34 male subjects (68 wrists) (Table 1), the Schaeffer's test demonstrated that the PL tendon was present in 60 wrists (88.2%): 42.6% in 29 right wrists and 45.5% in 31 left wrists. Of 8 absent cases (11.7%): 5 were on the right side (7.35%) and 3 were on the left side (4.41%). Whereas in 45 female subjects (90 wrists) (Table 1), Schaeffer's test demonstrated that the PL tendon was present in 78 wrists (86.6%): 41.1% in 37 right wrists and 45.5% in 41 left wrists. Of 12 absent cases (13.3%): 8 were on the right side (8.88%) and 4 were on the left side (4.44%) (Table 1).

The ultrasound examination also involved the same subjects of the Schaeffer's test. 149 of 158 wrists demonstrated the presence of the PL tendon by ultrasound examination method (94.3%) while absence was registered in 9 wrists (5.7%).

Of 34 male subjects (68 wrists) (Table 1), the ultrasound evaluation demonstrated that the PL tendon was present in 66 wrists (97%): 47.05% in 32 right wrists and 50% in 34 left wrists. About the 2 absent cases (2.9%): both were on the right side while reporting zero percent cases on the left side. Whereas in 45 female subjects (90 wrists) the ultrasound evaluation demonstrated that the PL tendon was present in 83 wrists (92.2%): 45.5% in 41 right wrists and 46.6% in 42 left wrists (Table 1). Of the seven wrists in which absence was registered (7.7%): 4 were on the right side (4.4%) and 3 were on the left side (3.3%). Overall, the Schaeffer's test gave a false-negative result for 11 subjects. No anatomical variations in the structure of the PL tendon, such as duplicated tendon or reversed PL muscle, were detected. *Chi-square* test results showed that the differences between the outcomes of physical examination and ultrasonography were significant ($p= 0.032$).

PL tendon morphometry by ultrasonographic evaluation

The thickness, width and circumference of the PL tendon and its distance from the median nerve measured at the wrist of all limbs by ultrasound are expressed as Mean±SD. For all the parameters measured, the Bahraini, Omani, Kuwaiti and Saudi samples did not show any statistically significant differences ($p>0.05$) among right and left sides, except the width and circumference, which were statistically significant in the Bahraini sample ($p=0.036; p=0.04$) (Table 2). The gender differences in morphometric measurements performed on the PL tendon by ultrasonography are expressed as Mean±SD in Table 3. The overall mean differences of morphometric measurements performed on PL tendon by ultrasonography in both genders are statistically significant for thickness ($p<0.0005$); width ($p=0.001$); circumference ($p=0.001$) and

Table 2. Morphometric measurements performed on right and left PL tendon by ultrasonography. Values are expressed as Mean ± SD.

Palmaris Longus Tendon morphometric measurements (mm) Ultrasonographic observations									
Population	Sample Size (No of Wrists)	Thickness		Width		Circumference		Distance from Median Nerve	
		Right	Left	Right	Left	Right	Left	Right	Left
Bahrain	66	1.18 ± 0.49	1.27 ± 0.36	3.96 ± 1.43	4.57 ± 0.79	8.88 ± 3.08	10.17 ± 1.70	1.12 ± 0.53	1.21 ± 0.43
Saudi Arabia	26	1.1 ± 0.45	1.24 ± 0.24	4.26 ± 1.46	4.82 ± 0.74	9.5 ± 3.20	10.25 ± 1.59	1.52 ± 0.76	1.42 ± 0.63
Kuwait	24	1.2 ± 0.50	1.10 ± 0.63	4.25 ± 1.45	3.93 ± 1.93	9.37 ± 3.17	8.42 ± 4.02	1.23 ± 0.58	1.08 ± 0.79
Oman	42	1.07 ± 0.32	1.1 ± 0.41	4.05 ± 1.13	3.98 ± 1.55	8.59 ± 2.55	8.44 ± 3.13	1.48 ± 0.67	1.29 ± 0.72
Overall	158	1.14 ± 0.44	1.19 ± 0.41	4.08±1.34	4.36±1.26	8.98±2.94	9.45±2.67	1.30±0.63	1.24±0.61

PL: palmaris longus

distance between the PL tendon and the median nerve (*p=0.023*) (Table 3). Data showed that the thickness, width, circumference of the PL tendon and its distance from median nerve were greater on the left side, except the distance of the PT from median nerve in females (Table 4).

DISCUSSION

Our study documented absence of the PL tendon in 12.7% of the wrists by physical examination and 5.7% of wrists by ultrasonography. Few previous studies conducted on Arab populations, on the basis of physical examination, showed extreme variation in its occurrence: PL was absent in 38.6% of studied Jordanians (Hassan and Jabeti, 2008); 50.8% in Egyptians (Raouf et al., 2013); 40.5% in Saudis (Alkhamis et al., 2017); 36.8% in Bahrainis (Sater et al., 2010). A subsequent study in Saudi Arabia, however, concluded a much lower rate (16.7%) of PL absence (Hussain, 2012). Based on extensive data review conducted on different examination methods (Table 5), we also noted that wide variation exists in PL absence from 4.5-50.8% in Pan Arabs and 16.7-40.5% in Gulf Arabs (Sater et al., 2010; Hussain, 2012; Alzahrani et al., 2017; Alkhamis et al., 2017). This wide variation could be due to ethnic differences, sample size and the types of specimens or examination methods used.

A study on 136 wrists reported that the incidence of tendon absence was 10% in ultrasonography and 14% in standard physical examination methods such as Schaeffer's test (Holzgrefe et al., 2019). In another study on 96 wrists, the tendon absence was detected for 19% by ultrasonography and 18% by physical examination methods; this study also confirmed that the Schaeffer's is the standard test that could reliably detect PL tendon presence/absence with a sensitivity and specificity of 94% (Johnson et al., 2020). This justifies why we used only Schaeffer's as the standard test in our study. Other than its absence, we did not observe any anomalous PL structure in our ultrasound examination, unlike the variations reported previously. Based on cadaveric dissection, it was reported that the different PL variations range from complete agenesis to changes in its location, size, shape and the insertion site (Reimann et al., 1994; Thejodhar et al., 2008). Olewnik et al. (2017) described three variant insertions of

Table 3. Morphometric measurements performed on male and female PL tendon by ultrasonography. Values are expressed as Mean ± SD.

Palmaris Longus Tendon morphometric measurements (mm) Ultrasonographic observations									
Population	Sample Size (No of Wrists)	Thickness		Width		Circumference		Distance from Median Nerve	
		Male	Female	Male	Female	Male	Female	Male	Female
Bahrain	66	1.33 ± 0.48	1.14 ± 0.36	4.51 ± 1.43	4.07 ± 0.91	9.88 ± 3.08	9.23 ± 2.01	1.23 ± 0.49	1.11 ± 0.47
Saudi Arabia	26	1.25 ± 0.27	0.70 ± 0.50	4.80 ± 0.74	3.15 ± 2.10	10.35 ± 1.60	7.28 ± 4.86	1.63 ± 0.60	0.60 ± 0.42
Kuwait	24	1.56±0.31	0.85±0.85	4.96 ± 0.61	3.47 ± 1.93	10.77 ± 0.89	7.55 ± 4.18	1.41 ± 0.62	0.97 ± 0.68
Oman	42	1.0 ± 0.50	1.10 ± 0.34	3.83 ± 2.09	4.04 ± 1.21	8.50 ± 4.28	8.52 ± 2.59	1.37 ± 0.87	1.39 ± 0.68
Overall	158	1.31± 0.42	1.06 ± 0.40	4.61±1.23	3.93±1.29	10.04±2.59	8.60±2.82	1.40±0.60	1.17±0.62

PL: palmaris longus

Table 4. Gender differences in morphometric measurements performed on PL tendon by ultrasonography. Values are expressed as Mean ± SD.

Gender	Thickness		Width		Circumference		Distance from Median Nerve	
	Right	Left	Right	Left	Right	Left	Right	Left
M (34)	1.29 ± 0.46	1.34 ± 0.38	4.4 ± 1.28	4.82 ± 1.17	9.74 ± 2.76	10.34 ± 2.42	1.35 ± 0.59	1.45 ± 0.61
F (45)	1.03 ± 0.40	1.09 ± 0.40	3.84 ± 1.36	4.01 ± 1.24	8.4 ± 2.98	8.79 ± 2.68	1.26 ± 0.66	1.09 ± 0.57

the PL and classified them as Type I, II and III. In Type I, the muscle inserted into the palmar aponeurosis (78.8% of the cases), whereas in Type II, a bifurcated muscle tendon was seen getting inserted to the palmar aponeurosis and flexor retinaculum (12.5% of cases), and in Type III, the tendon was seen fusing with the flexor carpi ulnaris and getting inserted into the palmar aponeurosis and pisiform bone (1.2% of the cases). These morphometric patterns suggest that PL is

Table 5. Prevalence of PL tendon absence reported in previous studies with different examination methods.

Study &Year	Country	Examination method	Number of examined upper limbs	% of PLT Absence
Schaeffer (1909)	USA	Schaeffer	800	22.5
Adachi (1909)	Japan	Cadaveric study	540	4.3
Nakano (1923)	China	Cadaveric study	95	2.1
Botar (1931)	Hungary	Cadaveric study	68	4.4
Reimann (1944)	USA	Cadaveric study	1600	12.8
George (1953)	Canada	Cadaveric study	552	15.2
Machado and DiDio (1967)	Brazil	Machado	758	3.7
Dvorakowa and Zvolsky (1975)	Czech Republic	Dvorakowa	816	11.6
Wang et al. (1983)	China	Cadaveric study	120	5.0
Troha et al. (1990)	USA	Thompson	400	4.0
Wehbe (1992)	USA	Cadaveric study	240	14.6
Dowdy et al. (1994)	Canada	Cadaveric study	52	5.8
Ceyhan and Mavt (1997)	Turkish	Schaeffer, Thompson, Reimann	14,000	64.0
Thompson et al. (2001)	Northern Irish	Thompson	600	25.0
Ito et al. (2001)	Japan	Cadaveric study	72	4.2
O' Sullivan and Mitchell (2002)	UK	Cadaveric study	47	53.2
Sebastin and Lim (2006)	Singapore	Schaeffer, Mishra, Pushpakumar, Thompson	658	4.6
Roohi et al. (2007)	Malaysia	Schaeffer	900	9.3
Mobarakeh et al. (2008)	Iran	Cadaveric study	128	29.6
Hassan and Jabeti (2008)	Jordan	Schaeffer	2040	38.6
Kapoor et al. (2008)	India	Schaeffer	1000	17.2
Gangata (2009)	Zimbabwe	Schaeffer, Mishra, Gangata	1780	1.5
Kose et al. (2009)	Turkey	Schaeffer, Mishra	2700	26.6
Mbaka and Ejiwunmi (2009)	Nigeria	Schaeffer, Mishra, Pushpakumar, Thompson	1200	6.7
Agarwal (2010)	India	Schaeffer, Mishra, Pushpakumar	770	11.8
Ertem et al. (2010)	Turkey	Schaeffer, Ultrasound study	124	39.0
Sater et al. (2010)	Bahrain	Schaeffer, Mishra	2086	36.8
Eric et al. (2011)	Serbia	Schaeffer, Mishra, Pushpakumar, Thompson	1084	25.1
Hiz et al. (2011)	Turkey	Schaeffer, Mishra, Hiz	2000	15.0
Kigera and Mukwaya (2011)	Uganda	Schaeffer, Mishra, Pushpakumar, Thompson	1600	4.4
Sankar et al. (2011)	India	Schaeffer, Mishra, Pushpakumar, Thompson	1884	28.0
Kocabiyik et al. (2011)	Turkey	Cadaveric study	48	39.6
Kyung et al. (2012)	South Korea	Schaeffer, Mishra, Gangata	538	4.1
Osonuga et al. (2012)	Ghana	Schaeffer, Mishra, Hiz	452	3.1
Sharma et al. (2012)	India	Schaeffer, Mishra, Pushpakumar, Thompson	800	16.25
Soltani et al. (2012)	USA	Schaeffer	1032	14.9
Hussain (2012)	Saudi Arabia	Schaeffer, Pushpakumar, Thompson	800	16.7
Barkats (2013)	Hungary	Schaeffer, Mishra, Pushpakumar, Thompson	770	32.2
Cetin et al. (2013)	Turkey	Schaeffer	1170	30.4
Morais et al. (2013)	Brazil	Schaeffer, Thompson	198	17.2
Rajani et al. (2013)	India	Schaeffer, Mishra, Pushpakumar, Thompson	400	9.5
Raouf et al. (2013)	Egypt	Schaeffer, Mishra, Pushpakumar, Thompson	772	50.8
Saxena (2013)	India	Schaeffer, Mishra, Pushpakumar, Thompson	852	26.5
Venter et al. (2014)	South Africa	Schaeffer	1412	24.4
Barkats (2015)	Ukraine	Schaeffer, Mishra, Pushpakumar, Thompson	1096	52.9
Mathew et al. (2015)	India	Cadaveric study	48	8.3
Nasiri et al. (2016)	Iran	Schaeffer, Mishra, Pushpakumar, Thompson	1124	13.2
Alzahrani et al. (2017)	Saudi Arabia	Schaeffer	662	15.1
Olewnik et al. (2017)	Poland	Cadaveric study	80	7.5
Karacan et al. (2017)	Turkey	Schaeffer, Mishra, Thompson	2100	37.8
Johnson et al. (2018)	USA	Cadaveric study	17	23.5
Dabrowski et al. (2018)	Poland	Schaeffer, Ultrasound imaging	42	11.9
Caetano et al. (2018)	Brazil	Cadaveric study	30	16.6
Our study, 2020	**Arabian Gulf Region**	**Schaeffer, Ultrasound imaging**	**158**	**12.7 (Schaeffer test) 5.7 (Ultrasound imaging)**

PL: palmaris longus

the most variable muscle in the human forearm. This high variability in its presence/absence and structure may be linked to its development, and it has been postulated that the absence of PL is hereditary and linked to the HOX gene, which is responsible for the regulation of its morphological development (Amthor et al., 1999). From our ultrasonographic examination, we also noticed statistically significant differences in terms of tendon structure among nationalities and gender. These variations could be either developmental or acquired.

A recent meta-analysis of studies suggest that the absence of PL is more common in females, especially on the left sides (Pekala et al., 2017). Our findings also suggest that the absence of PL is more frequent in females, but on the right side (Table 1). It has been argued that the functional tests are likely to overestimate the absence of PL; thus, the usage of ultrasound assessment prior to grafting is preferred (Pekala et al., 2017). This is the reason why we have used Schaeffer's test along with ultrasound imaging. Not surprisingly, the Schaeffer's test gave a false negative result for 11 wrists in our study (Table 1).

Studies report that the absence of PL has no adverse effects or functional disadvantages in daily activities. Due to this reason the PL tendon is often used for grafts. The tendon harvest is crucial in surgical procedures. Due to its proximity with the tendon, the median nerve is also prone for injury during this procedure, if its distance from the tendon is not assessed before the surgical procedure (Lawler and Adams, 2007). In such cases, the ultrasound findings of our study mentioning the distance between tendon and nerve are very useful for the surgeons to be aware of the risks associated during tendon harvest procedures. The distance from mid-portion of the inter-styloid area to the point where the tendon crossed the median nerve was between 2.63 mm (shortest) and 5.62 mm (greatest) (Olewnik et al., 2017). In our study, from the ultrasound images of the transverse sections, we have measured the distance of the tendon from the nerve (2cm proximal to distal wrist crease) and found that the range of distance was 1.30±0.63 mm (right side) and 1.24±0.61 mm (left side). Investigators have used different sites to measure the PL tendon using ultrasonography (Olewnik et al., 2017; Karacan et al., 2017; Johnson et al., 2018). A recent systematic review stated that the mean width (transverse diameter) of the PL tendon is 4.0±1.7 mm, ranging from 2.8 mm to 7.7 mm (Yammine and Eric, 2020). The level of the measurement reported in all those studies is different from point to point, ranging from the proximal end, midpoint and distal end of the tendon, respectively. Whereas in our study the level of measurement was 2 cm proximal to distal wrist crease and the mean width of PL tendon measured by ultrasonography was 4.08±1.34 mm and 4.36±1.26 mm on the right and left sides: 4.61±1.23 mm and 3.93±1.29 mm in male and females, respectively. The limitation of our study is that we did not do the ultrasonography of the whole muscle; we did not measure the whole length of the tendon, bearing in mind the fact that the assessment of the "PL tendon diameter" is less invasive than the "PL tendon length", as surgically and anatomically the diameter can easily be achieved through a transverse incision at the wrist before planning tendon harvest surgery.

CONCLUSION

Our study has documented both the topographic and ultrasonographic features of the PL tendon in a Gulf Arab population, and confirmed that the ultrasonography is more reliable for detecting the PL tendon than the most often used clinical test: i.e., Schaeffer's test. Our study provides the quantitative data on the diameters of the PL tendon at the wrist based on ultrasonographic assessment. These data may be helpful, especially for the surgeons in the region, for their potential application in orthopedic and reconstructive surgeries that use PL grafting.

ACKNOWLEDGEMENTS

Authors would like to thank all the students for their voluntary participation in the study. Our sincere thanks to CMMS, AGU for grant support (Grant number: G-E011-PI-11/18). We thank Dr. Ahmed Jaradat and Dr. Mohammed Ali Yunus Khan for their support in this project.

REFERENCES

ADACHI B (1909) Beiträge zur Anatomie der Japaner. XII. Die Statistik der Muskelvarietaten. *Z Morph Anthropol*, 12: 261-312.

AGARWAL P (2010) Absence of the palmaris longus tendon in Indian population. *Indian J Orthop*, 44(2): 212-215.

ALKHAMIS AA, ALSULTAN MH, ALAHMAD MS, SARAH A (2017) The frequency of palmaris longus absence among female students in King Faisal University in Al-Ahsa, Saudi Arabia. *Egyptian J Hospital Med*, 70 (11): 1959-1962.

ALZAHRANI MT, ALMALKI MA, ALTHUNAYAN TA, ALMOHAWIS AH, ALTURKI AT, UMEDANI L (2017) Clinical assessment of the congenital absence of palmaris longus and flexor digitorum superficialis muscles in young Saudi population. *Anat Res Int*, 2017: 5342497.

AMTHOR H, CHRIST B, PATEL K (1999) A molecular mechanism enabling continuous embryonic muscle growth - a balance between proliferation and differentiation. *Development*, 126(5): 1041-1053.

BARKATS N (2013) The prevalence of the palmaris longus muscle's agenesis in Hungarian students. *PoA*, 22: 28-33.

BARKATS N (2015) Change of the agenesis rate of palmaris longus muscle in an isolated village in Ukraine. *Folia Morphol*, 74(4): 470-474.

BOTAR J (1931) Sur quelques variations des muscles de l'avant-bras. *Bull Mem Soc Anthropol Paris*, 2: 25-33.

CAETANO EB, VIEIRA LA, FERREIRA CMB, CAVALHEIRO CS, ARCURI MH, SILVA JR LCNN (2019) Anatomical study of the branch of the palmaris longus muscle for its transfer to the posterior interosseous nerve. *Int J Morphol*, 37(2): 626-631.

CETIN A, GENC M, SEVIL S, COBAN YK (2013) Prevalence of the palmaris longus muscle and its relationship with grip and pinch strength: a study in a Turkish pediatric population. *Hand (NY)*, 8(2): 215-220.

CEYHAN O, MAVT A (1997) Distribution of agenesis of palmaris longus muscle in 12-18 years old age groups. *Indian J Med Sci*, 51(5): 156-160.

CHOO J, WILHELMI BJ, KASDAN ML (2017) Iatrogenic injury to the median nerve during palmaris longus harvest: An overview of safe harvesting techniques. *Hand*, 12(1): NP6-NP9.

CLEMENTE CD (1985) Anatomy of the Human Body. Lea and Febiger, Philadelphia.

DABROWSKI K, STANKIEWICZ-JOZWICKA H, KOWALCZYK A, MARKUSZEWSKI M, CISZEK B (2018) The sonographic morphology of musculus palmaris longus in humans. *Folia Morphol*, 77(3): 509-513.

DOWDY PA, RICHARDS RS, MCFARLANE RM (1994) The palmar cutaneous branch of the median nerve and the palmaris longus tendon: A cadaveric study. *J Hand Surg Am*, 19(2): 199-202.

DVORAKOWA M, ZVOLSKY P (1975) Absence of musculus palmaris longus in the Prague population. *Cas Lek Cesk*, 114(44): 1365-1368.

ERIC M, KOPRIVCIC I, VUCINIC N, RADIC R, KRIVOKUCA D, LEKSAN I, SELTHOFER R (2011) Prevalence of the palmaris longus in relation to the hand dominance. *Surg Radiol Anat*, 33(6): 481-484.

ERTEM K, SIGIRCI A, KARACA S, SIGIRCI A, KARAKOC Y, YOLOGLUS (2010) Ultrasonographic assessment of relationship between the palmaris longus tendon and the flexor retinacular ligament and the palmar aponeurosis of the hand. *Eur J Gen Med*, 7(2): 161-166.

GANGATA H (2009) The clinical surface anatomy anomalies of the palmaris longus muscle in the Black African population of Zimbabwe and a proposed new testing technique. *Clin Anat*, 22(2): 230-235.

GARAFFA G, SANSALONE S, RALPH DJ (2013) Penile reconstruction. *Asian J Androl*, 15(1): 16-19.

GEORGE R (1953) Co-incidence of palmaris longus and plantaris muscles. *Anat Rec*, 116(4): 521-523.

HASSAN AF, JABETI S (2008) Absence of the palmaris longus tendon in mid- eastern population. *J Bahrain Med Soc*, 20(2): 70-73.

HIZ O, EDIZ L, CEYLAN MF, GEZICI E, GULCU E, ERDEN M (2011) Prevalence of the absence of palmaris longus muscle assessed by a new examination test (Hiz-Ediz Test) in the population residing in the area of Van, Turkey. *J Clin Exp Investig*, 2(3): 254-259.

HOLZGREFE RE, ANASTASIO AT, FARLEY KX, DALY CA, MASON AR, GOTTSCHALK MB (2019) Detection of the palmaris longus tendon: physical examination versus sonography. *J Hand Surg Eur Vol*, 44(8): 800-804.

HUSSAIN FN (2012) Prevalence of congenital absence of palmaris longus tendon in young Jizani population of Saudi Arabia: A cross sectional study. *Pak J Med Sci*, 28(5): 865-869.

ITO MM, AOKI M, KIDA MY, ISHII S, KUMAKI K, TANAKA S (2001) Length and width of the tendinous portion of the palmaris longus: A cadaver study of adult Japanese. *J Hand Surg Am*, 26(4): 706-710.

JOHNSON CC, VUTESCU ES, MILLER TT, NWAWKA OK, LEE SK, WOLFE SW (2018) Ultrasound determination of presence, length and diameter of the palmaris longus tendon. *J Hand Surg Eur Vol*, 43(9): 948-953.

JOHNSON CC, ZUSSTONE E, MILLER TT, NWAWKA OK, LEE SK, WOLFE SW (2020) Clinical tests for assessing the presence and quality of the palmaris longus tendon: diagnostic accuracy of examination compared with ultrasound. *J Hand Surg Eur Vol*, 45(3): 292-298.

KAPOOR SK, TIWARI A, KUMAR A, BHATIA R, TANTUWAY V, KAPOOR S (2008) Clinical relevance of palmaris longus agenesis: Common anatomical aberration. *Anat Sci Int*, 83(1): 45-48.

KARACAN K, AKCAALAN M, BAYLAN H (2017) Evaluation of relationship between prevalence of palmaris longus muscle and handedness in Turkish population. *Int J Morphol*, 35(3): 1026-1030.

KIGERA JWM, MUKWAYA S (2011) Frequency of agenesis palmaris longus through clinical examination: An East African study. *PLoS One*, 6(12): e28997.

KOCABIYIK N, YILDIZ S, DEVELI S, OZAN H, YAZAR F (2012) Morphometric analysis of the palmaris longus muscle: A fetal study. *Anatomy*, 6-7: 42-47.

KOSE O, ADANIR O, CIRPAR M, KURKLU M, KOMURCU M (2009) The prevalence of absence of the palmaris longus: A study in Turkish population. *Arch Orthop Trauma Surg*, 129(5): 631-639.

KYUNG DS, LEE JH, CHOI IJ, KIM DK (2012) Different frequency of the absence of the palmaris longus according to assessment methods in a Korean population. *Anat Cell Biol*, 45(1): 53-56.

LALIT M, SINGLA RK, PIPLANI S (2014) Bifid inverted palmaris longus muscle – a case report. *Eur J Anat*, 18(3): 341-343.

LAWLER E, ADAMS BD (2007) Reconstruction for DRUJ instability. *Hand*, 2(3): 123-126.

LESLIE BM, OSTERMAN AL, WOLFE SW (2017) Inadvertent harvest of the median nerve instead of the palmaris longus tendon. *J Bone Joint Surg Am*, 99(14): 1173-1182.

MACHADO AB, DIDIO LJ (1967) Frequency of the musculus palmaris longus studied in vivo in some Amazon Indians. *Am J Phys Anthropol*, 27(1): 11-20.

MATHEW AJ, SUKUMARAN TT, JOSEPH S (2015) Versatile but temperamental: A morphological study of palmaris longus in the cadaver. *J Clin Diagn Res*, 9(2): AC01-AC03.

MBAKA GO, EJIWUNMI AB (2009) Prevalence of palmaris longus absence: A study in the Yoruba population. *Ulster Med J*, 78(2): 90-93.

MISHRA S (2001) Alternative tests in demonstrating the presence of palmaris longus. *Indian J Plast Surg*, 34: 12-14.

MOBARAKEH MK, PASHA MG, POOR MM (2008) Variation, length and width of tendinous portion of palmaris longus and forearm length and height: Is there a link? A cadaver study of adult Iranians. *Iran J Med Sci*, 33(3): 164-168.

MORAIS M, SANTOS W, MALYSZ T (2013) Agenesis of palmaris longus muscle: Is this a phenotype of variable expressivity? *J Morphol Sci*, 30(4): 249-253.

NAKANO T (1923) Beiträge zur Anatomie der Chinesen. Die Statistik der Muskelvarietaten. *Folia Anat Jpn*, 1: 273-282.

NASIRI E, POURGHASEM M, MOLADOUST H (2016) The prevalence of absence of the palmaris longus muscle tendon in the North of Iran: A comparative study. *Iran Red Crescent Med J*, 18(3): e22465.

O'SULLIVAN E, MITCHELL BS (2002) Association of the absence of palmaris longus tendon with an anomalous superficial palmar arch in the human hand. *J Anat*, 201(5): 405-408.

OLEWNIK L, WYSIADECKI G, POLGUJ M, TOPOL M (2017) Anatomic study suggests that the morphology of the plantaris tendon may be related to Achilles tendonitis. *Surg Radiol Anat*, 39(1): 69-75.

OSONUGA A, MAHAMA HM, BROWN AA, OSONUGA OA, SERBEH G, HARDING AN, HORMEKU AK (2012) The prevalence of palmaris longus agenesis among the Ghanaian population. *Asian Pac J Trop Dis*, 2: 887-889.

OZASA Y, WADA T, IBA K, YAMASHITA T (2018) Surgical treatment for partial rupture of the distal biceps tendon using palmaris longus tendon graft: A case report. *Acta Orthop Traumatol*, 52(4): 323-325.

PEKALA PA, HENRY BM, PEKALA JR, SKINNINGSRUD B, WALOCHA JA, BONCZAR M, TOMASZEWSKI KA (2017) Congenital absence of the palmaris longus muscle: A meta-analysis comparing cadaveric and functional studies. *J Plast Reconstr Aesthet Surg: JPRAS*, 70(12): 1715-1724.

PUSHPAKUMAR SB, HANSON RP, CARROLL S (2004) The 'two finger' sign. Clinical examination of palmaris longus (PL) tendon. *Br J Plast Surg*, 57(2): 184-185.

RAJANI S, PATEL S, RAJANI J, GANASVA A, DAMOR J (2013) Study of palmaris longus tendon agenesis through clinical examination in Gujarat region of India. *Int J Res Med*, 2(1): 83-87.

RAOUF HA, KADER GA, JARADAT A, DHARAP A, FADEL R, SALEM AH (2013) Frequency of palmaris longus absence and its association with other anatomical variations in the Egyptian population. *Clin Anat*, 26(5): 572-577.

REIMANN AF, DASELER EH, ANSON BJ, BEATON LE (1994) The palmaris longus muscle and tendon. A study of 1600 extremities. *Anat Rec*, 89(4): 495-505.

ROOHI AS, CHOON-SIAN L, SHALIMAR A, TAN GH, NAICKER AS, REHAB M (2007) A study on the absence of palmaris longus in a multiracial population. *Malays Orthop J*, 1(1): 26-28.

SANKAR KD, BHANU PS, JOHN SP (2011) Incidence of agenesis of palmaris longus in the Andhra population of India. *Indian J Plast Surg*, 44: 134-138.

SATER MS, DHARAP AS, ABU-HIJLEH MF (2010) The prevalence of absence of the palmaris longus muscle in the Bahraini population. *Clin Anat*, 23(8): 956-961.

SAXENA S (2013) A study on the absence/presence of the muscle Palmaris Longus in an Indian population. *Int J Biomed Res*, 2(1): 48-53.

SCHAEFFER JP (1909) On the variations of the palmaris longus muscle. *Anat Rec*, 3: 275-278.

SEBASTIN SJ, LIM AYT (2006) Clinical assessment of absence of the palmaris longus and its association with other anatomical anomalies: A Chinese population study. *Ann Acad Med Singap*, 35: 249-253.

SHARMA DK, SHUKLA CK, SHARMA V (2012) Clinical assessment of absence of palmaris longus muscle and its association with gender, body sides, handedness and other neighboring anomalies in a population of central India. *J Anat Soc India*, 61(1): 13-20.

SOLTANI AM, PERIC M, FRANCIS CS, NGUYEN TT, CHAN LS, GHIASSI A, STEVANOVIC MV, WONG AK (2012) The variation in the absence of the palmaris longus in a multiethnic population of the United States: an epidemiological study. *Plast Surg Int*, 2012: 282959.

THEJODHAR P, POTU BK, VASAVI RG (2008) Unusual palmaris longus muscle. *Indian J Plast Surg*, 41(1): 95-96.

THOMPSON JW, MCBATTS J, DANFORTH CH (1921) Hereditary and racial variations in the musculus palmaris longus. *Am J Phys Anthrop*, 4: 205-220.

THOMPSON NW, MOCKFORD BJ, CRAN GW (2001) Absence of the palmaris longus muscle: A population study. *Ulster Med J*, 70(1): 22-24.

TROHA F, BAIBAK GJ, KELLEHER JC (1990) Frequency of the palmaris longus tendon in North American Caucasians. *Ann Plast Surg*, 25(6): 477-478.

TRUSSLER AP, KAWAMOTO HK, WASSON KL, DICKINSON BP, JACKSON E, KEAGLE JN, JARRAHY R, BRADLEY JP (2008) Upper lip augmentation: palmaris longus tendon as an autologous filler. *Plast Reconstr Surg*, 121 (3): 1024-1032.

VASTAMAKI M (1987) Median nerve as free tendon graft. *J Hand Surg*, 12(2): 187-188.

VENTER G, VAN SCHOOR AN, BOSMAN MC (2014) Degenerative trends of the palmaris longus muscle in a South African population. *Clin Anat*, 27(2): 222-226.

WANG X, WEI B, LING T, HOU K (1983) Anatomy of palmaris longus and its clinical application. *Hebei Med*, 6: 53-55.

WEBER RV, MACKINNON SE (2007) Median nerve mistaken for palmaris longus tendon: restoration of function with sensory nerve transfers. *Hand*, 2(1): 1-4.

WEHBE MA (1992) Tendon graft donor sites. *J Hand Surg Am*, 17(6): 1130-1132.

YAMMINE K, ERIC M (2020) Morphometric analysis and surgical adequacy of palmaris longus as a tendon graft. A systematic review of cadaveric studies. *Surg Radiol Anat*, 42: 259-267.

Young coconut juice prevents neuronal cell death via ChAT, NMDAR1, and estrogen receptors in the hippocampus and prefrontal cortex of ovariectomized rats

Kolip Payanglee[1], Albert M. Hutapea[2], Nisaudah Radenahmad[1]

[1] Division of Health and Applied Sciences, Faculty of Science, Prince of Songkla University, Hat Yai, Songkhla, Thailand
[2] Department of Pharmacy, Faculty of Science, Universitas Advent Indonesia, Bandung, Indonesia

SUMMARY

Decreasing estrogen levels are associated with an increased risk of dementia and Alzheimer's disease (AD) in postmenopausal women. We used ovariectomized (OVX) rats as a model for postmenopausal women. Our studies showed that a high daily dose of 100 mL/kg body weight of young coconut juice (YCJ) helped prevent AD pathologies. We investigated the optimal dose for the neuroprotective effects of YCJ that would have least side effects following prolonged consumption and the neuroprotective effects of the YCJ acted via choline acetyltransferase (ChAT) and N-methyl-D-aspartate receptors (NMDAR1). Our results showed that rats receiving YCJ at a dose of 10 mL/kg BW/d had the least side effects in their liver and kidney. The ovariectomized rats that were given 10 mL/kg BW/d (OY10) and 20 mL/kg BW/d (OY20) of YCJ demonstrated significantly ($p<0.05$) higher vaginal scores, as compared to the control ovariectomized (OW) group, showed proestrus and estrus stages continuously throughout the ten weeks. A significant ($p<0.05$) increase was observed in the number of ChAT-ir, NMDAR1-ir, ERα-ir, and ERβ-ir pyramidal neurons in CA1, CA2 and CA3 hippocampal areas (HP) and prefrontal cortex (PF) brain regions following administration of YCJ. Moreover, there was a significant positive correlation among those number of ChAT-ir, NMDAR1-ir, ERα-ir, and ERβ-ir neurons. Our study indicated that YCJ at the lowest dose of 10 mL/kg BW/day has estrogenic effects using primarily screening vaginal smear, a test of epithelial cell changes in response to alterations in the concentration of the ovarian hormone. The mechanism of YCJ on preserving neuronal cells and prevent Alzheimer's pathologies, ChAT, and NMDAR1 antibodies were also investigated. Estrogenic effects of YCJ were also confirmed using estrogen receptor (ERα and ERβ) antibodies. In brief, YCJ has neuroprotective effects by preserving ChAT-ir and NMDAR1-ir neurons via ERα and ERβ.

Key words: Estrogen – Menopause – Young coconut juice – ChAT – NMDAR1 – Estrogen receptors

Corresponding author:
Dr. Nisaudah Radenahmad. Division of Health and Applied Sciences, Faculty of Science, Prince of Songkla University, Hat Yai, Songkhla, Thailand. E-mail: nisaudah.r@psu.ac.th

Submitted: November 13, 2020. **Accepted:** January 30, 2021

INTRODUCTION

Dementia is a significant cognitive impairment, and Alzheimer's disease (AD) is one of the leading causes of disability in postmenopausal women, a period when circulating estrogen is reduced (van Dijk et al., 2015). AD is a neurodegenerative disorder of the brain that progresses slowly characterized by the formation of amyloid beta (Aβ) and neurofibrillary tangles (Sezgin and Dincer, 2014).

Acetylcholine modulates cognitive performances, learning, and memory processes. Impaired cortical cholinergic neurotransmission may also contribute to Aβ plaque and neurofibrillary tangles in AD (Ferreira-Vieira et al., 2016). Several studies reveal that ovariectomy induces pathology of AD and causes changes in cholinergic systems. Schliebs and Arendt (2006) found a correlation between clinical dementia ratings and reductions in the numbers of cortical cholinergic markers such as choline acetyltransferase (ChAT), muscarinic and nicotinic acetylcholine receptor binding sites, as well as in the levels of acetylcholine. Carroll et al. (2007) found that ovariectomy-induced depletion of sex steroid hormones in adult female 3xTg-AD mice significantly increased amyloid-beta accumulation and worsened memory performance. However, treatment of these ovariectomized mice with estrogen, but not progesterone, prevented these effects. According to Szego et al. (2011), estrogen-pretreatment on Aβ-induced cholinergic neurodegeneration in the nucleus basalis magnocellularis (NBM) decreased cholinergic neuron loss and partly prevented fiber degeneration. Another group of researchers found that hormone replacement therapy (HRT) in OVX rats increased ChAT protein levels in the hippocampus (HP) and prefrontal cortex (PF) (Bohacek et al., 2008).

The short-term release of glutamate is involved in learning and memory (Collingridge and Singer, 1990). Glutamatergic neurotransmission in the neocortical regions and the hippocampus is severely disrupted in AD (Greenamyre, 1986; Maragos et al., 1987; Palmer and Gershon, 1990). It has been reported that an Aβ peptide blocks glutamate uptake, thus induces an increase of extracellular glutamate (Fernandez-Tome et al., 2004). Consequently, the extracellular glutamate level elevation induces excessive over stimulation of the N-methyl-D-aspartate receptors (NMDAR), which can trigger an intracellular Ca^{2+} influx leading to neuronal cell death (Lauderback et al., 2001).

The use of estrogen-based HRT in postmenopausal women can reduce the risk of AD but can also increase the risk of certain diseases like breast cancer (Bitzer et al., 2008), ovarian cancer (Zhou et al., 2008), and endometrial cancer (McCullough, 2008). Therefore, phytoestrogen could be a candidate for a safer alternative for exogenous estrogen in replacing HRT. Our previous studies have shown that young coconut juice (YCJ) (*Cocos nucifera* L., Arecaceae), known to contain β-sitosterol (Rattanaburee et al., 2014) delayed AD pathologies (Radenahmad et al., 2011) and prevented neuronal cell death (Radenahmad et al., 2009; Payanglee et al., 2017). In the present study, we further investigated the neuroprotective effects of YCJ in preserving neuronal cells via ChAT and NMDAR1 that represent the cholinergic and glutamatergic systems in the HP and PF. These areas are involved in cognitive function and spatial memory. Besides, we also investigated the optimal neuroprotective dose of YCJ that would cause the least side effects following its prolonged consumption by lowering the concentration of YCJ from 100 mL/kg BW to 10 mL/kg BW, 20 mL/kg BW, and 40 mL/kg BW.

MATERIALS AND METHODS

YCJ preparation

A large volume of YCJ was collected from Khlong Hoi Khong district, Hat Yai, Songkhla, Thailand. It was then dried, and the powder formed was kept at -30°C until used. The powder was freshly reconstituted and prepared daily for the oral intake. A complete description of YCJ, including its preparation and administration, is provided in our previous publication (Radenahmad et al., 2006).

Animals

Adult female Wistar rats (8-month-old and 250-300 g bw) were purchased from Mahidol University, Salaya campus. The animals were maintained on standard food pellet housed

in a room free from any source of chemical contamination, artificially illuminated (12h dark/light cycle) and thermally controlled (25 ± 1°C) and humidity (50 ± 5%) at the Animal House Laboratory, Faculty of Science, Prince of Songkla University, Hat Yai, Songkhla, Thailand. All animals were received humane care in compliance with the guidelines of the Animal Care and Use Committee of Prince of Songkla University and the National Institutes of Health (NIH publication 86-23 revised 1985. The protocol was approved under the license number 04/57).

Experimental design

A total of seventy rats were randomly divided into seven groups (Table 1a), with ten rats per group such as the first group, the baseline (BL); second, the sham-operated (SW); third, the OVX rats (OW); and the fourth, the OVX rats injected with exogenous estrogen (2.5 µg/kg BW), a dose of estradiol benzoate for three days a week (OB) given was the same as in the previous studies (Radenahmad et al., 2009; 2011). The fifth, sixth, and seventh groups consisted of OVX rats daily received 10 (OY10), 20 (OY20), and 40 (OY40) mL/kg BW/day of YCJ, respectively. The administration of EB and YCJ started one week after the ovariectomy was performed. SW and OW rats were forced-fed with injection vehicle (reverse osmosis water) instead. YCJ were treated once a day every day, began one week following ovariectomy. After ten weeks of feeding and injection treatment, the rats were sacrificed; the brains were fixed with 10% neutral formalin, processed through paraffin sectioning and immunohistochemical staining. Serum was collected for estradiol measurements using the chemiluminescent immunoassay (CIA) technique (ECLIA, Modular E 170C, Estradiol II 03000079 122, Roche, Germany).

Evaluation of the estrous cycle

Examining the effect of the estrogen-like-compound inYCJ on the vagina was performed using vaginal smears (Marcondes, 2002). Vaginal secretions were collected with a plastic pipette filled with 10 µL of normal saline. The samples containing cells were placed on microscopic glass slides and air-dried prior to staining and then stained with the Papanicolaou (Pap) stain before being examined with a light microscope. Scoring of vaginal smears was performed as follows:

Estrous cycle	Scores
Proestrus	3
Estrus	2
Metestrus	1
Diestrus	1

Immunohistochemistry

Fourteen 5-µm-thick sections collected from each block were prepared for cresyl violet stain and immunostaining (Table 1b). For immunostaining, the glass slides were coated by poly-L-lysine solution. Sections of uterus and ovary from normal female rats were used as positive controls for ERα, and ERβ immunostaining, respectively, and the staining process was performed according to the method previously described (Radenahmad et al., 2009; 2011; 2012). Please see the details of all antibodies, concentration, and manufacturer used for brain sections of each rat in Table 1b.

Quantitative analysis of immunoreactive cells

The total number of immunoreactive cells from the prefrontal cortex (PF) and the hippocampus (CA1, CA2, and CA3) were counted under light microscopy (LM) with 40x magnification power. The counting was performed by two blinded observers on each slide's ten random fields using an image analysis system (Samba microscopic image processor; Samba Technologies, Meylan, France). Readings from three sections pertaining to each antibody were averaged and expressed as the mean number of immunoreactive cells/mm^2.

Statistical analysis

Shapiro-Wilk test was applied to test the normal distribution. Statistical analysis was performed using the One-way ANOVA followed by LSD test available in the statistical program SPSS version 16.0 (SPSS, Inc., Chicago, IL, USA). Altman's nomogram was used for calculations of sample size. Random selection of the microscopic fields was achieved using a computer-generated list

of random numbers (Excel version 5.0). Results were expressed as mean ± SEM, and $p<0.05$ was considered significant.

RESULTS

Vaginal smear

The proestrus smear had a predominance of nucleated epithelial cells with a blue-purple stained nucleus and light pink stained cytoplasm (Fig. 1A, proestrus). A predominance of cornified cells was found in estrous smear (Fig. 1A, estrus). The metestrus smear showed densely packed leukocytes with blue-purple stained nucleus and a small cytoplasm and a few cornified cells (Fig. 1A, metestrus). The diestrus smear had only scattered nucleated epithelial cells consisting almost entirely of leukocytes (Fig. 1A, Diestrus).

As determined by vaginal smear cytology, all rats of the sham group (SW) exhibited four stages of the estrous cycle with an average score of 2.00±0.05, which was significantly higher than that of OW (1.17±0.02), OB (1.58±0.06), OY10 (1.24±0.03), OY20 (1.33±0.04) and OY40 (1.17±0.04) at $p<0.05$.

As determined by vaginal smear cytology, all rats exhibited four stages of the estrous cycle except the ovx rats (OW group), which was persistently in metestrus/diestrus. The average score of the SW group = 2.00±0.05, which was significantly higher than that of OW (1.17±0.02), OB (1.58±0.06), OY10 (1.24±0.03), OY20 (1.33±0.04), and OY40 (1.17±0.04) at $p<0.05$.

In summary, the average for the vaginal smear scoring of the estrus cycle for 70 days of the SW group was significantly ($p<0.05$) the highest, as compared to other groups (Figs. 1A, 1B). The OW group scores were significantly ($p<0.05$) lower compared to the OB, OY10, and OY20 groups. Vaginal smear scoring of the OB group was significantly ($p<0.05$) higher compared to the OY10 and OY40 groups. Surprisingly, the OY40 group scores were significantly ($p<0.05$) lower than those of the OY10 and OY20 groups.

Serum E2 level

The serum E2 level of the BL group was significantly ($p<0.05$) higher when compared to all the other groups, except for the SW group (Fig.

Table 1. Animal grouping (**a**); and antibodies, concentration, and manufacturer used for brain sections of each rat (**b**).

a. Animal grouping (10 rats per group)

Groups	Treatments
BL	Normal (normal control)
SW	Sham-operated, received reverse-osmosis water (sham control)
OW	Ovariectomized, received reverse-osmosis water (ovariectomized control)
OB	Ovariectomized, and injected with estradiol benzoate (EB, 2.5 μg/kg BW) 3 days a week, for 10 wks
OY10	Ovariectomized, received YCJ at 10 mL/kg BW/d for 10 wks
OY20	Ovariectomized, received YCJ at 20mL/kg BW/d for 10 wks
OY40	Ovariectomized, received YCJ at 40mL/kg BW/d for 10 wks

b. Immunostaining for each rat brain

Section No.	Staining
1	Cresyl violet, for histological orientation
2-4	Anti-ChAT antibody, 1:1,000 diluted (MAB5270-50UG[formerly Roche 1464272], EMD Millipore Corporation, Temecula, CA, USA)
5-7	Anti-NMDAR1 antibody, 1:2,000 diluted (MAB363, EMD Millipore Corporation, Temecula, CA, USA)
8-10	Anti-estrogen receptor α (aa-120-170) antibody, 1:500 diluted (MAB447, EMD Millipore Corporation, Temecula, CA, USA)
11-13	Anti-estrogen receptor β antibody, 1:2,000 diluted (PA1-310B, Thermo Fisher Scientific, Rockford, IL, USA)
14	Immunostaining, omitting primary antibodies (negative control)

2). Surprisingly, serum E2 levels of the OW, OB, and OY10 were not significantly different from those of the SW group because of the SW group's high SEM bar. Furthermore, E2 levels of the OY20 and OY40 groups were significantly lower than that of the SW group.

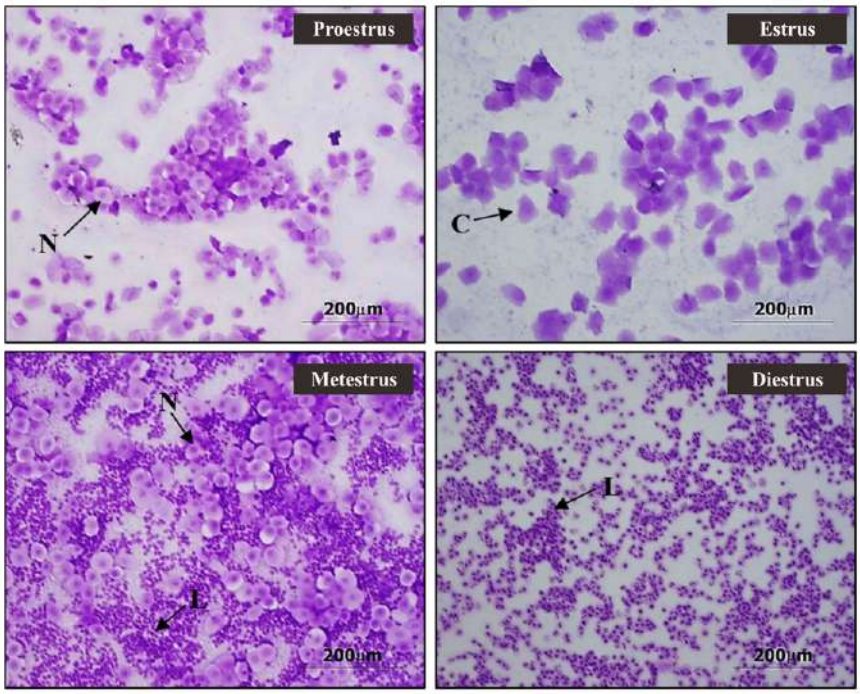

Fig. 1A.- Micrographs of vaginal smears using the Marcondes's method in all four stages. Proestrus = vaginal smear dominated by nucleated epithelial cells, that occur singly or in sheets; Estrus = period primarily consisting of cornified cells; Metestrus = many leukocytes appearing in this period along with a few cornified cells; Diestrus = smear consisting almost entirely of leukocytes; N = nucleated epithelial cells; L = leukocytes; C = cornified cells. Scale bars = 200 µm.

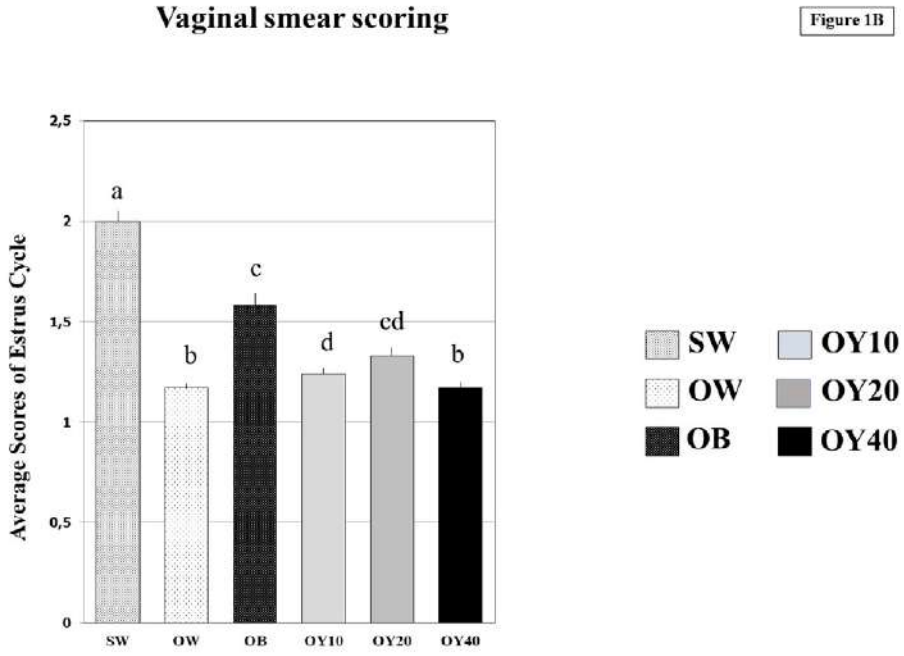

Fig. 1B.- Means of vaginal smear scoring of the estrus cycle for a period of 70 days in the six groups examined. Definition of each group was described in Table 1a. All different superscripts indicate statistical significance at $p<0.05$ level. SW = sham-operated group; OW = ovariectomized group; OB = ovariectomized rat receiving estradiol benzoate (EB) 2.5 µg/kgBW/day; OY10 = ovariectomized rat receiving YCJ 10 mL/kgBW/day; OY20 = ovariectomized rat receiving YCJ 20 mL/kgBW/day; OY40 = ovariectomized rat receiving YCJ 40 mL/kgBW/day.

Histomorphometry of immunoreactive (-ir) cells

Immunoreactivity of the anti-ChAT, anti-NMDAR1, anti-ERα, and anti-ERβ antibodies was detected in the cell bodies' cytoplasm, dendrites, and axons of the pyramidal neurons in all the seven groups examined for CA1, CA2, CA3, and PF (Figs. 3, 5, 6). The restoration of the serum E2 level following the oral intake of YCJ at 10 mL/kg BW (OY10), as demonstrated in Fig. 2, was associated with significant preservation in the neuronal cells compared to the OVX group, which did not receive any treatment. This condition was indicated by the significantly ($p<0.05$) higher number of neurons that were positive for ChAT, NMDAR1, ERα, and ERβ (Figs. 3 and 6). Interestingly, for some brain regions like CA1 in Fig. 3A, and PF in Fig. 3C, the number of these neurons of at least one group of YCJ treatment was also significantly ($p<0.05$) higher compared to the OB group.

After 70 days of treatment, when the numbers of ERα-ir and ERβ-ir cells were statistically correlated with that of ChAT with regression, an equation for ERα: y=0.522x+6.044 (p = .000) and for ERβ: y=0.411x+5.569 (p = .000), respectively, leading to the conclusion that the numbers of ChAT-ir neurons increased by way of ERα and ERβ activation (Fig. 4A).

Like ChAT, the regression equation for ERα: y =0.445x+8.109 (p = .000) and for ERβ: y=0.414x+6.269 (p = .000) leading to the conclusion that the numbers of NMDAR1-ir neurons increased by way of ERα and ERβ activation (Fig. 4B).

Furthermore, when the number of ChAT-ir neurons was correlated with that of NMDAR1-ir neurons, the p-value of the testing regression equation indicates p = .000, leading to the conclusion that these two types of neurons somehow have colocalized activity (Fig. 4C).

DISCUSSION

Alzheimer's disease (AD) is the most common neurodegenerative disease, accounting for more than 50% of all dementia types (Plassman et al., 2007). Currently, no treatments are available to stop, slow, or reverse the progression of the disease process (Master et al., 2015). The neuroprotective role of estrogen-containing hormone therapy is useful but controversial. The primary concern with estrogen therapy as hormone replacement therapy (HRT) is increased risk of venous thrombosis, coronary artery disease, breast and endometrial carcinoma, dysmenorrhea,

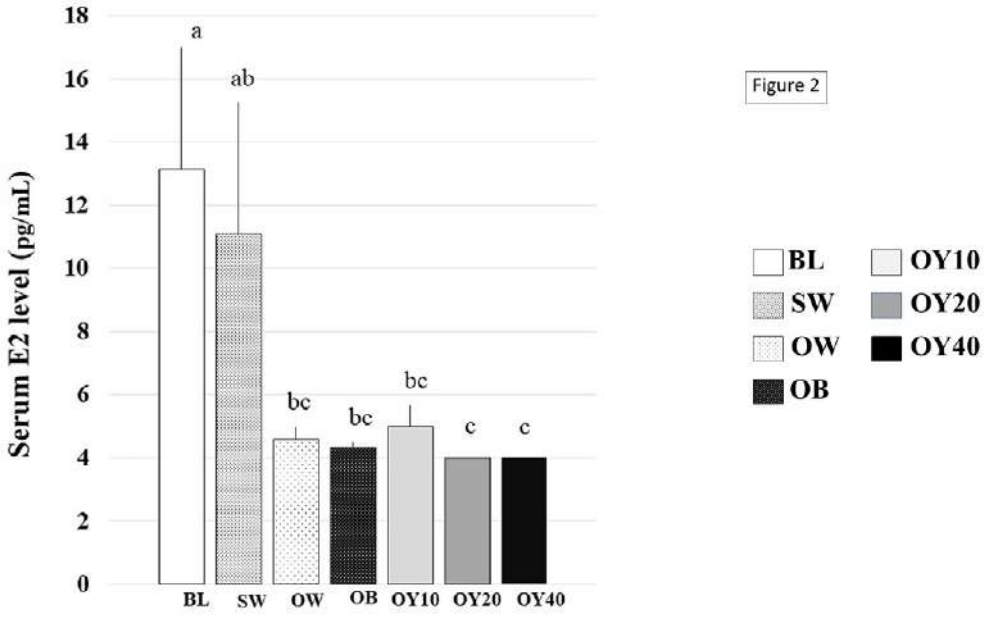

Fig. 2.- Serum estradiol (E2) levels (pg/mL) of the 7 groups examined. All different superscripts indicate statistical significance at $p<0.05$ level. BL = baseline control group; SW = sham-operated group; OW = ovariectomized group; OB = ovariectomized rat receiving estradiol benzoate (EB) 2.5 µg/kgBW/day; OY10 = ovariectomized rat receiving YCJ 10 mL/kgBW/day; OY20 = ovariectomized rat receiving YCJ 20 mL/kgBW/day; OY40 = ovariectomized rat receiving YCJ 40 mL/kgBW/day.

abnormal vaginal bleeding and hypersensitivity (Jamshed et al., 2014). Nowadays, plant-derived estrogen researches were explored to replace HRT. In previous work, we reported that YCJ at 100 mL/kg BW help halting AD pathologies (Radenahmad et al., 2009; 2011), but undesirable effects such as glycogen deposition in the liver occurred. Therefore, the lower doses of YCJ were investigated in this study to minimize the unfavorable side effects. A vaginal smear was applied to preliminary screening in living rats to ensure that such a lower dose of YCJ still had estrogenic activity,

The rat vaginal wall provides an excellent model to determine the estrogenic activity of estrogenic substances and is recognized as a simple, sensitive,

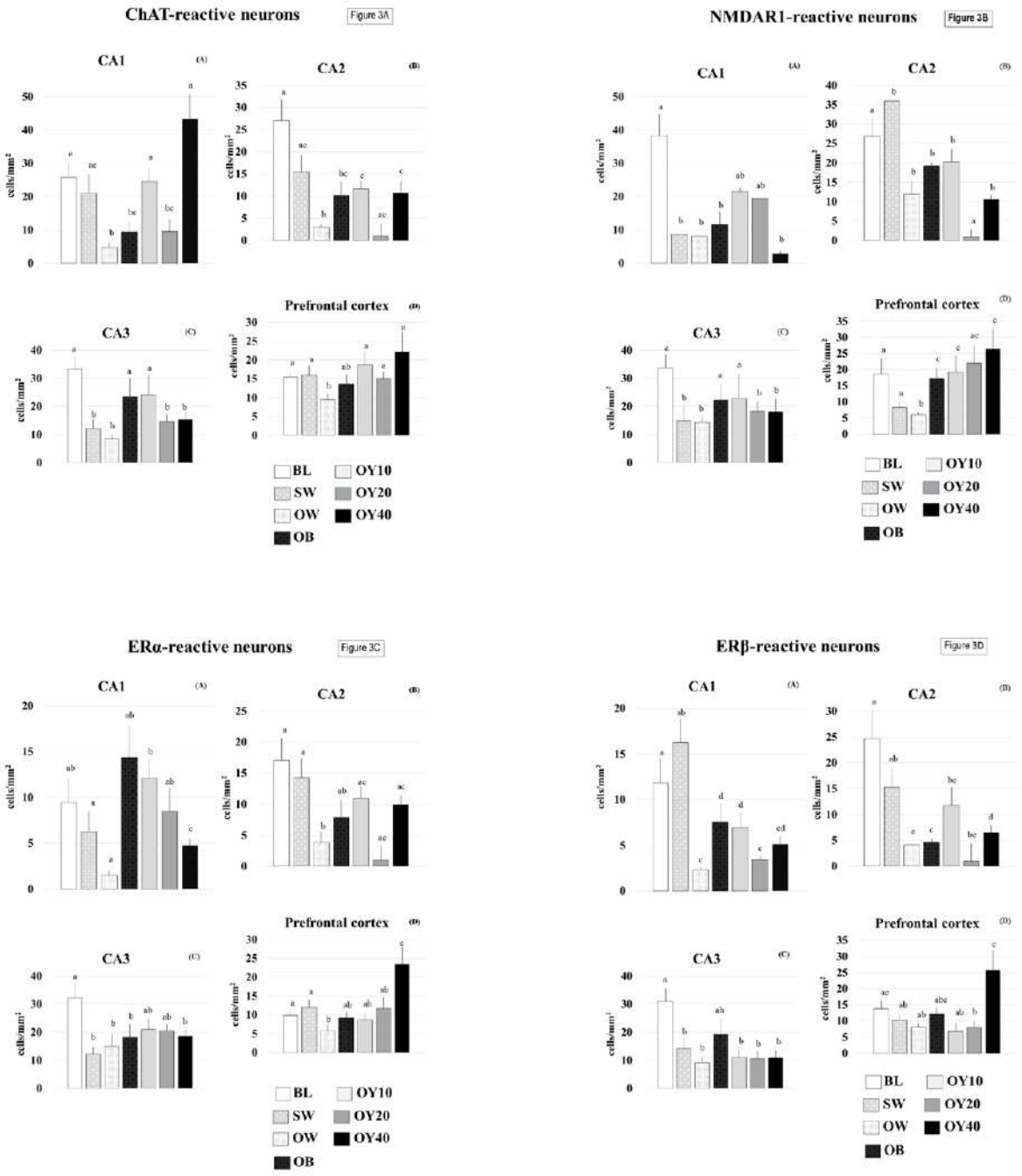

Fig. 3.- Number of ChAT-reactive neurons (**3A**), NMDAR1 (**3B**), ERα (**3C**), ERβ (**3D**) of the cornu ammonis (CA) of the hippocampus and areas of cerebral cortices in all groups of the rats tested. All different superscripts indicate statistical significance at $p<0.05$ level. BL = baseline control group; SW = sham-operated group; OW = ovariectomized group; OB = ovariectomized rat receiving estradiol benzoate (EB) 2.5 µg/kgBW/day; OY10 = ovariectomized rat receiving YCJ 10 mL/kgBW/day; OY20 = ovariectomized rat receiving YCJ 20 mL/kgBW/day; OY40 = ovariectomized rat receiving YCJ 40 mL/kgBW/day.

and inexpensive method (Parhizkar et al., 2011). The estrogenic-like compounds have been shown to affect the differentiation of the vaginal epithelium and enhance vaginal cornification (Laws et al., 2000; Burton and Wells, 2002). The present experiment confirmed the presence of a menopausal stage in OVX rats by monitoring the cellular differentiation of the vaginal epithelium for ten consecutive weeks. In the OVX group, the vaginal smear scores were low compared to the sham control rats. The OVX rats had diestrus and metestrus stages continuously throughout the

Figure 4

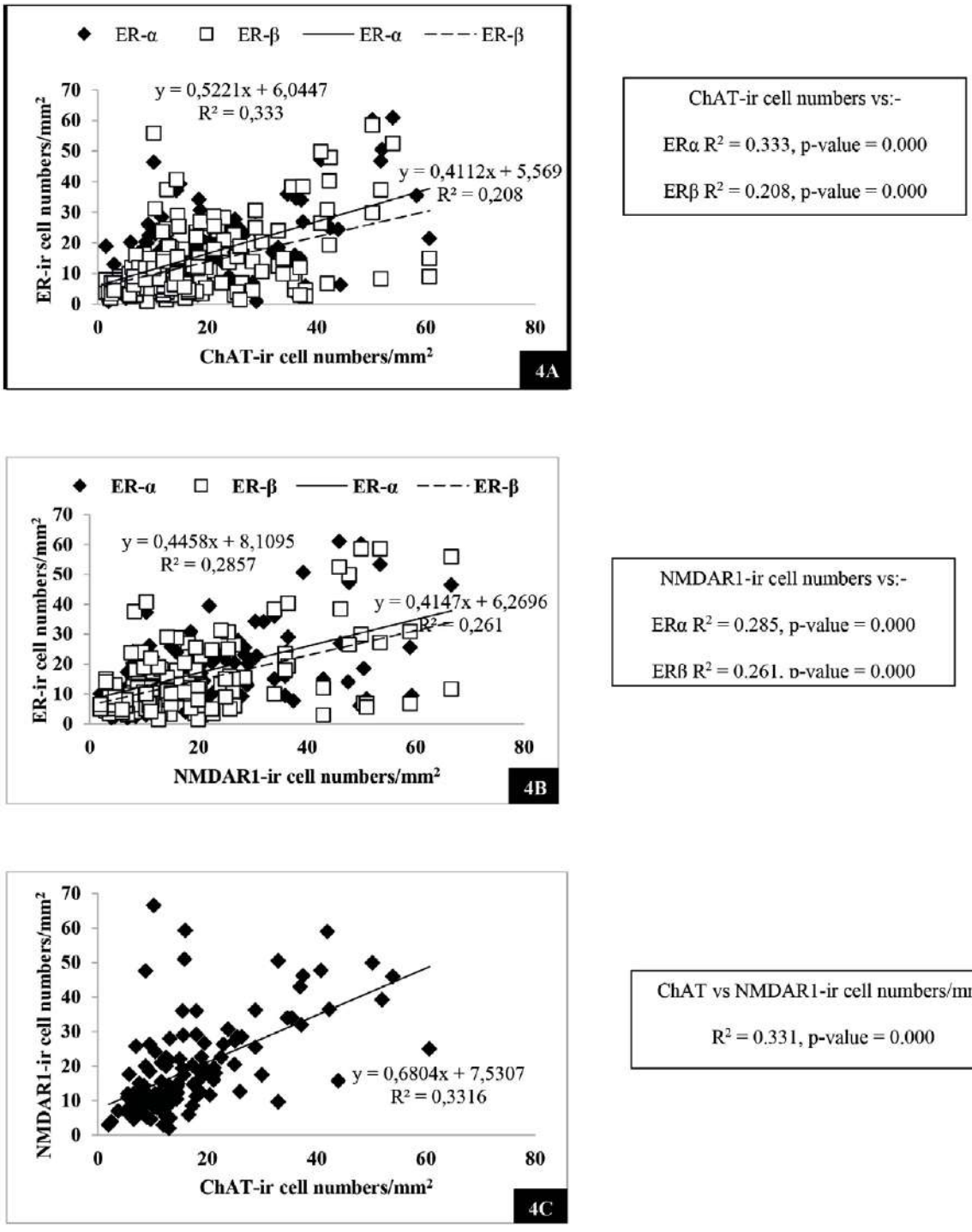

Fig. 4.- Plot of number of the ChAT-reactive neurons against the number of ERα- and ERβ- reactive neurons (**4A**), the NMDAR1-reactive neurons against the number of ERα- and ERβ- reactive neurons (**4B**) and the ChAT-reactive neurons against the number of NMDAR1-reactive neurons (**4C**), from the same rats and from all animal groups.

10-week period. The ovariectomized rats that fed with 10 mL/kg BW/d (OY10) and 20 mL/kg BW/d (OY20) of YCJ showed proestrus and estrus stages continuously throughout ten weeks treatment with higher vaginal scores at $p<0.05$ compared to the control ovariectomized (OW) group. Nevertheless, the vaginal smear scores of OY10 and OY20 groups were significantly lower compared to the OB. During proestrus, progesterone declines, and a preovulatory follicle undergoes its final growth phase (estradiol increases). Proestrus and estrus stages comprise the follicular phase indicating a high level of estrogen. Ovulation usually occurs during estrus. While metestrus and diestrus make up the luteal phase when the estrogen drops to a very low level (Jin et al., 2018). That vaginal smear of the OY40 group was not significantly different from the ovx (OW) group, and it was significantly lower than that of the SW, OB, OY10, and OY20 groups. That vaginal smear score of the OY40 group was in the metestrus cycle, indicating a deficient estrogen level.

We have previously demonstrated the effect of estrogen-like activities of YCJ in delaying AD pathologies, protecting neuronal cell death, accelerating wound healing, and preventing bone loss (Radenahmad et al., 2006; 2009; 2011; 2012; 2014; 2015; Yusuh et al., 2010; Suwanpal et al., 2011). In some of these studies, pyramidal neurons that use excitatory neurotransmitters, and non-pyramidal ones that use inhibitory neurotransmitters, were examined using antibodies against NF200 and parvalbumin (PV), respectively. More parameters were investigated using antibodies against ChAT and NMDAR1 in the hippocampus and prefrontal cortex, the brain regions involved with learning and memory function in the present study. Our results demonstrated that the protective

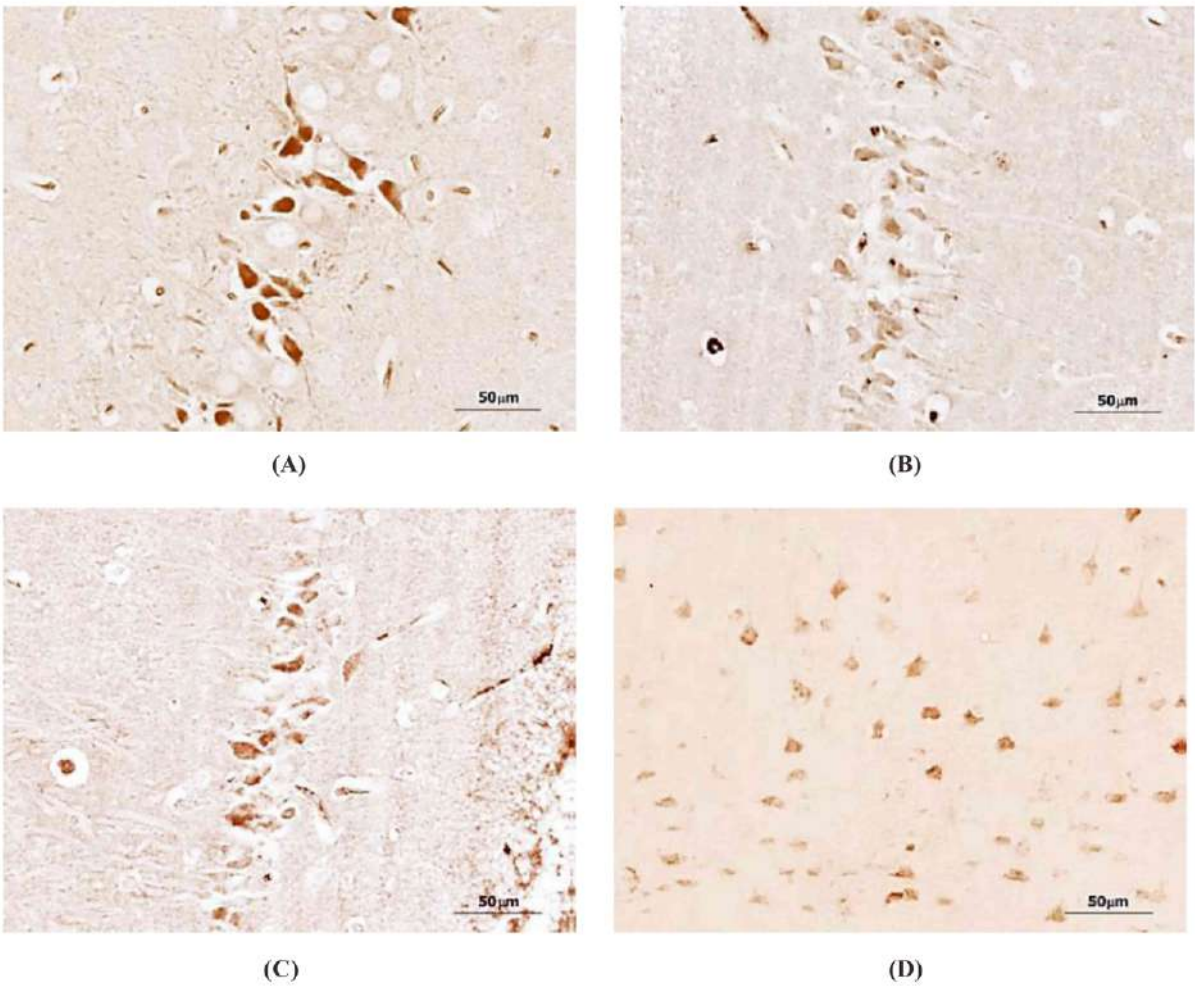

Fig. 5.- Examples of reactive neurons of YCJ-treated groups: **(A)** ChAT-reactive neurons in the CA2, **(B)**NMDAR1-reactive neurons in the CA1, **(C)** ERα-reactive neurons in the CA1 of the hippocampus and, **(D)** ERβ-reactive neurons in the prefrontal cortex of the brains. Scale bars = 50 µm.

effect of various dosages of YCJ on different brain regions is generated via its estrogen-like component. The results derived from the ERα and ERβ immunostaining and counting reflect an increase in the ERα- and ERβ-ir pyramidal neurons in the CA1, CA2, and PF regions. It was observed that there was a significant increase of cell densities in the hippocampus of the sham group. We suggest that this condition may be due to the compounds present in the food pellets. During the last decade, there has been a steady increase in research into the dietary factors that enhance neurogenesis in adults (Poulose et al., 2017). Results of clinical investigations show that polyphenols, vitamins B-9 and E, v-3 PUFAs, and non-nutrient phytochemicals improve adult neurogenesis in adultratsandmice (Shukitt-Hale et al., 2015; Reyes-Izquierdo et al., 2013; Dong et al., 2012; Moriya et al., 2011; Fernández-Fernández et al., 2012).

It has been reported that 58% of YCJ components consists of β-sitosterol alongside different sterols, such as, α spinasterol, stigmasterol, fucosterol, and stigmastatrienol (Rattanaburee et al., 2014) and the β-sitosterol has a similar structure to the animal cholesterol that functions as a sex steroid precursor (Moghadasian, 2000). It has also been reported that coconut extract is rich in phytohormones such as abscisic acid (ABA), auxin, gibberellins (GAs), and other cytokinins (Kobayashi et al., 1997; Ge et al., 2006; Wu and Hu, 2009), and due to its high content of β-sitosterol, stigmasterol and other flavonoids, its methanol extract has an estrogenic effect in rats (Salah et al., 2002). Coconuts contain trans-zeatin, a potent inhibitor of acetylcholinesterase that has been indicated to be effective for the treatment of AD and its associated dysfunctions (Heo et al., 2002; Kim et al., 2008). Besides, trans-zeatin also prevents the formation of amyloid β-protein with an important role in the development and

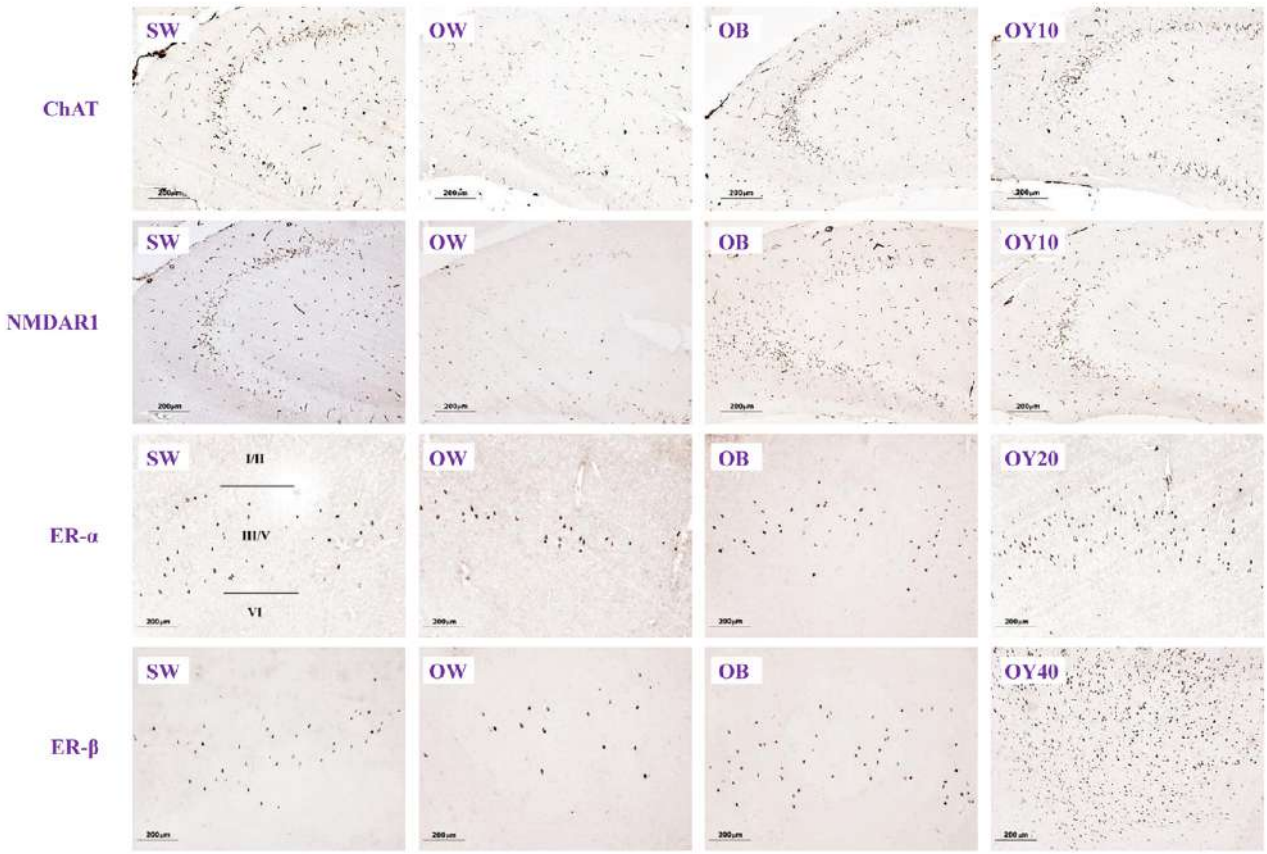

Fig. 6A.- Immunohistochemical sections showing the degree expression of ChAT-, NMDAR1-, ERα- and ERβ- positive neurons in the hippocampus (HP) and prefrontal cortex (PF) brain sections (10x). SW = sham-operated group; OW = ovariectomized group; OB = ovariectomized rat receiving estradiol benzoate (EB) 2.5 µg/kgBW/day; OY10 = ovariectomized rat receiving YCJ 10 mL/kgBW/day; OY20 = ovariectomized rat receiving YCJ 20 mL/kgBW/day; OY40 = ovariectomized rat receiving YCJ 40 mL/kgBW/day..

progress of AD (Choi et al., 2009) and showed anti-aging effects on human fibroblast cells (Rattan and Sodagam, 2005). In the current study, the protective role of YCJ against the disturbances of different reactive neurons in the brain of OVX rats is mainly due to its strong estrogenic effect, which facilitates the synthesis of endogenous estrogens.

We verified that the protective effect of various dosages of YCJ on different brain regions is generated via its estrogen-like component by the regression correlation graphs between ChAT-ir and NMDAR1-ir cell numbers with numbers of ER-ir cells. All those p-values are very significant at p-value = 0.000. Moreover, a significant positive correlation was found when correlation analysis was performed. Our results are in agreement with findings derived from other studies and can have important implications in the search by the scientific community for methods to preserve the brain cholinergic system due to the importance of

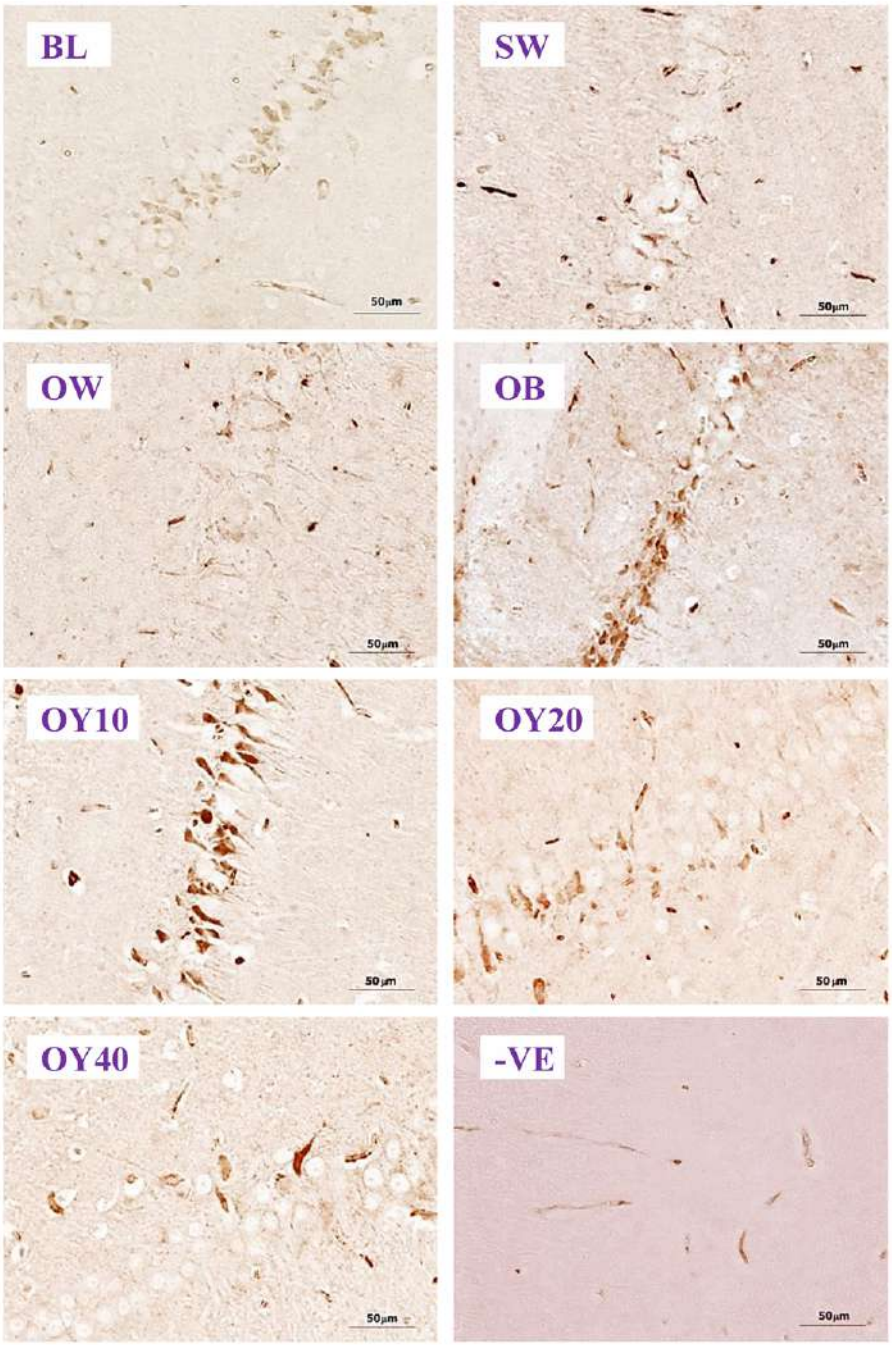

Fig. 6B.- Examples of higher magnification (40x) of ChAT-ir positive neurons in the CA1 of hippocampus. BL= baseline group; SW = sham-operated group; OW = ovariectomized group; OB = ovariectomized rat receiving estradiol benzoate (EB) 2.5 µg/kgBW/day; OY10 = ovariectomized rat receiving YCJ 10 mL/kgBW/day; OY20 = ovariectomized rat receiving YCJ 20 mL/kgBW/day; OY40 = ovariectomized rat receiving YCJ 40 mL/kgBW/day; -VE = negative control group.

the latter in controlling cerebral blood flow, cortical activity, cognitive functions, and cortical plasticity (Dang, 2010; Hall et al., 2001; Bohacek et al., 2008; Morissette et al., 2008; Schliebs and Arendt, 2006). They also can have important implications in the search for methods to preserve the brain glutamatergic system, which relies on NMDAR1 receptors that participate in the mechanism of long-term potentiation (LTP), the best-understood synaptic model of learning and memory (Sze et al., 2001). However, the double immunohistochemical staining of these ChAT-ir and NMDAR1-ir cells and ER-ir cells will be investigated to confirm this hypothesis in the near future.

Our previous studies demonstrated a significant degree of prevention of AD pathologies in OVX rats treated with YCJ at a daily high dose of 100 mL/kg BW. However, this dosage showed side effects that may be considered unfavorable, such as the deposition of glycogen in the liver. Therefore, in

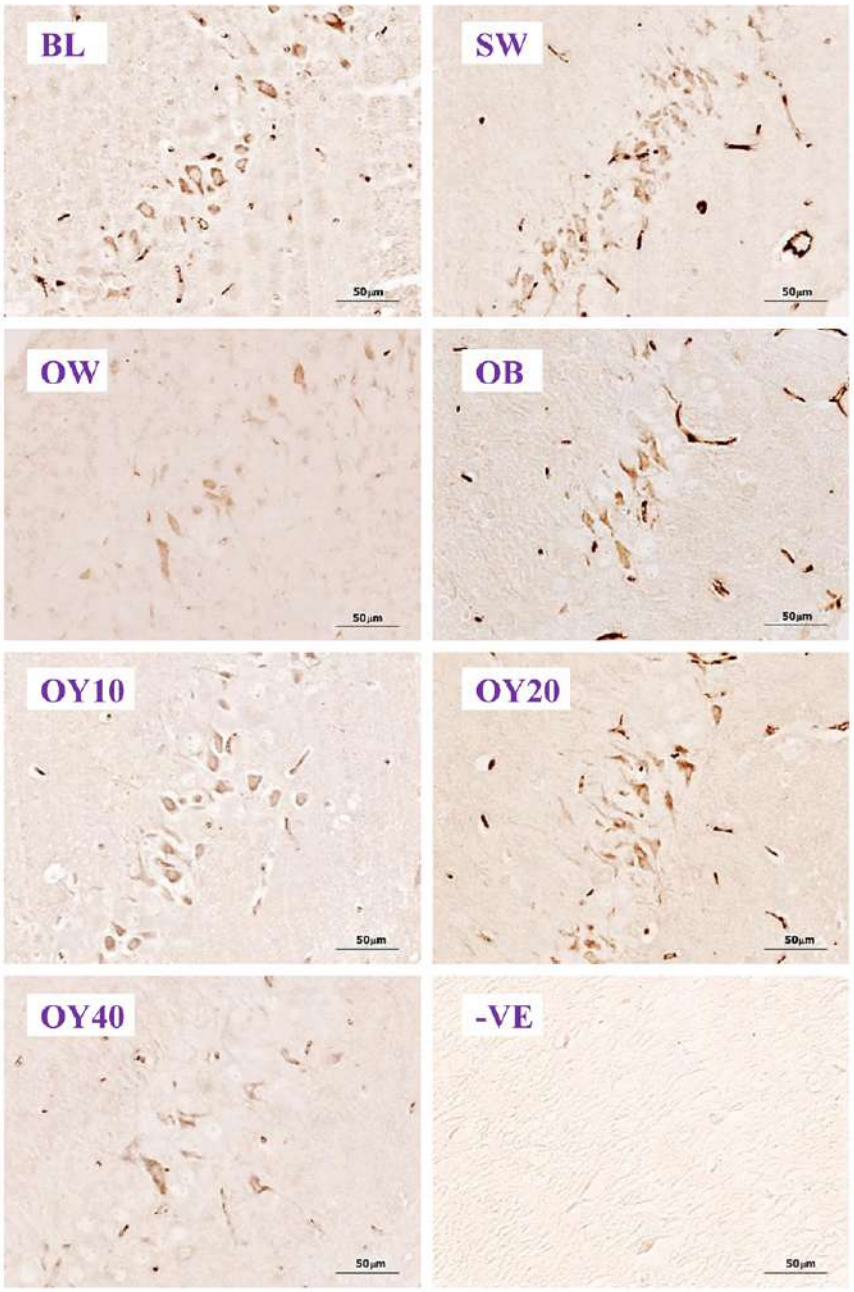

Fig. 6C.- Examples of higher magnification (40x) of NMDAR1-ir positive neurons in the CA2 of the hippocampus. BL= baseline group; SW = sham-operated group; OW = ovariectomized group; OB = ovariectomized rat receiving estradiol benzoate (EB) 2.5 µg/kgBW/day; OY10 = ovariectomized rat receiving YCJ 10 mL/kgBW/day; OY20 = ovariectomized rat receiving YCJ 20 mL/kgBW/day; OY40 = ovariectomized rat receiving YCJ 40 mL/kgBW/day; -VE = negative control group.

this study, we sought to optimize the YCJ dose by examining the effects of three lower doses, namely 10 mL, 20 mL, and 40 mL/kg BW/day. Our results showed that YCJ at 10 mL/kg BW/day was the optimal neuroprotective dose that preserved cholinergic and glutamatergic neurons in the CA1, CA2, CA3, and PF regions, without affecting the functional parameters of the liver or kidney (please see the details of lipid, liver and renal parameters in Payanglee et al., 2017).

Finally, YCJ seems to act as a selective estrogen receptor modulator (SERM). The results of other parameters investigated in bone, skin, calcium-binding proteins in the GI tract of the same model of both male and female rats confirmed this SERM activities of YCJ (some manuscripts were published, some are being in preparations). Pharmacological interventions using SERMs in estrogen deficiency cases often rely on its binding ability to the estrogen receptors (ERα and ERβ),

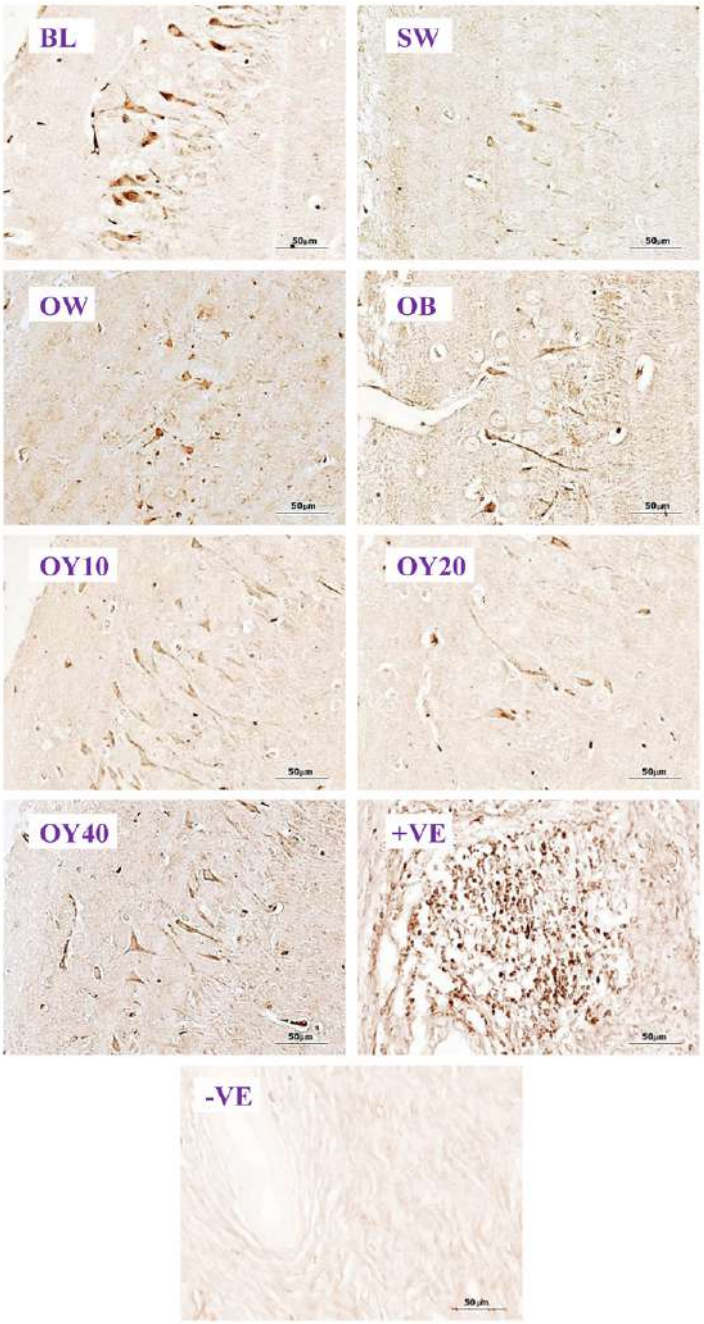

Fig. 6D.- Examples of higher magnification (40x) of ERα-ir positive neurons in the CA3 of hippocampus. BL= baseline group; SW = sham-operated group; OW = ovariectomized group; OB = ovariectomized rat receiving estradiol benzoate (EB) 2.5 µg/kgBW/day; OY10 = ovariectomized rat receiving YCJ 10 mL/kgBW/day; OY20 = ovariectomized rat receiving YCJ 20 mL/kgBW/day; OY40 = ovariectomized rat receiving YCJ 40 mL/kgBW/day; +VE = positive control group (uterus for ERα and ovary for ERβ); -VE = negative control group.

therefore acting as either agonists or antagonists depending on the pharmacological compounds present as well as the target tissues (Hadji, 2012). Phytoestrogens are plant derivatives that behave differently from estrogen and more like SERMs and have a higher affinity to ERβ (Oseni et al., 2008). We have previously reported that YCJ had beneficial effects on accelerating wound healing in OVX rats, whereby such wounds had a significantly higher degree of expression of ERβ than ERα (Radenahmad et al., 2012). Moreover, our recent study showed that β-sitosterol was a significant component of YCJ, which, in turn, was found to have binding affinities to both ERα and ERβ (Ratanaburee et al.,2014; Dang, 2010). In conclusion, the present study indicates that YCJ may affect preserving cholinergic and glutamatergic neurons via the ChAT and NMDAR1 in the brain regions, at least in part, via a SERM-like activity.

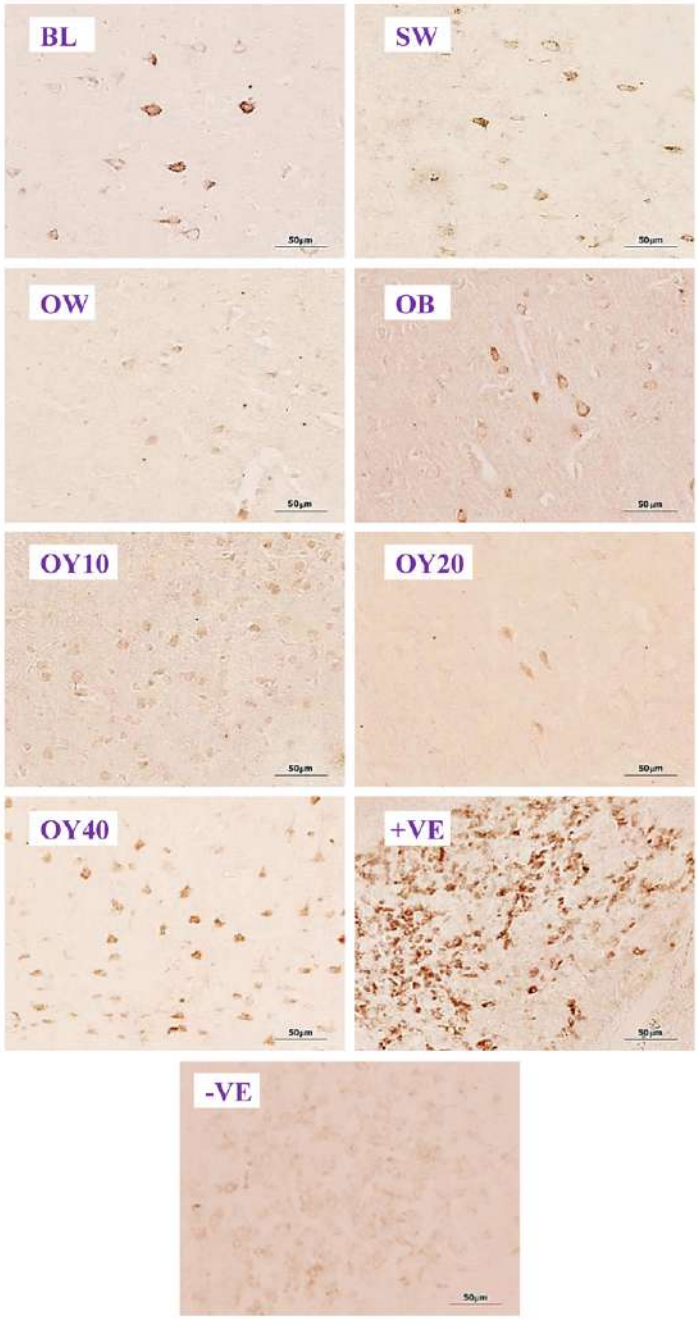

Fig. 6E.- Examples of higher magnification (40x) of ERβ-ir positive neurons in the prefrontal cortex. BL= baseline group; SW = sham-operated group; OW = ovariectomized group; OB= ovariectomized rat receiving estradiol benzoate (EB) 2.5 µg/kgBW/day; OY10 = ovariectomized rat receiving YCJ 10 mL/kgBW/day; OY20 = ovariectomized rat receiving YCJ 20 mL/kgBW/day; OY40 = ovariectomized rat receiving YCJ 40 mL/kgBW/day; +VE = positive control group (uterus for ERα and ovary for ERβ); -VE = negative control group.

CONCLUSION

The results of this study revealed that: (1) OVX rats showed the reduction of positive neurons due to the deficiency of estrogen hormone; (2) vaginal smear could be used as a preliminary screening estrogenic effect of YCJ; (3) YCJ treatment, at various doses tested, restored the decreased numbers of ChAT-, NMDAR1-, ERα- and ERβ-reactive neurons caused by ovariectomy to normal or close-to-normal levels, and (4) the effects of YCJ were comparable to those of EB treatment. In most cases, the dose of YCJ at 10 ml/kg BW was the best. The higher doses of YCJ (20 ml and 40 ml/kg BW), the more side effects in the liver and kidney and serum analysis parameters. For example, the higher doses of YCJ, the higher the total cholesterol, LDL, and triglyceride levels (please see details in Payanglee et al., 2017). These findings indicate that histological methods can effectively provide scientific evidence of neurodegenerative processes and treatment mechanisms. These findings suggest the potential therapeutic property of YCJ in preventing AD pathology in female rats caused by a lack of estrogen.

ACKNOWLEDGEMENTS

This work was supported by the government budget of the Prince of Songkla University**,** Grant code: SCI580566S. We thank the late Dr. Brian Hodgson from the Faculty of Pharmaceutical Science, Prince of Songkla University, for assistance with the English correction.

REFERENCES

BITZER J, KENEMANS P, MUECK AO (2008) Breast cancer risk in postmenopausal women using testosterone in combination with hormone replacement therapy. *Maturitas*, 59(3): 209-218.

BOHACEK J, BEARL AM, DANIEL JM (2008) Long-term ovarian hormone deprivation alters the ability of subsequent oestradiol replacement to regulate choline acetyltransferase protein levels in the hippocampus and prefrontal cortex of middle-aged rats. *J Neuroendocrinol*, 20(8): 1023-1027.

BURTON JL, WELLS M (2002) The effect of phytoestrogens on the female genital tract. *J Clin Pathol*, 55(6): 401-407.

CARROLL JC, ROSARIO ER, CHANG L, STANCZYK FZ, ODDO S, LAFERLA FM, PIKE CJ (2007) Progesterone and estrogen regulate Alzheimer-like neuropathology in female 3xTg-AD mice. *J Neurosci*, 27(48): 13357-13365.

COLLINGRIDGE GL, SINGER W (1990) Excitatory amino acid receptors and synaptic plasticity. *Trends Pharmacol Sci*, 11(7): 290-296.

CHOI SJ, JEONG CH, CHOI SG, CHUN JY, KIM YJ, LEE JM, SHIN DH, HEO HJ (2009) Zeatin prevents amyloid beta-induced neurotoxicity and scopolamine-induced cognitive deficits. *J Med Food,*12*:* 271-277.

DANG Z (2010) Comparison of relative binding affinities to fish and mammalian estrogen receptors: the regulatory implications. *Toxicol Lett*, 192(3): 298-315.

DONG S, ZENG Q, MITCHELL ES, XIU J, DUAN Y, LI C, TIWARI JK, HU Y, CAO X, ZHAO Z (2012) Curcumin enhances neurogenesis and cognition in aged rats: implications for transcriptional interactions related to growth and synaptic plasticity. *PlosOne*, 7(2): e31211.

FERNÁNDEZ-FERNÁNDEZ L, COMES G, BOLEA I, VALENTE T, RUIZ J, MURTRA P, RAMIREZ B, ANGLES N, REGUANT J, MORELLO JR, BOADA M, HIDALGO J, ESCORIHUELA M, UNZETA M (2012) LMN diet, rich in polyphenols and polyunsaturated fatty acids, improves mouse cognitive decline associated with aging and Alzheimer's disease. *Behav Brain Res*, 228(2): 261-271.

FERNÁNDEZ-TOMÉ P, BRERA B, ARÉVALO MA, DE CEBALLOS ML (2004) β-amyloid 25-35 inhibits glutamate uptake in cultured neurons and astrocytes: modulation of uptake as a survival mechanism. *Neurobiology Dis*, 15(3): 580-589.

FERREIRA-VIEIRA TH, GUIMARAES IM, SILVA FR, RIBEIRO FM (2016) Alzheimer's disease: Targeting the cholinergic system. *Curr Neuropharmacol,* 14(1): 101-115.

GE L, TAN S, YONG JWH, TAN SN (2006) Capillary electrophoresis for cytokinin analyses: A review. *Electrophoresis,* 27: 4779-4791.

GREENAMYRE JT (1986) The role of glutamate in neurotransmission and in neurologic disease. *Arch Neurol*, 43(10): 1058-1063.

HADJI P (2012) The evolution of selective estrogen receptor modulators in osteoporosis therapy. *Climacteric*, 15(6): 513-523.

HALL JM, COUSE JF, KORACH KS (2001) The multifaceted mechanisms of estradiol and estrogen receptor signaling. *J Biol Chem*, 276(40): 36869-36872.

HEO HJ, HONG SC, CHO HY, HONG B, KIM HK, KIM EK, SHIN DH (2002) Inhibitory effect of zeatin, isolated from *Fiatouavillosa*, on acetylcholinesterase activity from PC12 cells. *Mol Cells*, 13: 113-117.

JAMSHED N, OZAIR FF, AGGAWAL P, EKKA M (2014) Alzheimer disease in postmenopausal women: Intervene in the critical window period. *J Mid-life Health*, 5(1): 38-40.

JIN YK, BAE HS, LEE JY, YUM SY, KIM KM, KOO OJ, AILIA MJ (2018) The effect of gonadotropin-releasing hormone agonist on superovulation and estrous synchronization in female Sprague Dawley rat. *Reprod Fert Develop,* 30(1): 239-239.

KOBAYASHI H, MORISAKI N, TAGO Y, HASHIMOTO Y, IWASAKI S, KAWACHI E, NAGATA R, SHUDO K (1997) Structural identification of a major cytokinin in coconut milk as14-*O*-(3-*O*-[β-Dgalactopyranosyl-(1-->2)-α-D-galactopyranosyl-(1-->3)-α-L-arabinofuranosyl]-4-O-(α-L-arabinofuranosyl)-β-D-galactopyranosyl)-*trans*-zeatinriboside. *Chem Pharm Bull,* 45: 260-264.

KIM MJ, CHOI SJ, LIM ST, KIM HK, KIM YJ, YOON HG, SHIN DH (2008) Zeatin supplement improves scopolamine-induced memory impairment in mice. *Biosci Biotechnol Biochem,* 72: 577-581.

LAUDERBACK CM, HACKETT JM, HUANG FF, KELLER JN, SZWEDA LI, MARKESBERY WR, BUTTERFIELD DA (2001) The glial glutamate transporter, GLT-1, is oxidatively modified by 4-hydroxy-2-nonenal in the Alzheimer's disease brain: the role of Aβ1–42. *J Neurochem*, 78(2): 413-416.

LAWS SC, CAREY SA, FERRELL JM, BODMAN GJ, COOPER RL (2000) Estrogenic activity of octylphenol, nonylphenol, bisphenol A and methoxychlor in rats. *Toxicol Sci*, 54(1): 154-167.

MARAGOS WF, GREENAMYRE JT, PENNEY JR JB, YOUNG AB (1987) Glutamate dysfunction in Alzheimer's disease: a hypothesis. *Trends Neurosci*, 10(2): 65-68.

MARCONDES FK, BIANCHI FJ, TANNO AP (2002) Determination of the estrous cycle phases of rats: some helpful considerations. *Braz J Biol*, 62(4A): 609-614.

MASTERS CL, BATEMAN R, BLENNOW K, ROWE CC, SPERLING RA, CUMMINGS JL (2015) Alzheimer's disease. *Nat Rev Dis Primer,* 1: 15056.

MCCULLOUGH ML, PATEL AV, PATEL R, RODRIGUEZ C, FEIGELSON HS, BANDERA EV, GANSLER T, THUN MJ, CALLE EE (2008) Body mass and endometrial cancer risk by hormone replacement therapy and cancer subtype. *Cancer Epidem Biomar,* 17(1): 73-79.

MOGHADASIAN MH (2000) Pharmacological properties of plant sterols in vivo and in vitro observations. *Life Sci,* 67(6): 605-615.

MORISSETTE M, LE SAUX M, D'ASTOUS M, JOURDAIN S, AL SWEIDI S, MORIN N, ESTRADA-CAMARENA E, MENDEZ P, GARCIA-SEGURA LM, DI PAOLO T (2008) Contribution of estrogen receptors alpha and beta to the effects of estradiol in the brain. *J Steroid Biochem*, 108(3-5): 327-338.

MORIYA J, CHEN R, YAMAKAWA JI, SASAKI, K, ISHIGAKI Y, TAKAHASHI T (2011) Resveratrol improves hippocampal atrophy in chronic fatigue mice by enhancing neurogenesis and inhibiting apoptosis of granular cells. *Biol Pharm Bull,* 34(3): 354-359.

OSENI T, PATEL R, PYLE J, JORDAN VC (2008) Selective estrogen receptor modulators and phytoestrogens. *Planta Med*, 74(13): 1656-1665.

PALMER AM, GERSHON S (1990) Is the neuronal basis of Alzheimer's disease cholinergic or glutamatergic? *FASEB J,* 4(10): 2745-2752.

PARHIZKAR S, LATIFFAH A, LATIFF LA, RAHMAN SA (2011) Assessing estrogenic activity of Nigella sativa in ovariectomized rats using vaginal cornification assay. *Afr J Pharm Pharmaco*, 5(2): 137-142.

PAYANGLEE K, CHONPATHOMPIKUNLERT P, PANITYAKUL T, RADENAHMAD N (2017) Beneficial effects of young coconut juice on preserving neuronal cell density, lipid, renal, and liver profiles in ovariectomizedrats: A preliminary study. *Songklanakarin J Sci Technol*, 39(2): 237-243.

PLASSMAN BL, LANGA KM, FISHER GG, HEERINGA SG, WEIR DR, OFSTEDAL MB, BURKE JR, HURD MD, POTTER GG, RODGERS WL, STFFENS DC, WILLIS R, WALLACE RB (2007) Prevalence of dementia in the United States: The aging, demographics, and memory study. *Neuroepidemiology*, 29: 125-132.

POULOSE SM, MILLER MG, SCOTT T, SHUKITT-HALE B (2017) Nutritional factors affecting adult neurogenesis and cognitive function. *Adv Nutr*, 8(6): 804-811.

RADENAHMAD N, VONGVATCHARANON U, WITHYACHUMNARNKUL B, CONNOR RJ (2006) Serum levels of 17β-estradiol in ovariectomized rats fed young-coconut-juice and its effect on wound healing. *Songklanakarin J Sci Technol*, 28: 897-910.

RADENAHMAD N, SALEH F, SAWANGJAROEN K, RUNDORN W, WITHYACHUMNARNKUL B, CONNOR JR (2009) Young coconut juice significantly reduces histopathological changes in the brain that is induced by hormonal imbalance: A possible implication to postmenopausal women. *Histol Histopathol*, 24(6): 667-674.

RADENAHMAD N, SALEH F, SAWANGJAROEN K, VONGVATCHARANON U, SUBHADHIRASAKUL P, RUNDORN W, WITHYACHUMNARNKUL B, CONNOR JR (2011) Young coconut juice, a potential therapeutic agent that could significantly reduce some pathologies associated with Alzheimer's disease: novel findings. *British J Nutr*, 105(5): 738-746.

RADENAHMAD N, SALEH F, SAYOH I, SAWANGJAROEN K, SUBHADHIRASAKUL P, BOONYOUNG P, RUNDORN W, MITRANUN W (2012) Young coconut juice can accelerate the healing process of cutaneous wounds. *BMC Complem Altern M*, 12(1): 252.

RADENAHMAD N, BOONYOUNG P, KAMKAEW K, CHANCHULA K, KIRIRAT P (2014) Effects of young coconut juice on the numbers of argyrophil endocrine cells in the gastrointestinal tract of male rats: Novel preliminary findings. *Songklanakarin J Sci Technol*, 36: 599-606.

RADENAHMAD N, SUWANSA-ARD S, SAYOH I (2015) Young coconut juice accelerates cutaneous wound healing by downregulating macrophage migration inhibitory factor (MIF) in ovariectomized rats: Preliminary novel findings. *Songklanakarin J Sci Technol*, 37: 417-423.

RATTAN SIS, SODAGAM L (2005) Gerontomodulatory and youth-preserving effects of zeatin on human skin fibroblasts undergoing aging *in vitro. Rejuv Res,* 8: 46-57.

RATTANABUREE P, AMNUAIKIT T, RADENAHMAD N, PURIPATTANAVONG J (2014) Phytochemical study and its quantity and quality of fresh and freeze-dried young coconut juice (*Cocosnucifera L.*). In: *Advanced Materials Research*, 884: 490-493). *Trans Tech Ltd, Publications, Switzerland.*

REYES-IZQUIERDO T, NEMZER B, SHU C, HUYNH L, ARGUMEDO R, KELLER R, PIETRZKOWSKI Z (2013) Modulatory effect of coffee fruit extract on plasma levels of brain-derived neurotrophic factor in healthy subjects. *British J Nutr*, 110(3): 420-425.

SALAH AM, GATHUMBI J, VIERLING W, WAGNER H (2002) Estrogenic and cholinergic properties of the methanol extract of Ruelliapraetermissa Sceinf. ex. Lindau (Acanthaceae) in female rats. *Phytomed,* 9: 52-55.

SCHLIEBS R, ARENDT T (2006) The significance of the cholinergic system in the brain during aging and in Alzheimer's disease. *J Neural Transm*, 113(11): 1625-1644.

SEZGIN Z, DINCER Y (2014) Alzheimer's disease and epigenetic diet. *Neurochem Int*, 78: 105-116.

SHUKITT-HALE B, BIELINSKI DF, LAU FC, WILLIS LM, CAREY AN, JOSEPH JA (2015) The beneficial effects of berries on cognition, motor behavior and neuronal function in aging. *British J Nutr*, 114(10): 1542-1549.

SUWANPAL P, RADENAHMAD N, YUSUH M, EKSOMTRAMATE M, RUANGSRI P, CHANTANASUKSILPA A (2011) Effects of young-coconut juice on increasing mandibular cancellous bone in orchidectomized rats: Preliminary novel findings. *Songklanakarin J Sci Technol*, 33(6): 617-623.

SZE CI, BI H, KLEINSCHMIDT-DEMASTERS BK, FILLEY CM, MARTIN LJ (2001) N-methyl-D-aspartate receptor subunit proteins and their phosphorylation status are altered selectively in Alzheimer's disease. *J Neurol Sci*, 182(2): 151-159.

SZEGŐ ÉM, CSORBA A, JANÁKY T, KÉKESI KA, ÁBRAHÁM IM, MÓROTZ GM, PENKE B, PALKOVITS M, MURVAI U, KELLERMAYER MSZ, KARDOS J (2011) Effects of estrogen on beta-amyloid-induced cholinergic cell death in the nucleus basalismagnocellularis. *Neuroendocrinology,* 93(2): 90-105.

VAN DIJK GM, KAVOUSI M, TROUP J, FRANCO OH (2015) Health issues for menopausal women: The top 11 conditions have common solutions. *Maturitas*, 80(1): 24-30.

WU Y, HU B (2009) Simultaneous determination of several phytohormones in natural coconut juice by hollow fiber-based liquid-liquid-liquid microextraction-high performance liquid chromatography. *J Chromatogr*, 1216: 7657-7663.

YUSUH M, PHOCHANUKOON N, RADENAHMAD N, EKSOMTRAMATE M, RUANGSRI P, CHANTANASUKSILPA A, NITIRUANGJARAS A (2010) Changes of condyle cartilage in orchidectomized rats fed with young coconut juice: Novel preliminary findings. *Songklanakarin J Sci Technol*, 32(4): 333-339.

ZHOU B, SUN Q, CONG R, GU H, TANG N, YANG L, WANG B (2008) Hormone replacement therapy and ovarian cancer risk: a meta-analysis. *GynecolOncol*, 108(3): 641-651.

Gross and histological study of nasal and brain olfactory structures in the grasscutter (*Thryonomys swinderianus*, Temminck)

Boniface Kavoi[1,2], Rodi Ojoo[1,2], Kwadwo Boateng[2,3], Stephen Kiama[1]

[1] *Department of Veterinary Anatomy and Physiology, Faculty of Veterinary Medicine, University of Nairobi, Riverside Drive, Nairobi, Kenya*

[2] *School of Veterinary Medicine, College of Applied and Basic Sciences, University of Ghana, Legon, Accra, Ghana*

[3] *Animal Research Institute, Council for Scientific and Industrial Research, Achimota, Accra, Ghana*

SUMMARY

The major drawback of the efforts currently being made to domesticate grasscutters (GRCs) is the paucity of data on their biology particularly in connection with sensory related reactions. We investigated, both grossly and histologically, the qualitative and quantitative features of the GRC nasal and brain olfactory components with a view to understanding their morphofunctional adaptations. At the caudal roof of the nasal cavity, the olfactory mucosa (OM), whose basic histology was similar to that of other mammals, covered a set of five cylindrical-shaped ethmoturbinates. Olfactory bulb (OB) and olfactory brain components (OBC) (i.e., OB, olfactory tract and stria) constituted 0.55 and 1.26% of the entire brain volume respectively. Relative to the cerebral hemispheres, respective proportions for lengths and breadths were 72.23% for OBC and 34.38% for OB. Regarding the OM, epithelial height and axon bundle diameters were 76.3 ± 5.4 µm and 70.6 ± 8.6 µm respectively while volume fractions were 31.2 ± 4.4% for the bundles and 49.7 ± 5.1% for Bowman's glands. These findings reveal that the anatomical design of the GRC OM and OBC follows the general patterns observed in other mammals and are refined to levels that appear to correspond to demands in olfactory function vis-à-vis behavior and ecology.

Key words: Grasscutter – Morphometry – Nasal – Olfactory brain – Structures

INTRODUCTION

The grasscutter (GRC) (*Thryonomys swinderianus, Temminck 1827*), also known as the great cane rat or marsh cane-rat, is a rodent but not a rat proper (Opara, 2010). Rodents constitute the largest group among the mammalian orders, with about 2,277 species (Aydin et al., 2008). The GRC is indigenous to Africa and belongs to a small group of the so called African hystricognath rodents (Woods and Kilpatrick, 2005). Hystricomorpha, which are distinguished from other rodents by their skull structure, comprise of the families Thryonomydae (family of the GRCs), Hystricidae (porcupines), Bathyergidae (sand-diggers) and Petromuridae (African rock-rats) (Opara, 2010).

Corresponding author:
Boniface M. Kavoi (BVM, MSc, PhD). Department of Veterinary Anatomy and Physiology, Faculty of Veterinary Medicine, University of Nairobi, Riverside Drive, P.O. Box 30197-00100, Nairobi, Kenya. Phone: +254720895968; Fax: +254 02 4451770. E-mail: bmkavoi@uonbi.ac.ke.

Submitted: January 3, 2021. **Accepted:** January 30, 2021

GRCs are prevalent in the West African sub-region from Senegal to parts of the Cape Province including Ghana, Nigeria, Togo, Benin, and Côte d'Ivoire (Rosevear, 1969). In these places, GRCs are hunted aggressively for their meat, which the locals consider a delicacy (Matthews, 2008). Consequently, in the aforementioned countries, relentless efforts are being made to domesticate GRCs by raising them in cages for home consumption and for sale (Fa et al., 2002). Indeed, GRCs in these regions are considered "micro livestock" (Karikari and Nyameasem, 2009) or more precisely "livestock of tomorrow" (Opara, 2010). Moreover, rearing and breeding of captive GRCs for use as research models are becoming habitual practice (Jori et al., 2001; Ibe et al., 2017).

In the wild, GRCs inhabit reed-beds and riverbanks where they live in small groups led by a single male (Woods and Kilpatrick, 2005). These animals are nocturnal monogastric herbivores that live above the ground and feed on roots, shoots, and stems of various grasses (Williams et al., 2011). GRCs are considered wasteful feeders in that they cut grass with a characteristic tooth-chattering sound to obtain the more nutritious succulent inner nodes, leaving behind scattered pieces on the ground (Asibey, 1974). Humans have expanded into the GRCs' native habitats and this has forced GRCs to look for food and space in plantations (Opara, 2010). GRCs attain sexual maturity at the age of 7 months, when their body mass is 1.6-2.1 kg (Adu and Yeboah, 2003). In terms of appearance, GRCs have a thickset body, rounded ears, short nose, coarse bristle hair, spiny fur on the back (Fig. 1) and forefeet that are smaller than the hind. The body coat comprises a mixture of brown reddish and gray fur that varies depending on habitat (Jori and Chardonnet, 2001).

Data on the anatomy of the GRC is essential in understanding the basis for some of the behaviors it exhibits in its natural habitat, and which must be considered for its effective performance when reared and bred in cages. The anatomy of the GRC brain has been studied previously (Byanet et al., 2009; Ajayi et al., 2011; Byanet and Dzenda, 2014; Ibe et al., 2017), with little attention to the olfactory system. A study detailing the structure of reflex centers in the GRC brain revealed a relatively bigger caudal than rostral colliculi (Ibe et al., 2017), implying a better auditory than visual acuity. Besides, Opara (2010) opined that the poor visual acuity in the GRC makes communication to occur more effectively via auditory and olfactory senses. In this study, therefore, the gross, histologic and morphometric features of the GRC olfactory mucosa (OM) and olfactory brain components (OBC) are analyzed in an attempt to understand the neural substrates responsible for the reportedly better olfactory cue. Notably, results of this work add on to the growing literature on GRC anatomy. Furthermore, quantitative data recorded here may serve as an important taxonomic exponent of animals in the order Rodentia.

MATERIALS AND METHODS

Experimental animals

A total of ten healthy male captive-bred GRCs aged 13-15 months (2.8-3.2 kg bwt) were used. These were chosen from a colony raised in a conventional animal housing facility. The GRCs were transported from the housing facility in well ventilated wooden cages to the School of Veterinary Medicine, University of Ghana, anatomy laboratory, where they were immediately euthanized using pentobarbital sodium (140 mg/kg, intravenously). Perfusion fixation of the olfactory mucosae and brains was carried out through the left ventricle with saline followed by 10% formaldehyde. All procedures performed on the GRC were approved by the University's Animal Care and Use Committee and were in strict conformity to the guidelines provided in the Animals (Scientific Procedures) Act 1986.

Harvesting of the brains

Soon after perfusion fixation, the brains (n= 5 animals) were harvested as detailed in Ibe et al. (2017). In brief, the head was cut off from the rest of the body at the atlanto-axial joint using a sharp knife. This was followed by skinning and stripping off the cranial and facial muscles, and then breaking the skull to extract the brain in caudorostral and dorsoventral directions using scalpel blades, thumb forceps and a pair of scissors. The brain was then allowed to

fix further by immersing it overnight in 10% formaldehyde.

Harvesting and processing of the olfactory mucosa for histology

The ethmoidal conchae, onto which the olfactory mucosa (OM) lies, were harvested from the nasal cavity (n = 5 animals) following mid-sagittal sectioning of the skull and subsequent exposure of the conchae by dissecting out the nasal septum (Kavoi et al., 2010). The conchae were then transected perpendicular to their long axes into posterior, middle and anterior portions, from which tissue sub-segments for histology were selected by systematic random sampling.

The selected conchal pieces were decalcified in 5% EDTA (Alers et al., 1999), washed in distilled water and dehydrated in graded ethanol series (50, 70, 80, 90% and twice in 100%). This was followed by paraffin embedding and sectioning in the transverse plane at 5 µm using a rotary microtome (Leitz Wetzlar, Germany). Staining was then done in hematoxylin and eosin and Masson's trichrome using routine procedures.

Morphometric analysis

Volume and linear measurements were performed on the brain as illustrated in Kavoi and Jameela (2011). The volumes for the whole brain (WB), cerebral hemisphere (CH), olfactory bulb (OB) and olfactory bulb, tract and stria combined (OBC) were determined using the water displacement method (Scherle, 1970).

Linear measurements (greatest lengths and breadths) were carried out on the OB, OBC and CH as illustrated in Fig. 2. Vernier calipers, thread and meter rule were used to take the measurements and three trained technicians were involved in the exercise (intra and inter-observer errors = 2-3%).

Quantitative parameters of the OM were analyzed from 30-35 test fields generated from randomly selected histomicrographs (Kavoi et al., 2010; Kavoi et al., 2012). The parameters estimated included: 1) thickness of the olfactory epithelium, 2) diameter of axon bundles and 3) volume fractions of axon bundles and Bowman's glands. The protocols followed in carrying out these measurements are well outlined in Kavoi et al. (2012).

Data on morphometry were expressed as mean ± SD (standard deviation) and presented in tables. Comparisons of measurement values between OBC and the cerebrum or whole brain were expressed as ratios (%).

Fig. 1.- Photographs showing characteristic body features of grasscutters (*Thryonomys swinderianus*). Notice the spiny fur on the back of its thickset body, large rounded ears, short nose and prominent vibrissae.

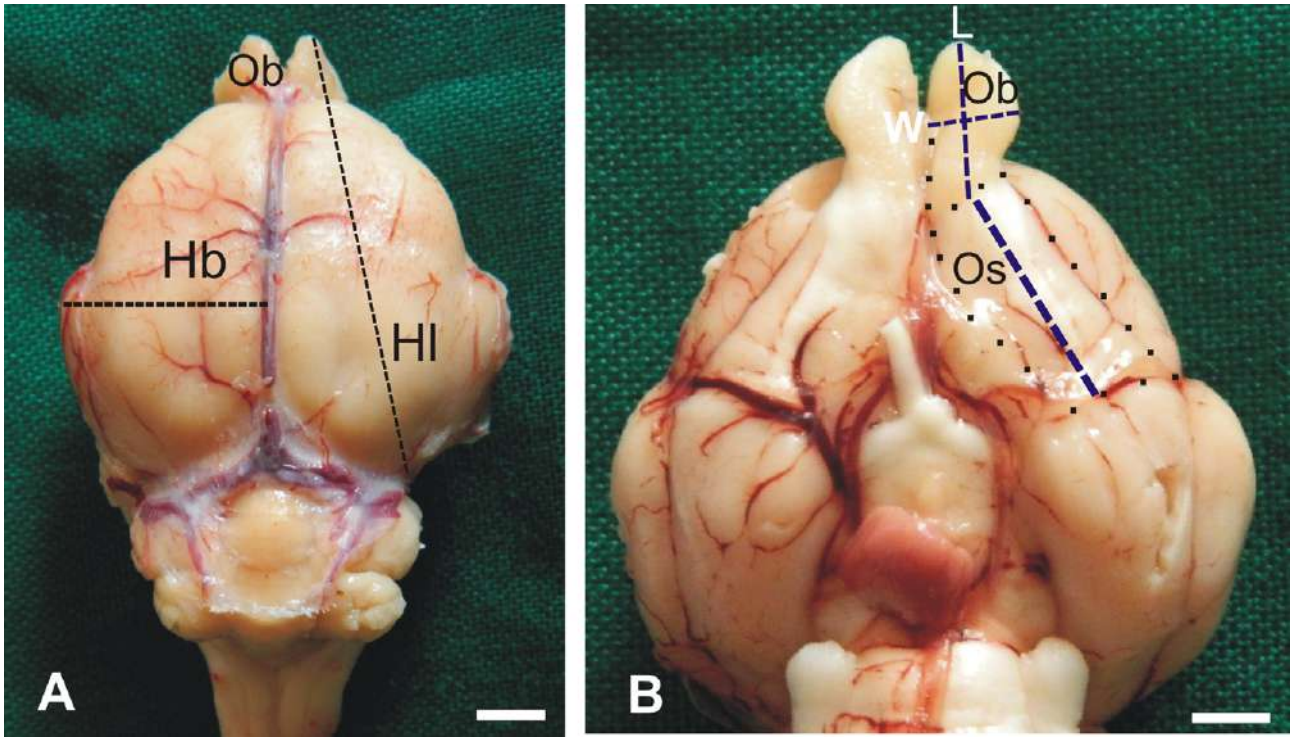

Fig. 2.- Macrographs showing how linear dimensions were estimated on the GRC brain. **A:** greatest length (Hl) and breadth (Hb) of the cerebral hemisphere were measured from the dorsal aspect of the brain. **B:** ventrally on the brain, the olfactory bulb (Ob) and olfactory tract and stria (Os) were dissected out (dotted lines) to allow measurement of their greatest lengths (L) and breadths (W). Scale bar = 5 mm in A and B.

RESULTS

Morphology

Grossly, the GRC OM was identified by its characteristic yellowish-brown color at the caudal roof of the nasal cavity, where it was covered by a set of five cylindrical ethmoturbinates (Fig. 3).

It is noted in Fig. 4 that the histological appearance of the GRC OM was basically similar to that of other mammalian species. The epithelium (Fig. 4A) was organized into a free zone, non-nuclear zone and nuclear zone, with the latter zone having an upper region of elongated supporting cell nuclei, middle portion of rounded olfactory cell nuclei and a lower row of basal cell nuclei. Embedded in the lamina propria (Fig. 4B) were Bowman's glands and olfactory nerve axon bundles. Here, the glands were of the mucus tubuloalveolar type, and were mainly confined in the upper two thirds of the propria. The lower third of the propria was predominated by axon bundles.

Morphometry

Volume measurements gave a value of 0.06 ± 0.008 cm^3 for OBs, 0.14 ± 0.05 cm^3 for OBC and 11.14 ± 0.72 cm^3 for CH (Table 1). This translates to volume ratios of 0.55 and 1.26% for OB: CH and OBC: CH respectively.

Linear dimensions for olfactory brain structures are shown in Table 2. In terms of length, the OBC was 23.51 ± 1.23 mm long while CH measured 32.55 ± 1.86 mm, thus giving an OBC: CH ration of 72.23%. For the breadths, values for OB and CH were 5.56 ± 0.81 and 16.17 ± 1.54, respectively, and therefore the OB: CH ratio was 34.38%.

Table 1. Mean volumes (± SD given in parentheses) of the GRC olfactory bulb (OB), olfactory bulb and stria combined (OBC) and whole brain (WB) in cubic centimeters and their ratios (%).

VOLUMES (cm^3)			RATIOS (%)	
OB	OBC	WB	OB: WB	OBC: WB
0.06 (0.008)	0.14 (0.05)	11.14 (0.72)	0.55	1.26

Table 2. Linear measurements (± SD given in parenthesis) of GRC olfactory brain structures and their ratios (%) with respect to cerebral hemispheres. OB stands for olfactory bulb, OBC- olfactory bulb & stria combined and CH- cerebral hemisphere.

LENGTH (mm)			BREADTH (mm)		
OBC	CH	Ratio (%)	OB	CH	Ratio (%)
23.51 (1.23)	32.55 (1.86)	72.23	5.56 (0.81)	16.17 (1.54)	34.38

In Table 3, respective values for olfactory epithelial height and axon bundle diameter were 76.3 ± 5.4 and 70.6 ± 8.6 µm, whereas volume fractions of Bowman's glands and axon bundles were 49.7 ± 5.1 and 31.2 ± 4.4 % respectively.

GRC data on lengths, breadths and volumes of olfactory structures with respect to the whole brain (in ratios %) are compared with those obtained earlier in other species in Table 4.

Table 3. Mean values (± SD given in parenthesis) for olfactory epithelial thickness and axon bundle diameter (in µm) and volume fractions (%) of Bowman's glands and axon bundles in the GRC.

MEASUREMENTS (µm)		VOLUME FRACTIONS (%)	
Epithelial thickness	Bundle diameter	Bowman's glands	Axon bundles
76.3 (5.4)	70.6 (8.6)	49.7 (5.1)	31.2 (4.4)

Table 4. Comparison of GRC brain morphometric parameters (ratios %) with those recorded earlier in the rufous sengi (Kavoi and Kisipan, 2019) and in the dog, goat and humans (Kavoi and Jameela, 2011). OBS, CH and WB denote olfactory brain components, cerebral hemisphere and whole brain, respectively.

RATIOS (%)	GRC	SENGI	DOG	GOAT	HUMAN
OBC: CH length	72.23	58.08	72.30	51.87	21.47
OB: CH breadth	34.38	28.97	42.91	29.73	8.94
OB: WB volume	0.55	0.44	0.31	0.18	0.01
OBC: WB volume	1.26	1.03	1.95	0.77	0.03

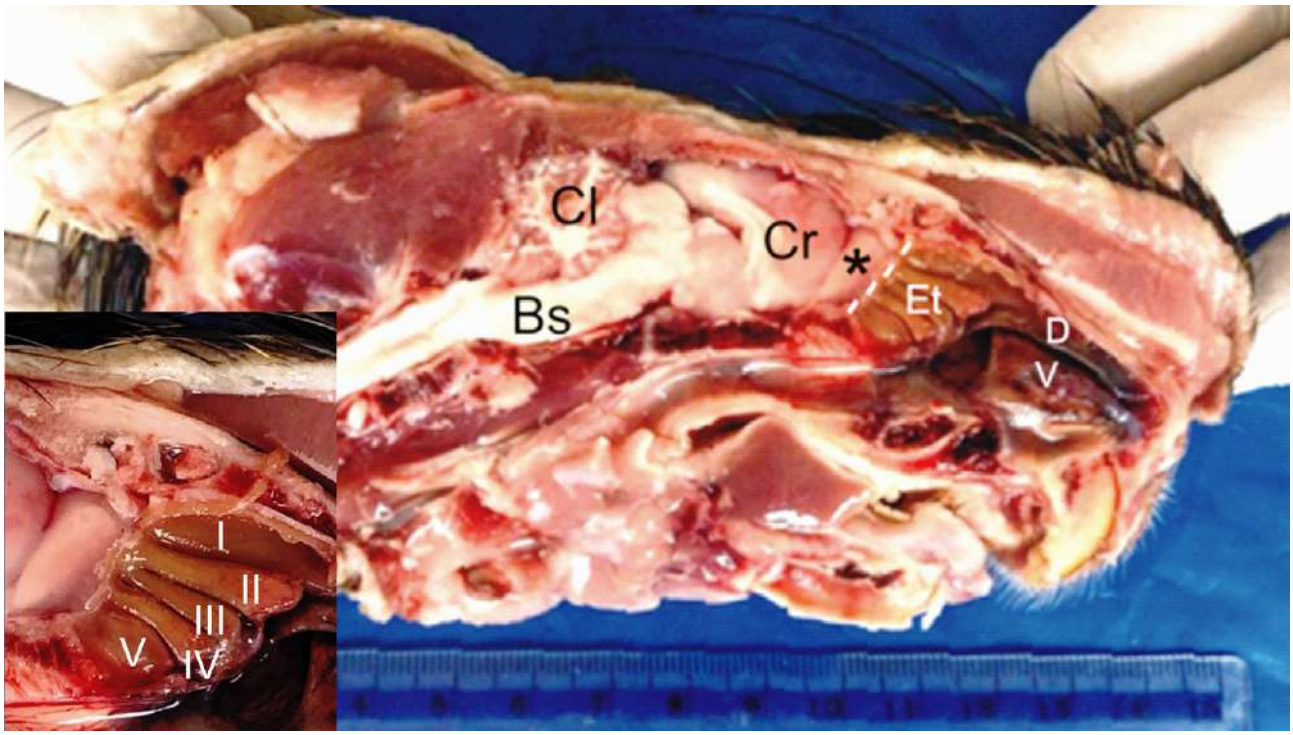

Fig. 3.- Macrograph of the left side of split head of GRC showing the location of the ethmoturbinates (Et) onto which the olfactory mucosa lies. The turbinates (inset) occur in a set of five and are cylindrical in shape. Cr- stand for cerebrum, Cl- cerebellum, Bs- brain stem, D- dorsal nasal concha, V- ventral nasal concha and (*)- olfactory bulb.

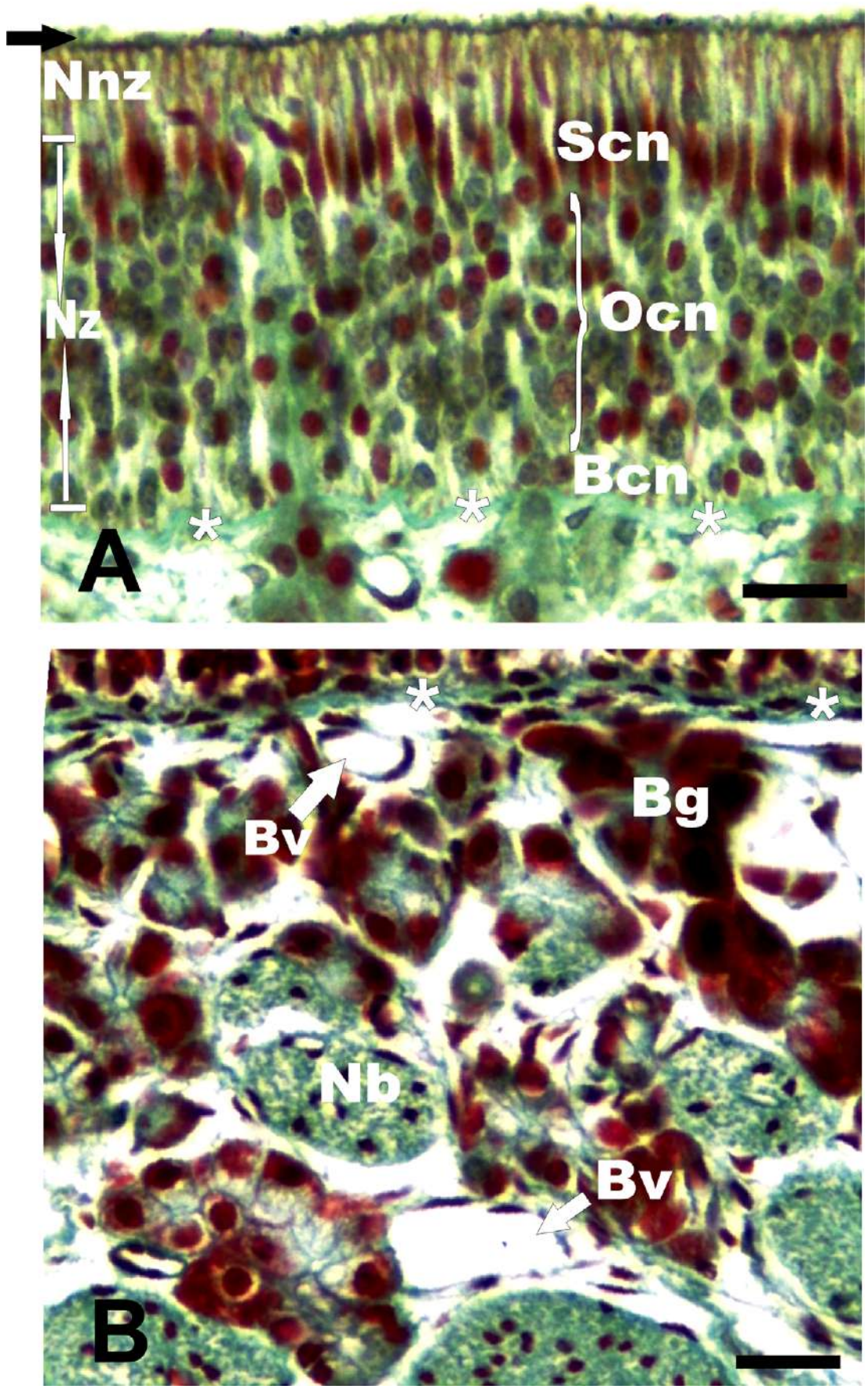

Fig. 4.- Light micrographs of the GRC olfactory mucosa. **A:** the epithelium is constituted by a nuclear zone (NZ), a non-nuclear zone (Nnz) and a mucociliary complex (arrow). The NZ has three regions: an upper region of elongated supporting cell nuclei (Scn), a middle region of olfactory cell nuclei (Ocn) and lower row of basal cell nuclei (Bcn) located just above the basement membrane (asterisks). **B:** the lamina propria containing tubuloacinar Bowman's glands (Bg), olfactory nerve axon bundles (Nb) and blood vessels (Bv), with the bundles taking a deeper position than the glands. A- H&E stain, B- Masson's trichrome stain. Scale bar = 20 µm in A, B.

DISCUSSION

GRCs are African hystricognath rodents prevalent throughout sub-Saharan Africa (Ibitoye et al., 2019). In West African countries, GRC flesh is very popular for domestic consumers, and as such GRCs are currently being captured from the wild for breeding as minilivestock and research models (Ibe et al., 2017). Indeed, GRC domestication has significantly impacted on the livelihood of rural communities in West Africa (Adu, 2002; Adedapo and Adekunle, 2013). This study explores the anatomy of structures of the GRC olfactory system in an effort to understand the adaptive physiology of the animal. The olfactory system is the epitome of communication, playing a critical role in the regulation of social, sexual, maternal and feeding behaviors in most mammals (Mota-Rojas et al., 2018). Olfaction first occurs in the cilia of the olfactory neurons in the mammalian nasal cavity and the generated signals are then transmitted to the olfactory cortex via synaptic connections with downstream neurons in the olfactory bulb (Field et al., 2003). To the best of our knowledge, this is the first study to describe and quantify anatomical features of the olfactory system in the GRC.

At the caudal roof of GRC nasal cavity, the OM covers a set of five cylindrical-shaped ethmoturbinates. Although the number of the ethmoturbinates did not differ much from that of other mammals, the complexity, shape and orientation varied from that of some mammals. In dogs (Kavoi et al., 2010), the ethmoturbinates form prominent lamellar folds that serve to elaborate the surface area covered by the OM, whereas in the naked mole rat (Onyono et al., 2017) the turbinates are less complex, and present tongue- and flap-like shapes. In the root rat (Onyono et al., 2017), the turbinates are highly branched and quite extensive, occupying dorsomedial, medial and lateral surfaces of the nasal cavity. Although assessment of olfactory acuity would best be based on finer structural details such as packing densities of olfactory cells and cilia numbers per olfactory neuron (Kavoi et al., 2010, 2012), the size and degree of folding of the olfactory area are considered important indicators of olfactory capability (Pihlström et al., 2005).

Histologically, cell arrangement in the GRC OM epithelium takes the usual mammalian pattern in which basal cell are placed lowermost, followed by olfactory cells and then supporting cells. The thickness of the GRC OM epithelium was estimated at 76.3 µm, a value that was higher than that recorded in rats (genus rattus) (Sakashita et al., 1995), rufous sengi (Kavoi, 2018), sheep and dogs (Kavoi et al., 2010), but lower when compared to rabbits (Kavoi et al., 2012), root rats and mole rats (Onyono et al., 2017). Within the lamina propria of the OM, volume fraction of axon bundles was 31.2%, a value that was less than that reported in the rabbit (Kavoi et al., 2012). Olfactory sensitivity has been shown to increase with increasing OM epithelial thickness (Raimund et al., 1991) and axon bundles size (Van Drongelen et al., 1978). We therefore presume that the above differences in morphometric values signify variations in odor detection abilities vis-à-vis olfaction needs and ecological adaptations among species.

Parameters of specific brain parts show differences that reflect functional requirements between and within species (Kaas and Collins, 2001). On the GRC brain, linear dimensions and volumes of OBCs were determined and correlated with those of the cerebrum and the entire brain. The ratios of OBC to that of the cerebrum in regard to length and breadth was 72.23 and 34.38% respectively. These values exceed those previously reported in the rufous sengi (Kavoi and Kisipan, 2019), human and goat (Kavoi and Jameela, 2011) but are less than in the dog (Kavoi and Jameela, 2011). Regarding volume, the GRC OB: brain and OBC: brain volume ratios were greater than in all the above-mentioned species except for the dog (Kavoi and Jameela, 2011) in which the ratio was greater. Kaas (2000) attributes changes in parameters of certain brain parts to the number of neurons, the size of such neurons and/or their connectivity and, indeed, Haehner et al. (2008) showed OB volume to increase with olfaction ability.

In conclusion, results of this work show the GRC to have an olfactory system whose structural design is much more sophisticated/better

specialized than that of many other mammals. The OM and OBS in this species are refined, both quantitatively and qualitatively, to levels that appear to correspond to olfaction needs pertaining to their behavior and ecology. As GRCs continue to receive more and more attention during domestication and use as research models, more anatomical work will be required to contribute to the understanding of the morpho-functional dynamics of its various organ systems. It is hoped that results of this investigation constitute a significant addition to the available database on the GRC anatomy. Moreover, data obtained here may find application in the broader areas of comparative anatomy and wildlife behavior. Future works should analyze the GRC olfactory system for ultrastructural characteristics.

ACKNOWLEDGEMENTS

We thank the Department of Animal Science, University of Ghana, for providing the GRCs for this work. Laboratory space, equipment and chemicals were made available by the School of Veterinary Medicine, University of Ghana, and also the Departments of Human Anatomy and Veterinary Anatomy and Physiology, University of Nairobi. Messrs. Derrick Asare, Kingsley Amoako and Ephraim Yawson helped in tissue harvesting.

REFERENCES

ADEDAPO A, ADEKUNLE A (2013) Economic aspects of grasscutter farming in Southwest Nigeria: Implications for sustainable adoption and conservation. *IJSER*, 4: 17-23.

ADU EK (2002) Research on grasscutter production in Ghana. In: Atta-Agyepong K, Weidinger R (eds). Proceedings of a Workshop on Promoting Grasscutter Production for Poverty Reduction in Ghana (16-18 October, 2002), Sunyani, Ghana.

ADU EK, YEBOAH S (2003) On the use of perineal stain as an index of sexual maturity and breeding condition in the male greater cane rat (*Thryonomys swinderianus*, Temminck). *Trop Anim Health Prod*, 35: 433-439.

AJAYI IE, OJO SA, ONYEANUSI BI, GEORGE BDJ, AYO JO, SALAMI SO, IBE CS (2011) Gross observations and morphometry of the medulla oblongata of the African grasscutter (*Thryonomys swinderianus*). *Vet Rec, 4*: 5-8.

ALERS JC, KRIJTENBERG PJ, VISSERS KJ, VAN DEKKEN H (1999) Effect of bone decalcification procedures on DNA in situ hybridization and comparative genomic hybridization: EDTA is highly preferable to a routinely used acid decalcifier. *J Histochem Cytochem*, 47: 703-710.

ASIBEY EOA (1974) The grasscutter (*Thryonomys swinderianus* Temminck) in Ghana. *Symp Zool Soc Lond*, 34: 161-170.

AYDIN A, YILMAZ S, OZKAN ZE, ILGUN R (2008) Morphological investigations on the circulus arteriosus cerebri in mole-rats (*Spalax Leucodon*). *Anat Histol Embryol*, 37: 219-222.

BYANET O, DZENDA T (2014) Quantitative biometry of body and brain in the Grasscutter (*Thryonomys swinderianus*) and African giant rat (*Cricetomys gambianus*): encephalization quotient implication. *Res Neurosci*, 3: 1-6.

BYANET O, ONYEANUSI BI, IBRAHIM NDG (2009) Sexual dimorphism with respect to the macro-morphometric investigations of the forebrain and cerebellum of the grasscutter (*Thryonomys swinderianus*). *Int J Morphol*, 27: 361-365.

FA JE, JUSTE J, BURN RW, BROAD G (2002) Bushmeat consumption of two ethnic groups in Bioko Island, West Africa. *Hum Ecol*, 30: 397-416.

FIELD PM, LI Y, RAISMAN G (2003) Ensheathment of the olfactory nerves in the adult rat. *J Neurocytol*, 32: 317-324.

HAEHNER A., RODEWALD A, GERBER JC, HUMMEL T (2008) Correlation of olfactory function with changes in the volume of the human olfactory bulb. *Arch Otolaryngol Head Neck Surg*, 134: 621-624.

IBE CS, IKPEGBU E, NZALAK O (2017) Relationship between age and brain stem allometry in the African grasscutter (*Thryonomys swinderianus* Temminck, 1827). *J S Afr Vet Assoc*, Vol 88.

IBITOYE O, KOLEJO O, AKINYEMI G (2019) Burgeoning and domestication of grasscutter (*Thryonomys swinderianus*) in a post-Ebola era: A reassessment of its prospects and challenges in Nigeria. *World Sci News*, 130: 216-237.

JORI F, CHARDONNET P (2001) Cane rat farming in Gabon. Status and Perspective. Proceedings of the 5th International Wildlife Ranching Symposium. Pretoria, South Africa, pp 33-51.

JORI F, COOPER JE, CASAL J (2001) Postmortem findings in captive cane rats (*Thryonomys swinderianus*) in Gabon. Vet. Rec, 148: 624-628.

KAAS JH (2000) Why is brain size so important: design problems and solutions as neocortex gets bigger or smaller. *Brain Mind*, 1: 7-23.

KAAS JH, COLLINS CE (2001) Evolving ideas of brain evolution. *Nature*, 411: 141-142.

KARIKARI PK, NYAMEASEM JK (2009) Productive performance and carcass characteristics of captive grasscutters (Thryonomys swinderianus) fed concentrate diets containing varying levels of guinea grass. *World Appl Sci J*, 6: 557-563.

KAVOI BM (2018) Light and scanning electron microscopy of the olfactory mucosa in the rufous sengi (*Elephantulus rufescens*). *Anat Histol Embryol*, 47:167-173.

KAVOI BM, JAMEELA H (2011) Comparative morphometry of the olfactory bulb, tract and stria in the human, dog and goat. *Int J Morphol*, 29: 939-946.

KAVOI BM, KISIPAN ML (2019) A gross morphometric study of olfactory brain components in the Rufous Sengi (*Elephantulus rufescens*). *Int J Morphol*, 37: 1003-1007.

KAVOI B, MAKANYA A, HASSANALI J, CARLSSON HE, KIAMA S (2010) Comparative functional structure of the olfactory mucosa in the domestic dog and sheep. *Ann Anat*, 192: 329-337.

KAVOI BM, MAKANYA AN, PLENDL J, KIAMA SG (2012) Morphofunctional adaptations of the olfactory mucosa in postnatally developing rabbits. *Anat Rec*, 295: 1352-1363.

MATTHEWS J (2008) The Value of Grasscutters. *World Ark*, (January-February, 2008), pp 23-24.

MOTA-ROJAS D, ORIHUELA A, NAPOLITANO F, MORA-MEDINA P, OROZCO-GREGORIO H, ALONSO-SPILSBURY M (2018) Invited review: Olfaction in animal behaviour and welfare. *CAB Rev*, 13: 1-13.

ONYONO PN, KAVOI BM, KIAMA SG, MAKANYA AN (2017) Functional morphology of the olfactory mucosa and olfactory bulb in fossorial rodents: The East African root rat (Tachyoryctes splendens) and the naked mole rat (Heterocephalus glaber). *Tissue Cell*, 49: 612-621.

OPARA MN (2010) The Grasscutter I: A livestock of tomorrow. *Res J For*, 4: 119-135.

PIHLSTRÖM H, FORTELIUS M, HEMILÄ S, FORSMAN R, REUTER T (2005) Scaling of mammalian ethmoid bones can predict olfactory organ size and performance. *Proc R Soc B*, 272: 957-962.

RAIMUND A, DIETER R, BURTON MS (1991) Ontogenetic changes in odor sensitivity, olfactory receptor area and olfactory receptor density in the rat. *Chem Senses*, 16: 209-218.

ROSEVEAR DR (1969) The Rodents of West Africa. British Museum Publications, London.

SAKASHITA H, MORIIZUMI T, ITO M, FURUKAWA M, KAWANO J OKOYAMA S, KITAO Y, KUDO M (1995) Differentiation of the olfactory epithelium during development. *Acta Otorrinolaringol*, 115: 93-98.

SCHERLE W (1970) A simple method for volumetry of organs in quantitative stereology. *Mikroskopie*, 26: 57-60.

VAN DRONGELEN W, HOLLEY A, DOVING KB (1978) Convergence in the olfactory system: Quantitative aspects of odor sensitivity. *J Theor Biol*, 71: 39-48.

WILLIAMS OS, OLA SI, BOLADURO BA, BADMUS RT (2011) Diurnal variation in ambient temperature and humidity in a pit pen grass-cutter (Thryonomys swinderianus) house in Ile-Ife. Proceedings of 36th Annual Conference Nigerian Society for Animal Production. *Abuja, Nigeria*, pp 111-113.

WOODS CA, KILPATRICK CW (2005) Infraorder Hystricognathi Brandt, 1855. In: Wilson DE, Reeder DM (eds). Ma*mmal Species of the World: a Taxonomic and Geographic Reference, 3rd ed.* The Johns Hopkins University Press, Baltimore, pp 1538-1600.

Anatomy knowledge retention in Australian osteopathic training: A comparative study

Raymond Blaich[1,2], Nalini Pather[3], Tania Prvan[4], Roger Engel[1], Anneliese Hulme[3], Goran Strkalj[3]

[1] Department of Chiropractic, Faculty of Medicine, Health and Human Sciences', Macquarie University, Sydney, Australia
[2] School of Health and Human Sciences, Southern Cross University, Lismore, New South Wales, Australia
[3] Department of Anatomy, School of Medical Sciences, Faculty of Medicine, University of New South Wales, Sydney, Australia
[4] Department of Mathematics and Statistics, Faculty of Science and Engineering, Macquarie University, Sydney, Australia

SUMMARY

Anatomy knowledge retention is an important consideration in the training of health professionals. In this study, musculoskeletal anatomy knowledge retention was measured in students enrolled in the osteopathic programs at Southern Cross University, Australia. The double-degree osteopathic program has recently undergone curriculum change from five years to four years. Anatomy knowledge in the final-year students of the four-year program was compared to final-year students in the five-year program. Anatomy knowledge amongst the final-year students was also compared to osteopathic practitioners. To measure anatomy knowledge, a test consisting of 20 multiple-choice questions was used, with ten low-order and ten high-order questions, based on the Blooming Anatomy Tool. Students enrolled in the osteopathic program were invited to participate. A total of 92 students participated from a total of 106 students (student response rate of 86.8%). 118 osteopathic practitioners (osteopaths) completed the anatomy knowledge test from a possible 2,546 Australian osteopaths (response rate 4.6%). Retrospective data of anatomy knowledge retention amongst chiropractic students enrolled at Macquarie University, Australia was used to compare with the osteopathic students. There were no differences in the measured level of anatomy knowledge in both low-order and high-order questions between osteopathic students and osteopaths. There were no differences in the measured level of anatomy knowledge in both low-order and high-order questions between senior (fourth-year) students in the four-year program and senior (fifth-year) students in the five-year osteopathic program. The results from this study indicate there is a consistent level of anatomy knowledge retention among osteopathic students and practitioners.

Key words: Gross anatomy education – Knowledge retention – Osteopathic education – Medical education – Musculoskeletal anatomy – Anatomy curriculum

ABBREVIATIONS

Anatomy knowledge retention (AKR)

Australian Osteopathic Accreditation Council (AOAC)

Bachelor of Clinical Sciences (BClinSc)

Basic Competency Examination (BCE)

Corresponding author:
Raymond Blaich. The School of Health and Human Sciences, Southern Cross University, PO Box 157 Lismore, New South Wales, 2480, Australia. E-mail: raymond.blaich@scu.edu.au

Submitted: January 9, 2021. **Accepted:** February 1, 2021

Master of Osteopathic Medicine (MOM)

Musculoskeletal (MSK)

Progress Test in Medicine (PTM)

Southern Cross University (SCU)

Macquarie University (MU)

Low-Order (LO)

High-Order (HO)

INTRODUCTION

Anatomy has long been considered an essential foundation in the training of medical and health practitioners (Turney, 2007, Louw et al., 2009; Ahmed et al., 2010; Diaz-Mancha et al., 2016; Estai & Bunt, 2016; Dayal et al., 2017; Losco et al., 2017; Farey et al.,2018; Blaich et al., 2019). The study of anatomy aids in preparing students for clinical practice (Sugard et al., 2010; Valenza, 2012) not only through teaching about the structures of the human body, but also in the development of non-traditional discipline-independent skills (Rizzolo, 2010; Lachman and Pawlina, 2006; Strkalj, 2014; Evans et al., 2018; Hildebrandt, 2019). These skills include professionalism, time-management, empathy, teamwork, and respect for the patient (Swartz, 2006; Bockers et al., 2010; Talarico, 2010; White et al., 2011; Talarico, 2012).

In health profession programs, anatomy education is predominantly delivered in the first two years of training. In these early years, biomedical sciences dominate the curricula, giving way to more clinically oriented disciplines later in the program (Strkalj, et al., 2011; Nabil et al., 2014; McBride and Drake, 2018; Giuriato, et al., 2019; Arantes et al., 2020; Lufler et al., 2020). This type of delivery leads to a time interval between the initial acquisition of biomedical knowledge such as anatomy and the clinical application of that knowledge (Lufler et al., 2020). Anatomy knowledge retention (AKR) is therefore an important factor to consider when designing programs for health professional education.

AKR is a complex domain. Numerous studies have demonstrated anatomy knowledge attrition (i.e., a decrease in anatomy knowledge) in the latter stages of health profession programs (Feigin et al., 2002; Prince et al., 2005; Feigin et al., 2007; Lazarus et al., 2012; Jurjus et al., 2014; Brunk et al., 2017; Farey et al., 2018; Lufler et al., 2020). However, others have shown an increase in AKR as students' progress through their programs (Humphreys et al., 2007; Hulme et al., 2019).

With recent significant changes in the content and delivery of anatomy within medical and health professions education (McBride and Drake, 2016; Day et al., 2018; Lufler et al., 2020), concerns have been raised about the level of AKR of students as they graduate and move into clinical practice (McKeown et al., 2003; Prince et al., 2005; Humphreys et al., 2007; Ahmed et al., 2010; Bergmann et al., 2011; Strkalj et al., 2011; Jurjus et al., 2014; Meyer et al., 2015; Doomernik et al., 2017). These concerns extend to a broad range of health professions, including chiropractic (Stkalj et al., 2011), podiatry (Diaz-Mancha et al., 2016), optometry (Backhouse et al., 2019), and nursing (Narnaware and Neumeier, 2020).

In addition, other factors that can influence AKR such as vertical integration of anatomy knowledge within curricula (Bergman et al., 2011; Parmar and Rathinam, 2011; Bergman et al., 2014), composition of assessments (Blunt and Blizzard, 1975; Feigin et al., 2002; Feigin et al., 2007; Jurjus et al., 2016), anatomy curricula requiring specific clinical context (D'Eon et al., 2006; Kerfoot et al., 2007; Custers, 2010; Dobson and Linderholm, 2015; Karpicke and Blunt, 2011; Karpicke, 2012; Smith et al., 2016; Dobson et al., 2017; Dayal et al., 2017; Williams and Mann, 2017; Castillo et al., 2018; Farey et al., 2018) and their cumulative effect on AKR have not been fully explored.

Assessing the effect of these factors is important for designing strategies to improve AKR. Different assessment tools have been used to assess AKR. These include the Progress Test in Medicine (PTM) (Brunk et al., 2017), the Basic Competency Examination (BCE) (Freedman and Bernstein, 1998; Childs, et al., 2005; Stockard and Allen, 2006), the carpal and tarsal bone tests (Valenza et al., 2012; Diaz-Mancha et al., 2016), and Bloom's taxonomy-ordered multiple-choice questions (Hulme et al., 2019). While these studies produced valuable results in AKR assessment of different student cohorts, the use of different assessment tools hampered the comparison of AKR across

disciplines and pedagogies. However, using the same AKR assessment tool on students from different discipline programs, and different educational institutions, demonstrated differences in levels of anatomy knowledge at similar stages of progression (Wass et al., 2001; Humphreys et al., 2007; Valenza et al., 2012; Brunk et al., 2016; Daiz-Mancha et al., 2016). This suggests that anatomy education within the health professions is a complex issue and that AKR may be dependent on both the anatomical region studied and the perceived importance of that anatomical region to the specific health discipline.

Studies focusing on AKR in medical (McKeown et al., 2003; Valenza et al., 2012; Nabil et al., 2014), physical therapy (Diaz-Muncha et al., 2016; Parmar and Rathinam, 2011; Valenza et al., 2012), podiatry (Castillo-Lopez et al., 2014), nursing (Zieber and Sedgewick, 2918; Narnaware and Neumeier, 2020), occupational therapy (Parmar and Rathinam, 2011), chiropractic (Strkalj et al., 2011), and osteopathic students (Stockard and Allen, 2006) did not compare levels of AKR with clinicians. Other studies focused on AKR in just clinicians such as medical practitioners (Spielmann and Oliver, 2005; Custers and Cute, 2011; Roche et al., 2011; Farey et al., 2018) and optometrists (Bakkum and Trachimowicz, 2015). These latter studies demonstrated that attrition of anatomy knowledge increased with time since graduation (Spielmann and Oliver, 2005; Custers and Cute, 2011; Bakkum and Trachimowicz, 2015). However, to date there has been only one investigation into AKR of musculoskeletal (MSK) anatomy in osteopathic students (Stockard and Allen, 2006), and no study of AKR in osteopathic practitioners within an Australian context.

This study had two aims. The first aim was to provide a preliminary assessment of musculoskeletal anatomy knowledge in the final-year osteopathic students at an Australian tertiary university, and thus their preparedness (in terms of anatomy knowledge) to enter the workforce. This was achieved through the comparison of the results of anatomy tests (focusing on the anatomy of limbs at two different cognitive levels) completed by the final-year osteopathic students and a sample of practicing osteopaths. In addition, test results of the final year students were compared with those of the final year chiropractic students from Macquarie University (MU). This comparison was considered valid because of the similarities between the two health professions, both focusing on musculoskeletal disorders and relying on manual therapy. The second aim was to assess anatomy knowledge of the final year students in two osteopathic programs, the old five-year program and the new four-year program.

MATERIALS AND METHODS

Student data was collected from students enrolled in the Master of Osteopathic Medicine (MOM) degree at Southern Cross University (SCU) in Lismore, New South Wales, Australia. Data were collected from osteopathic practitioners via an online discussion forum. The osteopathic program at SCU is a double-degree program consisting of an undergraduate Bachelor of Clinical Sciences (BClinSc) and a postgraduate MOM. Students must successfully complete both degrees to register as an osteopath in Australia. Both degrees are accredited with the Australian Osteopathic Accreditation Council (AOAC, 2020), the body responsible for osteopathic education accreditation in Australia.

The osteopathic program at SCU has recently undergone curriculum change through which duration to complete the double-degree program decreased from five to four years effectively reducing the MOM from two years to one year. The new, revised BClinSc degree remained three years in duration. The first student intake into the new four-year program commenced in February 2017. The main curriculum change in the new integrated program is that education is delivered and assessed within a clinically-oriented context with greater emphasis on evidence-based practice. The change included streamlining delivery to remove repetitious content, thereby improving the overall integration of the curriculum. This included the anatomical curriculum.

Anatomy curriculum at Southern Cross University

The anatomy curriculum in the revised program includes several anatomy units (subjects or

courses) spread over two teaching sessions per year. The university has three 13-week teaching sessions per academic year). All units follow a common format and include face-to-face lectures (1 hour per week), tutorials (1 hour per week) and anatomy laboratory practical classes with prosected specimens (2 hours per week). The exception to this is the histology and embryology unit which does not have practical classes. Table 1 outlines the anatomy units in the old five-year and new four-year osteopathic programs at SCU.

Table 2 describes the content of each of the units listed in Table 1. In session 1 of year one in the new four-year program, there is a shared introductory unit covering the basic concepts of anatomy. Two osteopathic specific units (Osteopathic Science

Table 1. Anatomy curricula of the SCU osteopathic programs.

The 5-year osteopathic program (old program)				
	Teaching Session 1 Units		**Teaching Session 2 Units**	
Year	**Unit Code**	**Unit title**	**Unit Code**	**Unit title**
1	BIO01302	Human Anatomy *	BIO00209	Biomechanics & Kinesiology *
	BIO00207	Mechanics for Movement *	SCI10473	Histology & Embryology *
2	SCI10475	Neuroscience *		
	SCI10474	Advanced Visceral Anatomy		
The 4-year osteopathic program (new program)				
1	BIO01302	Human Anatomy *	OST71005	Osteopathic Science 1
2	OST71006	Osteopathic Science 2		
	SCI10475	Neuroscience *		

*= shared unit. i.e. common unit for several health science programs including Osteopathy.

Table 2. Anatomy syllabi of the SCU units.

The 5-year osteopathic program (Old program)	
Unit title	**Unit description**
Human Anatomy*	Introductory anatomy
Mechanics for Movement	MSK gross anatomy
Biomechanics & Kinesiology	MSK gross anatomy
Histology & Embryology	Microscopic anatomy Developmental anatomy
Neuroscience*	Neuroanatomy
Advanced Visceral Anatomy	Visceral anatomy
The 4-year osteopathic program (New program)	
Unit title	**Unit description**
Human Anatomy*	Introductory anatomy
Osteopathic Science 1	MSK gross anatomy Spinal gross anatomy
Osteopathic Science 2	MSK gross anatomy Pectoral girdle Upper extremity Cranial anatomy Pelvic girdle Lower extremity
Neuroscience*	Neuroanatomy

*: Units common to both the old five-year and new four-year programs.
MSK: musculoskeletal anatomy

1 and Osteopathic Science 2) are delivered in session 2 of year 1 and session 1 of year 2. These units include an in-depth study of the functional, clinical and biomechanical anatomy of each anatomical region. Osteopathic Science 1 covers the vertebral column (axial skeleton), and visceral anatomy while Osteopathic Science 2 covers the pectoral girdle and upper limb, pelvic girdle, lower limb, and the cranium. Student learning is supported by online resources delivered via the Blackboard learning management system (Blackboard Inc. Version 3.9.2). Students can access these online resources at any time and are used for both summative and formative assessment activities.

Participant Population

Participants in this study were the senior osteopathic students (both fifth-year students in the old five-year program and fourth-year students in the new four-year program) in the osteopathic programs at SCU and osteopathic practitioners working in private practice. Student data was collected from students enrolled in the MOM at SCU in Lismore, Australia. Eligible students were invited to participate during scheduled classes. Introducing the new four-year course while the old five-year course was being 'taught out' meant that there were two cohorts of students studying the same material at different stages of their respective courses. Table 3 details the different student cohorts and the stage of their respective programs.

Data were collected from osteopathic practitioners via two avenues: an online discussion forum, and direct paper-based. Collected data included age, gender, and year of graduation. Online osteopathic practitioners were recruited Australia-wide via an online forum. This online forum was sponsored by Osteopathy Australia, the osteopathic profession's peak professional body. For the direct approach, ten osteopathic practitioners attending a local osteopathic educational meeting, were invited to participate.

The Test Instrument

To measure anatomy knowledge, a 20-question test instrument in a multiple-choice format was used that assessed knowledge of musculoskeletal (MSK) anatomy of the upper and lower limbs. This instrument had originally been developed and validated to assess the MSK anatomical knowledge of chiropractic students at Macquarie University in Sydney, Australia (Hulme et al., 2019). The test consisted of two components: 10 lower cognitive order (Low-order LO) questions requiring simple recall of anatomical detail; and 10 higher cognitive order (High-order HO) questions requiring analysis, application and integration of anatomy knowledge as it pertained to a clinical setting. The LO and the HO questions were evenly distributed throughout the test to improve compliance by avoiding participants' becoming discouraged when encountering more difficult questions (HO) mid-test. The classification into two cognitive orders was based on the Blooming Anatomy Tool, a set of discipline specific criteria utilising Bloom's Taxonomy that classifies cognitive levels of anatomy knowledge for multiple-choice questions (Anderson et al., 2001; Thompson and O'Loughlin, 2015; Morton et al., 2017; Day, 2018). Students were given the opportunity to participate in class with no prior warning to prevent biasing the results through pre-test preparation. Participating students were asked to keep the test questions confidential from other students. All data were de-identified.

Participant recruitment and Data collection

Student data were collected near the end of the 2020 academic year (November). Fourth- and fifth year-students were invited to participate during one

Table 3. Student cohort in new 4-year program & the old 5-year program.

Academic Year	Year 2	Year 3	Year 4	Year 5
2018	New 4-year course	Old 5-year course	Nil	Nil
2019	New 4-year course	New 4-year course	Old 5 -year course	Nil
2020	Nil	New 4-year course	New 4-year course	Old 5-year course

of their final classes for the year. They were informed that the test was not a summative assessment and did not count towards their final grade in the unit. Students were provided with a written copy of the test and given 20 minutes to complete it.

Osteopathic practitioners asked to participate in this study were recruited by both direct and indirect means. Direct means involved contact with the chief investigator at a local osteopathic educational gathering in 2019. Practitioners were invited to participate and provided with a hard copy of the test if they agreed to participate and provide consent. The indirect approach involved inviting practitioners to participate via an online discussion forum run by the national osteopathic association in 2020. Participation was voluntary and anonymous. There was no personal identification information collected from any of the participants as part of this study.

Statistical Analysis

Data were recorded and collated using MS Excel (Microsoft Corporation, version 16, 2016). All statistical calculations were performed using Statistical Package for Social Sciences (SPSS), version 23 (IBM Corp, Armonk, NY). Descriptive data, including means and standard deviations were calculated where appropriate. Mean scores were calculated for the correct number of low-order, high-order and total questions answered. Data were compared using paired t-tests. A p-value of less than 0.005 was considered statistically significant (i.e., using 0.5 % significance) for all analysis.

Ethics Approval

Ethics approval to collect data for this study was provided by two Human Research Ethics Committees (HRECs): Southern Cross University (approval number: ECN-14-242) and Macquarie University (Reference number: 52020907722092).

RESULTS

Participants

In total, 224 participants completed the questionnaires (106 students and 118 practitioners). For the students, this represented an 86.8% response rate (Table 4). According to the Australian Health Practitioner Regulation Agency (AHPRA), there were 2,546 registered osteopathic practitioners in Australia as of 30th of June 2018 (OBA, 2020). A total of 118 practitioners completed the questionnaire: 111 online and 7 paper-based, representing a response rate of 4.6% (118/2546).

Comparison of knowledge retention of students and practitioners

To ascertain whether there were differences between anatomy knowledge of osteopathic students, osteopathic practitioners, and chiropractic students at a different institution, knowledge retention was assessed using LO and HO questions. Using the independent-samples median test, scores were compared for the following (Tables 5 and 6):

1. Final-year osteopathic students in 2020: Year-four and Year-five.
2. Final-year osteopathic students in 2020 and osteopathic practitioners.
3. Year-5 final-year osteopathic students at SCU to Year-5 final-year chiropractic students at Macquarie University (MU).

Retrospective comparisons were also made with previous data of AKR among chiropractic students (Hulme et al., 2019) and compared with SCU students.

There were no differences between the fifth-year osteopathic students and fifth-year chiropractic students. All other comparisons revealed no differences in scores (LO, HO or total: LO + HO).

Age & Gender differences

There were no gender differences in any of the participant populations. There was a difference in the mean age of practitioners compared to both student groups (year 2 and year 5). While this is not surprising given, a practitioner in Australia would have to be of post-graduate age.

DISCUSSION

A major objective of educating health practitioners is the development of a sound knowledge -base which can be readily applied,

integrated and synthesised to a clinical setting. The measurement of AKR can be used as a way of assessing whether this educational objective has been achieved. This study evaluated AKR in osteopathic students and osteopathic practitioners. The results demonstrated little attrition of knowledge amongst students and practitioners. Comparison between osteopathic and chiropractic students at a similar stage in their programs showed there was a difference in AKR.

Anatomy knowledge and program length

There were no differences in student mean scores, between the shorter four-year program and the longer five -year program at SCU implying students appeared to be equally effective in learning anatomy over a shorter duration. These results are not surprising as the new SCU anatomy curriculum was designed to be vertically integrated. This is consistent with the findings from similar studies (McBride and Drake, 2016; Wilson et al., 2018; Hulme et al., 2019; Zhao et al., 2020) that measured anatomy knowledge in medical students enrolled in an integrated problem-based learning curriculum (McBride and Drake, 2016; Wilson et al., 2018; Zhao et al., 2020), and chiropractic students enrolled in a standard program (Hulme et al., 2019).

The results from the present study provide evidence that graduates of a four-year osteopathic program are as ready to enter the health care workforce as those from a five-year program, with respect to their knowledge of MSK anatomy. This conclusion supports the change to a shorter program at SCU.

Table 4. Study participants.

SCU Student groups			**Participants**	**Response Rates (%)**	**Mean age (years)**		
Program year	**Academic Year**	**Number of students enrolled**			**Mean**	**Median**	**SD**
5	2018	23	14	60.8	31.7	29.0	9.2
5	2019	27	25	92.6			
4	2020	24	24	100.0	32.0	33.3	8.4
5	2020	32	29	90.6	35.0	33.0	9.9
Total		106	92	86.8			
Practitioners							
Osteopathic Practitioners		Potential Participants*					
Online, remote	2018	2546	111	4.6	37.7	37.0	9.2
Paper-based	2018		7				
Total practitioners			118				

*= total number of Australian osteopathic practitioners registered with OBA 2018

Table 5. Summary of knowledge retention comparisons by group.

	Academic year			
	2018	**2019**	**2020**	**2020**
4th year students vs 5th year students			year 4 (n=24)	year 5 (n=29)
Osteopathic students vs Osteopathic practitioners	Practitioners (n=118)		year 4 (n= 24)	year 5 (n=29)
Osteopathic students vs Chiropractic students	year 5 (n=14)	year5 (n=25) *year 5 (n=44)	year 5 (n=29)	

* indicate chiropractic students from Macquarie University (raw data obtained from Hulme et al., 2019). All other students are from SCU.

Table 6. Summary of comparison of AKR in students and practitioners.

Cohorts	LO			HO			Total (LO + HO)		
	Mean (x/10)	SEM	SD	Mean (x/10)	SEM	SD	Mean (x/20)	SEM	SD
SCU Year 4 students	6.0	0.39	1.9	3.5	0.26	1.3	9.6	0.54	2.6
SCU Year 5 students	6.3	0.29	1.5	3.6	0.24	1.3	10.1	0.36	1.9
P values [a]	0.996			0.962			0.966		
SCU Year 4 students	6.00	0.39	1.9	3.5	0.26	1.3	9.6	0.54	2.6
SCU Year 5 students	6.31	0.29	1.5	3.6	0.24	1.3	10.0	0.36	1.9
Practitioners	6.10	0.19	2.1	4.4	0.13	1.4	10.6	0.28	3.0
P values [a]	0.671			0.089			0.494		
Practitioners < 10 years since graduation	6.12		2.1	4.2		1.26	10.33		2.76
Practitioners ≥ 10 years since graduation	6.25		2.2	4.6		1.59	10.88		3.30
P values [b]	0.744			0.111			0.340		
SCU Year 5 students	5.5		1.8	4.5		1.3	10.0		2.5
MU Year 5 students	5.5		1.7	4.4		2.0	9.9.		3.0
P values [c]	0.968			0.834			0.876		

[a] p values using Independent-Samples Median Test; [b] p values using Two sample t-tests; [c] p values using Two sample-t tests, appealed to Central Limit Theorem.
AKR= anatomy knowledge retention; SCU = Southern Cross University; MU = Macquarie University; * = significant difference ($p<0.0005$). LO: Low order; HO: High order

The results can be explained by the configuration of the new four-year program with its integrated curriculum where biomedical and clinical sciences are taught within a more clinically oriented context (Brauer et al., 2015; Johnston and Vaughan, 2020). Although there is still a predominance of biomedical sciences in the early years of the program followed by clinical learning in the later years (Craig et al., 2010; Talarico and Painter, 2020), the integrated approach includes clinical context for the content covered in the earlier years so as to enhance learner engagement and content retention (Erkonen et al., 1992; Norman, 2009; Bridges et al., 2016; Quintero et al., 2016; Farey et al., 2018).

AKR in osteopaths

It was expected that there would be difference in AKR between students and practitioners and that anatomy knowledge attrition would increase with length in time in practice (Bakkum and Trachomowicz, 2015). Surprisingly, there were no differences in AKR between osteopaths and senior students and no attrition of anatomy knowledge in osteopaths. The findings of the present study contradict findings from other studies that investigated AKR in health practitioners (Custers and Cate, 2011; Bakkum and Trachimowicz (2015). These studies demonstrated decreasing AKR over time. Bakkum and Trachimowicz (2015) studied knowledge of the microanatomy of the retina in fourth-year optometry students (n=35), optometry faculty members (n=41) and optometrists in private practice (n=96), and found a steady and consistent trend of knowledge attrition with years from graduation. The longer the private practice optometrists had been in practice, the less retinal layers they were able to correctly identify.

In a study of AKR in medical students (n= 25) and practicing doctors (n=25; junior doctors: n=15; senior doctors: n=10), the doctors were able to correctly identify more of the carpal bones compared to the medical students (Spielmann and Oliver, 2006). Furthermore, the senior doctors with more clinical experience performed better than the medical students and junior doctors. This is to be expected, although

caution is advised, as this study used a very small sample size and the carpal bones test is a crude and very limited measure of anatomy knowledge. A study also using the carpal bones test found similar results (i.e., poor AKR) in medical graduates (n=102) undertaking specialty-training in Accident & Emergency medicine, or trauma/orthopaedics (Roche et al., 2011).

The discrepancy in results from these studies and the present study can be explained by the different anatomy knowledge measurement tool used. The present study used the MSK anatomy knowledge test, which is a more comprehensive measurement of anatomy knowledge compared to the narrow carpal bone test, which is limited in its ability to measure anatomy knowledge.

Using a knowledge test covering a range of basic biomedical sciences including anatomy, physiology, biochemistry, and pathophysiology, a long-term study of medical students (n=65) and medical practitioners (n=75) reported better performances by students compared to practitioners with length in practice a contributing factor (Custers and Cate, 2011). Similarly, licensed physical therapists (n=182) scored better than physical therapy students on the BCE tool (Childs et al., 2005), supporting the concept that there is a difference between anatomical knowledge and clinical competency with that knowledge (Jassen et al., 2014). In an Australian study that also used the BCE to measure MSK knowledge in general practitioners (n=47) and orthopaedic interns (n=66), general practitioners scored higher (Broadhurst et al., 2002). These results are to be expected as the BCE assesses clinical management as well as MSK anatomy knowledge and general practitioners had experienced broader clinical management than the orthopaedic interns. Taken together the choice of test may be a factor in determining results in an AKR test and could explain the difference in results in the present study. The context of the curriculum and the emphasis placed on the learners' perception of the relevance of the anatomy being taught may also affect the level of AKR (Bergman et al., 2014).

Comparison between osteopathic and chiropractic students

As there are many similarities between the scope of practice of chiropractic and osteopathy, it was considered appropriate to compare AKR among students from the two professions. Both professions focus on the MSK system and related disorders and share a common reliance on manual therapy as an intervention. Data on AKR in chiropractic students at MU has been reported in the literature and was made available to the researchers (Hulme et al., 2019). Data from fifth-year chiropractic students at MU was compared to performances with fifth-year osteopathic students at SCU.

There were no differences in AKR between the fifth-year osteopathic and chiropractic students. It was anticipated that both fifth-year student cohorts would perform similarly in the AKR test, as these students were at the conclusion of their formal studies and about to enter the workforce as health practitioners.

Both programs included integrated curricula (Hulme et al., 2019) and both had received full accreditation by the relevant accrediting bodies. The difference in AKR in students could be attributed to the anatomy syllabus component of the new osteopathic (four-year) program.

Our findings are consistent with similar comparisons of AKR in students in other health professions. These include studies using the carpal bone test in fifth-year Australian chiropractic students (n=44), who did much better than second-year chiropractic students (n=47) (Meyer et al., 2015); fifth-year chiropractic students (n=84) who did much better than final-year medical students (Strkalj et al., 2011); and third-year Spanish physical therapy (PT) students (n= 54) who did better than third-year Spanish medical students (n=80) (Valenza et al. (2012). Contradicting these results, Dayal et al. (2017) found that first-year Australian physiotherapy students (n=129) were better at correctly identifying the carpal bones compared to their fourth-year (n=113) counterparts. In a study of Spanish podiatry students (first-years n=145 and fourth-years n=109), Castillo-Lopez et al. (2014)

found no difference in anatomy knowledge when using the tarsal bones test. These conflicting findings can be explained by the use of different tests, both of which are a narrow measure of AKR that is not indicative of other components of anatomy knowledge.

Limitations

It is important to state that AKR as measured in the present study does not equate to clinical competency. Even though HO questions were included, these questions do not give any indication of clinical competency. Measuring clinical competency is more complex than measuring AKR (Miller 1990; Wass et al., 2001). The format and nature of anatomy assessment can strongly influence anatomy learning and AKR (Logan et al., 2011; Bergman et al., 2014). This study did not include how anatomy was assessed within the programs, or the timing of anatomy assessments.

This study only measured AKR and did not investigate the factors which could influence AKR. Further studies should include focus groups with osteopathic students to discuss factors in anatomy learning that they consider important to improve AKR and better prepare them for clinical practice (Bergman et al., 2014; Farey et al., 2018). These factors could then be used by curricula planners to improve anatomy learning outcomes.

All data gathered as part of this study was cross-sectional in nature. Longitudinal data of AKR would provide more methodological rigour and validity. Measuring AKR in the same student cohorts at multiple time points would help to achieve this.

This study was not designed to be a comprehensive assessment of all AKR at a single educational institution (e.g., SCU). The test instrument used in this study was limited to only measuring MSK anatomy knowledge. Other aspects of the anatomy curriculum were not measured such as the sub-disciplines visceral anatomy, spinal anatomy, microanatomy (histology), developmental anatomy (embryology), neuroanatomy, and radiographic anatomy. Measuring what constitutes a passable or satisfactory mean test score, or what level of anatomy knowledge could be considered as ample for safe and effective osteopathic clinical practice were considered beyond the scope of this study and therefore not identified.

As participation in this study was voluntary and did not from part of the formal anatomy assessments, the number of participants in the various student cohorts may not be representative of the entire student cohort. As all data used in this study was obtained anonymously, it was not possible to measure an individual's performance over time with only mean scores used for comparisons. The small student sample sizes are a result of the small number of students enrolled in the osteopathic programs at SCU and could be considered a limitation with respect to the generalisability of these results.

The study also used a small number of MCQs as the knowledge retention assessment tool.

The theory-based MCQs are easy and quick to mark, eliminate potential bias, and increase inter-examiner reliability. This tool may not thoroughly assess anatomy knowledge and it is recommended that a more comprehensive set of questions be used in future studies in order to assess anatomy knowledge more thoroughly.

Future Directions

As these results may not be comparable with other educational institutions, further investigations could include conducting similar studies at other osteopathic educational institutions in Australia and overseas to validate these findings on a broader scale. Additionally, expanding the scope of assessments to include other parts of the anatomy curriculum, e.g., visceral anatomy, spinal anatomy, histology, embryology, and neuroanatomy, would improve our understanding of anatomy knowledge retention. To improve anatomy knowledge amongst students, others have suggested the addition of anatomy instructions where students revisit key anatomical concepts so as to improve their ability to transfer anatomy knowledge to a clinical setting (Lazarus et al., 2012; Jurjus et al., 2016).

CONCLUSION

There is a consistent level of anatomy knowledge retention among Australian osteopathic students and practitioners. Shortening the length of an osteopathic program does not appear to affect the level of musculoskeletal anatomy knowledge in graduating students in a vertically integrated curriculum. The results from the present study can assist in informing the development of a core anatomy curriculum for osteopathic education within the Australian context, and can also contribute to the standardisation of a minimum level of anatomy knowledge required for students entering clinical practice.

REFERENCES

AHMED K, ROWLAND S, PATEL V, KHAN RS, ASHRAFIAN H, DAVIES DC, DARZI A, ATHANASIOU T, PARASKEVA PA (2010) Is the structure of anatomy curriculum adequate for safe medical practice? *Surgeon,* 8(6): 318-324.

ANDERSON LW, KRATHWOHL DR, AIRASIAN PW, CRUIKSHANK KA, MAYER RE, PINTRICH PR, RATHS J, WITTROCJ MC (2001) A taxonomy for learning, teaching, and assessing: A revision of Bloom's taxonomy of educational objectives. Abridged 1st Ed. Allyn & Bacon, Boston, MA, pp 352.

ARANTES M, ANDRADE JP, BARBOSA J, FERREIRA MA (2020) Curricular changes: The impact on medical students' knowledge of neuroanatomy. *BMC Med Educ*, 20(1): 20.

AUSTRALIAN OSTEOPATHIC ACCREDITATION COUNCIL (2020) Accreditation. 2016 http://www.osteopathiccouncil.org.au/accreditation.html, [Accessed: 18/12/20]

BACKHOUSE S, TAYLOR D, ARMITAGE JA (2019) Is this mine to keep? Three-dimensional printing enables active, personalized learning in anatomy. *Anat Sci Educ,* 12(5): 518-528.

BAKKUM BW, TRACHOMOWICZ RA (2015) Retention of knowledge of retinal microanatomy by optometric students, faculty, and practitioners. *Optometric Educ,* 40(2): 77-82.

BERGMAN EM, VAN DER VLEUTEN CP, SCHERPBIER AJ (2011) Why don't they know enough about anatomy? A narrative review. *Med Teach,* 33(5): 403-409.

BERGMAN EM, DE BRUIN AB, HERRLER A, VERHEIJEN IW, SCHERPBIER AJ, VAN DER VLEUTEN CP (2013) Student's perceptions of anatomy across the undergraduate problem-based learning medical curriculum: A phenomenographical study. *BMC Med Educ,* 13(1): 151-152.

BERGMAN EM, VERHEIJEN IW, SCHERPBIER AJ, VAN DER VLEUTEN CP, DE BRUIN AB (2014) Influences on anatomical knowledge: The complete arguments. *Clin Anat*, 27(3): 296-303.

BERGMAN EM, DE BRUIN AB, VORSTENBOSCH MA, KOOLOOS JG, PUTS GC, LEPPINK J, SCHERPBIER AJ, VAN DER VLEUTEN CP (2015) Effects of learning content in context on knowledge acquisition and recall: A pretest-posttest control group design. *BMC Med Educ,* 15(1): 133.

BLAICH R, PATHER N, LUO K, STRKALJ G (2019) Australian osteopathic practitioners' perceptions of the clinical relevance of anatomy. *Inter J Morph,* 37(1): 319-323.

BLUNT MJ, BLIZARD PJ (1975) Recall and retrieval of anatomical knowledge. *Med Educ,* 9(4): 255-263.

BOCKERS A, JERG-BRETZKE L, LAMB C, BRINKMANN A, TRAUE HC, BOCKERS TM (2010) The gross anatomy course: An analysis of its importance. *Anat Sci Educ,* 3(1): 3-11.

BRAUER DG, FERGUSON KJ (2015) The integrated curriculum in medical education: AMEE Guide No. 96. *Med Teach,* 37(4): 312-322.

BRIDGES S, YIU CKY, BOTELHO MG (2016) Design considerations for an integrated, problem-based curriculum. *Med Sci Educ,* 26(3): 365-373.

BRUNK I, SCHAUBER S, GEORG W (2017) Do they know too little? An inter-institutional study on the anatomical knowledge of upper-year medical students based on multiple choice questions of a progress test. *Ann Anat,* 209: 93-100.

CASTILLO-LOPEZ JM, DIAZ-MANCHA JA, HEREDIA-RIZO AM, FERNANDEZ-SEGUIN LM, POLO-PADILLO J, DOMINGUEZ-MALDONADO G, MUNUERA PV (2014) The tarsal bone test: A basic test of health sciences students' knowledge of lower limb anatomy. *BioMed Res Int*, 2014: 939163.

CASTILLO JM, PARK YS, HARRIS I, CHEUNG JJH, SOOD L, CLARK MD, KULASEGARAM K, BRYDGES R, NORMAN G, WOODS N (2018) A critical narrative review of transfer of basic science knowledge in health professions education. *Med Educ,* 52(6): 592-604.

CHILDS JD, WHITMAN JM, SIZER PS, PUGIA ML, FLYNN TW, DELITTO A (2005) A description of physical therapists' knowledge in managing musculoskeletal conditions. *BMC Musculoskel Disorders,* 6(1): 32.

CRAIG S, TAIT N, BOERS D, McANDREW D (2010) Review of anatomy education in Australia and New Zealand medical schools. *ANZ J Surg,* 80(4): 212-216.

CUSTERS EJ (2010) Long-term retention of basic science knowledge: a review study. *Adv Health Sci Educ,* 15(1): 109-128.

CUSTERS EJ, CATE OTJ (2011) Very long-term retention of basic science knowledge in doctors after graduation. *Med Educ,* 45: 422-430.

DAY LJ (2018) A gross anatomy flipped classroom effects performance, retention, and higher-level thinking in lower performing students. *Anat Sci Educ,* 11(6): 565-574.

DAYAL MR, OWENS O, GIBSON W, STRKALJ G (2017) Anatomical knowledge retention in physiotherapy students: A preliminary assessment. *Int J Anat Res,* 5(1.2): 3474-3479.

D'EON MF (2006) Knowledge loss of medical students on first year basic science courses at the University of Saskatchewan. *BMC Med Educ,* 6(1): 5.

DIAZ-MANCHA JA, CASTILLO-OPEZ JM, MUNUERA-MARTINEZ PV, FERNANDEZ-SEGUIN LM, POLO-PADILLO J, HEREDIA-RIZO AM (2016) A comparison of fourth-year health science student's knowledge of gross lower and upper limb anatomy: A cross-sectional study. *J Manip Physiol Ther,* 39(6): 450-457.

DOBSON JL, LINDERHOLM T (2015) The effect of selected "desirable difficulties" on the ability to recall anatomy information. *Anat Sci Educ,* 8(5): 395-403.

DOBSON JL, PEREZ J, LINDERHOLM T (2017) Distributed retrieval practice promotes superior recall of anatomy information. *Anat Sci Educ,* 10(4): 339-347.

DOOMERNIK DE, VAN GOOR H, KOOLOOS JG, TEN BROEK RP (2017) Longitudinal retention of anatomical knowledge in second-year medical students. *Anat Sci Educ,* 10(3): 242-248.

DRAKE RL (2007) A unique, innovative, and clinically oriented approach to anatomy education. *Acad Med,* 82(5): 475-478.

ERKONEN WE, ALBANESE MA, SMITH WL, PANTAZIS NJ (1992) Effectiveness of teaching radiologic image interpretation in gross anatomy: A long-term follow-up. *Invest Radiol,* 27(3): 264-266.

ESTAI M, BUNT S (2016) Best teaching practices in anatomy education: A critical review. *Ann Anat,* 208: 151-157.

EVANS DJ, PAWLINA W, LACHMAN N (2018) Human skills for human[istic] anatomy: An emphasis on nontraditional discipline -independent skills. *Anat Sci Educ,* 11(3): 221-224.

FAREY JE, BUI DT, TOWNSEND D, SURESHKUMAR P, CAR S, ROBERTS C (2018) Predictors of confidence in anatomy for work as a junior doctor: A national survey of Australian medical students. *BMC Med Educ,* 18(1): 174.

FEIGIN D, MAGID D, SMIRNIOPOULOS J, CARBOGNIN S (2007) Learning and retaining normal radiographic chest anatomy does preclinical exposure improves student performance? *Acad Radiol,* 14(9): 1137-1142.

FEIGIN DS, SMIRNIOTOPULOS JG, NEHER TJ (2002) Retention of radiographic anatomy of the chest by 4th-year medical students. *Acad Radiol,* 9(1): 82-88.

FREEDMAN KB, BERNSTEIN J (1998) The adequancy of medical school education in musculoskeletal medicine. *J Bone Joint Surgery,* 80-A(10): 1421-1427.

GIURIATO R, STRKALJ G, MEYER AJ, PATHER N (2019) Anatomical sciences in chiropractic education: A survey of chiropractic programs in Australia. *Anat Sci Educ,* 13(1): 37-47.

HILDEBRANDT S (2019) The role of history and ethics of anatomy in medical education. *Anat Sci Educ,* 12(4): 425-431.

HULME AK, LUO K, STRKALJ G (2019) Musculoskeletal anatomy knowledge retention in the Macquarie University chiropractic program: A cross-sectional study. *Anat Sci Educ,* 13(2): 182-191.

HUMPHREYS BK, SULKOWSKI A, McINTYRE K, KASIBAN M, PATRICK AN (2007) An examination of musculoskeletal cognitive competency in chiropractic interns. *J Manip Physiol Ther*, 30(1): 44-49.

JANSSEN SA, VAN DER MEULEM SP, SHOSTROM VK, LOMNETH CS (2014) Enhancement of anatomical learning and developing clinical competence of first-year medical and allied health profession students. *Anat Sci Educ,* 7(3): 181-190.

JOHNSON S, VAUGHAN B (2020) 'We need one more hour solely based on anatomy.... Give us anatomy!': Early-year learner perceptions of anatomy within an integrated and case-based learning osteopathy curriculum. *Intern J Osteo Med,* 36: 49-54.

JURJUS RA, LEE J, AHLE S, BROWN KM, BUTERA G, GOLDMANN EF, KRAPF JM (2014) Anatomical knowledge retention in third-year medical students prior to obstetrics and gynecology and surgery rotations. *Anat Sci Educ,* 7(1): 461-468.

JURJUS RA, BROWN RA, GOLDMAN E, GALOOSIAN A, BUTERA G, KRAPF JM (2016) Curricular responses to increase recall and transfer of anatomical knowledge into the obstetrics/gynecology clerkship. *Anat Sci Educ,* 9(4): 337-343.

KARPICKE JD (2012) Retrieval-based learning: Active retrieval promotes meaningful learning. *Curr Dir Psychol Sci,* 21(3): 157-163.

KARPICKE JD, BLUNT JR (2011) Retrieval practice produces more learning than elaborative studying with concept mapping. *Science,* 331(6018): 772-775.

KERFOOT BP, DE WOLF WC, MASSER BA, CHURCH PA, FEDERMAN DD (2007) Spaced education improves the retention of clinical knowledge by medical students: A randomised controlled trial. *Med Educ,* 41(1): 23-31.

LACHMAN N, PAWLINA W (2006) Integrating professionalism in early medical education: The theory and application of reflective practice in the anatomy curriculum. *Clin Anat,* 19(5): 456-460.

LAZARUS MD, CHINCHILLI VM, LEONG SL, KAUFFMAN GLJ (2012) Perceptions of anatomy: Critical components in the clinical setting. *Anat Sci Educ,* 5(4): 187-199.

LOGAN JM, THOMPSON AJ, MARSHAK DW (2011) Testing to enhance retention in human anatomy. *Anat Sci Educ,* 4(5): 243-248.

LOSCO CD, GRANT WD, ARMSON A, MEYER AJ, WALKER BF (2017) Effective methods of teaching and learning anatomy as a basic science: A BEME systematic review: BEME Guide no. 44. *Med Teach,* 39(3): 234-243.

LOUW G, EIZENBERG N, CARMICHAEL SW (2009) The place of anatomy in medical education: AMEE Guide no 41. *Med Teach,* 31(5): 373-386.

LUFLER RS, LAZARUS MD, STEFANIK JJ (2020) The spectrum of learning and teaching: The impact of a fourth-year anatomy course on medical student knowledge and confidence. *Anat Sci Educ,* 13(1): 19-29.

McBRIDE JM, DRAKE RL (2016) Longitudinal cohort study on medical student retention of anatomical knowledge in an integrated problem-based learning curriculum. *Med Teach,* 38(12): 1209-1213.

McBRIDE JM, DRAKE RL (2018) National survey on anatomical sciences in medical education. *Anat Sci Educ,* 11(1): 7-14.

McKEOWN PP, HEYLINGS DJA, STEVENSON M, McKELVEY KJ, NIXON JR, McCLUSKEY D (2003) The impact of curricular change on medical students' knowledge of anatomy. *Med Educ*, 37(11): 954-961.

MEYER AJ, ARMSON A, LOSCO CD, LOSCO B, WALKER BF (2015) Factors influencing student performance on the carpal bone test as a preliminary evaluation of anatomical knowledge retention. *Anat Sci Educ,* 8(2): 133-139.

MILLER GE (1990) The assessment of clinical skills/competence/performance. *Acad Med,* 65(9 Suppl): S63-S67.

MORTON DA, COLBERT-GETZ JM (2016) Measuring the impact of the flipped anatomy classroom: The importance of categorizing an assessment by Bloom's taxonomy. *Anat Sci Educ,* 10(2): 170-175.

NABIL NM, AL-MOUSLY N, OUSLY, N. AlWATHNANI S, ABDULDAIEM A, AL-ISSA H (2014) Medical Students' perception on anatomy knowledge relevance and retention during clerkship. *J Contemp Med Educ,* 2(3): 147-151.

NARNAWARE Y, NEUMEIER M (2020) Second-year nursing students' retention of gross anatomical knowledge. *Anat Sci Educ,* 13(2): 230-236.

NORMAN G (2009) Teaching basic science to optimize transfer. *Med Teach*, 31(9): 807-811.

OSTEOPATHY BOARD OF AUSTRALIA (2020) 2019/2020 Annual Report. Retreived from https://www.osteopathyboard.gov.au/News/Annual-report.aspx [Assessed 21/11/20]

PARMAR SK, RATHINNAM BA (2011) Introduction of vertical integration and case-based learning in anatomy for undergraduate physical therapy and occupational therapy students. *Anat Sci Educ,* 4(3): 170-173.

PRINCE KJ, SCHERPBIER AJ, VAN MAMEREN H, DRUKKER J, VAN DER VLEUTEN CP (2005) Do students have sufficient knowledge of clinical anatomy? *Med Educ,* 39(5): 326-332.

QUINTERO GA, VERGEL J, ARREDONDO M, ARIZA M-C, GOMEZ P, PINZON-BARRIOS A-M (2016) Integrated medical curriculum: Advantages and disadvantages. *J Med Educ Curricular Devel,* 2016(3): 133-137.

RAUPACH T, ANDERSEN JC, MEYER K, STROBEL L, KOZIOLEK M, JUNG W, BROWN J, ANDERS S (2016) Test-enhanced learning of clinical reasoning: A crossover randomised trial. *Med Educ,* 50(7): 711-720.

RIZZOLO L, RANDO W, O'BRIEN M, HAIMS A, ABRAHAMS J, STEWART W (2010) Design, implementation, and evaluation of an innovative anatomy course. *Anat Sci Educ,* 3(3): 109-120.

ROCHE A WILLIAMS G, WHARTON D, BROWN D (2011) Physical and radiographic identification of the bones of the wrist by junior doctors. *J Hand Surg Eur*, 36(2): 107-110.

SMITH MA, BLUNT JR, WHIFFEN JW, KARPICKE JD (2016) Does providing prompts during retrieval practice improve learning? *Appl Cognit Psychol,* 30(4): 544-553.

SPIELMANN PM, OLIVER CW (2005) The carpal bones: A basic test of medical students' and junior doctor's knowlegde of anatomy. *Surgeon,* 3(4): 257-259.

STOCKARD AR, ALLEN TW (2006) Competence levels in musculoskeletal medicine: Comparison of osteopathic and allopathic medical graduates. *J Am Osteop Assoc,* 106(6): 350-355.

STRKALJ G (2014) The emergence of humanistic anatomy. *Med Teach,* 36(10): 912-913.

STRKALJ G, SCHRODER T, PATHER N, SOLYALI V (2011) A Preliminary assessment of the fifth-year chiropractic students' knowledge of anatomy. *J Altern Complement Med,* 17(1): 63-66.

SUGARD K, ABRAHAMS P, KHURANA A (2010) The anatomy of anatomy: A review for its modernization. *Anat Sci Educ,* 3(2): 83-93.

SWARTZ WJ (2006) Using gross anatomy to teach and assess professionalism in the first year of medical school. *Clin Anat,* 19(5): 437-441.

TALARICO Jr EF (2010) A human dissection training program at Indiana university school of medicine-northwest. *Anat Sci Educ,* 3(2): 77-82.

TALARICO Jr EF (2012) A change in paradigm: Giving back identity to donors in the anatomy wet laboratory. *Clin Anat,* 26(2): 161-172.

TALARICO Jr EF, PAINTER SD (2020) Small team-based medical imaging of human cadavers: An innovative tool for interdisciplinary learning in human gross anatomy and radiologic scineces. *Eur J Anat,* 24(2): 141-154.

THOMPSON AR, O'LOUGHLIN VD (2015) The blooming taxonomy tool (BAT): A discipline-specific rubric for utilising Bloom's taxonomy in the design and evaluation of assessments in the anatomical sciences. *Anat Sci Educ,* 8(6): 493-501.

TURNEY BW (2007) Anatomy in a modern medical curriculum. *Ann R Coll Surg Engl,* 89(2): 104-107.

VALENZA MC, CASTRO-MARTIN E, VALENZA G, GUIRAO-PINEIRO M, DE-LA-LLAVE-RINCON AI, FERNANDEZ-DE-LAS-PENAS C (2012) Comparison of third-year medical and physical therapy students' knowledge of anatomy using the carpal bone test. *J Manip Physiol Therap,* 35(2): 121-126.

WASS V, VAN DER VLEUTEN C, SHATZER J, JONES R (2001) Assessment of clinical competence. *Lancet,* 357(9260): 945-949.

WHITE MT, BORGES NJ, GEIGER S (2011) Preceptions of factors contributing to professional identity development and speciality choice: A survey of third and fourth-year medical students. *Ann Behav Sci Med Educ,* 17(1): 18-23.

WILLIAMS AD, MANN BD (2017) Improved knowledge gain and retention for third-year medical students during surgical journal club using basic science review. A pilot study. *Am J Surg,* 213(2): 238-243.

WILSON JS, ALVAREZ J, DAVIES BC, DUERINCKX AJ (2018) Cost-effective teaching of radiology with pre-clinical anatomy. *Anat Sci Educ,* 11(2): 96-206.

ZHAO X, GOLDMAN E, BANANI T, KLINE K, BROWN K, LEE J, JUJUS RA (2020) The process of curricular integration and its effects on anatomical knowledge retention. *Clin Anat,* 33(6): 960-968.

ZIEBER M, SEDGEWICK M (2018) Competence, confidence and knowledge retention in undergraduate nursing students. A mixed method study. *Nurse Educ Today,* 62: 16-21.

No changes in muscle fibre type composition in rat multifidus muscle following lesion of the lumbar intervertebral disc

Heleen Docter, Jaimy D. van den Hout, Wendy Noort, Jaap van Dieën, Huub Maas

Department of Human Movement Sciences, Faculty of Behavioural and Movement Sciences, Vrije Universiteit Amsterdam, Amsterdam Movement Sciences, The Netherlands

SUMMARY

The multifidus muscle has been proposed to play an important role in the development and recurrence of low-back pain (LBP). In line with this, fibre type composition has been found to be altered in humans with LBP. This study aims to investigate the changes in muscle fibre type composition of the multifidus muscle after stab disc lesion in the rat.

Data were obtained from 24 male Wistar rats randomly assigned to the intervention group, in which the L4/L5 intervertebral disc was stabbed, or the control group, in which no intervention was applied. At 7, 14 and 28 days post-intervention, two fascicles of the multifidus muscle between L3 and S1 were removed bilaterally for analysis of fibre type composition. The rats' multifidus muscle consisted for the largest part of type IIB fibres in both the intervention (53 ± 10% across all time points) and the control group (53 ± 9% across all time points). We found no effects of disc lesion on the proportion of type I, IIA, IIX and IIB fibres. These results indicate that the fibre type composition of the multifidus muscle is not affected by disc lesion within the time period (28 days) studied. A different functional role of the multifidus muscle in the rat compared to humans, reflected in the high proportion of fast muscle fibres in the rat's multifidus muscle, may explain our findings. Differences between species in fibre type composition should be taken into account when using rats as a model to investigate the mechanisms causing (chronic) LBP in humans.

Key words: Low-back pain – Animal model – Spine – Degeneration – Muscle fibre type

INTRODUCTION

Chronic low-back pain (LBP) is a common disorder in humans (Heidari et al., 2015; Shraim et al., 2015). Despite its high prevalence, the mechanisms causing chronic LBP are not fully understood. Mechanical dysfunction of the spine, resulting in instability, has been suggested to be involved in the development of LBP (Panjabi, 1992). Three systems are involved in stabilizing the spine: the passive system including ligaments and intervertebral discs, the active system comprising the trunk musculature and the neural

Corresponding author:
Huub Maas. Department of Human Movement Sciences, Faculty of Behavioural and Movement Sciences, Amsterdam Movement Sciences, Vrije Universiteit Amsterdam, Van der Boechorststraat 9, 1081 BT, The Netherlands. E-mail: h.maas@vu.nl

Submitted: July 31, 2020. **Accepted:** February 4, 2021

system (Panjabi, 1992). Dysfunction of one of these systems can lead to spinal instability and potentially contribute to LBP.

The three systems may also affect each other. Cortical and spinal cord excitability have been found to be changed after disc lesion (Hodges, 2009). This likely leads to an altered activation of parts of the active system (D'hooge et al., 2013; Hodges, 2009; Hodges et al., 2013; Hodges et al., 2006; MacDonald et al., 2011; MacDonald et al., 2009, 2010; Stokes and Young, 1984). Possibly mediated by such changes in activation, disc degeneration seems to induce degenerative changes in the multifidus muscle (Maas et al., 2018). The multifidus muscle is thought to play an important role in stabilization of the spine (Ward et al., 2009). Degeneration of the multifidus muscle may in turn cause increased and uncontrolled disc deformation, which eventually results in disc degeneration (Panjabi, 1992). Deformation of the intervertebral disc (IVD) has been related to low back pain, indicated by an odds ratio of 1.12 to 3.32 between degeneration and LBP (van Tulder et al., 1997). The interdependence of the stabilizing systems suggests that the multifidus muscle may have an important role in the development and rehabilitation of LBP.

In addition to microscopic structural alterations (Cagnie et al., 2015) and atrophy (Danneels, 2000; Hides et al., 2008; Hides et al., 1994) in the lumbar muscles, a change in the fibre type composition has been found in patients with LBP. In human skeletal muscle, three different fibre types can be identified based on their structural and functional characteristics: type I, type IIA and type IIX fibres. These fibre types form a continuum of increasing force production, increasing speed and decreasing endurance capacity respectively (Schiaffino and Reggiani, 2011). Specifically, type IIX fibres appear to occupy a larger area in patients with LBP than in control participants (Cagnie et al., 2015; Goubert et al., 2016; Mannion, 1999). The studies with human participants have a cross-sectional design, making identification of causal relationships impossible. Animal models appear warranted to unravel potential mechanisms underlying chronic LBP. Rats are widely used animal models to investigate surgically induced IVD degeneration (Shi et al., 2018). In contrast to humans, rat muscles have an additional fibre type—i.e., type IIB. Muscle fibres of this type are functionally comparable to the type IIX fibres found in humans. The type IIB fibres in rats have a greater cross-sectional area, can generate more force and shorten at higher velocities than the same type of fibres in humans (Schiaffino and Reggiani, 2011).

The multifidus muscle shows structural and functional similarities between rats and humans. In both rats and humans, the multifidus lies superficial of the spine and each fascicle spans up to three segments of the spine. Electromyography recordings in adult rats show tonic activity of the multifidus muscle during both rest and motor activity (Geisler et al., 1996). The continuous activity pattern is in line with the assumption that the multifidus muscle acts as a stabilizer as in humans (Ward et al., 2009). To our knowledge, the effects of disc lesion on fibre type composition have not been investigated in rats.

The aim of the present study was to investigate changes in muscle fibre type composition of the multifidus muscle after stab disc lesion in rats. We hypothesized that an IVD lesion would inhibit multifidus muscle activation, resulting in a transition from slow to fast muscle fibres.

MATERIALS AND METHODS

Animals

24 Adult male Wistar rats (Harlan Laboratories) were randomly divided in an intervention (stabbing the L4/5 disc) group (n=12) and a control group (n=12). Surgical and experimental procedures agreed with the guidelines and regulations concerning animal welfare and experimentation set forth by the Dutch law and were approved by the Committee on Ethics of Animal Experimentation at the Vrije Universiteit Amsterdam (FBW 13-03).

Surgical procedures and experimental setup

In the intervention group, buprenorphine (Temgesic®, Schering-Plough) was administered subcutaneously (0.1 ml/100 g body mass) half an

hour prior to the surgery. After being anesthetized, using isoflurane gas (1-3%), a tenotomy knife (blade length 30 mm, thickness 0.4 mm) was used to penetrate the IVD by 2.5 mm (up to nucleus pulposus) between lumbar vertebrae L4 and L5 using a transperitoneal-ventral approach (Rousseau et al., 2004). After surgery, rats were kept in a large cage (0.55×0.33×0.20 m) with access to food and water *ad libitum*. Up to two days after the surgery, carprofen (Rimadyl®, Pfizer) was administered subcutaneously (once a day, 0.1 ml/100 g body mass) to prevent pain. After administration of carprofen, no behavioural changes were observed. For more details see Maas et al. (Maas et al., 2018). The control group did not undergo surgery.

The control and intervention groups were further randomly divided in three subgroups: 7 days (n=4), 14 days (n=4) and 28 days (n=4). Body mass at the day of tissue harvesting, which is related to age (Huijing and Maas, 2016), was similar between time points (Table 1). At the different time points, the rats were deeply anesthetized with intraperitoneally injected urethane (for details see Maas et al., 2018) and the fascicle running from L3 to L6 and the fascicle running from L4 to S1 were removed as one piece at both sides (Figure 1). After surgery, the rats were euthanized by an intracardiac injection with an overdose Euthasol 20% (Euthasol®, AST farma, Oudewater, The Netherlands).

Excised multifidus fascicles were frozen with liquid nitrogen and stored in cryotubes at -80°C. The fascicles of the left side were sliced transversally (10 µm) in a cryostat (MICROM HM 550, Thermo Scientific™, Waltham, USA) at -22°C. First, 1/3 was cut off at both ends, ensuring that the slices contained both fascicles (Figure 2A). Three slices were put on a Superfrost Plus adhesion slide (Thermo Scientific™, Waltham, USA). The multifidus of one rat of the intervention group (14 days) could not be analysed, because the tissue was not of sufficient quality. Fibre-type composition was assessed by immunofluorescence analysis of myosin heavy chain (MHC) expression (Bloemberg and Quadrilatero, 2012), using primary antibodies BA-D5, SC-71, BF-F3, and 6H1, for MHC-I, MHC-IIA, MHC-IIB, and MHC-IIX, respectively and secondary antibodies Alexa Fluor 488 IgG_{2b}, for MHC-1, 647 IgM for MHC-IIB, and MHC-IIX and 448 IgG_1, for MHC-IIA (all from Fisher Scientific, Landsmeer, The Netherlands). To control for possible differences between the left and right sides, the right multifidus muscle of three rats was also investigated. We found no left-right differences in fibre type composition.

For further analysis, the stained slides were scanned using a fluorescence microscope (Axiovert 200, Zeiss, Jena, Germany) with a CCD camera (PCO AG, SensiCam, Kelheim, Germany) and the program Slidebook (version 5.0, Intelligent Imaging Innovations, inc., Denver, USA).

Measurements

Four squares, spatially distributed within the muscle section, were selected for analysis (Figure 2B). The number of fibres was counted manually, using ImageJ (http://imagej.nih.gov/ij). Each area contained a total of 60 to 70 fibres, the whole cross-section included about 600 fibres. In some muscles, the quality of the staining for type IIX fibres was poor. Therefore, all fibres not identified as type I, IIA or IIB were classified as type IIX fibres.

Statistics

To test for effects of IVD lesion on muscle fibre type proportion, a two-way ANOVA (SPSS version 24, IBM, Armonk, NY, USA) was applied for each of the fibre types, with between-subject factors time (7, 14 or 28 days) and intervention (disc lesion or

Table 1. Body mass (g) of rats at the day tissues were harvested.

	7-days post-op	14-days post-op	28-days post-op
IVD lesion	282 ± 9	300 ± 10	350 ± 11
Controls	254 ± 18	312 ± 11	360 ± 10

N = 4 for each experimental group and time point. *Note*. Adapted from "Effects of intervertebral disc lesion and multifidus muscle resection on the structure of the lumbar intervertebral discs and paraspinal musculature of the rat", by Maas et al. (2018), *Journal of Biomechanics*, 70: 228-234.

control). If a significant interaction was found, the effects of intervention were tested using an independent samples t-test with Bonferroni correction for each time point and the effects of time for each intervention were tested using a one-way ANOVA and Bonferroni post hoc tests.

RESULTS

For the proportion of type I, IIA, IIX and IIB fibres, neither significant effects of time or intervention were observed, nor a significant interaction (Tables 2, 3; Fig. 3). Rat multifidus muscle consisted for the largest part of type IIB

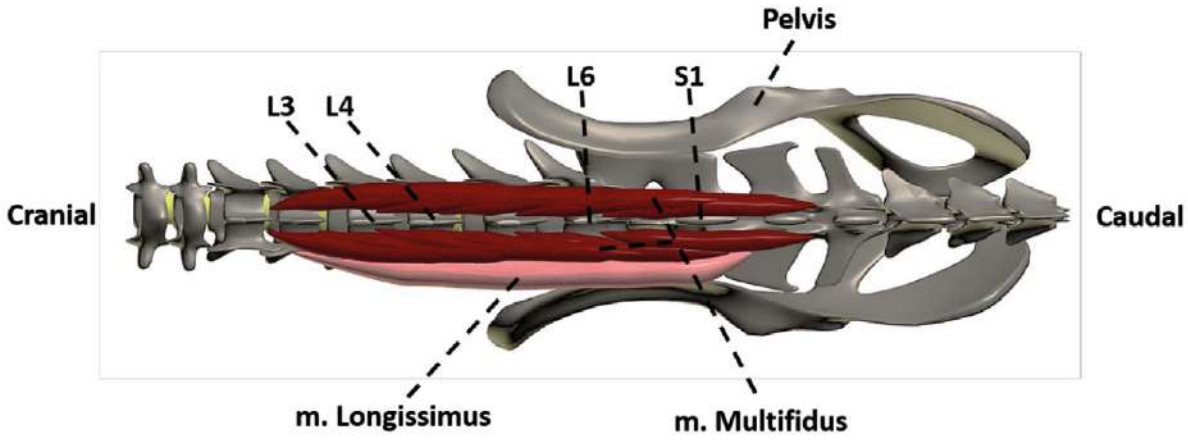

Fig. 1.- Dorsal view of the spine of a rat. The deep red muscle represents the multifidus muscle and the light red muscle represents the longissimus muscle. The fascicles of the multifidus muscle from L3 to L6 and from L4 to S1 were harvested.

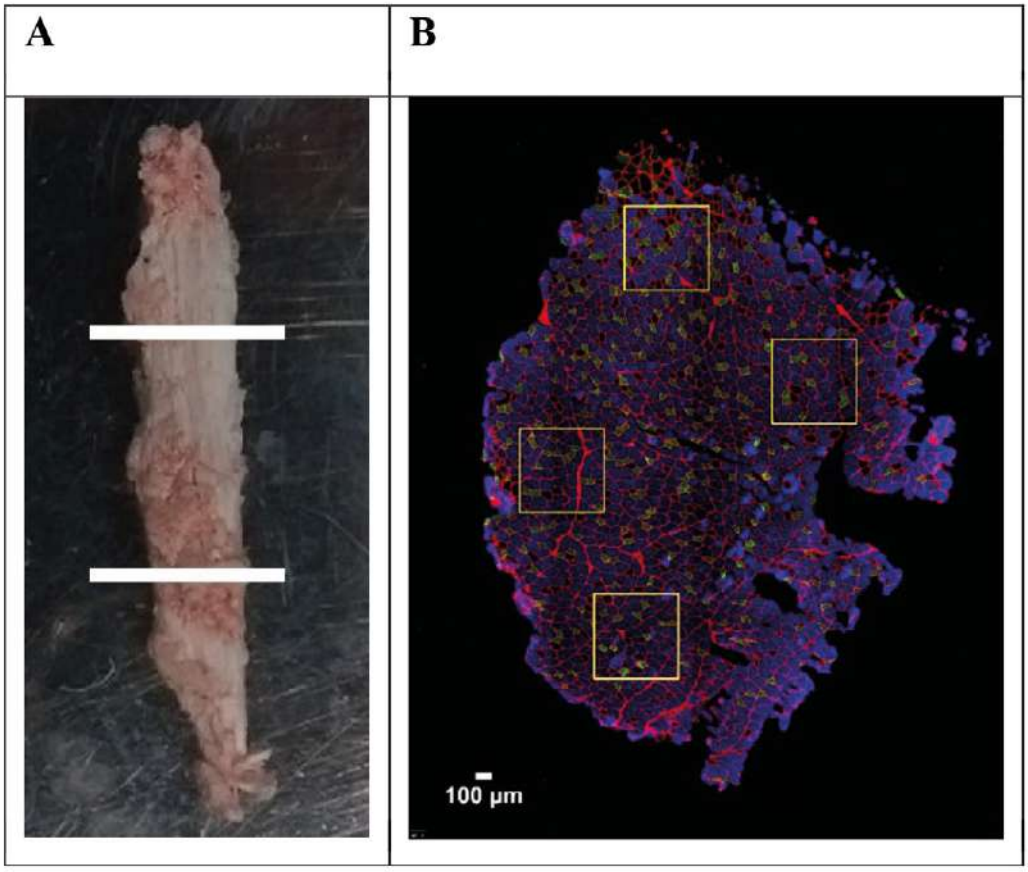

Fig. 2.- A: A typical example of a fascicle of which 1/3 of both sides was removed before the muscle was sliced; **B:** Typical sample of the chosen areas for the determination of the fibre type proportions.

fibres in both the intervention (53 ± 10% across all time points) and the control group (53 ± 9% across all time points).

DISCUSSION

The aim of this study was to investigate the effects of a lumbar disc lesion on fibre type composition of rat multifidus muscle. In contrast

Table 2. Results of the two-way ANOVA for the proportion of the different fibre types, including the degrees of freedom (df), F-value, p-value and power.

Fibre type		df	F-value	p-value	Power
Type I	Time	2,17	0.301	0.744	0.090
	Intervention	1,17	0.986	0.335	0.155
	Interaction	2,17	3.394	0.058	0.559
Type IIA	Time	2,17	0.154	0.859	0.070
	Intervention	1,17	0.037	0.849	0.054
	Interaction	2,17	1.215	0.321	0.229
Type IIX	Time	2,17	1.368	0.281	0.254
	Intervention	1,17	0.660	0.428	0.120
	Interaction	2,17	0.034	0.966	0.054
Type IIB	Time	2,17	0.998	0.389	0.195
	Intervention	1,17	2.147	0.162	0.281
	Interaction	2,17	3.438	0.056	0.565

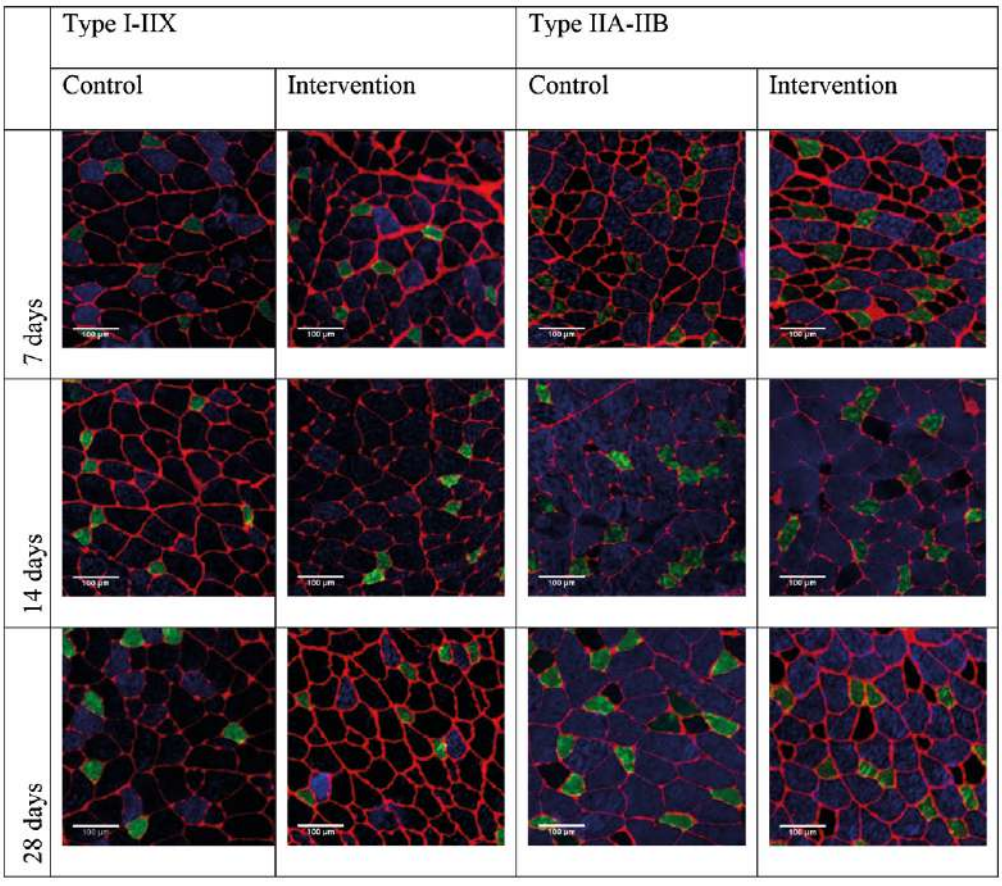

Fig. 3.- Fibre type staining for type I-IIX and type IIA-IIB in the intervention and control group. In the two left panels, green represents type I (antibodies BA-D5 and Alexa Fluor 488 IgG2b) and blue represents type IIX fibres (antibodies 6H1 and 647 IgM). In the two right panels, green represents type IIA (antibodies SC-71 and IgG1) and blue represents type IIB (antibodies BF-F3 and 647 IgM). The red lines represent the connective tissue, stained with wheat germ agglutinin.

with our hypothesis, the disc lesion did not affect the fibre type proportions within the first 28 days after the intervention.

The rats in our study received an anterior stab incision in the IVD to mimic spinal dysfunction, a potential cause of LBP in humans. The area occupied by type IIX fibres appears increased in people with LBP, compared to abled-bodied people (Cagnie et al., 2015; MacDonald et al., 2006; Mannion, 1999). In sheep, a transition from slow to fast muscle fibres at 24 weeks and 6 months after a lateral stab incision has been reported (Hodges, 2014, 2015). In contrast to the abovementioned studies, we did not find a similar transition in the rat model.

There are several possible explanations for our negative preliminary findings. The follow-up time (28 days) might have been too short to detect changes in fibre type composition. However, both overloading and unloading in the rat have resulted in significant fast-to-slow transition even within 14 days (Baldwin et al., 1990; Cornachione et al., 2008; De Souza et al., 2011; Degens et al., 2008; Feng et al., 2016; Fisher and Brown, 1998; Gardiner et al., 1991; Herbison et al., 1984; McCall et al., 2009; Oakley and Gollnick, 1985; Roy et al., 2005; Van der Meer et al., 2011; Watt et al., 1984), demonstrating the plasticity of the muscle tissue of rats. We cannot exclude that time has been a factor, but the plasticity of rat muscles makes it unlikely that the time frame is an explanation for our negative findings.

Another reason for our negative findings might be the ability of rats to recover from a disc lesion in a relatively short time. In two out of four rats analysed 28 days after stab incision, the lumbar IVD appeared to be recovered (Maas et al., 2018). Such resilience of the intervertebral discs was not found in sheep (Osti et al., 1990).

Finally, our negative findings may be explained by the functional role of the multifidus muscle of the rat, as reflected in its phenotype. Our findings indicate that the multifidus muscle in control rats contains predominantly (>60%) fast glycolytic (type IIX and IIB) fibres (Table 3), suggesting that this muscle is active predominantly during rapid movements. This differs substantially from the fibre type distribution and muscle function of the multifidus in humans. Human muscle does not express the type IIB myosin heavy chain isoform. In healthy humans, percentages of 54%-74.3% are reported for type I fibres, 16.4%-30.2% for type IIA fibres and 4.6%-22.34% for type IIX fibres (Cagnie et al., 2015; Goubert et al., 2016; Mannion, 1999). The high prevalence of fast glycolytic fibres has also been reported for rodents other than Wistar rats (Schilling, 2009), and follows the ancestral pattern for primates (Neufuss et al., 2014). The orthograde posture and locomotor behaviour of hominoid primates might be related to the slow phenotype of their back muscles (Neufuss et al., 2014). It should be noted that the fibre type composition of the multifidus in sheep, for which a slow-to-fast muscle fibre type transition was found (see above), is similar to rats, i.e., ±73% fast muscle fibres, ±23% slow muscle fibres and ±4% intermediate muscle fibres (Hodges, 2014). This suggests that not only the fibre type composition, but other anatomical or physiological differences (e.g., tissue resilience) are responsible for our negative results.

There are some limitations that should be considered. First, a substantial inter-individual variation was found in muscle fibre type

Table 3. General overview of the percentages of muscle fibre type proportions (mean ± SD) for the intervention and control group at 7, 14 and 28 days after the stab disc lesion.

	7 days		**14 days**		**28 days**	
	Control (n=4)	Intervention (n=4)	Control (n=4)	Intervention (n=3)	Control (n=4)	Intervention (n=4)
Type I	9±7	20±4	19±9	11±5	9±9	16±9
Type IIA	12±5	17±4	14±5	13±10	17±5	13±4
Type IIX	18±8	21±9	13±3	14±2	16±5	18±6
Type IIB	62±13	43±9	56±12	63±7	60±6	54±9

proportions. This will reduce the power to find small differences. A high variability in percentage type I fibres has also been reported for other muscles of the rat (Eng, 2008). The high variation could be a result of an inequal distribution of the muscle fibre types within the cross-section of the muscle of one sample. In this study, the four analysed areas were systematically chosen following predetermined rules (see Methods, Fig. 2), such that the areas were representative for the whole muscle.

Another limitation of this study is the absence of a sham lesion in the control group. It is possible that the surgery damaged the abdominal wall, which may have resulted in reduced physical activity of the rats. Considering that we observed no effects of multifidus resection on the IVD in our previous study (Maas et al., 2018), and no differences with the control group in the present study, we deem confounding by this limitation unlikely.

Variances found within the investigated groups are especially important in case of small sample sizes. The groups studied in this research included 4 (and in one group 3) animals. Despite the limited sample numbers, the relative area of the nucleus pulposus was significantly smaller after the stab incision in the same group of rats 14 days after intervention (Maas et al., 2018). Moreover, there was no main effect of intervention at all time points. Thus, our conclusion that fibre type composition was not affected by a disc lesion was actually based on twelve rats, not four.

We conclude that muscle fibre type composition of the multifidus muscle was not affected by disc lesion in rats within a four-week time period. Differences between quadrupedal mammals and humans in fibre type composition and tissue resilience should be considered when using rats as a model to investigate the mechanisms causing (chronic) LBP in humans.

ACKNOWLEDGEMENTS

We would like to thank Guus Baan for help with the surgical procedures and for the drawing shown in Figure 1. Paul Hodges is acknowledged for the discussions about this work.

REFERENCES

BALDWIN KM, HERRICK RE, ILYINA-KAKUEVA E, OGANOV VS (1990) Effects of zero gravity on myofibril content and isomyosin distribution in rodent skeletal muscle. *FASEB J*, 4: 79-83.

BLOEMBERG D, QUADRILATERO J (2012) Rapid determination of myosin heavy chain expression in rat, mouse, and human skeletal muscle using multicolor immunofluorescence analysis. *PloS One*, 7(4): e35273.

CAGNIE B, DHOOGE F, SCHUMACHER C, DE MEULEMEESTER K, PETROVIC M, VAN OOSTERWIJCK J, DANNEELS L (2015) Fibre typing of the erector spinae and multifidus muscles in healthy controls and back pain patients: a systematic literature review. *J Manipulative Physiol Ther*, 38: 653-663.

CORNACHIONE A, CAÇÃO-BENEDINI LO, SHIMANO MM, VOLPON JB, MARTINEZ EZ, MATTIELLO-SVERZUT AC (2008) Morphological comparison of different protocols of skeletal muscle remobilization in rats after hindlimb suspension. *Scand J Med Sci Sports*, 14: 453-461.

D'HOOGE R, HODGES PW, TSAO H, HALL L, MACDONALD DA, DANNEELS L (2013) Altered trunk muscle coordination during rapid trunk flexion in people in remission of recurrent low back pain. *J Electromyography Kinesiol*, 23: 173-181.

DANNEELS LA, VANDERSTRAETEN GG, CAMBIER DC, WITVROUW EE, DE CUYPER HJ (2000) CT imaging of trunk muscles in chronic low back pain patients and healthy control subjects. *Eur Spine J*, 9: 266-272.

DE SOUZA RWA, AGUIAR AF, CARANI FR, CAMPOS GER, PADOVANI CR, SILVA MDP (2011) High-intensity resistance training with insufficient recovery time between bouts induce atrophy and alterations in myosin heavy chain content in rat skeletal muscle. *Anat Rec: Adv Integrat Anat Evol Biol*, 294: 1393.

DEGENS H, KOŞAR ŞN, HOPMAN MT, DE HAAN A (2008) The time course of denervation-induced changes is similar in soleus muscles of adult and old rats. *Appl Physiol Nutrition Metab*, 33: 299-308.

ENG CM, SMALLWOOD LH, RAINIERO MP, LAHEY M, WARD SR, LIEBER RL (2008) Scaling of muscle architecture and fiber types in the rat hindlimb. *J Exp Biol*, 211: 2336-2345.

FENG HZ, CHEN X, MALEK MH, JIN JP (2016) Slow recovery of the impaired fatigue resistance in postunloading mouse soleus muscle corresponding to decreased mitochondrial function and a compensatory increase in type I slow fibres. *Am J Physiol Cell Physiol*, 310: C27l.

FISHER JS, BROWN M (1998) Immobilization effects on contractile properties of aging rat skeletal muscle. *Aging Clin Exp Res*, 10: 59-66.

GARDINER PF, JASMIN BJ, CORRIVEAU P (1991) Rostrocaudal pattern of fibre-type changes in an overloaded rat ankle extensor. *J Appl Physiol*, 71: 558-564.

GEISLER HC, WESTERGA J, GRAMSBERGEN A (1996) The function of the long back muscles during postural development in the rat. *Behav Brain Res*, 80: 211-215.

GOUBERT D, VAN OOSTERWIJCK J, MEEUS M, DANNEELS L (2016) Structural changes of lumbar muscles in non-specific low back pain: a systematic review. *Pain Physician*, 19: E985-E1000.

HEIDARI P, FARAHBAKHSH F, ROSTAMI M, NOORMOHAMMADPOUR P, KORDI R (2015) The role of ultrasound in diagnosis of the causes of low back pain: a review of the literature. *Asian J Sports Med*, 6(1): e23803.

HERBISON GJ, JAWEED MM, DITUNNO JR JF (1984) Recovery of reinnervating rat muscle after cast immobilization. *Exp Neurol*, 85: 239-248.

HIDES JA, STOKES MJ, SAIDE MJGA, JULL GA, COOPER DH (1994) Evidence of lumbar m. multifidus muscle wasting ipsilateral to symptoms in patients with acute/subacute low back pain. *Spine*, 19: 165-172.

HIDES J, GILMORE C, STANTON W, BOHLSCHEID E (2008) M. multifidus size and symmetry among chronic LBP and healthy asymptomatic subjects. *Man Ther*, 13: 43-49.

HODGES PW, HOLM AK, HANSSON T, HOLM S (2006) Rapid atrophy of the lumbar m. multifidus follows experimental disc or nerve root injury. *Spine*, 31: 2926-2933.

HODGES PW, GALEA MP, HOLM S, HOM AK (2009) Corticomotor excitability of back muscles is affected by intervertebral disc lesion in pigs. *Eur J Neurosci*, 29: 1490-1500.

HODGES PW, COPPIETERS MW, MACDONALD DA, CHOLEWICKI J (2013) New inseight into motor adaptation to pain revealed by a ombination of modelling and empirical approaches. *Eur J Pain*, 17: 1138-1146.

HODGES PW, JAMES G, BLOMSTER L, HALL L, SCHMID AB, SHU C, LITTLE J, MELROSE J (2014) Can proinflammatory cytokine gene expression explain m. multifidus muscle fibre changes after an intervertebral disc lesion? *Spine*, 40: 1057-1071.

HODGES PW, JAMES G, BLOMSTER L, HALL L, SCHMID A, SHU C, LITTLE C, MELROSE J (2015) Multifidus muscle changes after back injury are characterized by structural remodeling of muscle, adipose and connective tissue, but not muscle atrophy. *Mol Morphol Evid*, 40: 1057-1072.

HUIJING P, MAAS H (2016) Adaptation of physiological cross-sectional area and serial number of sarcomeres after tendon transfer of rat muscle. *Scand J Med Sci Sports*, 26: 244-255.

MAAS H, NOORT W, HODGES PW, VAN DIEËN J (2018) Effects of intervertebral disc lesion and m. multifidus muscle resection on the structure of the lumbar intervertebral discs and paraspinal musculature of the rat. *J Biomech*, 70: 228-234.

MACDONALD DA, MOSELEY GL, HODGES PW (2006) The lumbar multifidus: Does the evidence support clinical beliefs? *Man Ther*, 11: 254-263.

MACDONALD DA, MOSELEY GL, HODGES PW (2009) Why do some patients keep hurting their back? Evidence of ongoing back muscle dysfunction during remission from recurrent back pain. *Pain*, 142(3): 183-188.

MACDONALD DA, MOSELEY GL, HODGES PW (2010) People with recurrent low back pain respond differently to trunk loading despite remission from symptoms. *Spine*, 35: 818-824.

MACDONALD DA, DAWSON AP, HODGES PW (2011) Behavior of the lumbar multifidus during lower extremity movements in people with recurrent low back pain during symptom remission. *J Orthop Sports Phys Ther*, 41: 155-164.

MANNION AF (1999) Fibre type characteristics and function of the human paraspinal muscles: normal values and changes in association with low back pain. *J Electromyography Kinesiol*, 9: 363-377.

MCCALL GE, HADDAD F, ROY RR, ZHONG H, EDGERTON VR, BALDWIN KM (2009) Transcriptional regulation of the myosin heavy chain IIb gene in inactive rat soleus. *Muscle Nerve*, 40: 411-419.

NEUFUSS J, HESSE B, THORPE SKS, VEREECKE EE, D'AOUT K, FISCHER MS, SCHILLING N (2014) Fibre type composition in the lumbar perivertebral muscles of primates: implications for the evolution of orthogrady in hominoids. *J Anat*, 224: 113-131.

OAKLEY CR, GOLLNICK PD (1985) Conversion of rat muscle fiber types. *Histochemistry*, 83: 555-560.

OSTI OL, VERNON-ROBERTS BFRD, FRASER R (1990) Anulus tears and intervertebral disc degeneration. An experimental study using an animal model. *Spine*, 15: 762-767.

PANJABI MM (1992) The stabilizing system of the spine. Part I. Function, dysfunction, adaptation, and enhancement. *J Spinal Disord*, 5: 383-389.

ROUSSEAU MA, BASS EC, LOTZ JC (2004) Ventral approach to the lumbar spine of the Sprague-Dawley rat. *Lab Animal*, 33: 43-45.

ROY RR, ZHONG H, SIENGTHAI B, EDGERTON VR (2005) Activity dependent influences are greater for fibres in rat medial gastrocnemius than tibialis anterior muscle. *Muscle Nerve*, 32: 473-482.

SCHIAFFINO S, REGGIANI C (2011) Fiber types in mammalian skeletal muscles. *Physiol Rev*, 91: 1447-1531.

SCHILLING N (2009) Metabolic profile of the perivertebral muscles in small therian mammals: implications for the evolution of the mammalian trunk musculature. *Zoology*, 112: 279-304.

SHI C, QIU S, RIESTER SM, DAS V, ZHU B, WALLACE AA, VAN WIJNEN AJ, MWALE FCLJ, SAKAI D, VOTTA-VELIS G, YAN W, IM H (2018) Animal models for studying the etiology and treatment of low back pain. *J Orthop Res*, 36: 1305-1312.

SHRAIM M, CIFUENTES M, WILLETTS JL, MARUCCI-WELLMAN HR, PRANSKY G (2015) Length of disability and medical costs in low back pain: do state workers' compensation policies make a difference? *J Occup Environ Med*, 57: 1275-1283.

STOKES M, YOUNG A (1984) The contribution of reflex inhibition to arthrogenous muscle weakness. *Clin Sci*, 67(1): 7-14.

VAN DER MEER SF, JASPERS RT, JONES DA, DEGENS H (2011) The time course of myonuclear accretion during hypertrophy in young adult and older rat plantaris muscle. *Ann Anat*, 193: 56-63.

VAN TULDER MW, ASSENDELFT WJ, KOES BW, BOUTER LM (1997) Spinal radiographic findings and nonspecific low back pain: a systematic review of observational studies. *Spine*, 22: 427-434.

WARD SR, KIM CW, ENG CM, GOTTSCHALK LJ, TOMIYA A, GARFIN SR, LIEBER RL (2009) Architectural analysis and intraoperative measurements demonstrate the unique design of the m. multifidus muscle for lumbar spine stability. *J Bone Joint Surg*, 91: 176-185.

WATT PW, GOLDSPINK G, WARD PS (1984) Changes in fibre type composition in growing muscle as a result of dynamic exercise and static overload. *Muscle Nerve*, 7: 50-53.

Evaluation of the morphology and angles of celiac trunk

Azad Hekimoglu, Onur Ergun

Diskapi Yildirim Beyazit Training and Research Hospital, Department of Radiology, Ankara, Turkey

SUMMARY

The objective of this study is to investigate the morphology, direction, and the origin angle of the celiac trunk. The abdominal CT images of the included 304 patients (165 males, 139 females) were retrospectively evaluated in the axial and sagittal planes following the formation of the multiplanar images. The mean age of the patients was 51 years (17-91 years). Calibration of the celiac trunk and the length between the origin of the trunk and the first branching were measured. The angle between the abdominal aorta and the celiac trunk at the level of the origin at the sagittal plane and the direction of the distal part of the trunk at the axial plane were also evaluated.

The mean length of the celiac trunk was 28.11 mm (11.1-44.6 mm) and the mean diameter was 8.05 mm (5.9-10.5 mm). There was a statistically significant difference between males and females for the length and diameter of the celiac trunk. The mean origin angle of the celiac trunk was 121.20° at the sagittal plane. There was no statistically significant difference between males and females for the origin angle of the celiac trunk. Regarding the axial images, celiac trunk had a straight direction in 187 patients (61.5%), a rightward direction in 111 patients (36.5%) and a leftward direction in 6 patients (1.9%). We believe that the knowledge about the morphology, origin angle, and direction of the celiac trunk can be a guide for the interventional radiological procedures and decrease the risk of possible complications.

Key words: Celiac trunk – Morphological findings – Multidetector computed tomography

INTRODUCTION

The celiac trunk, which is the first and one of the most important branches of the aorta, originates at the level of diaphragm's aortic hiatus and upper edge of the first lumbar vertebra. Its three branches (left gastric artery, splenic artery and common hepatic artery) are responsible for the perfusion of the liver, gall bladder, pancreas, spleen, stomach, distal esophagus and proximal duodenum (White et al., 2015).

As the celiac trunk is the most important structure supplying the upper gastrointestinal system, knowledge about its morphology and variations is critical for the management of the surgical and interventional radiological procedures in the upper abdomen. There are several studies on the morphology and variations of the celiac trunk and they showed that variations of the celiac trunk are not rare (Iezzi et al., 2008; Marco-Clement et al., 2016; Ozbülbül, 2011). The majority of these

Corresponding author:
Azad Hekimoglu, M.D. Dışkapı Yıldırım Beyazıt Eğitim ve Araştırma Hastanesi, Radyoloji Bölümü, Dışkapı, 06110, Ankara, Turkey.
Phone: 00 90 312 5962619 / Mobile: 00 90 506 7559485. E-mail: azadhekimoglu@gmail.com

Submitted: November 21, 2020. **Accepted:** February 13, 2021

studies had been focused on the branching of the celiac trunk and on the classification related to the branching (Iezzi et al., 2008; Marco-Clement et al., 2016; Panagouli et al., 2013).

In our study, our objective was to investigate the corpus of the celiac trunk: in other words, the part between the origin of the trunk and the bifurcation instead of the branching of the trunk. The length, diameter of the celiac trunk and the rate of stenosis were also examined. In addition, we measured the direction of the celiac trunk at the axial plane and the angle of the origin from the aorta at the sagittal plane.

MATERIALS AND METHODS

The CT images of 320 patients, who had undergone contrast-enhanced CT angiography due to any reason in our hospital, were investigated in a retrospective study design. In 4 of the evaluated patients, the common hepatic artery and gastrosplenic trunk originated separately from the aorta. In 2 patients, the left gastric artery, common hepatic artery and splenic artery originated individually. In 8 patients, there was a gastrosplenic trunk and the common hepatic artery originated from the superior mesenteric artery (SMA). In one patient, the celiac trunk and the superior mesenteric artery formed together the celiacomesenteric trunk, and finally another patient had the history of a previous surgery related to the vascular structures of the upper abdomen. Depending on the abovementioned findings, these 16 patients were excluded from the study. The mean age of the included 304 patients was 51 years (17-91 years) and 165 of them were males (Table 1).

The abdominal CT angiography examination was performed with a 128-slice multi-detector CT scanner (GE, Optima CT 660). The images were created with the following parameters: 120kV, 60-100mA, and 0.625mm slice thickness. Arterial CT angiography images were obtained by placing region-of-interest (ROI) in the descending aorta, and by administering 80-100 ml of contrast intravenously at 300 psi and 4 ml / sec. The thin-slice imaging data obtained at the axial plane in all patients were obtained from PACS and evaluated retrospectively. Multiplanar reformatted (MPR) and maximum intensity projection (MIP) images were created. As the celiac trunk is easily visible at the sagittal plane, we preferred the axial and sagittal planes for the evaluation. All CT images were evaluated by two radiologists and the reports were prepared after the consensus between them.

First, calibration of the celiac trunk and the length between the origin of the trunk and the first branching were measured. The angle between the abdominal aorta and the celiac trunk at the level of the origin at the sagittal plane and the direction of the distal part of the trunk at the axial plane were also evaluated. A straight truncal direction within the abdominal aorta margins were considered as *straight*, as *rightward* if this direction exceeded the imaginary line drawn from the right margin of abdominal aorta towards the anterior, and as *leftward* if the direction exceeded the imaginary line drawn from the left margin of abdominal aorta towards the anterior (Fig. 1). Finally, we checked

Table 1. Demographical and radiological characteristics.

	Female	**Male**	**Total**
Patient	139 (45.7%)	165 (54.3%)	304
Age	53.16	50.16	(p=0.126)
No stenosis	121 (40%)	147 (48.2%)	268 (88.2%)
Mild stenosis	14 (4.6%)	11 (3.6%)	25 (8.2%)
Severe stenosis	4 (1.3%)	7 (2.3%)	11 (3.6%)
Straight forward direction	82 (27%)	105 (34.5%)	187 (61.5%)
Rightward direction	54 (17.8%)	57 (18.7%)	111 (36.5%)
Leftward direction	3 (0.99%)	3 (0.99%)	6 (1.98%)

the presence and grade of stenosis in the origin of the celiac trunk. Stenosis was evaluated in two grades as mild (<50%) and severe (>50%) (Fig. 2).

The data of our study were analyzed with the SPSS v21 software package and normally-distributed parameters were assessed with the T-test. The Mann-Whitney U test was used for the angle of the celiac trunk.

RESULTS

The mean length of the celiac trunk (segment between the origin and the first branching) in the included 304 individuals was 28.11 mm (11.1-44.6 mm), and the mean diameter was 8.05 mm (5.9-10.5 mm). The mean length of the celiac trunk was 27.13 mm and mm in females and males respectively, and the difference was statistically significant.

The mean diameter of the celiac trunk was 7.83 mm and 8.24 mm in females and males respectively, and the difference was also statistically significant (Table 2).

Stenosis was observed in the celiac trunk in a total of 36 patients (11.8%). Twenty- five patients (8.2%) were categorized as mild (<50%), while the remaining 11 patients as severe (>50%). Poststenotic dilatation in the celiac trunk was observed in 4 of the patients with severe stenosis. Eighteen patients with stenosis were female (14 mild, 4 severe). Similarly, 18 male patients had stenosis (11 mild, 7 severe) (Table 1).

The origin angle between the celiac trunk and the abdominal aorta was between 90° and 150° at the sagittal plane in the participating 304 individuals (mean value=121.20°) (Fig. 3). The origin angle of the celiac trunk was 124.32° and 118.58° in females and males respectively, and the difference was not statistically significant (p=0.05) (Table 2).

Regarding the direction of the celiac trunk in the axial images, the trunk had a straight course in 187 patients (61.5%), while it had a rightward and leftward direction in 111 (36.5%) and 6 patients (1.9%) respectively (Table 1).

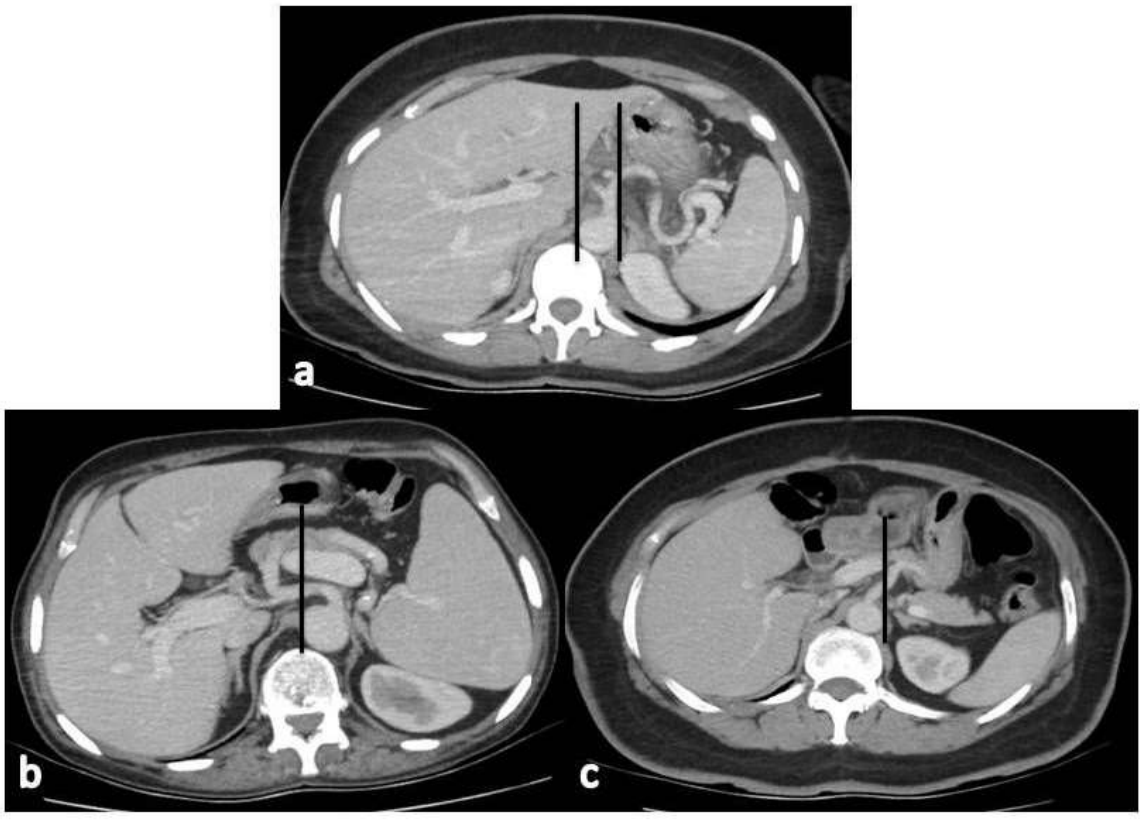

Fig. 1.- Axial contrast-enhanced abdominal CT image **a.** Direction of the celiac trunk is straight forward within the imaginary lines at the margins of abdominal aorta. **b.** Rightward direction of the celiac trunk. **c.** Leftward direction of the celiac trunk.

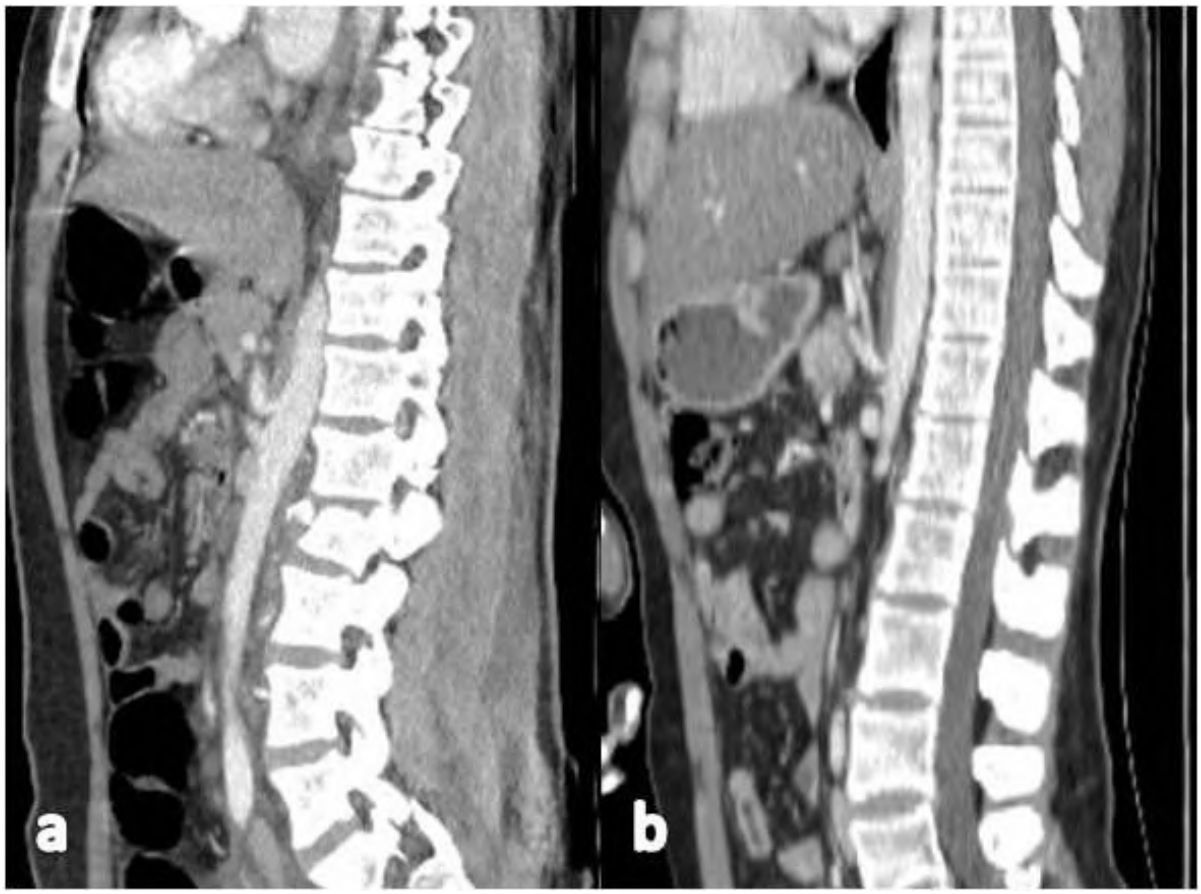

Fig. 2.- Sagittal contrast-enhanced abdominal CT images. **a.** Mild stenosis at the origin of the celiac trunk (<%50); **b.** Severe stenosis (>%50).

Table 2. Length, diameter and angle differences of the celiac trunk between females and males with p values.

	Female	**Male**	**p**
Length	27.13	28.93	<0.05
Diameter	7.83	8.24	<0.05
Origin angle	124.32˚	118.58˚	=0.05

DISCUSSION

The abnormal embryonic development of the ventral splanchnic arteries may lead to different vascular variations. Therefore, knowledge about the morphology of the celiac trunk is necessary for the planning of the upper abdominal surgeries and angiographic interventional procedures like transarterial chemoembolization for the liver tumors. The identification of the vascular variations is important not only for both anatomic and embryological knowledge but also for the prevention of the complications during the surgery and invasive radiological procedures. Parallel to the developments in the CT technology, multi-detector computed tomography (MDCT) became a valuable tool for the imaging of the celiac trunk and branches. MDCT angiography, which enables the definition of the anatomic variants apart from the normal anatomy, is a suitable and minimally invasive method for the evaluation of the celiac structure. It enables the avoidance of the complications related to the conventional angiography (Cavdar et al., 1997; Koops et al., 2004; Winston et al., 2007; Sone et al., 2008; Sahani et al., 2002).

In our study, the segment between the origin of the celiac trunk and the first branching was evaluated and the length and diameter of the celiac trunk were primarily measured. The mean length of the celiac trunk was reported 23 mm in a previous study performed with MDCT (Araujo Neto et al., 2015) and 26 mm in a study performed

on cadavers (Panagouli et al., 2011). The mean length of the celiac trunk was 28.11 mm in our study. Furthermore, the mean diameter of the celiac trunk was reported 8 mm in an MDCT study (Panagouli et al., 2011) and 7.9 mm in another study performed on cadavers (Silveira et al., 2009). Our result was 8.05 mm, which was compatible with the previous studies. In our study, we determined significant differences between males and females for the length and diameter of the celiac trunk. The dimension of these parameters was significantly higher in males compared to females.

Although the distal part of the celiac trunk is free and its position may minimally change according to the localization of the intraabdominal organs, breathing condition and lying position of the patient, we believe that the origin of the celiac trunk will be not much affected from this condition (Fig. 4). Measurements showed that the origin angle between the celiac trunk and aorta was between 90° and 150° with a mean value of 121.2°. Although it was not statistically significant, we noticed that the angle of the celiac trunk was wider in females compared to males and directed towards inferior. In addition, we determined that the celiac trunk had straight anterior direction in 61.5% of patients at the axial planes. We observed that it had a rightward direction in 36.5% and a leftward direction in as less as 1.9% of patients. We concluded that the celiac trunk usually had a direction towards inferior and anterior and to a lesser direction rightwards, which can be a guide for the angiographic interventional procedures.

The median arcuate ligament syndrome (MALS), which is also known as the celiac artery compression syndrome or Dunbar syndrome, is a clinical condition caused by the compression of the celiac trunk by the median arcuate ligament. MALS was first recognized in the 1960s and reported to occur usually in slim women between the ages of 20 and 40 (Harjola, 1963; Dunbar et al., 1965; Horton et al., 2005). However, it was demonstrated with angiographic examinations that the celiac body compression may be encountered in normal population with changing rates (13-50%) (Szilagyi et al., 1972; Bron and Redman, 1969). It was stated that

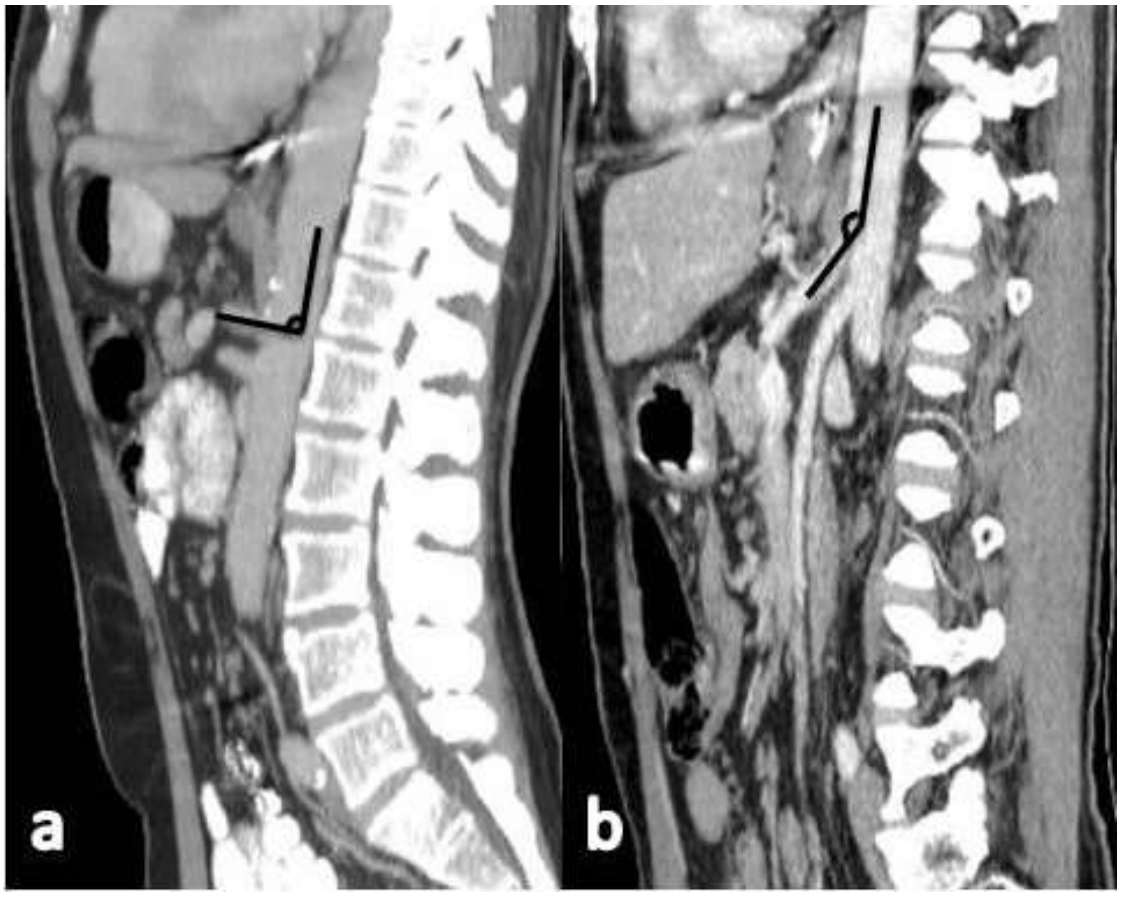

Fig. 3.- Sagittal contrast-enhanced abdominal CT image. Angle between the celiac trunk and abdominal aorta ranges between **a.** 90° and **b.** 150°.

the absence of MALS symptoms in cases with stenosis in the celiac trunk may be associated with the retrograde filling through SMA or other branches (Van Petersen et al., 2014). In our study, we observed stenosis in 11.8% of the cases at the celiac trunk origin, and all of them were attributed to compression of the median arcuate ligament.

The findings of the celiac artery stenosis caused by the median arcuate ligament in the CT scans were defined with the stenosis detected in the axial images and with the hook or "J" shape appearance in the sagittal reconstructions (Horton et al., 2005; Lee et al., 2018). However, in a study conducted by Petnys et al. (2018), the authors stated that the hook or "J" appearance should not be interpreted as a result of the external compression. They emphasized that the compression of the celiac axis by the median arcuate ligament occurred in 3.42% of the normal population but did not manifest any symptoms, a hook or "J" appearance was mostly not observed in this subgroup in the standard inspiratory phase CT imaging (Petnys et al., 2018). In our study, it was observed that this appearance changed in CT images taken at different dates in several patients. We think that the hook or "J" appearance in the distal of the celiac body may change depending on the respiratory condition of the patient, such as inspiration or expiration. (Fig. 4).

CONCLUSION

We conclude that the knowledge of the origin angles and the possible direction of the distal segment of the celiac trunk, as well as the vessel diameter, presence and degree of stenosis, provides useful information when planning endovascular treatments. This information may shorten the duration of the interventional procedures by suitable equipment selection, as well as decrease iatrogenic injuries.

REFERENCES

ARAUJO NETO SA, FRANCA HA, DE MELLO JUNIOR CF, SILVA NETO EJ, NEGROMONTE GR, DUARTE CM, CAVALCANTI NETO BF, DE FONSECA FARIAS RD (2015) Anatomical variations of the celiac trunk and hepatic arterial system: an analysis using multidetector computed tomography angiography. *Radiol Bras,* 48(6): 358-362.

BRON KM, REDMAN HC (1969) Splanchnic artery stenosis and occlusion: incidence, arteriographic and clinical manifestations. *Radiology,* 92: 323-328.

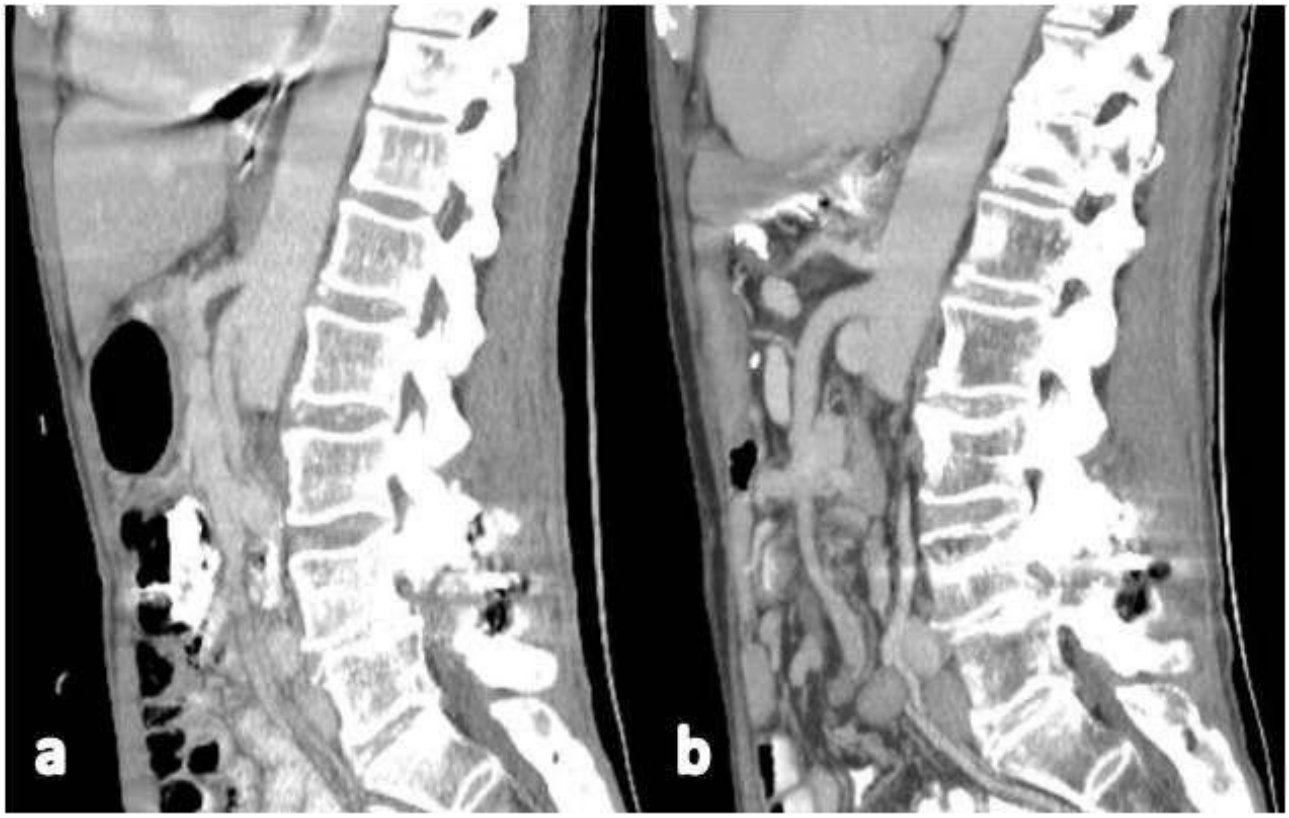

Fig. 4.- a, b. Sagittal contrast-enhanced abdominal CT images of a 61-year-old male patient taken on different dates. The distal part of the celiac trunk is displaced according to the position of the patient and intraabdominal organs while the angle of the origin is preserved.

CAVDAR S, SEHIRLI U, PEKIN B (1997) Celiacomesenteric trunk. *Clin Anat,* 10(4): 231-234.

DUNBAR JD, MOLNAR W, BEMAN FF, MARABLE SA (1965) Compression of the celiac trunk and abdominal angina. *Am J Roentgenol Radium Ther Nucl Med,* 95: 731-744.

HARJOLA PT (1963) A rare obstruction of the coeliac artery. Report of a case. *Ann Chir Gynaecol Fenn,* 52: 547-550.

HORTON KM, TALAMINI MA, FISHMAN EK (2005) Median arcuate ligament syndrome: Evaluation with CT angiography. *Radiographics,* 25: 1177-1182.

IEZZI R, COTRONEO AR, GIANCRISTOFARO D, SANTORO M, STORTO ML (2008) Multidetector-row CT angiographic imaging of the celiac trunk: anatomy andnormal variants. *Surg Radiol Anat,* 30: 303-310.

KOOPS A, WOJCIECHOWSKI B, BROERING DC, ADAM G, KRUPSKI-BERDIEN G (2004) Anatomic variations of the hepatic arteries in 604 selective celiac and superior mesenteric angiographies. *Surg Radiol Anat,* 26: 239-244.

LEE KH, YU ML, CHEUNG M (2018) The hooked proximal celiac artery. *Abdom Radiol,* 43(3): 753-754.

MARCO-CLEMENT I, MARTINEZ-BARCO A, AHUMADA N, SIMON C, VALDERRAMA JM, SANUDO J, ARRAZOLA J (2016) Anatomical variations of the celiac trunk: cadaveric and radiological study. *Surg Radiol Anat,* 38(4): 501-510.

OZBÜLBÜL NI (2011) CT angiography of the celiac trunk: anatomy, variants and pathologic findings. *Diagn Interv Radiol,* 17(2): 150-157.

PANAGOULI E, LOLIS E, VENIERATOS D (2011) A morphometric study concerning the branching points of the main arteries in humans: relationships and correlations. *Ann Anat,* 193: 86-99.

PANAGOULI E, VENIERATOS D, LOLIS E, SKANDALAKIS P (2013) Variations in the anatomy of the celiac trunk: A systematic review and clinical implications. *Ann Anat,* 195(6): 501-511.

PETNYS A, PUECH-LEAO P, ZERATI AE, RITTI-DIAS RM, NAHAS WC, NETO ED, DE LUCCIA N (2018) Prevalence of signs of celiac axis compression by the median arcuate ligament on computed tomography angiography in asymptomatic patients. *J Vasc Surg,* 68(6): 1782-1787.

SAHANI D, SAINI S, PENA C, NICHOLS S, PRASAD SR, HAHN PF, HALPERN EF, TANABE KK, MUELLER PR (2002) Using multidetector CT for preoperative vascular evaluation of liver neoplasms: technique and results. *AJR Am J Roentgenol,* 179: 53-59.

SILVEIRA LA, SILVEIRA FBC, FAZAN VPS (2009) Arterial diameter of the celiac trunk and its branches. Anatomical study. *Acta Cir Bras,* 24: 43-47.

SONE M, KATO K, HIROSE A, NAKASATO T, TOMABECHI M, EHARA S, HANARI T (2008) Impact of multislice CT angiography on planning of radiological catheter placement for hepatic arterial infusion chemotherapy. *Cardiovasc Intervent Radiol,* 31(1): 91-97.

SZILAGYI DE, RYAN RL, ELLIOTT JP, SMITH JP (1972) The celiac artery compression syndrome: does it exist? *Surgery,* 72: 849-863.

VAN PETERSEN AS, KOLKMAN JJ, MEERWALDT R, HUISMAN AB, VAN DER PALEN J, ZEEBREGTS CJ, GEELKERKEN RH (2014) Mesenteric stenosis, collaterals, and compensatory blood flow. *J Vasc Surg,* 60: 111-119.

WHITE RD, WEIR-MCCALL JR, SULLIVAN CM, MUSTAFA SA, YEAP PM, BUDAK MJ, SUDARSHAN TA, ZEALLEY IA (2015) The celiac axis revisited: anatomic variants, pathologic features, and implications for modern endovascular management. *Radiographics,* 35(3): 879-898.

WINSTON CB, LEE NA, JARNAGIN WR, TEITCHER J, DEMATTEO RP, FONG Y, BLUMGART LH (2007) CT angiography for delineation of celiac and superior mesenteric artery variants in patients undergoing hepatobiliary and pancreatic surgery. *AJR Am J Roentgenol,* 189: W13-19.

Anatomical variations of the left coronary artery: a cadaveric and radiological study

Hanan D. Yassa[1], Gaber H. Abdelfatah[1], Nourhan T. Sabra[1], Abd Elwakeel E. Essawy[2]

[1] Department of Anatomy and Embryology, Faculty of Medicine, Beni-Suef University, Beni-Suef, Egypt

[2] Department of Anatomy and Embryology, Faculty of Medicine, Cairo University, Cairo, Egypt

SUMMARY

The present study was designed to assess the incidence of different anatomical variations of the left coronary artery (LCA) and their branches. Also, it was designed to study the dominance pattern of coronary arteries. It was carried out on 30 human adult cadaveric hearts, 200 three-dimensional coronary computed tomographic angiography (3D-CCTA) scans, and 200 coronary catheterization angiography obtained from the Anatomy, Radiology, and Cardiology Department, Beni-Suef, Cairo as well as El Minia University. The current work revealed that there was not any case of higher take-off origin of the left coronary artery. The incidence of the LCA branching mode was 74.1%, 24.18%, and 0.46% for the bifurcation, trifurcation, and tetrafurcation, respectively. A statistically significant correlation between the diagonal branches of the left anterior descending artery and the mode of branching of the LCA had been demonstrated. The incidence of coronary artery dominance was 77%, 14%, and 9% for right, left, and co-dominant pattern. It can be concluded that perfect knowledge of the anatomical variations of the mode of branching of the LCA is essential for cardiologists and radiologists, during diagnostic and therapeutic cardiac procedures.

Key words: Heart – Left coronary artery – Diagonal artery – Myocardial bridge – Coronary dominance

LIST OF ABBREVIATIONS

CCTA: Coronary computed tomography angiography.

CT: Computed tomography.

CX: Circumflex artery.

D: Diagonal branch.

LAD: Left anterior descending artery.

LCA: Left coronary artery.

MB: Myocardial bridge.

OM: Obtuse marginal artery.

PDA: Posterior descending artery.

RCA: Right coronary artery.

RI: Ramus intermedius artery.

INTRODUCTION

Ischemic heart disease caused 7 million deaths all over the world in 2010, an increase of 35% since 1990 (Lozano, 2012). Whatever the etiology and pathophysiology of coronary artery disease are, the coronary artery remains the seat of the disease process. The increasing use of diagnostic

Corresponding author:
Nourhan Tharwat Sabra. Department of Anatomy and Embryology, Faculty of Medicine, Beni-Suef University, Beni-Suef, Egypt. Phone: 002-01100229244. E-mail: nor.th_2009@yahoo.com

Submitted: November 6, 2020. **Accepted:** February 21, 2021

and therapeutic interventional procedures necessitates that a sound basic knowledge of coronary artery pattern with dominance is essential (Das et al., 2010).

The anatomy of the coronary arteries has been described for at least three centuries. However, most of the reports are based on views and perspectives obtained from gross specimens (Fiss, 2007; Young et al., 2011).

The arterial supply of the heart is provided by the right and left coronary arteries. They are located between the epicardium and myocardium; these vessels arise from the bulbous aorta as two branches of the ascending aorta (Snell, 2011). The left main coronary artery originates from the left coronary sinus of Valsalva (Moore and Dalley, 2006). The morphology of the left coronary artery has been reported to present wide variability regarding its length, caliber, and mode of branching. Its trunk divides into several ways: bifurcation into left anterior descending (LAD) and circumflex (CX) branches, or trifurcation into LAD, CX, and median or ramus intermedius (RI) arteries (Beg et al., 2015). Tetra- and pentafurcation patterns of branching have been also mentioned (Reig and Petit, 2004; Roy et al., 2014). The bifurcation pattern has been described as the most frequent one (Chougule et al., 2014).

Recently, technical advances in computed tomography (CT) have improved image quality, diagnostic performance, and accuracy of coronary CT angiography (CCTA) (Graidis et al., 2015). Dose-reduction strategies have reduced radiation dose to an acceptable level, even lower than that from conventional coronary angiography (Altin et al., 2015). Three- dimensional CCTA is a noninvasive imaging modality, which can effectively show complex anatomy and variations of the coronary arteries (Erol et al., 2013).

Cardiac catheterization remains the gold standard in the diagnosis of coronary artery anomalies. The objective of angiocardiography is to establish the integrity and source of the coronary arteries (Takeuchi et al., 1979).

MATERIAL AND METHODS

Cadaveric Study

This descriptive study was done in 30 adult cadaveric hearts in the Department of Anatomy at Beni-Seuf, Cairo, and El Minia Universities of Medicine. The adult cadaveric hearts of both genders (aged 24-68 years) without any obvious pathology were included. The hearts with any gross pathology, traumatic damage, or congenital anomalies were excluded from the study. The heart was taken out by incising the fibrous pericardium and great vessels like aorta, pulmonary trunk, superior vena cava, inferior vena cava, and pulmonary veins. The specimens were collected, numbered, and preserved in a 10% formalin solution. The visceral pericardium and subepicardial fat were removed. The LCA and its branches were carefully dissected out and followed till their termination. The origin, course and termination of variations in varous branches, if any, were noted. To determine the dominant circulation, the origin of PIVA was noted in each specimen. Photographs of each specimen were taken using a digital camera, numbered, and labeled. The events followed were well-matched with the ethical standards for human experimentation. The ethical committee approved the study.

Radiological study

Coronary CT Angiography (CCTA):

Two hundred adult individuals of both genders (aged 24–68 years, free from major cardiac complaints and previous bypass surgery) were subjected to 3D-CCTA in certified radiology centers. Imaging was performed on 320-row CT scanners (Aquilion ONE, Toshiba Medical Systems, Tochigi-ken, Japan).

The main trunk of LCA was followed from its orifice until its division into the left anterior descending (LAD) and circumflex (CX) arteries. Its mode of branches was observed and recorded (Kini et al., 2007).

Coronary catheterization (coronary angiogram):

Two hundred adult individuals of both sexes, free from major cardiac complaints, atherosclerotic lesions in coronary arteries, history of coronary stent insertion, and previous bypass surgery were subjected to coronary angiogram in the Cardiology Department at Beni-Suef University.

Statistical analysis

After compilation of collected data, an analysis was done using Statistical Package for Social Sciences (SPSS), version 20 (IBM, Chicago, USA).

Qualitative data were expressed as frequency and percentage. Chi-square test or Fisher's exact test was used to examine the relation between qualitative variables. The differences were considered statistically significant when the p-value was <0.05.

RESULTS

Out of 430 hearts (30 cadavers, 200 3D CT angiography, and 200 coronary catheterizations), the overall incidence of the different patterns of LCA branching mode was 0.23% in which LCA continues as LAD (one branch), 74.1% in bifurcation, 24.18% in trifurcation, and 0.46% in tetrafurcation patterns. And the incidence of absent LCA was 0.93% as LAD and LCX (Table 1) (Figs. 1,2,3).

The diagonal (D) branches of the LAD artery were found in 319 hearts out of 319 with the bifurcation pattern (100%), 101 out of 104 hearts with the trifurcation pattern (97%), and 0 out of 2 hearts with the tetrafurcation pattern (0.0%). A significant relationship was detected between the incidence of the diagonal branches and the mode of branching of the LCA (Table 2) (Figs. 1,2,3).

The myocardial bridge was identified to obscure parts of the course of some branches of the LCA. Myocardial bridges were identified to obscure parts of the course of some branches of the LCA in 3 of 30 dissected cadaveric hearts. They were noticed to cross parts of the LAD and RI arteries. In CCTA, the myocardial bridges were observed in 27 of 200 scans (13.5%).

The myocardial bridges were observed in 30 out of 230 studied hearts (cadaver and CCTA only) (13.01%): 21 out of 168 hearts (12.5%) in the bifurcation pattern and 9 out of 59 hearts (15.2%) in the trifurcation pattern and 0 out of 2 hearts (0.0%) in the tetrafurcation pattern. The myocardial bridge could not be seen in the coronary catheterization. A significant relationship was detected between the incidence of these bridges and the mode of branching of the LCA (Table 3) (Figs. 1, 2).

In the present study, the right coronary artery (RCA) showed abnormal origin from LCA and its branches as fellow: from LCA in 0.23% (1 case), from LCX in 0.23% (1 case), and from LAD in 0.93% (4 cases) (Table 4) (Fig. 3).

According to coronary circulation, the posterior descending (PD) artery arose from RCA in 77%. These were called 'right dominant'. And PDA arose from LCX in 14% of studied hearts called 'left dominant' and in 9% both arteries gave origin to PDA. These were called 'balanced type' or 'co-dominant' (Figs. 4, 5).

DISCUSSION

Cardiovascular diseases are the leading cause of mortality worldwide, being responsible for about one-third of all deaths. With the increasing load of coronary heart diseases, the detailed anatomy

Table 1. Incidence of branching patterns of the left coronary artery.

	Frequency	Percent
Absent LCA (Separate ostium from aorta)	4	0.93%
Left Coronary has one branch (LAD)	1	0.23%
Bifurcation	319	74.1%
Trifurcation	104	24.18%
Tetra furcation	2	0.46%
Total	430	100%

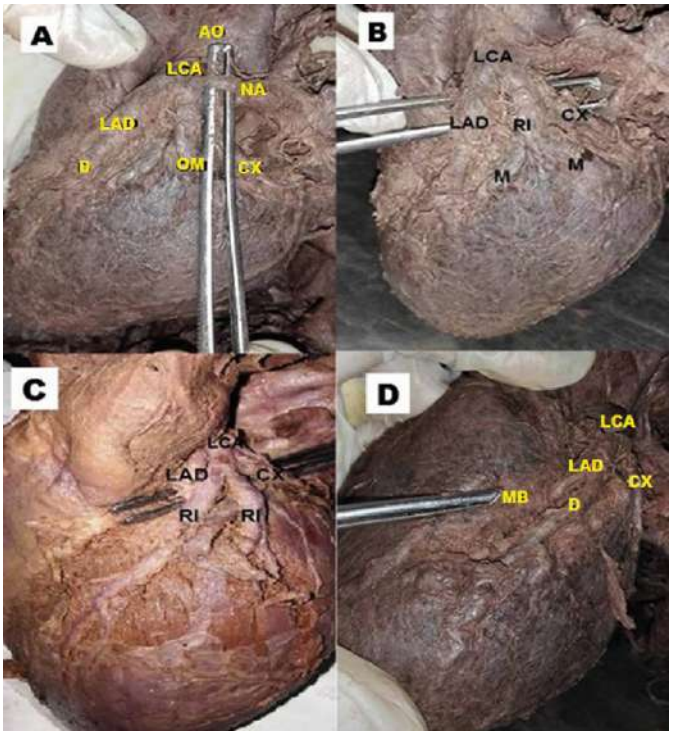

Fig. 1.- A dissected human heart. **A:** bifurcation pattern of the left coronary artery (LCA) into the left anterior descending (LAD) and circumflex (CX) arteries. The LAD artery gives a diagonal (D) branch and the CX gives an obtuse marginal (OM) branch. Note: AO is referred to as ascending aorta and NA is referred to as a sinoatrial nodal branch of the left coronary artery. **B:** trifurcation pattern of the left coronary artery (LCA) into the left anterior descending artery (LAD), one ramus intermedius (RI), and circumflex artery (CX) branches. The RI artery appears equal in size to the LAD and gives muscular branches (M) to the left ventricle. **C:** left coronary artery (LCA) dividing into four branches (tetrafurcation): left anterior descending (LAD), circumflex (CX) and two ramus intermedius (RI) arteries. **D:** left coronary artery (LCA) dividing into two branches: left anterior descending (LAD) and circumflex (CX). Myocardial bridge (M.B.) interrupting the course of LAD is also observed.

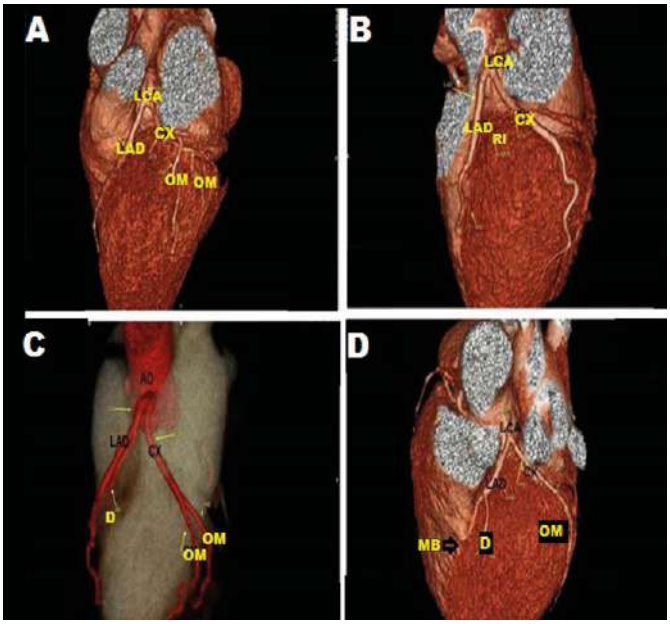

Fig. 2.- 3D CT coronary angiography. **A:** The left coronary artery (LCA) dividing into left anterior descending (LAD) and circumflex (CX) arteries. Two obtuse marginal (OM) arteries are branches of CX. **B:** The left coronary artery (LCA) dividing into left anterior descending (LAD) and circumflex (CX) arteries. A diagonal branch (D) is seen arisen from LAD and obtuse marginal (OM) is seen arise from CX. **C:** The left anterior descending (LAD) and circumflex (CX) arteries are arising directly from the ascending aorta (AO) by a separate ostium and the left coronary artery (LCA) is absent. A diagonal branch (D) is seen arisen from LAD and obtuse marginal (OM) is seen arise from CX. **D:** The left coronary artery (LCA) dividing into left anterior descending (LAD) and circumflex (CX) arteries. A diagonal branch (D) is seen arisen from LAD and obtuse marginal (OM) is seen arise from CX. Myocardial bridge (M.B.) interrupting the course of LAD is also observed.

of coronary arteries has been investigated by medical professionals (Tomar et al., 2013).

30 postmortem hearts, 200 3D CCTA scans, and 200 catheterization angiographies were enrolled in the present study to investigate the different patterns of the mode of branching of the left coronary artery. The current work has revealed that, in most of the specimens (99.07%), the LCA has arisen from the left posterior aortic sinus of the ascending aorta. This finding runs with what is reported by most authors (Kulkarnil and Metha, 2012; Dombe et al., 2012; Erol et al., 2013). The

Table 2. Relation between the diagonal (D) branches of the LAD artery and the branching patterns of the LCA.

Bifurcation Pattern		**LAD Diagonal No.**					
		0	**1**	**2**	**3**	**4**	**Total**
Bifurcation	Count	0	60	202	55	2	**319**
	% within LCA branch	0.0%	18.8%	63.3%	17.2%	0.6%	**100%**
Trifurcation	Count	3	72	22	6	1	**104**
	% within LCA branch	2.88%	69.2%	21.2%	5.8%	1%	**100%**
Tetrafurcation	Count	2	0	0	0	0	**2**
	% within LCA branch	100 %	0.0%	0.0%	0.0%	0.0%	**100%**
Total	Count	5	132	224	61	3	**425**
	% of Total	1.2%	31.1%	52.7%	14.4%	0.7%	**100%**
Chi- Square Tests							
Pearson Chi-Square				**P-value: 0.001**			

Significant: $p \leq 0.05$.

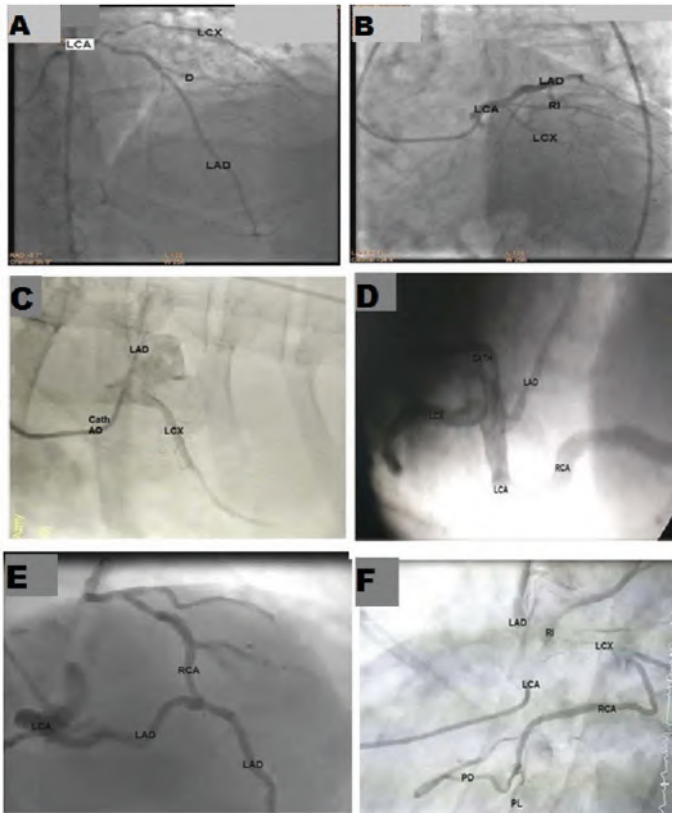

Fig. 3.- Coronary catheterization angiography study showing: **A:** The left coronary artery (LCA) dividing into left anterior descending (LAD) and circumflex (LCX) arteries (bifurcation). One diagonal (D) is seen as a branch of LAD. **B:** The left coronary artery (LCA) dividing into 3 branches: left anterior descending (LAD), circumflex (LCX), and ramus intermedius (RI) arteries (Trifurcation). **C:** Absent left coronary artery (LCA). As left anterior descending (LAD) and left circumflex (LCX) arteries arise from separate ostium from the aorta. **D:** The left coronary artery (LCA) is dividing into left anterior descending (LAD) and left circumflex (LCX) arteries and also gives rise to the right coronary artery (RCA) from its beginning. **E:** The left coronary artery (LCA) is dividing into left anterior descending (LAD) and left circumflex (LCX) arteries. The right coronary artery (RCA) is raised from LAD. **F:** The left coronary artery (LCA) is dividing into left anterior descending (LAD), left circumflex (LCX), and ramus intermedius (RI) arteries. RCA is raised from LCX. RCA is terminated into two terminal branches (PL and PD).

location and level of the coronary ostia are essential for the successful performance of a coronary angiogram (Taylor et al., 2000). In the present study, the LCA has been observed to run between the pulmonary trunk and left atrial appendage in all cases. This is coincident with most of the studies met within the literature (Cademartiri et al., 2008; Jacobs, 2010). The left coronary artery has been frequently mentioned to exhibit variations regarding the mode of its branching; it might be bifurcated, trifurcated, tetrafurcated or even pentafurcated (Ajayi et al., 2013). In the current investigation, the incidence of patterns of branching mode of the left coronary artery in all studied hearts (dissected and scanned), was 74.1% (bifurcated), 24.18% (trifurcated), and 0.46% (tetrafurcated). The incidences of the branching pattern of LCA reported in several large-scale studies are summarized in Table 5.

In the present work, the frequency of the bifurcation pattern of the LCA is more than threefold that of the trifurcation pattern (74.1% vs 24.18%). This is in agreement with Tomar et al. (2013), who mentioned that the incidence of the trifurcation pattern was about one-third that of the bifurcation pattern (24% vs 76%). Fazliogullari et al. (2010) reported a nearly equal incidence of both bifurcation and trifurcation patterns. The contradiction between these reported results and ours could be explained on grounds of the different approaches used for defining the ramus intermedius (RI) artery of the LCA.

Some authors consider the RI as an artery located in the angle between the LAD and CX arteries (Reig and Petit, 2004). Other authors considered that the RI artery as that originated from the vertex of the angle between LAD and CX arteries or from the initial millimeters of the LAD or CX artery themselves (Angelini et al., 1999). The present study has followed the way of identification of the RI artery that was mentioned by Reig and Petit. (2004).

The ramus intermedius (RI) artery represents an essential source of collateral blood flow in

Table 3. Relation between the incidence of the myocardial bridges and the branching patterns of the LCA.

Furcation Pattern		**Myocardial bridge**		
		Absent	**Present**	**Total**
Bifurcation	Count	147	21	168
	% within LCA_branch	87.5%	12.5%	100.0%
Trifurcation	Count	50	9	59
	% within LCA_branch	84.7%	15.2%	100.0%
Tetrafurcation	Count	2	0	2
	% within LCA_branch	100.0%	0.0%	100.0%
Total	Count	199	30	229
	% within LCA_branch	86.89%	13.1%	100.0%
Chi-Square Tests				
Pearson Chi-Square		**P -value**: 0.001		

Table 4. Frequency of the origin of the right coronary artery RCA.

	Frequency	**Percent**
Normal	423	98.37
Higher origin above sinus	1	0.23
From LCA	1	0.23
From LCX	1	0.23
From LAD	4	0.93
Total	430	100.0

coronary insufficiency (Surucu et al., 2004; Shammas et al., 2009). The trifurcation of the LCA usually has no adverse hemodynamic effects and may play a protective role against the development of myocardial ischemia (Abuchaim et al., 2009). However, this pattern could cause technical difficulties in catheterization and might be a source of complication or misdiagnosis (Shammas et al., 2007; Koşar et al., 2009).

In the present study, a significant correlation between the incidence of the diagonal branches of the LAD artery and the branching patterns of LCA. Similar findings were reported by Reig and Petit. (2004)

In all the studies the majority of hearts were right dominant. Even though right dominance is predominant, the LCA is almost always considered more important than the RCA, as it is the major source of blood flow to the left ventricle in almost all humans even in those with anatomical right dominance.

The left dominance has been found to have significantly higher mortality than the right dominance and mixed dominance types (Goldberg et al., 2007). Dominance also plays an important role in the inferior wall infarcts of the heart. Inferior wall infarcts, although less extensive than anterior wall infarcts, are more important as they can cause various degrees of atrioventricular blocks in approximately 30% of cases (Agrawal and Arya, 2016).

In the present study, the incidence of left coronary dominance was assessed to be

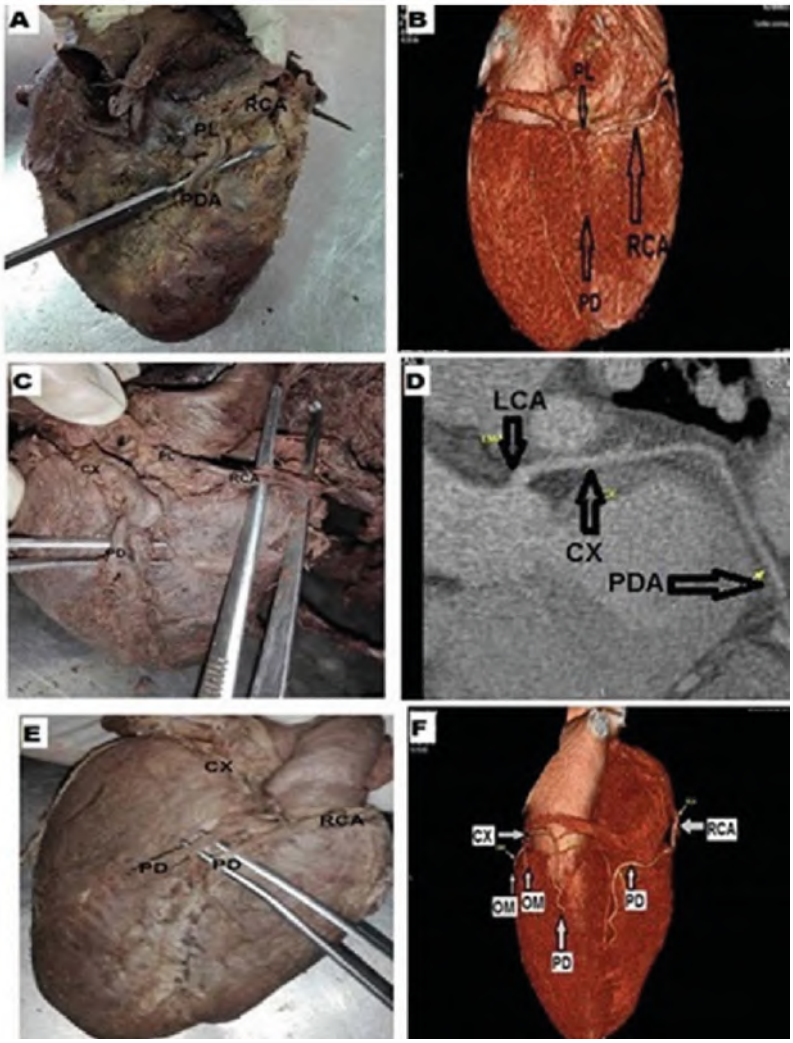

Fig. 4.- Pictures of **A:** Cadaver dissection and **B:** 3D CT angiography. Both of them showing the right coronary artery (RCA) termination into a posterior descending artery (PDA) and posterolateral artery (PL) in the right dominant heart. **C:** Cadaver dissection and **D:** 3D CT angiography showing a left dominance pattern where the posterior descending artery (PD) arose from the circumflex artery (CX), not from the right coronary artery (RCA). RCA is terminated by giving the posterolateral artery (PL). **E:** Cadaver dissection and **F:** 3D CT angiography showing a balanced pattern where the posterior descending artery (PD) arises from both the right coronary artery (RCA) and circumflex artery (CX), and both PD lying within the posterior interventricular sulcus.

13.5% of all hearts studied. Our left-dominant incidence is nearly similar to that reported by Fazliogullari et al. (2010) 14%. This incidence, herein, is lower than that reported by Ortale et al. (2005) who found that left coronary dominance is 25%.

In the present study, myocardial bridges are found across some of the branches of the LCA in 30 out of the 230 hearts. The current work has revealed a statistically significant relationship between the furcation pattern of LCA and the myocardial bridges. These results tally with the studies made by Loukas et al. (2006) and Beg et al. (2015).

Myocardial bridges may compress the coronary vessel underneath and compromise myocardial blood supply. Cases of sudden cardiac death where myocardial bridging is the only postmortem finding have been reported (Saidi et al., 2010).

The present investigation has demonstrated variations in the origin and branching pattern of the LCA. These variations could have

Table 5. A comparison of the frequency of LCA branching pattern among various studies.

Authors / Year of study	Type of study	Population / Number of cases	Bi-furcation	Tri-furcation	Quadri-furcation
Ballesteros and Ramirez (2008)	Cadaver	154 case Colombians	52%	42.2%	5.8%
Fazliogullari et al. (2010)	Cadaver	50 case Turkish	46%	44%	10%
Kulkarnil and Mehta (2012)	Coronary cath. angio.	107 case Indians	88.46%	11.54%	-
Ajayie et al. (2013)	Coronary cath. angio.	151 case South Africans	80.8%	18.5%	0.7%
Tomar et al. (2013)	CT angio.	50 case Indians	76%	24%	-
Beg et al. (2015)	Cadaver	40 case North Indians	47.5%	42.5%	10%
Nguyen and Talarico (2018)	Cadaver	125case Vietnamese	50.4%	44%	5.6%
Present study (2020)	Cadaver, CT angio & cath. angio.	230 case Egyptians	74.1%	24.18%	0.46%

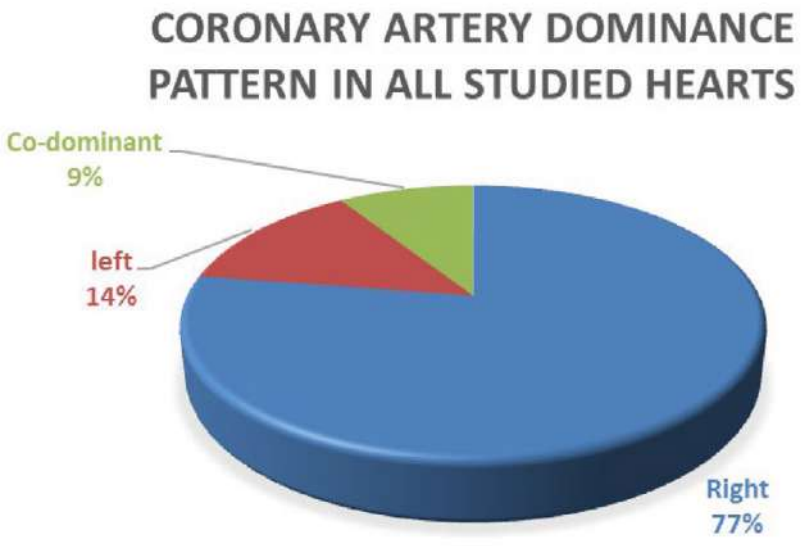

Fig. 5.- A pie chart demonstrating the coronary artery dominance pattern in all studied hearts.

anatomical, pathophysiological, diagnostic, and therapeutic implications. Moreover, before coronary revascularization procedures, precise evaluation and description of the coronary artery tree is greatly needed, in order to report possible coronary variations or anomalies which may cause technical difficulties during coronary interventional procedures and end in catastrophic complications for the patient.

CONCLUSIONS

A detailed study of LCA would be of use to cardiologists and interventional radiologists to predefine the abnormalities by invasive and non-invasive studies. Knowledge of individual and racial variations in coronary arteries is essential for the diagnosis and treatment of coronary artery patients. This morphological study may be helpful for interventional cardiologists and radiologists in diagnosis and in avoiding vascular trauma during diagnostic and therapeutic procedures.

ACKNOWLEDGEMENTS

The authors wish to thank Mohamed Gebreel, M.D. of radiology, who helps us in understanding the C.T coronary angiography. We are also grateful to Khaled Hussein, Msc of cardiology for his valuable guidance in reading the cardiac catheterizations.

REFERENCES

ABUCHAIM DCS, SPERA CA, FARACO DL, FILHO JMR, MALAFAIA O (2009) Coronary dominance patterns in the human heart investigated by corrosion casting. *Revista Brasileira de Cirurgia Cardiovascular*, 24(4): 514-518.

AGRAWAL R, ARYA RS (2016) Anatomical study of coronary dominance and variations of posterior interventricular artery in cadaveric human heart. *Int J Sci Res*, 5(3): 531-534.

AJAYI NO, LAZARUS L, VANKER EA, SATYAPAL KS (2013) Anatomic parameters of the left coronary artery: an angiographic study in a South African population. *Int J Morphol*, 31(4): 1393-1398.

ALTIN C, KANYILMAZ S, KOC S, GURSOY YC, BAL U, AYDINALP A, YILDIRIR A, MUDERRISOGLU H (2015) Coronary anatomy, anatomic variations and anomalies: a retrospective coronary angiography study. *Singapore Med J*, 56(6): 339-345.

ANGELINI P, VILLASON S, CHAN AV, DIEZ JG (1999) Normal and anomalous coronary arteries in humans. In: Angelini P (ed). *Coronary artery anomalies. A comprehensive approach*. Lippincot Williams & Wilkins, Philadelphia, pp 27-79.

BALLESTEROS LE, RAMIREZ LM (2008) Morphological expression of the left coronary artery: a direct anatomical study. *Folia Morphol*, 67(2): 135-142.

BEG MRU, SINGH A, GOEL S, GOEL AK, GOEL V, GOYAL P, SURANA A, SINGH NK, DHANDA MS (2015) Anatomical variations of coronary artery and frequency of median artery: A cadaveric study from Northern India. *Int Arch Integ Med IAIM*, 2(5): 88-94.

CADEMARTIRI F, LA GRUTTA LL, MALAGÒ R, ALBERGHINA F, MEIJBOOM WB, PUGLIESE F, MAFFEI E, PALUMBO AA, ALDROVANDI A, FUSARO M, BRAMBILLA V, CORUZZI P, MIDIRI M, MOLLET NRA, KRESTIN GP (2008) Prevalence of anatomical variants and coronary anomalies in 543 consecutive patients studied with 64-slice CT coronary angiography. *Eur Radiol*, 18(4): 781-791.

CHOUGULE P, SILOTRY N, CHAVAN L (2014) Variation in branching pattern of coronary arteries. *Int J Sci Res*, 3(8): 270-273.

DAS H, DAS G, DAS DC, TALUKDAR K (2010) A study of coronary arterial dominance in the population of Assam. *J Anat Soc India*, 59(2): 187-191.

DOMBE DD, ANITHA T, GIRI PA, DOMBE SD, AMBIYE MV (2012: Clinically relevant morphometric analysis of left coronary artery. *Int J Biol Med Res*, 3(1): 1327-1330.

EROL C, KOPLAY M, PAKSOY Y (2013) Evaluation of anatomy, variation and anomalies of the coronary arteries with coronary computed tomography angiography. *Anatolian J Cardiol*, 13(2): 154-164.

FAZLIOGULLARI Z, KARABULUT AK, DOGAN NU, UYSAL II (2010) Coronary artery variations and median artery in Turkish cadaver hearts. *Singapore Med J*, 51(10): 775-780.

FISS DM (2007) Normal coronary anatomy and anatomic variations. *App Radiol*, 36: 14-26.

GOLDBERG A, SOUTHERN D, GALBRAITH PD, TRABOULSI M, KNUDTSON ML, GHALI WA (2007) Coronary dominance and prognosis of patients with acute coronary syndrome. *Am Heart J*, 154(6): 1116-1122.

GRAIDIS C, DIMITRIADIS D, KARASAVVIDIS V, DIMITRIADIS G, ARGYROPOULOU E, ECONOMOU F, GEORGE D, ANTONIOU A, KARAKOSTAS G (2015) Prevalence and characteristics of coronary artery anomalies in an adult population undergoing multi-detector row computed tomography for the evaluation of coronary artery disease. *BMC Cardiovasc Disorders*, 15(1(: 112.

JACOBS JE (2010) Computed tomographic evaluation of the normal cardiac anatomy. *Radiol Clinics North Am*, 48(3): 701-710.

KINI S, BIS KG, WEAVER L (2007) Normal and variant coronary arterial and venous anatomy on high-resolution CT angiography. *AJR Am J Roentgenol*, 188(6): 1665-1674.

KOSAR P, ERGUN E, OZTURK C, KOSAR U (2009) Anatomic variations and anomalies of the coronary arteries: 64slice CT angiographic appearance. *Diagnostic Intervent Radiol*, 15(4): 275-283.

KULKARNIL JP, MEHTA L (2012) Main left coronary artery system – angiographic anatomy. *IOSR J Dental Med Sci*, 3(2): 5-7.

LOUKAS M, CURRY B, BOWERS M, LOUIS RG, BARTCZAK A, KIEDROWSKI M, KAMIONEK M, FUDALEJ M, WAGNER T (2006) The relationship of myocardial bridges to coronary artery dominance in the adult human heart. *J Anat*, 209(1): 43-50.

LOZANO R (2012) Global and regional mortality from 235 causes of death for 20 age groups in 1990 and 2010: a systematic analysis for the Global Burden of Disease Study 2010. *Lancet*, 380(9859): 2095-2128.

MOORE K, DALLEY AF (2006) Clinically Oriented Anatomy. Lippincott Williams & Wilkins, Baltimore, Chapter 5, pp 9-156.

NGUYEN VH, TALARICO JR EF (2018) A morphometric anatomical study on the division of the left main coronary artery and myocardial bridges. *Eur J Anat*, 22 (4): 355-365.

ORTALE JR, FILHO JM, PACCOLA AMF, LEAL JG, SCARANARI CA (2005) Anatomy of the lateral, diagonal and anterosuperior arterial branches of the left ventricle of the human heart. *Brazilian J Cardiovasc Surg*, 20(2): 149-158.

REIG J, PETIT M (2004) Main trunk of the left coronary artery: anatomic study of the parameters of clinical interest. *Clin Anat*, 17(1): 6-13.

ROY S, GUPTA A, NANRAH BK, VERMA M, SAHA R (2014) Morphometric study of left coronary artery trunk in adult human cadavers: a study on the eastern region population anatomy section. *J Clin Diagnost Res*, 8(2): 7-9.

SAIDI H, ONGETI WK, OGENG'O J (2010) Morphology of human myocardial bridges and association with coronary artery disease. *African Health Sci*, 10(3): 242-247.

SHAMMAS NW, DIPPEL EJ, AVILA A, GEHBAUER L, FARLAND L, BROSIUS S, JERIN M, WINTER M, STOAKES P, BYRD J, MAJETIC L, SHAMMAS G, SHARIS P, ROBKEN J (2007) Long-term outcomes in treating left main trifurcation coronary artery disease with the Paclitaxel-Eluting stent. *J Invasive Cardiol*, 19(2): 77-82.

SHAMMAS NW, SHAMMAS GA, JERIN M, PARIKH A, COIN K, DIPPEL E, SHARIS P, ROBKEN J (2009) Treatment of left main coronary trifurcation lesions with the Paclitaxel drug-Eluting stent: mid-term outcomes from a tertiary medical center. *J Invasive Cardiol*, 21(7): 321-325.

SNELL RS (2011) Clinical anatomy by regions. *Lippincott Williams and Wilkins*, Chapter 3, pp 86-87.

SURUCU HS, KARAHAN ST, TANYELI E (2004): Branching pattern of the left coronary artery and an important branch. *The median artery. Saudi Medical Journal*; 25(2):177-81.

TAKEUCHI S, IMAMURA H, KATSUMOTO K, HAYASHI I, KATOHGI T, YOZU R, OHKURA M, INOUE T (1979) New surgical method for repair of anomalous left coronary artery from pulmonary artery. *J Thoracic Cardiovasc Surg*, 78(1): 7-11.

TAYLOR AM, THORNE SA, RUBENS MB, JHOOTI P, KEEGAN J, GATEHOUSE PD, WIESMANN F, GROTHUES F, SOMERVILLE J, PENNELL DJ (2000) Coronary artery imaging in grown up congenital heart disease complementary role of magnetic resonance and X-ray coronary angiography. *Circulation*, 101(14): 1670-1678.

TOMAR S, AGA P, SHARMA PK, MANIK P, SRIVASTAVA AK (2013) Normal and variant anatomy of left coronary artery: 64-multi detector computed tomography (MDCT) coronary angiographic depiction in North Indian population. *Int J Sci Res*, 3(8): 1-17.

WANG SP, JAO YT, HAN SC (2008) Acute coronary syndrome due to high aortocoronary junction of the right coronary artery: the value of multislice CT. *Int J Cardiol*, 123: 59-61.

YOUNG PM, GERBER TC, WILLIAMSON EE, JULSRUD PR, HERFKENS RJ (2011) Cardiac imaging: Part 2, normal, variant and anomalous configurations of the coronary vasculature. *AJR Am J Roentgenol*, 197(4): 816-826.

Vacuum packaged embalmed dogs for veterinary surgery practicing

Isabela Del Ponti[1], Giovana C. Vieira[1], Laura G. Soares[1], Alessandra Rodrigues[1], Natália T.B. Costa[1], Geovana C. Ferreira[1], Alisson D.S. Fechis[2], Andréa B.P.S. Queiroz[1], Fabrício S. Oliveira[1]

[1] Department of Animal Morphology and Physiology, School of Agrarian and Veterinary Science, São Paulo State University (UNESP), Jaboticabal, São Paulo, Brazil

[2] Department of Veterinary Animal Pathobiology, School of Agrarian and Veterinary Sciences, São Paulo State University (UNESP), Jaboticabal, São Paulo, Brasil

SUMMARY

It is imperative to have a lot of discretion regarding animals' use in research and teaching activities. Consequently, the search for alternative methods that do not cause academic or scientific damage is essential. This research aims to determine the maximum rupture force and the rupture elongation of the skin and the students' evaluation of the embalmed dogs' cadaver for veterinary surgery classes. Cadavers were injected with 120 mL/kg of a 20% sodium chloride, 1% nitrite and 1% sodium nitrate solution, and 150 mL/kg of alcohol with 5% glycerin and kept in vacuum packages between 0 to 4°C. Eight dogs constituted group 1, and three skin samples were collected on day 0 (fresh samples/before fixation) and during the next seven consecutive days. Only days 2 and 6 were different from the control. Group 2 was analyzed by 46 undergraduate students during the veterinary surgery classes, who completed a form about malleability and incision/suture of the tissue. Using a scale from zero to ten, the reached value was 7.95, and 100% of the students approved the use of embalmed dogs for surgical training. The anatomical technique had an excellent cost-benefit ratio in addition to reduced environmental impact. The method maintained malleability and quality of incision and suture in surgical practice.

Key words: Anatomy – Conservation – Learning – Malleability – Teaching

INTRODUCTION

Great wisdom is very important in the use of animals in research and teaching activities. It is therefore important to look for alternative methods that do not bring academic or scientific harm.

Several alternative methods currently optimize animal welfare in the teaching of veterinary surgery (Oliveira, 2008). These methods aim to replace live animals' use, generating similar or superior learning to the students (Silva et al., 2007). A negative emotional state can hinder more complex cognitive mechanisms, that is, block significant learning. Some students feel uncomfortable and even shocked in classes with live animals, and what happens is just visual

Corresponding author:
Andréa Barros Piazzon de Souza Queiroz. Department of Animal Morphology and Physiology, School of Agrarian and Veterinary Science, São Paulo State University (UNESP), Jaboticabal, 14884-900 São Paulo, Brazil. E-mail: andrea.queiroz@unesp.br

Submitted: November 18, 2020. **Accepted:** February 21, 2021

memorization and not meaningful learning in many of these situations (Paixão, 2008).

Several kinds of research have demonstrated the effectiveness of using chemically prepared cadavers for veterinary surgery classes. That provides greater acceptance by students and better learning (Silva et al., 2004), and animals that died in shelters, veterinary clinics, and hospitals could be used as substitutes for live animals (Silva et al., 2007; Mathews et al., 2010).

Still, there were no significant differences in surgical performance in veterinary medicine students trained on a cadaver or live animals (Carpenter et al., 1991; Silva et al., 2007). The use of chemically preserved cadavers was approved by 95.7% of the veterinary medicine students (Silva et al., 2007).

Interest in the biomechanical properties of animal biological tissues is increasing. A significant focus is on comparative studies between preserved and fresh samples, generating data that contribute to improved surgical techniques. Besides, the search for alternative materials is a new option for animal experimentation models (Camargo et al., 2014).

The anatomical specimens are fixed to avoid tissue deterioration. Fixation is essential, as it keeps the tissues firm, insoluble, and protected (Rodrigues, 2010). Thus, the excellent conservation does not allow the material to deteriorate and prevents the proliferation of pathogens that may cause disease in laboratory workers (Corrêa, 2003). The most common substances used for cadaver preservation are formaldehyde, glycerin, ethyl alcohol, and phenol (Rodrigues, 2010).

Formaldehyde is the most widely used fixative, commonly in a 10% aqueous solution. It quickly penetrates tissues (six millimeters in twelve hours) and is commonly used in anatomy laboratories (Rodrigues, 2010). In addition to being harmful to health, it poses a severe environmental risk, as the improper handling and disposal of carcasses and effluents can contaminate the environment (WHO, 1991).

The current model that comes closest to reality is the fresh corpse. However, it needs freezing, has a limited working time due to rapid putrefaction, and can be an infection risk. The saturated salt solutions are a simple method, with a low risk of infection and cost, contributing to the wide use of preserved cadavers for surgical training (Hayashi et al., 2016).

The curing salt solution is an alternative to formaldehyde for the long-term preservation of dogs' anatomical specimens subjected to dissection at the Szent István University of Science, Hungary (Werdelmann and Gerics, 2016) and Berlin (Janczyk et al., 2010). The cadavers presented high quality of softness and color of the tissues immersed in the solution, contrasting with the stiffness and gray color caused by formaldehyde (Werdelmann and Gerics, 2016), without environmental and health risks (Janczyk et al., 2010).

Surgical training was performed on dogs' cadavers fixed with ethyl alcohol (AE) and preserved in 30% sodium chloride solution (30% SCAS) for eight months with good biomechanical quality of tissues (Rocha et al., 2018), as well as it was taken in cats for seven months (Zero et al., 2020). The dogs' cadavers obtained an average score of 7.32 ± 1.63, and 75.67% of the students were in favor of using cadavers for surgical training and 80% in favor of using chemically prepared cadavers (Rocha et al., 2019).

The process of curing meat is a traditional practice in the food industry and consists of the injection of nitrite, nitrate, sodium chloride, and sugar into the meat. By a combined action, these components have a pronounced effect on the products' characteristics and stability. Nitrite stabilizes the typical red color, improves the organoleptic characteristics, and mainly inhibits C. botulinum (Leitão, 1978).

Vacuum packaging is considered a modified atmosphere. There is a change in air pressure by reducing oxygen, thus causing a decrease in the regular respiratory activity of food and the microbial population, leading to a reduction in deterioration (Young et al., 1988). The vacuum also promotes a decline in oxidation and muscle strength values, which causes the softness of the product (Leonel, 2008).

This study aimed to determine the maximum rupture force (in Newtons - N) and the rupture elongation (in cm) of the skin in dogs' cadavers chemically prepared with ethyl alcohol and curing salt and the evaluation of undergraduate veterinary medicine students through the practice of incision and suture of the skin.

MATERIAL AND METHODS

The dogs' cadavers were from the Zoonosis Control Center in Ribeirão Preto, SP, in a process approved by the Municipal Legal Department (process 02.2014.000027-1). Sixteen specimens, male and female, died from causes that did not involve evident morphological alteration, such as large tumor masses or bone fractures. The animals were frozen (freezer at -18°C) after death and then transported to the Laboratory of Animal Anatomy at UNESP Jaboticabal, SP, located 50 km away.

The animals' weight 7.87 ± 2.57, a body score between 4 and 5 on a 1 to 9 scale, considered the ideal by Laflamme (1997). They were thawed in a horizontal refrigerator at 4-6°C and trichotomized. They were then divided into two groups: group 1 for the biomechanical analysis of the skin and group 2 for the practical evaluation of cutaneous suture and incision.

In group 1, three skin fragments were collected, which became the control samples for immediate biomechanical analysis.

The common carotid artery was dissected for the anatomical technique, and a 40x12 cannula was inserted on it. A solution containing 200 g/L of sodium chloride, 10g/L sodium nitrite, and 10g/L of sodium nitrate (CS) was injected with a 60ml syringe (120 ml/Kg), followed by pure ethyl alcohol with 5% glycerin (EAG) (150 ml/Kg). Each corpse was placed in a plastic bag and vacuum-packed (Fig. 1) in a professional machine (Cetro® DZ Q600 DE) and kept in a horizontal refrigerator between 0 and 4°C, with a digital thermometer attached to the refrigerator's sealing cover on the outside.

Fig. 1.- Dog's corpse placed in a plastic bag and vacuum-packed in a professional machine.

For the biomechanical analyzes of the skin, three samples were collected for seven consecutive days (breaking the vacuum packaging and re-do it again). The corpse was positioned in the right lateral decubitus and divided into four quadrants. A stainless-steel mold of 1x5 cm was placed on the side of the thorax, parallel and 5 cm from the median plane, in such a way that the first analysis (day 0) and the following analyses (days 1, 2, 3) were made on this antimere and the other four analyzes (days 4, 5, 6, 7) were made on the other antimere (Fig. 2). With a scalpel (blade number 23), the skin was excised, three sequential samples were collected in the transverse direction of the dog's skin tension line (Fig. 2). After each analysis, the animal was placed in a plastic bag and vacuum-packed again.

An EMIC® Universal Testing Machine - model DL-2000, present in our Department, was used to assess tissue resistance. The load cell was 500N, the load application speed was 100 mm/min, and the free space between the grips was 20 mm. The equipment belongs to the Laboratory of Surgical Anatomy of the Department of Animal Morphology and Physiology of FCAV - UNESP – Jaboticabal (Fig. 3).

For this group, statistics were performed using the software R 3.6.1 for Windows, comparing the maximum rupture force (MRF) of the skin and the rupture of elongation (RE) at all days to the control samples (D0). The MRF Cramer-Von Mises normality test and the Kruskal-Wallis test was performed. And for the RE, the Cramer-Von Mises normality test, the F test, ANOVA, and Tukey test (5%) were applied.

Cadavers from group 2 were chemically prepared as previously described and analyzed by 46 students from graduation from the veterinary surgical technique classes, between days 3 and 5 of conservation, which was the days with the best biomechanical results. A form was distributed to the students, which contained statements for evaluating scores related to skin malleability and incision/suture of the tissue (Fig. 4). In every class, fresh animals were taken for proper comparison with the prepared ones. Values from 1 (terrible) to 10 (excellent) were assigned to compare the animals prepared to compared to the fresh ones. The students were instructed to make an incision in the prepared animal's skin, followed by a separate simple suture with nylon. For the statics analyses the Student's T-test (5%) was used.

Fig. 2.- Dog's cadaver in left lateral decubitus demonstrated sample collection (day 4, 5, 6 and 7) on the right antimere.

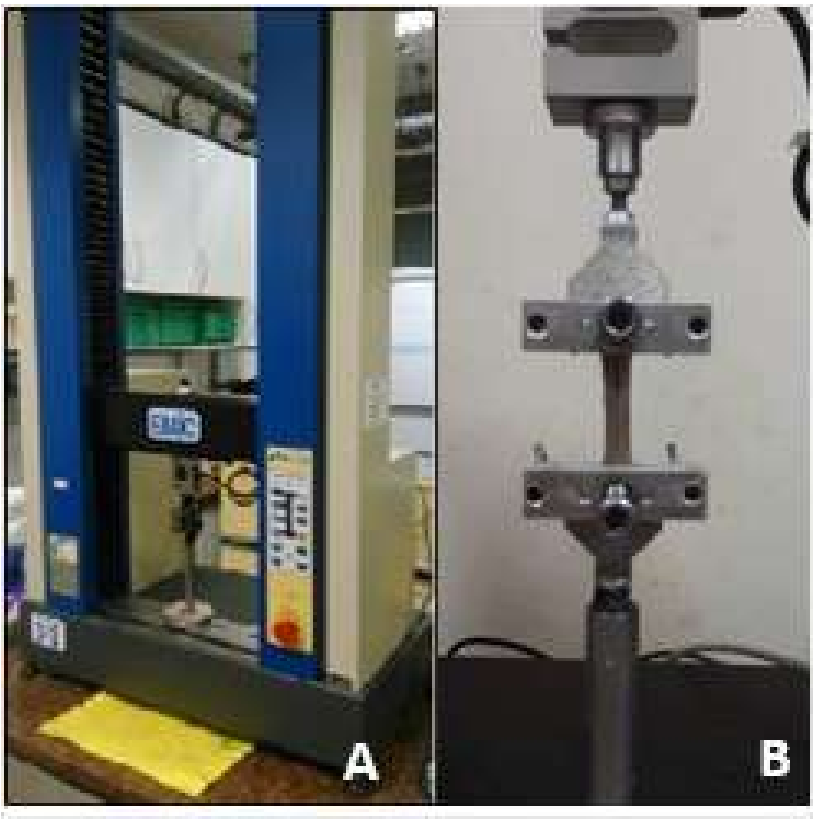

Fig. 3.- A: emic® universal testing machine used for the traction test. B: jejunum sample of an embalmed dog during traction test.

FORM

The questions should be answered based on the ease/difficulty in performing the Surgical technique and how close the corpses' morphological appearance/malleability is to what is considered real/ideal.

Rate from 1 (terrible) to 10 (excellent).

Skin resistance to incision/suture_____

Malleability of the skin_____

Adapted from de Silva et al., 2007

1. Before the surgical procedure began, you were for or against the use of corpses in teaching the surgical technique?

   a( ) in favor b( ) against

2. Have you changed your opinion?

   a( ) yes b( ) no

3. What kind of class do you prefer?

   a) Lessons with a live animal, euthanized after class.

   b) Inicial training in chemically prepared cadavers, followed by including animals from the Veterinary Hospital, who came for elective surgery, for example, orchiectomy or ovariohysterectomy.

Fig. 4.- Form used for research.

RESULTS

For group 1 the maximum rupture force (MRF) of the skin and the rupture of elongation (RE) at all days was compared to the control samples (D0), as shown in Table 1.

Table 1. Means and standard deviations of the MRF.

Days	MRF
D0	175.53±116.32
D1	179.90±112.18
D2	157.82±95.74
D3	141.26±92.09
D4	139.73±94.29
D5	160.78±119.41
D6	162.31±80.76
D7	152.18±114.56

In MRF, the Cramer-Von Mises normality test was performed ($p < 0.05$), and $P = 0.2276$, so then the Kruskal-Wallis test ($P = 0.8560$). There was no significant difference between treatments, and data did not show normality even after undergoing BoxCox transformation.

In the RE, the Cramer-Von Mises normality test ($p < 0.05$) was applied ($p=0.2145$), and box cox transformation was taken. Therefore, the F test was significant ($p < 0.0001$). Thus, the averages of treatments differ from the control, and to complement the ANOVA, the Tukey test (5%) was taken, which allowed for comparison of the means. Only days 2 and 6 were different from the control in skin biomechanics.

Table 2. ANOVA table with RE statistics.

	GL	SQ	QM	F Value	P Value
Treatments	7	1.05	0.15	4.348	<0.0001
Residues	173	5.97	0.04		

In group 2, in which undergraduate students evaluated the animals, there was no significant difference ($p=0.0517$) between the scores given in malleability for fresh (9.05±1.05) or chemically prepared skin (8.45±0.83), by the 5% Student T-test. In incision, there was a significant difference ($p = 0.0160$) between the scores attributed in fresh (9.15±0,81) or chemically prepared skin (8.55±0.69). The same was observed in the suture, in which fresh skin obtained better evaluation by students (9.20±0,77) when compared to embalmed one (7.95±1.19), and this difference was statistically significant ($p = 0.0003$) by the Student´s T-test 5%.

Regarding the questions, 100% of the students favored using cadavers to perform surgical techniques. All students preferred the initial training in chemically prepared cadavers, followed by surgery classes with live animals.

Table 3. Tukey test evaluation of RE averages.

Days	Mean	
D0	1.56±0.07	a
D1	1.56±0.07	a
D2	1.47±0.07	b
D3	1.56±0.09	a
D4	1.56±0.08	a
D5	1.57±0.11	a
D6	1.47±0.09	b
D7	1.56±0.09	a

* Means followed by different letters differ from each other (Tukey test at 5%).

DISCUSSION

The use of chemically prepared cadavers to teach surgical techniques in veterinary medicine graduation is an alternative to using live animals. Surgical training using cadavers reduces costs and increases exercise repeatability (Oliveira, 2008).

Like the ones in this research, the use of chemically prepared animals is a trend in universities worldwide and avoids the euthanasia of thousands of specimens for surgical training (Balcombe, 2000).

Surgical training on chemically prepared dogs' cadavers proved to present excellent acceptance by undergraduate veterinary students, and even preferable to live animals as the first contact with

the surgery, providing better learning (Knight, 2007), similar to the 93.29% (Silva et al., 2003) prepared with the modified Larssen solution or the 81.08% (Rocha et al.,2019) of the students that preferred to perform the first surgical training in cadavers prepared with ethyl alcohol.

All the students were satisfied with the embalmed specimens' experience, which is consistent with another Brazilian study presenting 75.67% of approval in the use of chemically prepared cadavers for veterinary surgery practicing (Rocha et al., 2019).

The result of our research using cadavers chemically prepared with curing salts and ethyl alcohol with glycerin proved to be effective. The results were similar to those obtained in another study using the same fixative and preservative but in cat cadavers (Fração et al., 2019) and used in human cadavers for up to 12 months (Goyri-O'neill et al., 2013).

The anatomical technique used was similar to the one that used EA for fixation and 30% SCAS for preserving dogs for up to 4 months, aiming for surgical training in skin and intestines (Rocha et al., 2018), common carotid arteries (Cerqueira et al., 2017) and external jugular veins (Pelogia et al., 2018). However, the malleability and subjective evaluation of the cadavers' color of our study was considered superior to the technique used previously according to the data in our forms.

The skin maintained its softness and color, differently from what happens when solutions with formaldehyde are used (Groscurth et al., 2001; Hayashi et al., 2016). However, there was a statistical difference compared to the fresh corpse. The malleability, incision, and suture have always been more significant than 7.95, on a scale from zero to ten (with the fresh corpse representing an almost maximum score in the evaluated criteria, considered ideal). The excellent quality of the chemically prepared dogs for surgical training is similar to the reported in soft tissues of cadavers prepared with EA for fixation, but kept in 30% SCAS tanks for up to 4 months (score 7.32 ± 1.63) (Rocha et al., 2019).

There was no statistical difference between the control and samples' mean, except on the D2 and D6, which demonstrated that might be due to minimal collection error or grasping on the universal testing machine. Good maintenance of tissue resistance during the research and the anatomical technique maintained the skin's biomechanical characteristics for up to 7 days, only with the cadaver vacuum-packed and refrigerated at 2-6°C. In vacuum packaging, the air is removed, inactivating aerobic bacteria, preventing product deterioration with better quality and longer shelf life (Mantilla et al., 2010). The same was reported in a study in which the EA solution combined with the 30% sodium chloride tank was used to conserve dog cadavers for up to 4 months (Rocha et al., 2018).

In a study using cats chemically prepared with the same anatomical technique used in this experiment (EAG and CS) and preserved for 90 days but with no vacuum, the MFR of the skin samples ranged from 254.19 ± 183.25N (fresh / control samples) to 234.68 ± 108.17N (Fração et al., 2019). In our study with vacuum-packed dogs, the MRF ranged from 175.53 ± 116.32 to 152.18 ± 114.56 after seven days of storage. This MRF was lower in our research because the dog's skin is 0.5-5 mm thick, while in the cat, the thickness is 0.4-2 mm (Affolter and Moore, 1994), thus demonstrating that the cat's skin is more elastic than the dog.

CONCLUSION

The anatomical technique, which uses EAG and CS, associated with vacuum packaging, has an excellent cost-benefit ratio, in addition to reduced environmental impact. Furthermore, it is an effective method for preserving the biomechanical characteristics of the skin for seven days. Also, it was observed that the technique maintains malleability, ease of incision, and suture in surgical training, which is recommended for the training and practice of veterinary surgery.

ACKNOWLEDGEMENTS

The authors wish to thank Fundação de Amparo à Pesquisa do Estado de São Paulo, FAPESP (process 2018/18567-0) and Usina São Martinho, Pradópolis, SP, Brazil.

REFERENCES

AFFOLTER VK, MOORE K (1994) Histologic features of normal canine and feline skin. *Clin Dermatol,* 12: 491-497.

BALCOMBE J (2000) The use of animals in higher education: problems, alternatives and recommendations. The Humane Society Press, Washington, DC.

CAMARGO AD, CAMARGO PC, LEAL LM, GARCIA FILHO SP, MARTINS LL, SHIMANO AC, MACHADO MRF (2014) Propriedades tensiométricas do peritônio da paca (Cuniculus paca) a fresco e conservado em glicerina 98%. *Pesq Vet Bras,* 34: 185-191.

CARPENTER LG, DONALD L, PIERMATTEI DL, SALMAN MD, ORTON C, NELSON AW, SMEAK DD, JENNINGS PB, TAYLOR RA (1991) A comparison of surgical training with live anesthezed dogs and cadavers. *Vet Surg,* 20: 373-378.

CERQUEIRA ESF, PELOGIA MES, SILVEIRA CPB, FECHIS ADS, ROCHA TASS, LAUS JL, OLIVEIRA FS (2017) Suture analysis and arterial traction test in dogs fixed on alcohol and preserved on saline solution aiming surgical practice. *GARJMMS*, 6: 292-295.

CORRÊA WR (2003) Isolation and identification of filamentous fungi found in anatomical pieces preserved in 10% formalin solution. Institute of Research and Development, University of the Valley of Paraíba, 59p.

FRAÇÃO VC, ZERO RC, RODRIGUES A, FERREIRA BN, FECHIS ADS, ROCHA TASS, IOZZI MT, OLIVEIRA FS (2019) Analysis of the skin of cats' corpses chemically prepared with ethylic alcohol and curing salt aiming veterinary surgical practice - chronic effect on biomechanics and students' evaluation. *CPQ Medicine*, 4: 01-08.

GOYRI-O'NEILL J, PAIS D, FREIRE FA, RIBEIRO P, O'NEILL ABA, RAMOS S, MARQUES CN (2013) Improvement of the embalming perfusion method: The innovation and the results by light and scanning electron microscopy. *Acta Med Por*, 26: 188-194.

GROSCURTH P, EGGLI P, KAPFHAMMER J, RAGER G J, HORNUNG P, FASEL JDH (2001) Gross Anatomy in the surgical curriculum in Switzerland: improved cadaver preservation, anatomical models, and course development. *New Anat*, 265: 254-256.

HAYASHI S, NAITO M, KAWATA S, QU N, HATAYAMA N, HIRAI S, ITOH M (2016) History and future of human cadaver preservation for surgical training: from formalin to saturated salt solution method. *Anat Sci Int*, 91: 1-7.

JANCZYK P, WEIGNER J, BECKER AL, KAESSMEYER S, PLENDL J (2011) Nitrite pickling salt as an alternative to formaldehyde for embalming in veterinary anatomy—A study based on histo- and microbiological analyses. *Ann Anat*, 193: 71-75.

KNIGHT A (2007) The effectiveness of humane teaching methods in veterinary education. *ALTEX*, 24: 91-109.

LAFLAMME D (1997) Development and validation of a body condition score system for cats: a clinical tool. *Feline Practice*, 25: 13-18.

LEITÃO MFF (1978) Microrganismos patogênicos na carne e derivados. *ITAL*, 59: 15-48.

LEONEL FR (2008) Irradiação e qualidade da carne de frango congelada e embalada a vácuo. Doctorate Thesis. Faculdade de Ciências Agrárias e Veterinárias – Unesp, Campus de Jaboticabal. *Jaboticabal*, SP.

MANTILLA SPS, BORGES SM, VITAL H (2010) Atmosfera modificada na conservação de alimentos. *Rev Acad Ciência Agrário Ambiente*, 8: 437-448.

MATHEWS KG, RILEY K, LASCELLES BDX, DERNELL WS (2010) Preparation of canine and feline cadavers for surgical laboratories. *Vet Surg*, 39: 224-225.

OLIVEIRA HP (2008) Situação atual do ensino da técnica cirúrgica e da clínica cirúrgica. *Ciênc Vet Tróp*, 11: 93-94.

PELOGIA MES, CERQUEIRA ESF, SILVEIRA CPB, ROLIM GS, FECHIS ADS, ROCHA TASS, LAUS JL, OLIVEIRA FS (2018) Suture and venous traction test analysis in dogs fixed in alcohol and preserved in saline solution. *Pesq Vet Bras*, 38: 1834-1837.

PAIXÃO RL (2008) Métodos substitutivos ao uso de animais vivos no ensino - Repensando o que aprendemos com os animais no ensino. *Ciênc Vet Tróp*, 11: 88-91.

ROCHA TASS, YANAGIHARA GR, SHIMANO AC, ROLIM GS, SANTOS CCC, FECHIS ADS, OLIVEIRA FS (2018) Biomechanical analysis of the skin and jejunum of dog cadavers subjected to a new anatomical preservation technique for surgical teaching. *J Plastination*, 30: 16-23.

ROCHA TASS, SANTOS CCC, IOZZI MT, DIAS RS, ZERO RC, CARDOZO MV, OLIVEIRA FS (2019) Chemically prepared dog cadavers in teaching of surgical technique - evaluation by students of a veterinary medicine course. *Acta Sci Anat*, 1: 136-140.

RODRIGUES H (2010) Técnicas anatômicas. *GM Gráfica & Editora*. Vitória-ES. 269p.

SILVA RMG, MATERA JM, RIBEIRO AACM (2003) Avaliação de ensino da técnica cirúrgica utilizando cadáveres quimicamente preservados. *Revista de Educação Continuada em Medicina Veterinária e Zootecnia do CRMV-SP*, 6: 1-3.

SILVA RMG, MATERA JM, RIBEIRO AACM (2004) Preservation of cadavers for surgical technique training. *Vet Surg*, 33: 606-608.

SILVA RMG, MATERA JM, RIBEIRO AACM (2007) New alternative methods to teach surgical techniques for veterinary medicine students despite the absence of living animals. Is that an academic paradox? *Anat Hist Embryol*, 36: 220-224.

YOUNG LL, REVIERE RD, COLE B (1988) Fresh meats: a place to apply modified atmospheres. *Food Sci Technol*, 42: 65-69.

WERDELMANN R, GERICS B (2016) Preservation of specimens for students-formaldehyde vs. salt-based fixative: 182. *Anat Histol Embryol*, 45: 93-94.

WHO – World Health Organization (1991) IPCS International Programme on Chemical Safety – Formaldehyde - *Health and Safety Guide*. n.57. Available in: <http://www.inchem.org>.

ZERO RC, SHIMANO AC, CARDOZO MV, SANTOS CCC, FECHIS ADS, ROCHA TASS, OLIVEIRA FS (2020) Cadáveres de gatos preparados químicamente para la enseñanza de técnicas quirúrgicas: análisis biomecánico de piel y yeyuno. *Rev Investig Vet Perú*, 31: e1617.

Role of stem cell therapy in diabetic nephropathy in rats: biochemical, histological and immunohistochemical study

Ahmed Y. Sedeak[1], Hanan D. Yassa[1], Azza S. Moawad[3], Abdalwakel A. Mohammed[2], Gaber H. Abdelfatah[1]

[1] Anatomy and Embryology Department, Faculty of Medicine, Beni-Suef University, Egypt

[2] Anatomy and Embryology Department, Faculty of Medicine, Cairo University, Egypt

[3] Histology Department, Faculty of Medicine, Beni-Suef University, Egypt

SUMMARY

Diabetes mellitus is one of the main causes of death due to the complications that involve many organs such as heart, kidney, retina and others. Mesenchymal stem cells (MSCs) have been demonstrated to be effective in treatment of diabetes. This paper aims to evaluate the effect of stem cells in the treatment of diabetic nephropathy, clarifying their role in oxidative stress and inflammation. 30 adult male albino rats were equally divided into 3 groups. Control group (group I) received 1ml saline by intra-peritoneal (IP) injection. Streptozotocin-treated group (group II) received Streptozotocin (STZ) (60 mg/kg BW, I.P.) for induction of diabetes, then were sacrificed after 4 weeks. Steptozotocin + Stem cell-treated group (group III) received STZ, were left for 4 weeks, and then they were injected once intravenously with 1 million units of MSC and sacrificed after 4 weeks. Blood glucose, serum urea and creatinine were checked. The kidney sections were examined Histologically with H&E and PAS Stain and immunohistochemically for endothelial Nitric Oxide Synthase (eNOS). A morphometric study and statistical analysis were performed. DM led to increased levels of glucose, urea and creatine. Also, DM caused inflammation, degeneration and decreased eNOS immunoexpression of the kidney. The administration of MSCs improved the levels of glucose, urea and creatinine. Also, MSCs decreased the pathological changes and increased eNOS immunoexpression in the kidney. MSCs have effective therapeutic role in treating diabetic nephropathy.

Key words: Diabetes – Nephropathy – Mesenchymal stem cell – eNOS – Oxidative stress

INTRODUCTION

Diabetes mellitus (DM) is one of the most prevalent non-communicable metabolic diseases. Recent years have showed a sudden increase of diabetes all over the world. The International Diabetes Federation (IDF) reported that the number of diabetic populations will increase from 415 million in 2015 to 642 million by 2040 (Peng et al., 2018).

Corresponding author:
Ahmed Yahia Sedeak. Faculty of Medicine, Beni-Suef University, Department of Anatomy and Embryology, Beni Suef, Egypt. E-mail: yehiaa930@yahoo.com

Submitted: November 10, 2020. **Accepted:** March 11, 2021

The effectiveness of MSCs was demonstrated in the treatment of diabetes and its complications, including microvascular complications such as retinopathy (Yang et al., 2010) and nephropathy (Fang et al., 2012), and macrovascular complications such as cardiomyopathy (Abdel Aziz et al., 2008).

Diabetic nephropathy is a major microvascular complication in patients with diabetes, and remains the leading cause of chronic kidney disease, accounting for approximately a half of all end-stage renal disease worldwide (Kanwar et al., 2011).

Streptozotocin (STZ) is one of antibiotics that obtained from Streptomyces achromogenes. It has been widely used for inducing experimental diabetes mellitus in a variety of animals, as it causes degeneration of pancreatic β cells causing insufficient insulin secretion (Mousa et al., 2016).

Stem cell treatment is a recent type of intervention strategy that is introduced into the damaged tissues in order to treat diseases or injuries. Many medical researchers believe that stem cell treatment has the potential to change the prospect of human diseases and alleviate suffering. The stem cells are able to proliferate and give rise to subsequent generations with variable degrees of differentiation capacities. This ability offers significant potential for the generation of tissues that can replace diseased and damaged tissues in the body (Mousa et al., 2016).

Mesenchymal stem cells (MSCs) secrete numerous factors, such as nitric oxide and prostaglandin E2, which enhance antioxidant defenses, inhibit oxidation factors and reduce necrosis of the cells (Pulavendran et al., 2010; Berardis et al., 2015). Furthermore, immune modulation of MSCs inhibits inflammatory cell proliferation, thereby exerting anti-inflammatory effects (Volarevic et al., 2014).

The goal of this study was to reveal the changes induced by diabetes on the kidney clarifying the possible therapeutic effects of MSCs through histological, immunohistochemical and biochemical studies.

MATERIALS AND METHODS

The study was carried out at the Animal House of the Faculty of Medicine, Cairo University, according to the guide lines used for the care and the use of laboratory animals (code of ethical approval is 018-61).

Experimental animals

The study was performed on 30 adult male albino rats of an average weight 150-180 g. The rats were acclimatized in the laboratory for a period of two weeks before performing the experiment. They were manipulated in cages made of metal under standard laboratory and pathogen-free environmental conditions. The rats were nourished using standard levels of the rodent water and food. These rats were equally divided into 3 groups:

Control group (group I): this group received 1ml saline by intra-peritoneal (IP) injection.

Streptozotocin-treated group (group II): this group received Streptozotocin (STZ) (60 mg/kg body weight (BW), I.P.) for induction of diabetes; then they were sacrificed after 4 weeks (Srinivasan et al., 2005).

Steptozotocin+ Stem cell-treated group (group III): this group received STZ for induction of diabetes and left for 4 weeks, then these rats were intravenously injected with 1 million units of bone marrow-derived mesenchymal stem cells (BM-derived MSCs) only for one time. After 4 weeks of being treated with stem cells, these rats were sacrificed (Ngoc et al., 2011).

Chemicals

Streptozotocin (STZ) was obtained from Sigma Company (St. Louis Mo, USA) in the form of powder solvent. Each vial of Streptozotocin powder contain 1 gram of Streptozotocin-active ingredient with the chemical name, N(Methylnitrosocarbamoyl)-α-D-glucosamine Streptozotocin.

Induction of DM: STZ (60 mg/kg BW) was dissolved in 0.1M sodium citrate buffer in the Biochemistry department, Faculty of Medicine, Cairo University. Preparation of the solution was done at pH 4.5 and then injected intravenously within 15 min. The aim of this procedure is to induce T1DM (Cesaretti et al., 2010).

Diagnosis of Diabetes: Polydipsia and Polyphagia were observed in adult rats within three days of

injection of streptozotocin and this suggested DM due to destruction of β-cells of Langerhans islet cells (Bluestone et al., 2010). Diagnosis of diabetes was approved by elevation of blood glucose level (Ikebukuro et al., 2002). Rats with blood glucose levels more than 200 mg/dL were considered diabetic (Cesaretti et al., 2010).

Treatment of DM: Preparation of Labeled bone marrow-derived mesenchymal stem cells was done in the stem cell unit, Biochemistry department, Faculty of Medicine, Cairo University. These stem cells were given by single I.V. injection in a dose of 1ml of about (1×10^6 cells/rat) 4 weeks after confirmation of diabetes (Kajiyama et al., 2010). The treatment was allowed only to the third group suspended in 1 ml normal saline (Carr et al., 2008).

Isolation and culture of bone marrow-derived mesenchymal stem cells (BM-derived MSCs) (Jiang et al., 2010):

5-bromo-2′-deoxy-uridine (BrdU) labeled MSCs were prepared at Medical Biochemistry Department, Faculty of medicine, Cairo University.

Isolated and cultivation of BM-derived MSCs were carried out for 4 weeks. Adult rats were euthanized and bilateral femora and tibias were removed under sterile conditions and placed in Dulbecco's modified eagle medium (DMEM; Gibco/BRL). Flushing out of MSCs was performed with DMEM using a syringe fitted with a 23-guage needle. This was followed by gently pipetting bone marrow from each bone many times to separate cells.

Then the cells were washed two times using DMEM, centrifuged 2250 rpm for 15min, and cultured in DMEM supplemented with 10% fetal bovine serum (GibcoBRL), 100 U/ml penicillin G and 100mg/ml streptomycin (GibcoBRL) at $2.5x10^5/cm^2$. The cells were incubated at 37 ºC in humidified 95% air and 5% CO2.

3 days later, elimination of non-adherent cells was done. Addition of fresh complete culture medium DMEM was done and then replaced every 3 or 4 days. When the cells become 80-90% confluent over 14 days, they were harvested with 0.25% trypsin and one mmol EDTA (GibcoBRL) for 3 min at 37° C, replanted in six-well disk at $1.5x10^5/cm^2$ and again grown to near confluence. Dilution of cells was obtained by adding water 1:2 per passage to expand the culture.

Fluorescence phase-contrast microscope (Axiocam MR R3, Carl Zeiss, Germany) was used to observe the rats MSCs every 2 or 3 days.

Biochemical study

At the end of the experiment of each group, collection of blood samples were carried out using fine heparinized capillary tube. The blood samples were delivered into centrifuge tubes and the plasma was collected and used for the determination of glucose, urea and creatinine.

Anaesthesia of the rats was performed using mild ether inhalation then subsequent sacrifice of these rats was done by cervical dislocation to avoid chemical injury (Liu et al., 2013). The rats' kidneys were excised immediately and carefully.

Histological study

The kidneys were dissected, fixed in 10% formalin overnight, processed for paraffin blocks and sectioned at 5 µm thickness. Sections of paraffin were used in:

1. Hematoxylin & Eosin stain (Kiernan, 2015)
2. PAS (Bancroft and Gamble, 2008)
3. Immunohistochemical study using endothelial nitric oxide synthase (eNOS) (Takahashi and Harris, 2014): Primary antibody: endothelial Nitric Oxide Synthase (eNOS) antibody, a mouse monoclonal [M221] antibody (IgG1) (Abcam Medical, Cambridge, USA, catalogue number ab76198) to eNOS and it consists of recombinant part of mouse eNOS protein which contained residues of amino acid in the C-terminal region. It is liquid and stored at -20°C in 0.05% sodium azide. Heart section was used as a standard positive control. One of the kidney sections was used as a negative control by avoiding application of the primary antibody.

Fluorescent microscopic examination

Kidney Sections of STZ+stem cell group were submitted to fluorescent microscopy

examination to clarify fluorescent labeled mesenchymal stem cells (Fig. 1). It was done by detecting the Bromodeoxyuridine (BrdU) - positive cells in the sections. The sections were immunostained using mouse anti-BrdU (1:100, Neomarkers), and goat anti-mouse Ig GFITC (1:100, Kpl).

Morphometric study

Using a Leica Quin 500 (Leica Ltd, Cambridge, UK) computerized image analysis system, the morphometric studies were done for the intensity of the eNOS immunoexpression in the kidney sections.

Statistical analysis *(Emsley et al, 2010)*:

Analysis of Statistics was done using SPSS software, version 16. All data will be expressed as mean ± SD. One way analysis of variance (ANOVA) test will be used for comparison between rat groups. The results of Statistics were considered significant when the p-values were < 0.05.

RESULTS

No deaths were detected in rats.

Biochemical results

The mean values of glucose, urea and creatinine levels of STZ group were significantly increased as compared with the control group (P-value < 0.05) (Table 1).

The mean value of glucose, urea and creatinine levels of STZ+ Stem cell-treated group were significantly decreased as compared with the STZ treated group (P-value < 0.05) (Table 1).

HISTOLOGICAL RESULTS

H and E stain results (Figs. 5, 6)

In the control group, H&E-stained sections of the kidneys revealed normal renal architecture in the form of Malpighian corpuscles formed of a glomerulus surrounded by Bowman's capsule, proximal and distal convoluted tubules (Fig. 2).

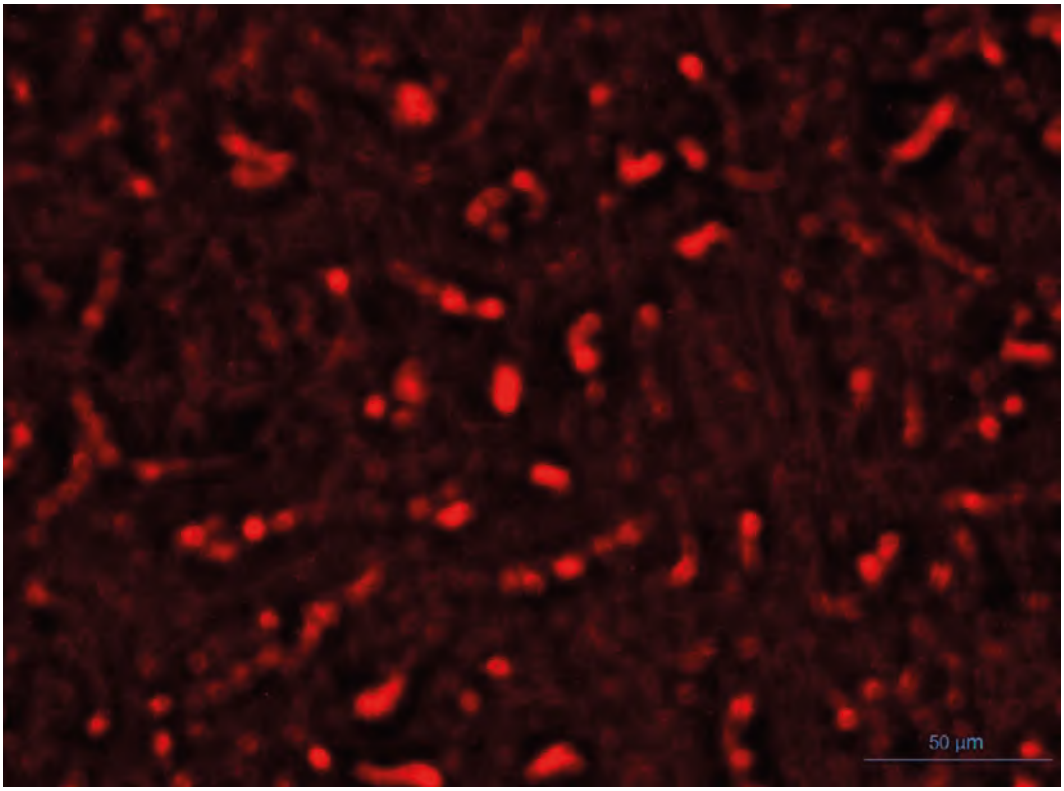

Fig. 1.- Fluorescent microscopic kidney section of the STZ+MSCs group shows fluorescent illumination of fluorescent-labeled mesenchymal stem cells. Scale bar = 50 µm.

Table 1. Comparison between all groups (control, STZ treated and STZ+ Stem cell-treated G) regarding blood glucose level, urea level, creatinine level and intensity of eNOS immunoexpression in the kidney sections (mean ± standard deviation).

Groups	Blood glucose level	Urea level	Creatinine level	Intensity of eNOS immunoexpression
Control	92.62 ± 6.49	37.9 ± 3.84	0.21 ± 0.02	33180870 ± 2446319
STZ treated	284.84 ± 19.18*	72.1 ± 9.06*	0.93 ± 0.25*	7887416 ± 1071690*
STZ+ Stem cell-treated	142.93 ± 13.10	47.3 ± 5.25	0.32 ± 0.06	28624580 ± 2121946

*Significant (P< 0.05) compared with other groups.

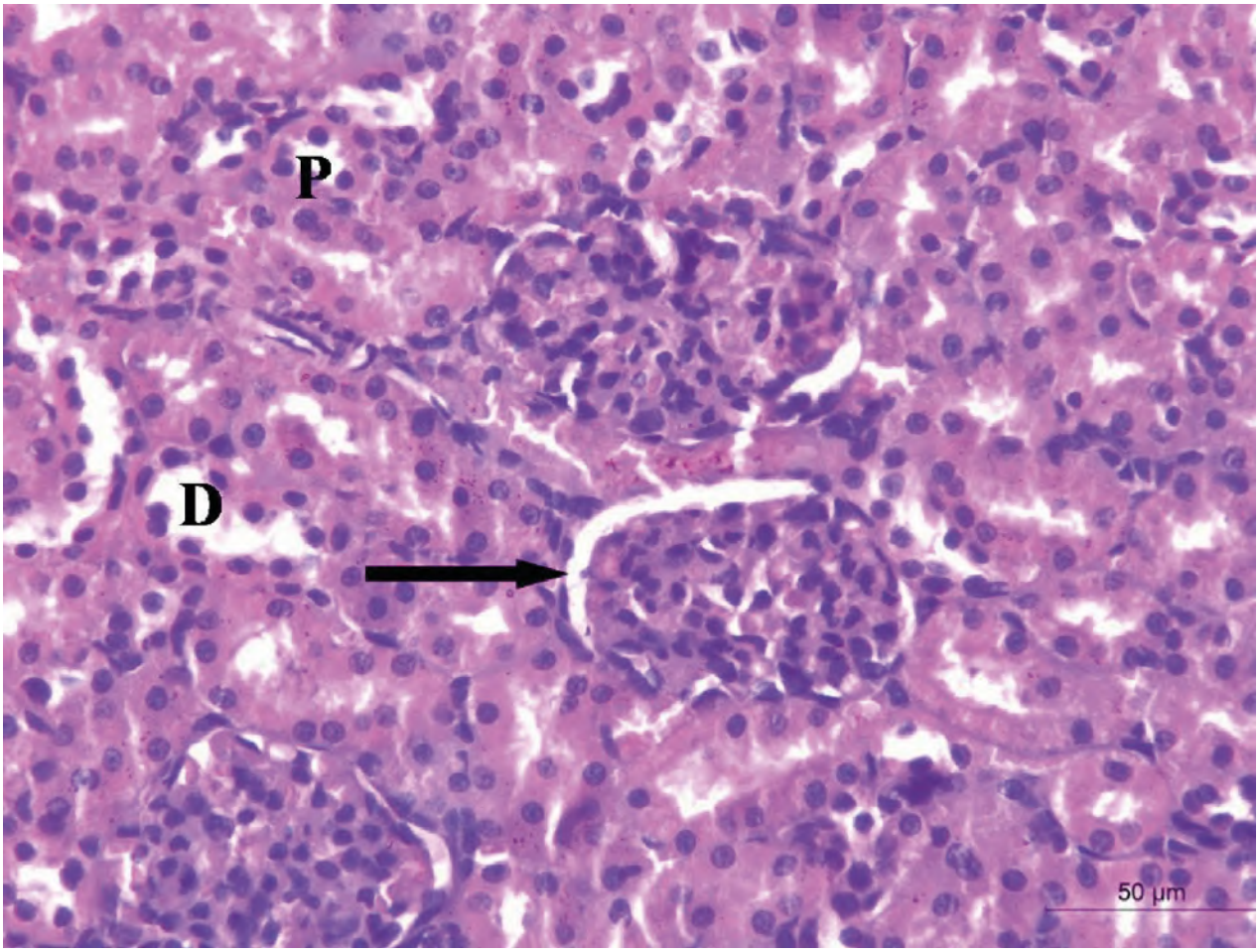

Fig. 2.- A renal cortical section of the control group shows normal Malpighian renal corpuscle formed of a glomerulus surrounded by Bowman's capsule (arrow), proximal convoluted tubule (P) and distal convoluted tubule (D). Scale bar = 50 µm.

In the STZ-treated group, renal sections showed hypertrophic glomeruli and obliteration of the capsular spaces (Fig. 3). Renal sections also revealed cytoplasmic vacuolization of the tubular cells (Figs. 3, 4). Multiple tubules with intraluminal acidophilic masses and congested blood vessels were demonstrated (Fig. 4). There was massive mononuclear cellular infiltration (Fig. 3).

The kidneys of STZ+ Stem cell-treated group revealed normal Malpighian corpuscles formed of a glomerulus surrounded by Bowman's capsule corpuscle and normal tubules whereas some tubules were dilated (Fig. 5).

PAS stain results (Fig. 6)

Using PAS stain, the control kidneys displayed the parietal layer of the Bowman's capsule, the basement membrane of renal tubule and the brush border of the proximal convoluted tubule. However, in STZ-treated group, there was thickening of parietal layer of the Bowman's capsule, as well as basement membrane of the

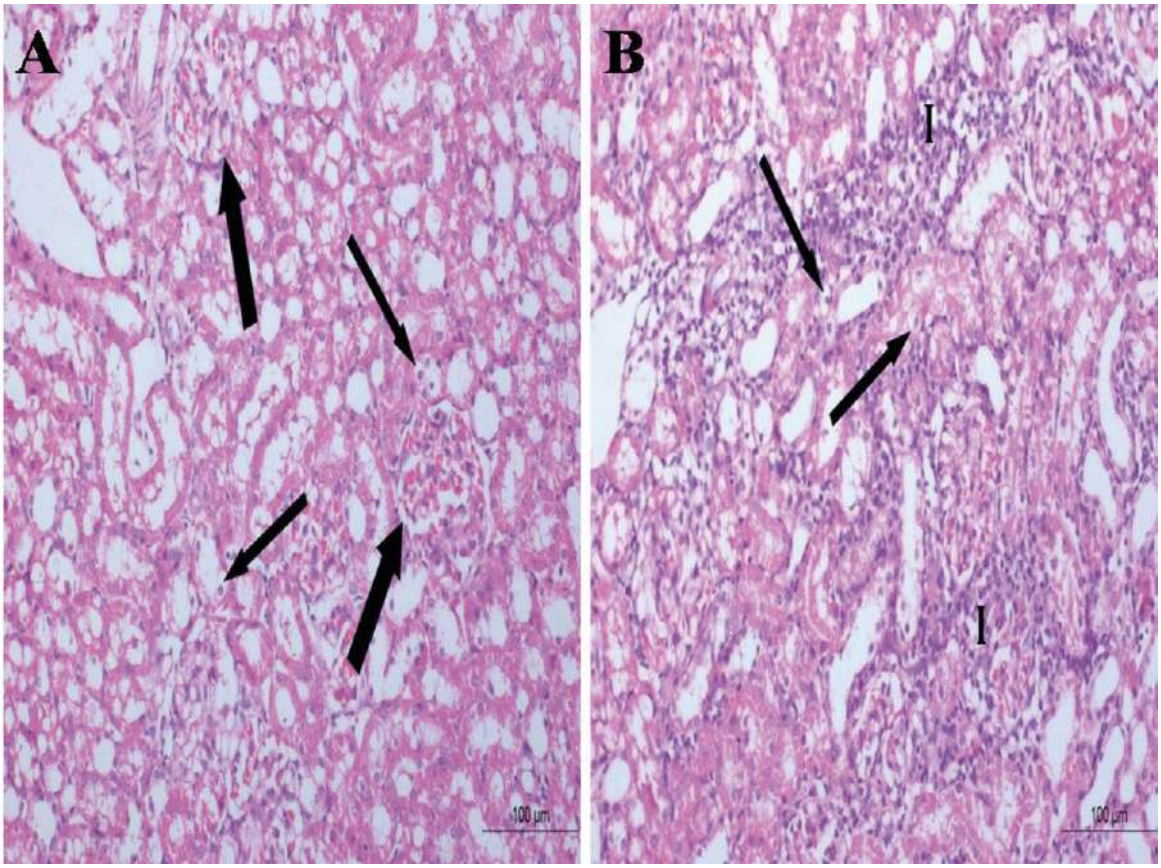

Fig. 3.- Renal cortical sections of the STZ treated group. **(A)** hypertrophic glomeruli and obliteration of the capsular spaces (thick arrow) and cytoplasmic vacuolation of the renal tubules (thin arrows). **(B)** massive mononuclear cellular infiltration (I) and cytoplasmic vacuolizations of the tubular cells (arrows). Scale bars = 100 µm.

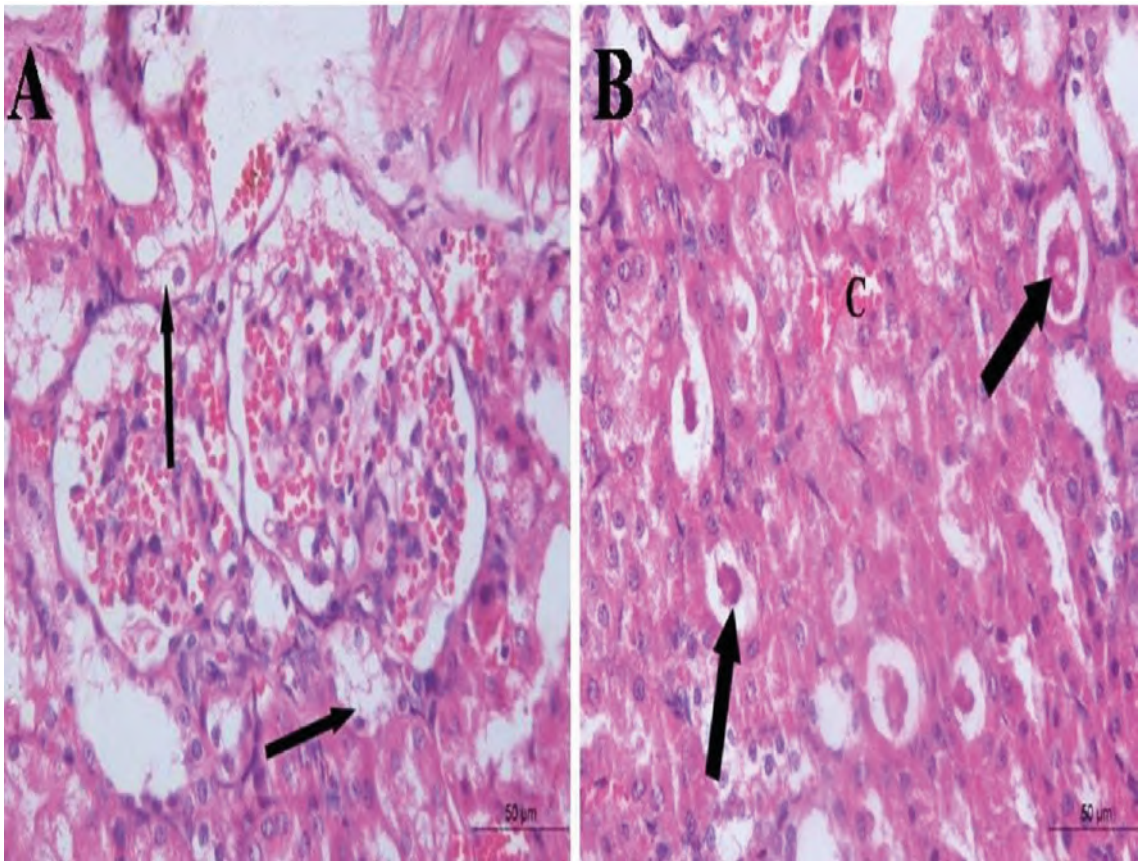

Fig. 4.- Renal cortical section of the STZ treated group. **(A)** cytoplasmic vacuolization of the tubular cells (arrows). **(B)** multiple tubules with intraluminal acidophilic masses (thick arrows) and congested blood vessels (C). Scale bars = 50 µm.

renal tubules. Partial loss of brush border of some proximal convoluted tubules was detected. While, in STZ+ Stem cell-treated group, there was thin parietal layer of the Bowman's capsule and basement membrane of renal tubule. Brush border of proximal convoluted tubules could be seen mostly intact.

***Immunohistochemical results* (Fig. 7)**

Immunohistochemical staining of the kidneys for (eNOS) demonstrated positive eNOS immunoexpression in the glomerular vascular endothelial cells. However, in STZ-treated group, immunohistochemical staining of the kidneys for (eNOS) demonstrated less intensity of the eNOS immunoexpression in the glomerular vascular endothelium in comparison with the control group. While the STZ+ Stem cell-treated group showed increased intensity of the eNOS immunoexpression.

Morphometric results

The intensity of eNOS immunoexpression in STZ group was significantly decreased as compared with the control group (P-value < 0.05) (Table 1).

The intensity of eNOS immunoexpression in STZ+stem cell group showed a significant increase as compared with the STZ treated group (P-value < 0.05) (Table 1).

DISCUSSION

In the present work, the diabetic rats developed diabetic nephropathy detected biochemically and histologically. Regarding the biochemical results of the kidney, renal dysfunction is detected by elevated serum urea and creatinine. Similar to the current work, Abdel Aziz et al., (2014) reported that one of the most sensitive and dramatic indicators of kidney injury is the increase of creatinine and urea level in the circulation following STZ administration.

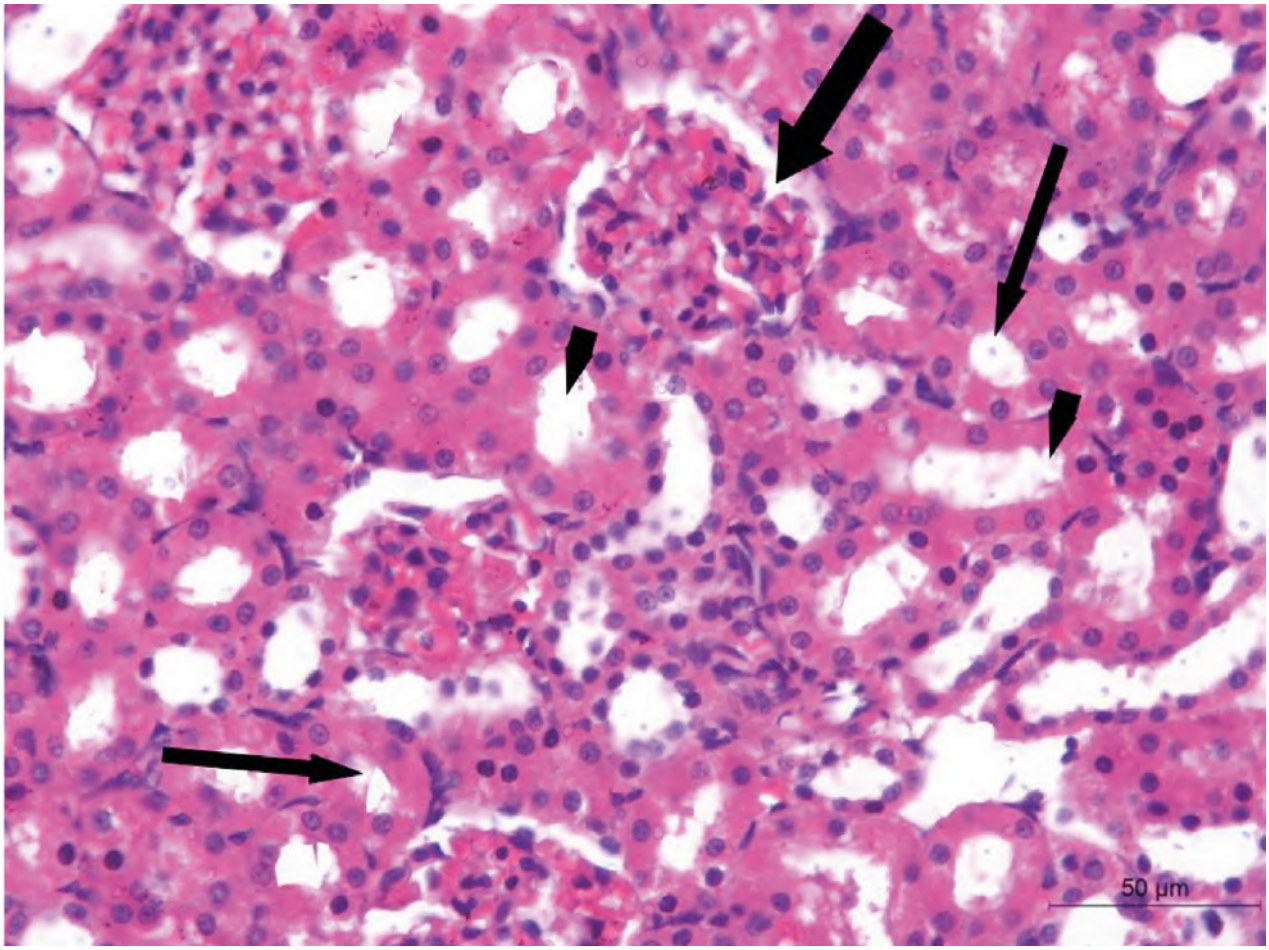

Fig. 5.- Renal cortical section of the STZ+ stem cell treated group shows apparently normal Malpighian corpuscle (thick arrow) and tubules (thin arrows) and some dilated tubules (arrow heads). Scale bar = 50 µm.

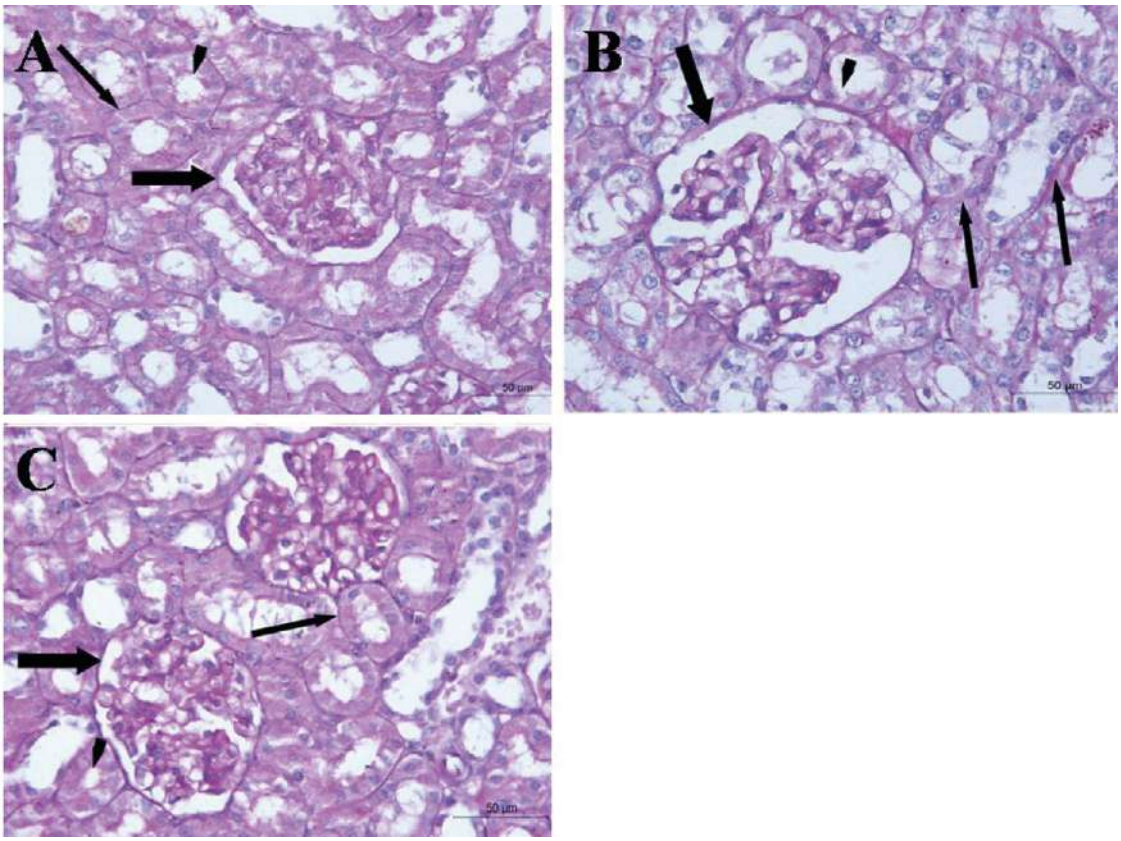

Fig. 6.- PAS-stained renal cortical sections of control (**A**), STZ treated (**B**) and STZ+ stem cell treated (**C**) groups. (B) shows in comparison with (A) thickening of parietal layer of Bowman's capsule (thick arrow) as well as basement membrane of renal tubules (thin arrows). Partial loss of brush border of some proximal convoluted tubules could be seen (arrowhead). (C) shows thin parietal layer of Bowman` s capsule and basement membrane of renal tubule. Brush border of proximal convoluted tubules could be detected mostly intact. Scale bars = 50 µm.

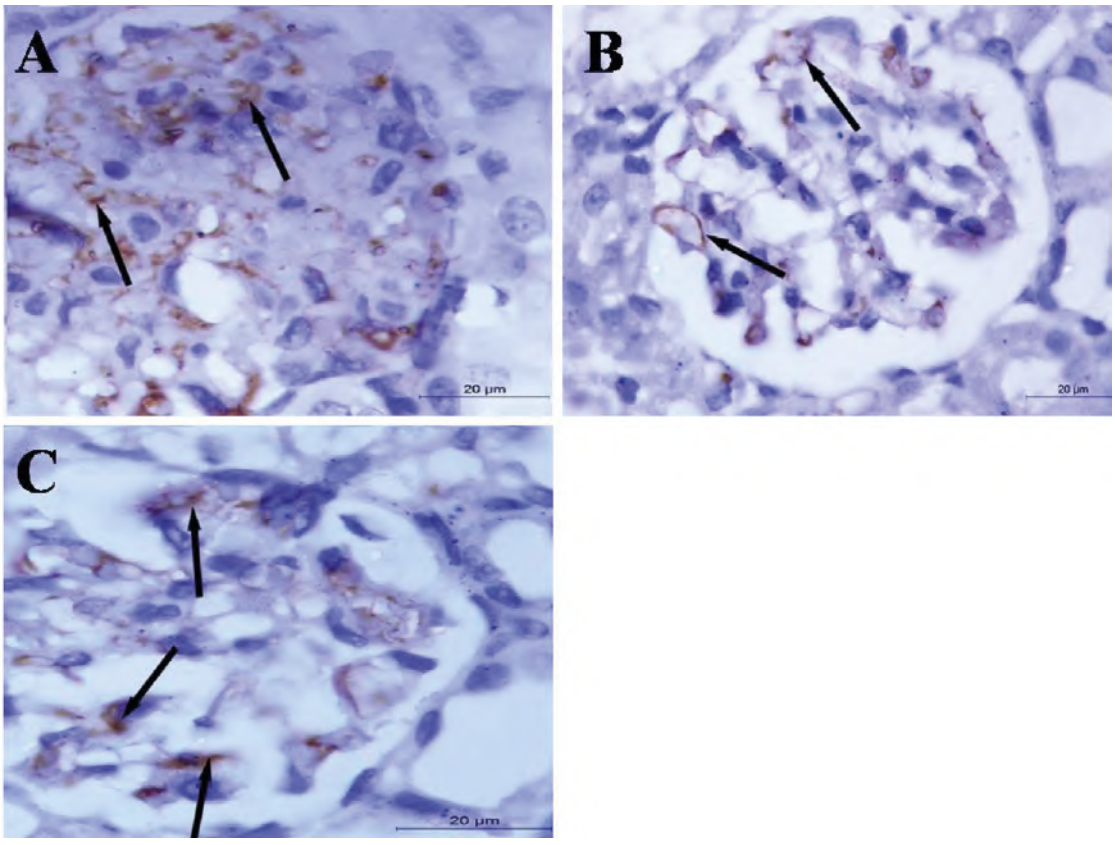

Fig. 7.- eNOS immunostained renal sections of control (**A**), STZ treated (**B**) and STZ+ stem cell treated (**C**). (A) shows brown coloration (positive eNOS immunoexpression) in the glomerular vascular endothelium (arrows). (B) shows decreased intensity of the eNOS immunoexpression while (C) shows an increase of the intensity. Scale bars = 20 µm.

The results of the current study are in accordance with Kaur et al. (2015), who reported that the single dose administration of STZ in rats has been shown to produce diabetic nephropathy (DN) after 6 weeks, and stated that the serum creatinine levels were noted to be increased markedly in STZ treated rats on day 42nd as compared to the control group. Also, Lu et al. (2007) and Shaker et al. (2015) reported that urea and creatinine levels were increased in DN rat model induced by streptozotocin.

Multiple mechanisms contribute to the development and outcomes of diabetic nephropathy such as an interaction between hyperglycemia-induced metabolic and hemodynamic changes and genetic predisposition, which sets the stage for kidney injury (Li et al., 2018).

Another theory was detected by Mousa et al. (2016) who postulated that the elevation in serum urea and creatinine of STZ diabetic animals could be attributed to the functional and/or morphological changes in the kidneys.

However, Sriram and Subramanian (2011) showed that the increased concentrations of urea and creatinine in blood was due to diabetic oxidative stress and impaired balance of nitrogen coupled with lowered protein synthesis.

The current work detected that administration of BM-MSCs in diabetic rats showed a significant improvement of kidney functions (urea and creatinine) as compared with diabetic group. This was agreed with Mousa et al. (2016) and Humphreys and Bonventre (2008), who detected an improvement of kidney functions after administration of stem cells, and this may be due to homing of MSCs to injured tissue causing its regeneration by its direct differentiation ability or by the paracrine factors released by MSCs. In agreement of the current study, the results of Semedo et al. (2009b) showed a significant improvement in kidney function in the diabetic group treated intravenously with a single dose of one million of MSCs per rat compared to DN group.

Abdel Aziz et al. (2014) reported that the administration of MSCs led to the amelioration of some functional parameters such as serum creatinine and urea levels. They referred this improvement in kidney function in MSCs-treated group to their paracrine action via different growth factors such as VEGF, TGF-β and TNF-α and antiapoptotic effects via Bax and Bcl2 genes.

Regarding the histological results, STZ injection caused structural alterations in the renal glomeruli which appeared hypertrophic with narrowed or obliterated Bowman` s space. These findings were similar to that of Shaker et al. (2015) and Zhou et al. (2009) who reported that kidney samples of diabetic nephropathy group showed exaggerated mesangial proliferation and thickened basement membrane.

Additionally, Patel et al. (2009) found that DM led to an elevation in oxidative damage inducing considerable injury in the glomeruli, disorders in matrix protein synthesis and increase in transforming growth factors-beta (TGF-β). However, Takahashi and Harris (2014) found that the diabetic nephropathic changes in the form of glomerular hypertrophy, mesangial expansion and nodular glomerulosclerosis were due to not only oxidative stress but also due to insulin resistance, hyperinsulinemia and hyperlipidemia.

In the present work, diabetic nephropathy was characterized by degenerated renal tubular cells with intraluminal acidophilic hyaline material that considered as hyaline casts. Moreover, there was a significant interstitial mononuclear cellular infiltration. This is in agreement with results reported by (Mundt and Shanahan, 2011).

These findings were analogous to the findings of Li et al. (2018), who indicated that renal morphologic abnormalities in DN rats including tubular degeneration, dilatation and protein cylinders at 8 weeks after STZ injection, confirming diabetic renal injury.

In the current study, light microscopic examination of the renal sections revealed the regaining of the normal appearance of most of the renal tissue including glomeruli, proximal and distal convoluted tubules in mesenchymal stem cell treated group after STZ administration. Comparable findings were observed by Asanuma et al. (2011) and Nagaishi et al. (2016) who revealed the therapeutic use of stem cells in diabetic nephropathy.

Many postulations were suggested to explain the mechanism of stem cells therapy in diabetic nephropathy. MSCs protects against diabetic nephropathy by restoring the biochemical alterations as well as inhibition of oxidative stress and pro-inflammatory gene expression levels suggesting a potential clinical use of MSCs to prevent the onset and progression of diabetic nephropathy according to Fang et al. (2012).

Another explanation is that the use of MSCs in type 1 diabetes (T1D) was based upon their immunoregulatory properties, which may help to rescue peripheral tolerance toward pancreatic β cells by reshaping the immune response and blocking their damage by autoreactive T cells (Fiorina et al., 2011). A study made by Lee et al. (2006) mentioned that in diabetic mice, MSCs homed and promoted repair of pancreatic islets and renal glomeruli. The results raised the possibility that MSCs may be useful in enhancing insulin secretion and perhaps improving the renal lesions that develop in patients with diabetes mellitus.

Antioxidant effect of MSCs was suggested to be mediated through modulation of pathways associated with the activation of antioxidant pathways such as superoxide dismutase and glutathione peroxidase (Lanza et al., 2009). Transplantation of MSCs decreases inflammatory response of kidney in diabetic nephropathy. This leads to modulation of the inflammation via increasing IL10 cytokine and delays the progression of diabetic nephropathy. This beneficial effect is thought to be due to the anti-inflammatory factors such as IL10 produced by MSCs that are secreted in a paracrine fashion (Semedo et al., 2009b).

In the present work, PAS-stained kidney sections revealed marked thickening of parietal layer of Bowman`s capsule. The basement membranes of proximal and distal convoluted tubules were also thickened with loss of apical brush border of some proximal convoluted tubules. These results were in compliance with the finding of many researchers such as Wang et al. (2013), Nagaishi et al. (2016) and Li et al. (2018).

In STZ+ Stem cell-treated group, there were regaining the thin parietal layer of Bowman`s capsule, thin basement membrane of renal tubule and intact brush border of proximal convoluted tubules.

In the current work, the eNOS immunoexpression is detected in the glomerular endothelial cells of the kidneys of the control group. The glomerular endothelium of diabetic kidneys showed a significant decrease in the intensity of the eNOS immunoexpression compared to the endothelium of control kidneys. Also, there was a significant increase in the intensity of the eNOS immunoexpression in the glomerular endothelial cells of the kidneys in the STZ +stem cell treated group compared to the diabetic group. These findings were also detected by Aktug et al. (2012), who found that eNOS expression in the glomerular endothelial cells and the visceral and parietal layers of the capsule were stronger in the controls when compared to the diabetic group. According to their results, hyperglycemia inhibits eNOS leading to reduced nitric oxide production in endothelial cells. Inhibition of eNOS was correlated with glomerular cell loss due to apoptosis.

Animal models have explored the mechanisms by which the eNOS deficiency causes advanced DN and provided many new insights into the pathogenesis of DN (Takahashi and Harris, 2014). Hyperglycemia down regulates the expression and activity of eNOS and decreases the bioavailability of NO, which aggravates diabetic nephropathy according to (Casey et al., 2004).

Oxidative stress appears to be the most important pathogenic factor in underlying diabetic complications (Dave and Kalia, 2007). Higher levels of reactive oxygen species can induce the production of inflammatory cytokines in the kidney which enhances DN progression. One of the sources of inflammatory cytokines is bone marrow-derived cells that excessively infiltrate the kidneys fusing with the tubular epithelial cells causing parenchymal cells to produce cytotoxic tumor necrosis factor alpha (TNF-α) and caspase-3 which leads to degeneration and apoptosis in STZ-induced diabetes (Nagaishi et al., 2016).

CONCLUSION

MSCs transplantation can improve the levels of blood glucose and kidney functions (urea and creatinine) in STZ-induced diabetic rats. Also stem cells ameliorate the pathological changes of the kidneys in diabetic rats. Thus, stem cells provided a new line of treatment strategies in diabetes and diabetic nephropathy.

REFERENCES

ABDEL AZIZ MT, EL-ASMAR MF, HAIDARA M, ATTA HM, ROSHDY NK, RASHED LA, SABRY D, YOUSSEF MA, ABDEL AZIZ AT, MOUSTAFA M (2008) Effect of bone marrow-derived mesenchymal stem cells on cardiovascular complications in diabetic rats. *Med Sci Monit*, 14(11): BR 249-255.

ABDEL AZIZ MT, WASSEF MA, AHMED HH, RASHED L, MAHFOUZ S, ALY MI, HUSSEIN RE, ABDEL AZIZ M (2014) The role of bone marrow derived-mesenchymal stem cells in attenuation of kidney functions in rats with diabetic nephropathy. *Diabetology Metab Synd*, 6: 34-44.

AKTUG H, CETINTAS VB, KOSOVA B, OLTULU F, DEMIRAY SB, CAVUSOGLU T, AKARCA SO, YAVASOGLU A (2012) Dysregulation of NOS activity and Bcl-2&caspase-3 gene expression in renal tissue of STZ-induced diabetic rats. *Turk J Med Sci*, 42(5): 830-838.

ASANUMA H, VANDERBRINK BA, CAMPBELL MT, HILE KL, ZHANG H, MELDRUM DR, MELDRUM KK (2011) Arterially delivered mesenchymal stem cells prevent obstruction-induced renal fibrosis. *J Surg Res*, 168: e51-e59.

BANCROFTJ, GAMBLE M (2008) Theory and Practice of Histological Techniques. 5th ed. Churchill-Livingstone, London, Edinburgh, New York, Philadelphia, St Louis, Sydney and Toronto, pp 126-127, 150, 171, 601-612.

BERARDIS S, SATTWIKA D, SOKAL E (2015) Use of mesenchymal stem cells to treat liver fibrosis. *World J Gastroenterol*, 3: 742-758.

BLUESTONE JA, HEROLD K, EISENBARTH G (2010) Genetics, pathogenesis and clinical interventions in type 1 diabetes. *Nature*, 464: 1293-1300.

CARR CA, STUCKEY DJ, TATTON L (2008) Bone marrow-derived stromal cells home to and remain in the infarcted rat heart but fail to improve function: an in vivo cine-MRI study. *Am J Physiol Heart Circ Physiol*, 295(2): H533.

CASEY GR, JOYCE M, NAGLE RG, CHEN G, BOUCHIER-HAYES D (2004) Pravastatin modulates early diabetic nephropathy in an experimental model of diabetic renal disease. *J Surg Res*, 123: 176-181.

CESARETTI ML, GINOZA M, RIBEIRO AB, KOHLMANN OJ (2010) Systemic hemodynamic and left ventricular function of diabetic-induced hypertensive rats. *Arq Bras Endocrinol Metabol*, 54(9): 842-851.

DAVE GS, KALIA K (2007) Hyperglycemia induced oxidative stress in type-1 and type-2 diabetic patients with and without nephropathy. *Cell Mol Biol*, 53(5): 68-78.

EMSLEY R, DUNN G, WHITE IR (2010) Mediation and moderation of treatment effects in randomized controlled trails of complex interventions. *Stat Methods Med Res*, 19: 237-270.

FANG Y, TIAN X, BAI SH, JUN FAN J, HOU W, TONG H, LI D (2012) Autologous transplantation of adipose-derived mesenchymal stem cells ameliorates streptozotocin-induced diabetic nephropathy in rats by inhibiting oxidative stress, pro-inflammatory cytokines and the p38 MAPK signaling pathway. *Int J Mol Med*, 30: 85-92.

FIORINA P, VOLTARELLI J, ZAVAZAVA N (2011) Immunological applications of stem cells in type 1 diabetes. *Endocr Rev*, 32(6): 725-754.

HUMPHREYS BD, BONVENTRE JV (2008) Mesenchymal stem cells in acute kidney injury. *Annu Rev Med*, 59: 311-325.

IKEBUKURO K, ADACHI Y, YAMADA Y, FUJIMOTO S, SEINO Y, OYAIZU H (2002) Treatment of streptozotocin-induced diabetes mellitus by transplantation of islet cells plus bone marrow cells via portal vein in rats. *Transplantation*, 73(4): 512-518.

JIANG TS, CAI L, JI WY, HUI YN, WANG YS, HU D, ZHU J (2010) Reconstruction of the corneal epithelium with induced marrow mesenchymal stem cells in rats. *Mol Vis*, 16: 1304-1316.

KAJIYAMA H, HAMAZAKI TS, TOKUHARA M, MASUI SH, OKABAYASHI K, OHNUMA K, YABE SH, YASUDA K, ISHIURA SH, OKOCHI H, ASASHIMA M (2010) Pdx1-transfected adipose tissue-derived stem cells differentiate into insulin-producing cells in vivo and reduce hyperglycemia in diabetic mice. *Int J Dev Biol*, 54: 699-705.

KANWAR YS, SUN L, XIE P, LIU FY, CHEN S (2011) A glimpse of various pathogenetic mechanisms of diabetic nephropathy. *Annu Rev Pathol*, 6: 395-423.

KAUR M, SACHDEVA S, BEDI O, KAUR T, KUMAR P (2015) Combined effect of hydrogen sulphide donor and losartan in experimental diabetic nephropathy in rats. *J Diabetes Metab Dis*, 14: 63.

KIERNAN JA (2015) Staining with dyes in one or two colors. In: *Histological and Histochemical Methods: Theory and Practice*, 5th ed. Scion Publishing Ltd., Vantage Business Park, Bloxham Road, Banbury, UK, pp 137-169.

LANZA C, MORANDO S, VOCI A, CANESI L, PRINCIPATO MC, SERPERO LD, MANCARDI G, UCCELLI A, VERGANI L (2009): Neuroprotective mesenchymal stem cells are endowed with a potent antioxidant effect in vivo. *J Neurochem*, 110: 1674-1684.

LEE RH, SEO MJ, REGER RL, SPEES JL, PULIN AA, OLSON SD, PROCKOP DJ (2006) Multipotent stromal cells from human marrow home to and promote repair of pancreatic islets and renal glomeruli in diabetic NOD/SCID mice. *Proc Natl Acad Sci USA*, 103: 17438-17443.

LIU S, ZHAO C, YANG C, LI X, HUANG H, LIU N, LI S, WANG X, LIU J (2013) Gambogic acid suppresses pressure overload cardiac hypertrophy in rats. *Am J Cardiovasc Dis*, 3(4): 227-238.

LI Y, LIU J, LIAO G, ZHANG J, CHEN Y, LI L, LIU F, CHEN B, GUO G, WANG C, YANG L, CHENG J, LU Y (2018) Early intervention with mesenchymal stem cells prevents nephropathy in diabetic rats by ameliorating the inflammatory microenvironment. *Int J Mol Med*, 41: 2629-2639.

LU Q, YIN XX, WANG JY, GAO YY, PAN YM (2007) Effects of Ginkgo biloba on prevention of development of experimental diabetic nephropathy in rats. *Acta Pharmacol Sin*, 28: 818-828.

MOUSA F, ABDEL AZIZ KK, ABDEL GAWAD H, MAHMOUD SS, ELGAMEL MS (2016) Bone marrow-derived mesenchymal stem cells infusion ameliorates hyperglycemia, dyslipidemia, liver and kidney functions in diabetic rats. *Int J Sci Res (IJSR)*, 5(2): 1624-1631.

MUNDT L, SHANAHAN K (2011) Graff's Textbook of Routine of Urin analysis and Body Fluids, 2nd edition, Lippincott Williams & Wilkins, Philadelphia.

NAGAISHI K, MIZUE Y, CHIKENJI T, OTANI M, NAKANO M, KONARI N, MINEKO FM (2016) Mesenchymal stem cell therapy ameliorates diabetic nephropathy via the paracrine effect of renal trophic factors including exosomes. *Sci Rep*, 6: 34842.

NGOC K, VAN PHUC P, NHUNG T, THUY D, NGUYET M (2011) Improving the efficacy of type 1 diabetes therapy by transplantation of immunoisolated insulin-producing cells. *Human Cell*, 24: 86-95.

PATEL SS, SHAH RS, GOYAL RK (2009) Antihyperglycemic, antihyperlipidemic and antioxidant effect of Dihar, a polyherbal an ayurvedic formulation in streptozotocin induced diabetic rat. *Int J Exp Biol*, 471: 564-570.

PENG BY, DUBEY NK, MISHRA VK, TSAI FC, DUBEY R, DENG WP, WEI HJ (2018) Addressing stem cell therapeutic approaches in pathobiology of diabetes and its complications. *J Diabetes Res*, 2018: 7806435.

PULAVENDRAN S, VIGNESH J, ROSE C (2010) Differential anti-inflammatory and anti-fibrotic activity of transplanted mesenchymal vs. hematopoietic stem cells in carbon tetrachloride induced liver injury in mice. *Int Immunopharmacol*, 4: 513-519.

SEMEDO P, PALASIO CG, OLIVEIRA CD, FEITOZA CQ, GONCALVES GM, CENEDEZE MA, WANG PM, TEIXEIRA VP, REIS MA, PACHECO-SILVA A, CAMARA NO (2009) Early modulation of inflammation by mesenchymal stem cell after acute kidney injury. *Int Immunopharmacol*, 9: 677-682.

SHAKER OG, NASSAR YH, ASHOUR SS, HAMMAM OA (2015) Effect of mesenchymal stem cells on diabetic nephropathy in experimental animals. *Med J Cairo Univ*, 83(1): 1113-1122.

SRINIVASAN K, VISWANAD B, ASRAT L, KAUL CL, RAMARAO P (2005) Combination of high-fat diet-fed and low-dose streptozotocin-treated rat: a model for type 2 diabetes and pharmacological screening. *Pharmacol Res*, 52: 313-332.

SRIRAM PG, SUBRAMMANIAN S (2011) Fistin, a bioflavonoid ameliorates hyperglycemia in streptozotocin-induced experimental diabetes in rats. *Int J Pharmac Sci Rev Res*, 6 (1): 68-74.

TAKAHASHI T, HARRIS RC (2014) Role of endothelial nitric oxide synthase in diabetic nephropathy. lessons from diabetic eNOS knockout mice. *J Diabetes Res*, 2014: 590541.

VOLAREVIC V, NURKOVIC J, ARSENIJEVIC N, STOJKOVIC M (2014) Concise review: therapeutic potential of mesenchymal stem cells for the treatment of acute liver failure and cirrhosis. *Stem Cells*, 32: 2818-2823.

WANG SH, LI Y, ZHAO J, ZHANG J, HUANG Y (2013) Mesenchymal stem cells ameliorate podocyte injury and proteinuria in a type 1 diabetic nephropathy rat model. *Biol Blood Marrow Transplant*, 19: 538-546.

YANG Z, LI K, YAN X, DONG F, ZHAO C (2010) Amelioration of diabetic retinopathy by engrafted human adipose-derived mesenchymal stem cells in streptozotocin diabetic rats. *Graefes Arch Clin Exp Ophthalmol*, 248: 1415-1422.

ZHOU P, HOHM S, OLUSANYA Y, HESS DA, NOLTA JA (2009) Human progenitor cells with high aldehyde dehydrogenase. *Hepatol*, 49(6): 1992-2000.

Influence of global cerebral ischemia/ reperfusion injury on rat dentate gyrus and the possible protective effect of beetroot (*Beta vulgaris L.*) extract

Samah Elsayed[1], Mostafa El-Habeby[1], Neveen El-Sherif[1], Marwa Al-Gholam[1]

Department of Anatomy and Embryology, Faculty of Medicine, Menoufia University, Menoufia, Egypt

SUMMARY

The dentate gyrus is a sensitive region of the brain for learning and memory, and is thus vulnerable to post-ischemic changes. So, this work aimed to study the histological changes in the dentate gyrus after right common carotid artery occlusion/ reperfusion. To the best of our knowledge, this research is the first attempt to demonstrate the beneficial protective role of red beetroot supplementation. Forty-two adult male albino rats were divided randomly into: Group I, consisting of 18 rats and were subdivided into control, red beetroot extract (RBE), and sham; Group II, right common carotid artery occlusion (RCCAO) group (n=12). This group had unilateral common carotid artery occlusion on the right side for 90 minutes followed by reperfusion for one week. Group III: RCCAO+RBE group (n=12): received RBE (500 mg/kg/day/oral) for 22 days, and on day 15 were subjected to RCCAO then reperfusion for one week. At the end of the experiment, the dentate gyrus sections were subjected to histological, immunohistochemical, and morphometric analyses for the expression of Caspase-3, glial fibrillary acidic protein (GFAP), Heat shock protein 70 (HSP70), Tumor necrosis factor-alpha (TNF-α). Besides, tissue nitric oxide, superoxide dismutase, and malonaldehyde levels were measured. Results: RBE ameliorates the ischemic induced dentate gyrus neurodegenerative changes. The number of granular cells and their Nissl's granules content were significantly increased. This study clarified that red beetroot extract exerted its effects via regulating oxidative stress, inflammation, and apoptosis. Besides, this study detected that the beneficial effect of RBE was also mediated by modulating HSP70 expression and the astroglial response to the injury. Conclusion: Red beetroot extract showed an anti-ischemic potential providing new insight into its significance as a neuroprotective agent.

Key words: Red beetroot extract – Ischemia/ Reperfusion injury – Dentate gyrus

INTRODUCTION

According to the World Health Organization, 15 million people suffer strokes worldwide each

Corresponding author:
Samah Sayed Hassan Elsayed. Department of Anatomy and Embryology, Faculty of Medicine, Menoufia University, Menoufia, Egypt. Phone: 01205290320. E-mail: samah.fakhreldean@gmail.com.
Marwa Abdel-Samad Al-Gholam. Phone: 01025079077. E-mail: marwaelgholam@yahoo.com

Submitted: August 29, 2020. **Accepted:** March 1, 2021

year (Virani et al., 2020). Of these, 5 million die, and another 5 million are permanently disabled (Mozaffarian et al., 2016). Stroke is the second cause of death after ischemic heart disease, and over a third of deaths by stroke occur in developing countries. Arab countries constitute populations with a similar lifestyle and diet that may influence stroke risk, type, and survival after stroke (Benamer and Grosset, 2009). The incidence of stroke in low-income and middle-income countries exceeded that in high-income countries by 20% (Lee et al., 2015). In Egypt, according to recent estimates, the overall prevalence rate of stroke is 963/100,000 inhabitants (Abd-Allah and Moustafa, 2014).

The main symptoms involve impairments in vision, body movement, and speaking. It can include unconsciousness, blindness, problems with coordination, and weakness in the body. Other effects that may result from brain ischemia are stroke, cardiorespiratory arrest and irreversible brain damage (Lozano et al. ,2013). Oxidative stress, leukocyte infiltration, platelet activation and aggregation, complement activation, and breakdown of the blood-brain barrier (BBB) are the major mechanisms of reperfusion injury. These mechanisms ultimately lead to edema or hemorrhagic transformation (Kim and Johnston, 2011). Despite stroke being a serious life-threatening risk and causing disability, the only effective accepted treatment is tissue plasminogen activators. However, the duration limitations of this treatment mean that it can only be given to a small proportion of patients, 1-2% (Goldstein, 2007).

Despite decades of intense research, the beneficial treatment of stroke remains limited (Lozano et al., 2013). In light of this, the search for effective means ameliorating cerebral ischemia-reperfusion injury (CIRI) is one of the major problems of experimental medicine and biology (Goldstein, 2007).

The powerful antioxidant, anti-inflammatory, and vascular-protective effects offered by beetroot and its constituents have been proved by several in vitro and in vivo human and animal studies (Clifford et al., 2015).

Consequently, the present study was designed to investigate, for the first time to the best of our knowledge, the protective effect of red beetroot extract on the post-ischemic dentate gyrus neurodegeneration.

MATERIALS AND METHODS

Chemicals

Red Beetroots (Beta vulgaris) were purchased from a local market. One kilogram of Fresh Red Beetroots was exhaustively macerated by soaking in 70% (1.5 L) ethanol for three successive days after washing with tap water and cutting into small pieces. Then this alcoholic extract was concentrated under reduced pressure using a rotatory evaporator till complete drying (Biochemistry Department, Faculty of Science, Menoufia University, Egypt) (El Gamal et al., 2014). The resulted extract (RBE, 150 g) was later suspended in distilled water.

Animals

Forty-two adult male albino rats with an average weight of 200-250 grams were used in this study. They were obtained from Ain shams Animal House, Cairo, Egypt. The animals were kept under controlled conditions of temperature and humidity and provided with water and a balanced diet. The light / darkness cycle was fixed at 12:12 h. The procedure was approved by the ethics committee on the animal experiment of the Faculty of Medicine, Menoufia University, Egypt following the international regulations on care and use of laboratory animals.

The rats were randomly divided into 3 groups:

Group I consisted of 18 rats and were subdivided into 3 subgroups. Subgroup Ia (n=6): animals were fed a regular diet. Subgroup Ib (n = 6): the rats were subjected to a sham surgical procedure on day 15 and left without treatment. Subgroup Ic (n=6): the rats received red beetroot extract (RBE) (500 mg/kg/day/orally) (El Gamal et al., 2014) for 22 days.

Group II: (RCCAO) group (n = 12). This group had unilateral common carotid artery occlusion on the right side for 90 minutes (Mentari et al.,2018) followed by reperfusion for one week.

Group III: (RCCAO+RBE) protected group (n = 12). The rats received red beetroot extract (RBE) (500 mg/kg/day/orally) (El Gamal et al., 2014) for 22 days and were subjected to the same surgical procedure as the group II followed by reperfusion for one week.

Surgical procedure

Induction of cerebral ischemia/reperfusion was carried out using the standard method (Mentari et al., 2018). Overnight fasted rats were anesthetized with thiopental sodium (30 mg/kg). A midline ventral incision was made in the throat. The right common carotid artery was located and freed from the surrounding tissue and vagus nerve. Global cerebral ischemia was induced by occluding the carotid artery on the right side with a clamp. After 90 min of global cerebral ischemia, the clamp was removed to allow the reperfusion of blood through the carotid artery. Rats were maintained at 37°C on a heated surgical platform. All surgical procedures were carried out under sterile conditions. The surgical procedure was done at Ain Shams University, Faculty of Medicine, Egypt.

At the end of the experiment, rats were deeply anesthetized using ketamine (90 mg/kg) and xylazine (15 mg/kg) intraperitoneally, then decapitated. The dentate gyrus sections were subjected to biochemical, histological, immunohistochemical, and morphometric analyses.

Evaluation methods

Histological study

A coronal section was performed in the cerebral hemisphere into two halves to reach the site of the dentate gyrus and then fixed in 10% buffered formaldehyde solution; then the specimens were dehydrated, cleared, and embedded in paraffin blocks. Serial coronal sections were cut 5 µm thick and stained with hematoxylin and eosin (H & E) for routine histological examination and with toluidine blue (TB) to detect Nissl's granules.

Immunohistochemical study

The paraffin sections on poly-L-lysin-coated slides were deparaffinized and rehydrated. Endogenous peroxidase was blocked by inserting the sections in 3% hydrogen peroxide (H2O2). The microwave antigen retrieval procedure was performed. The sections were incubated with primary anti Heat shock protein 70 (HSP70 antibody); a marker for oxidative stress-cytoplasmic and nuclear expression (rabbit polyclonal antibody, Midco Trade Company, Giza, Egypt); anti-Caspase-3 antibody; an apoptotic marker cytoplasmic expression, (rabbit polyclonal antibody, Dako, Carpinteria California, USA); anti-Glial fibrillary acidic protein (GFAP) antibody; a marker for astrocyte activation (rabbit polyclonal antibody, Midco Trade Company, Giza, Egypt) and anti-*Tumor necrosis factor-alpha* (TNF-α) antibody, expressed in the cytoplasm of granular cells (mouse monoclonal antibody, Gene tex company, Cairo, Egypt). After that, the biotinylated goat-polyvalent secondary antibody was applied. The sections were then incubated in preformed streptavidin-peroxidase and, finally, we applied the prepared DAB substrate chromogen (3,3′-diaminobenzidine tetrahydrochloride). The slides were counterstained with hematoxylin to be examined under a light microscope.

Biochemical study

Preparation of brain tissue for estimation of biochemical parameters related to oxidative stress. The brain of each animal was removed and washed with cooled 0.9% saline, kept on ice, and subsequently blotted on filter paper, then weighed and homogenized with cold phosphate buffer (0.1M, pH 7.4) using a Remi homogenizer. The homogenization procedure was performed as quickly as possible under completely standardized conditions. The homogenate was centrifuged at 1,000 rpm and 4°C for 3 min, and the supernatant was divided into two portions, one of which was used for measurement of Malondialdehyde (MDA). The remaining supernatant was again centrifuged at 12,000 rpm at 4°C for 15 min and used for the measurement of superoxide dismutase (SOD) levels by standard methods (PanelKevin et al., 1985).

Morphometric assessment

For histological and immunohistochemical quantitative assessment, from each section six non-overlapping fields (400x) were randomly

captured by a Leica Microscope DML B2/11888111 equipped with a Leica camera DFC450. The different parameters including the thickness of the granular layer, number of granular cells, the color intensity of toluidine blue, number of GFAP positive cells, Caspase-3 positive cells and HSP70 positive cells, and the area percentage of TNF-α immunoreaction were assessed in the fields taken from at least six sections/animal using image J software (Maryland, USA) and averaged per field for each animal. The calculated data for at least six animals/experimental group and the biochemical results were subjected to statistical analysis.

Statistical analysis

Mean ± SD was used to present the collected data. Data analysis was carried out using SPSS (Inc., Chicago, IL, USA) version 23 on IBM compatible computer. The obtained data were analyzed using one way-ANOVA followed by the post hoc Bonferroni test. The results were considered statistically significant when the p-values were <0.05.

RESULTS

Examination of all subgroups in group I showed the same histological findings and revealed no statistically significant difference in all the examined parameters between them. So we considered all as a control group.

Histological results

In H&E-stained sections, the hippocampus appears as a pair of interlocking C-shaped structures: Ammon's horn and the dentate gyrus. The dentate gyrus of the control group was formed of molecular, granular, and polymorphic layers (Fig. 1a). The granular layer was formed of multiple regular rows of well-organized, compactly arranged granular cells that were arranged in a V-shaped configuration forming upper and lower blades. Each granular cell appeared elliptical with basophilic cytoplasm, large vesicular nucleus, and prominent nucleolus. Both molecular and polymorphic layers were formed mainly of the eosinophilic neuropil matrix within which neuroglia was embedded. Microglia with rod-shaped nuclei, oligodendroglia with small dark nuclei and perinuclear halos, and astrocytes with oval vesicular nuclei were observed (Fig. 1b). In the RCCAO group, there was a disturbing arrangement of the granular cells that appeared degenerated with shrunken hyperchromatic nuclei, perinuclear halos, and lost nuclear details. The neuropil showed many vacuolations and congested blood vessels. Moreover, the number of astrocytes was increased compared with the control group (Fig. 1c). In the RCCAO+RBE group, many normal granular cells were observed with only some pyknotic ones and few ghost cells. The neuropil was regularly organized except for the presence of few vacuolations and less congested blood vessels. Besides, few astrocytes were observed. Few spindle-shaped cells were detected in SGZ. (Fig. 1d). Statistically, the thickness of the granular blades was significantly decreased ($P<0.05$) in the RCCAO group compared with the control one. However, it showed a significant increase ($P<0.05$) in the RCCAO+RBE group compared to the RCCAO group (Fig. 2).

Moreover, the number of the granular cells was significantly decreased ($P<0.05$) in the RCCAO group compared to the control one (61±2.89 vs. 124.16±1.69). However, it showed a significant increase ($P<0.05$) in the RCCAO+RBE group compared with the RCCAO group (116.83±2.75 vs. 61±2.89) (Table 1, Fig. 2).

In toluidine blue-stained sections, the cytoplasm of the granular cells of the control group was filled with dense dark blue Nissl's granules. In the RCCAO group, the Nissl's granules content appeared faint blue. In the RCCAO+RBE group, the Nissl's granules content appeared dark blue (Fig. 3). Statistically, a significant decrease ($P<0.001$) in the color intensity was observed in the RCCAO group as compared to the control group (84.66±1.64 vs. 140.73±5.74). Even so, there was a significant increase ($P<0.001$) in the RCCAO+RBE group as compared to the RCCAO group (116.73±4.13 vs. 84.66±1.64) (Table 1, Fig. 3d).

Immunohistochemical results

In GFAP-stained sections, the RCCAO group showed a significant increase ($p<0.001$) in the number of astrocytes compared to the control group (30.66±4.5 vs. 3.16±1.61). In the RCCAO

group treated with red beetroot extract, there was a significant decrease (p<0.001) in the number of astrocytes compared to the RCCAO group (12. 65±1.75 vs. 30.66±4.5) (Fig. 3a-c and Fig. 4a).

In HSP70 stained sections, the RCCAO group showed a significant increase (P<0.01) in the number of HSP positive cells compared to the control group (16.33±2.5 vs. 5.46±0.86). However, in RCCAO groups treated with beetroot extract, a more significant increase (P<0.001) in this percentage was observed compared to the RCCAO group (30.33±5.58 vs. 16.33±2.5) (Fig. 3d-f and Fig. 4b).

In Caspase-3-stained sections, the RCCAO group showed a significant increase (P<0.001) in the caspase positive cells compared to the control group (55.48±4.15 vs. 5.42±.17). In the RCCAO group treated with beetroot, a significant decrease (P<0.001) in this percentage was observed compared to the RCCAO group (34.75±1.17 vs. 55.48±4.15) (Fig. 3g-i, Fig. 4c).

In TNF-alpha stained sections, the RCCAO group showed a significant increase (P<0.001) in its area percentage compared to the control group (1.46±0.86 vs. 29.33±2.52). RCCAO groups treated with red beetroot extract showed a significant decrease (P<0.001) in area percentage of TNF-alpha compared to the RCCAO group (12.32±3.04. vs29.33±2.52) (Fig. 3j-l, Fig. 4d).

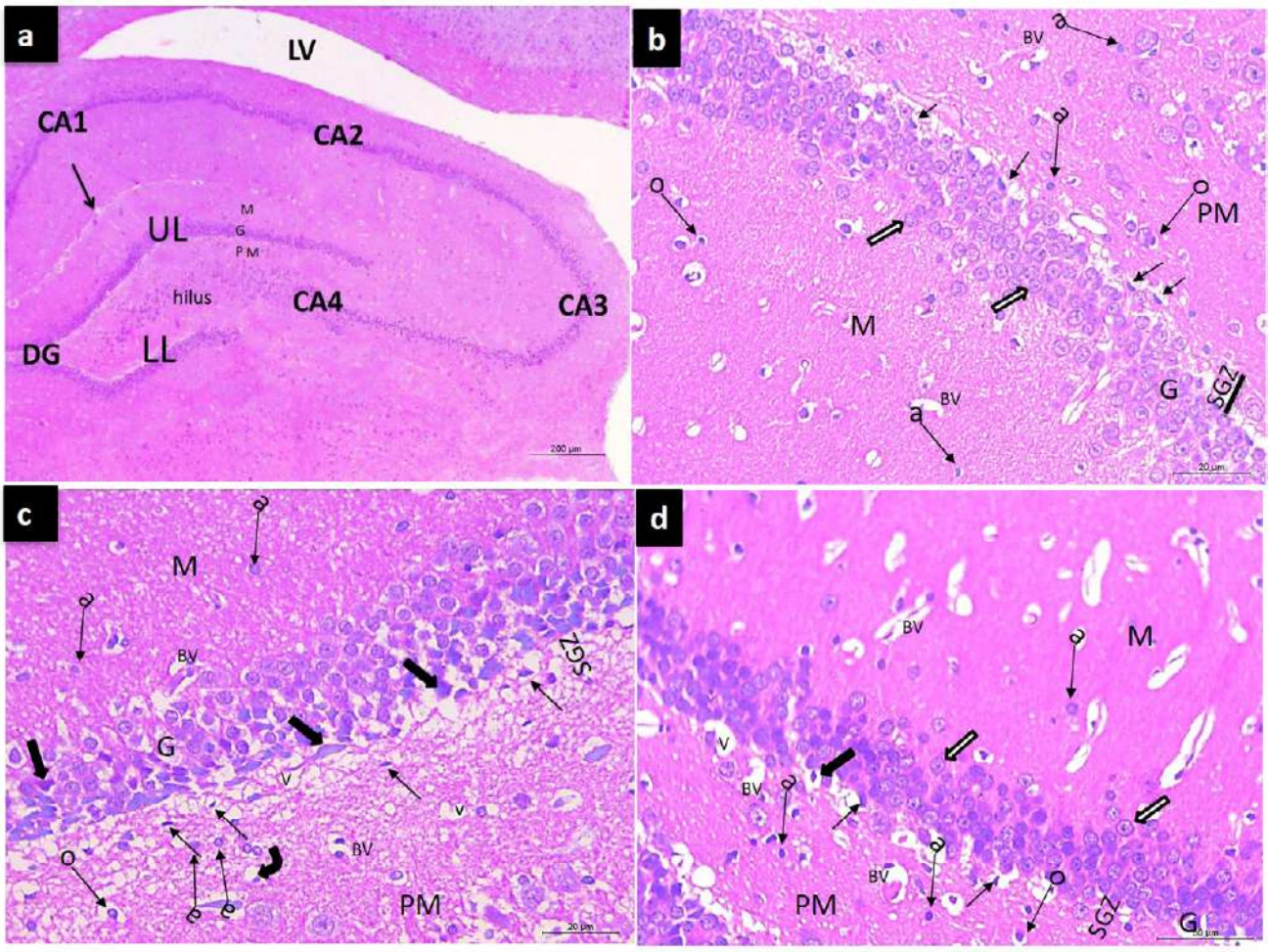

Fig. 1.- Representative photomicrographs **(a)** of coronal sections at the hippocampus and the dentate gyrus (DG), the dentate gyrus is formed of upper limb (UL), lower limb (LL), every limb formed of three: molecular (M), Granular (G) and polymorphic (PM) layers and stem in between, with a narrow hippocampal sulcus (arrow) in between. The hippocampus proper is composed of four areas: CA1, CA2, CA3, and CA4. The cavity of the lateral ventricle (LV). **(b)** The control group is showing the three layers of dentate gyrus: the molecular (M), Granular (G), and polymorphic (PM) layers. The Granular layer is formed of multiple regular rows of the Granular cells that appear tightly elliptical cells with basophilic cytoplasm (white arrows). Oligodendroglia; dark small nuclei and perinuclear halo (o), and astrocyte; oval vesicular nuclei (a) are scattered inside the neuropil. **(c)** The RCCAO group showing pyknotic granular cells (thick arrows), vacuolations (V), congested blood vessels (BV), degenerated oligodendroglia (bent arrow), and numerous astrocytes (a). the SGZ shows an increased number of spindle-shaped cells (thin arrows). **(d)** RCCAO group treated with beetroot extract showing many normal granular cells (white arrows) but some pyknotic (thick arrows) and are still present. Normal oligodendroglia (o), few astrocytes (a), few vacuolations (V), and a small number of spindle cells (thin arrows) of SGZ are observed within the neuropil. Scale bars: a = 200 µm); b, c, d = 20 µm, ×400).

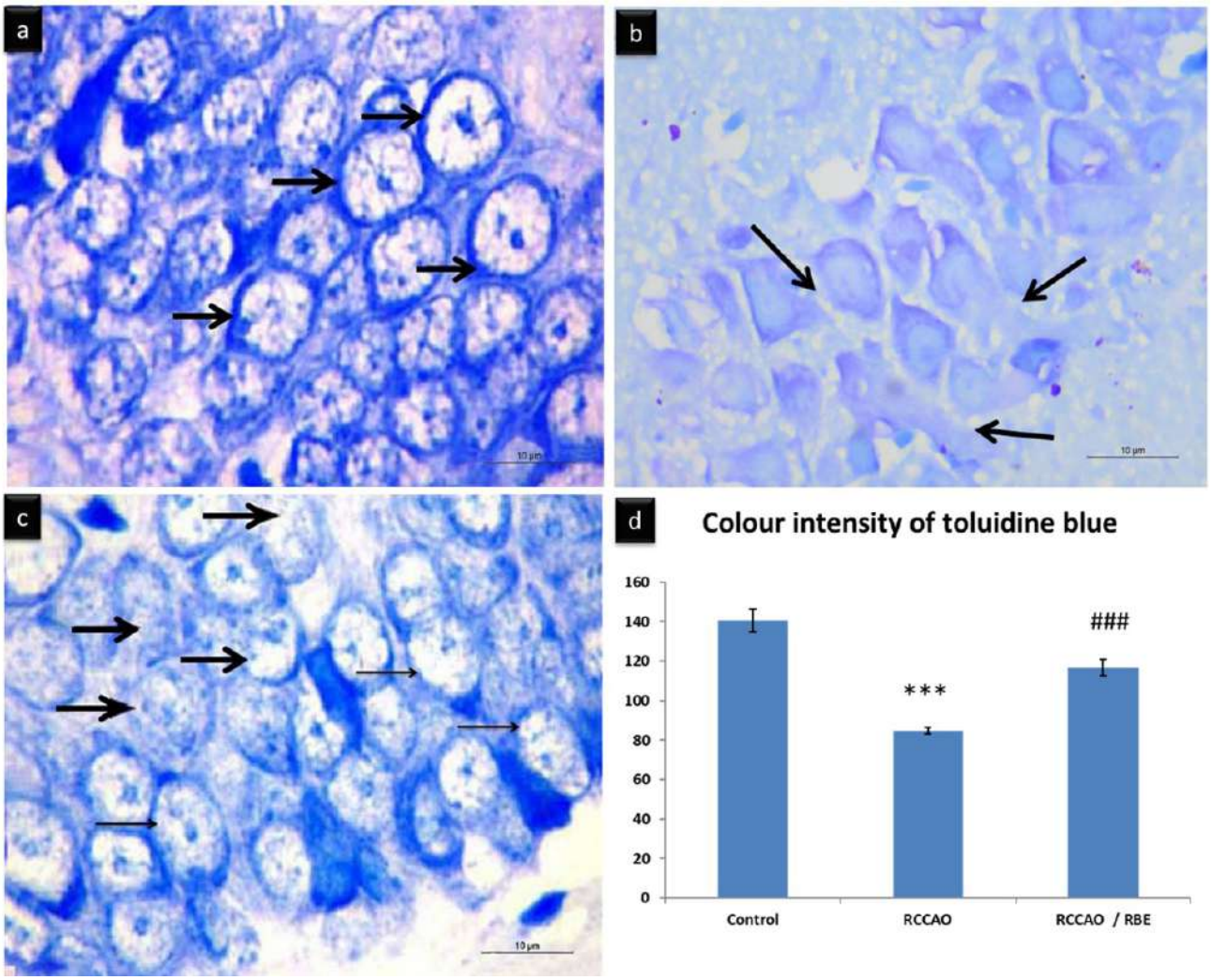

Fig. 2.- Representative micrographs of TB-stained sections in the dentate gyrus. **(a)** control group showing dense dark blue Nissl's granules content inside the cytoplasm of the granular cells (thick arrows). **(b)** RCCAO group showing an apparent decrease of Nissl's granules content inside the cytoplasm of the granular cells that appeared faint blue (arrows). **(c)** RCCAO+RBE treated with beetroot extract showing increased Nissl's granules content in many of the granular cells which appeared dark blue (thin arrow) with only a few faint blue Nissl's granules (thick arrow). Scale bars a-c = 10 µm, ×1000). **(d)** Mean color intensity (pixel) of Nissl's granules. *** p < 0.001compared with control, ### P< 0.001compared with RCCAO.

Table 1. Histological results.

Group Parameter	Control Mean±SD	RCCAO Mean±SD	RCCAO=RBE Mean±SD
Number of the granular cells	124.16±1.69	101±1.09*	116.83±0.75#
The thickness of upper dentate blade layer (µm)	75.5±5.24	66.16±3.86*	72±3.68#
The thickness of lower dentate blade layer (µm)	49.45±2.46	38.27±4.77*	42.07±1.88#

RCCAO: right common carotid artery occlusion, RCCAO+RBE: right common carotid artery occlusion + Red beetroot extract. *p<0.05 Comparison between RCCAO and control, # P < 0.05 Comparison between RCCAO+RBE and RCCAO.

Biochemical results

A significant increase in MDA level was observed in the RCCAO group (P<0.001) as compared with the control group. However, there was a significant decrease in its level in the RCCAO+RBE protected group (P<0.05) as compared with the RCCAO group (Table 2).

In this study we assessed the level of NO, which has an important role in the formation of oxidative damage and whose expression has also been detected in neural cells. There was a significant increase in NO level in the RCCAO group (p<0.001) compared to the control. It has been observed that red beetroot extract administration decrease (P<0.05) reperfusion injury and regresses the NO levels (Table 2).

Antioxidant marker tissue (SOD) activity is a major defense mechanism that protects the cells against oxidants. In this study, antioxidants decreased significantly in the RCCAO group ($p<0.001$) compared to the control group, while pretreatment with red beetroot extract decreases ($P<0.05$) reperfusion injury and regresses the NO levels (Table 2).

DISCUSSION

Ischemic stroke is one of the major leading causes of death and common causes of adult disability worldwide (Evenson et al., 1999). Considering the poor prognosis of ischemic stroke, protective therapies are being investigated to decrease neurological complications of its patients. Consequently, the present study was designed to investigate, for the first time to the best of our knowledge, the possible protective effect of red beetroot extract on the post-ischemic dentate gyrus neurodegeneration.

Examination of the dentate gyrus of the ischemia group showed small dark-stained nuclei in the granule cell layer and areas of cell loss. The same results were obtained by Irmak et al. (2003), who stated that cerebral ischemia up-regulated the expression of a transcription factor that has a pivotal role in mediating inflammatory response and reactive oxygen species (ROS) protein. This overproduction of ROS, inflammation, and oxidative stress leads to neuronal injury (Irmak

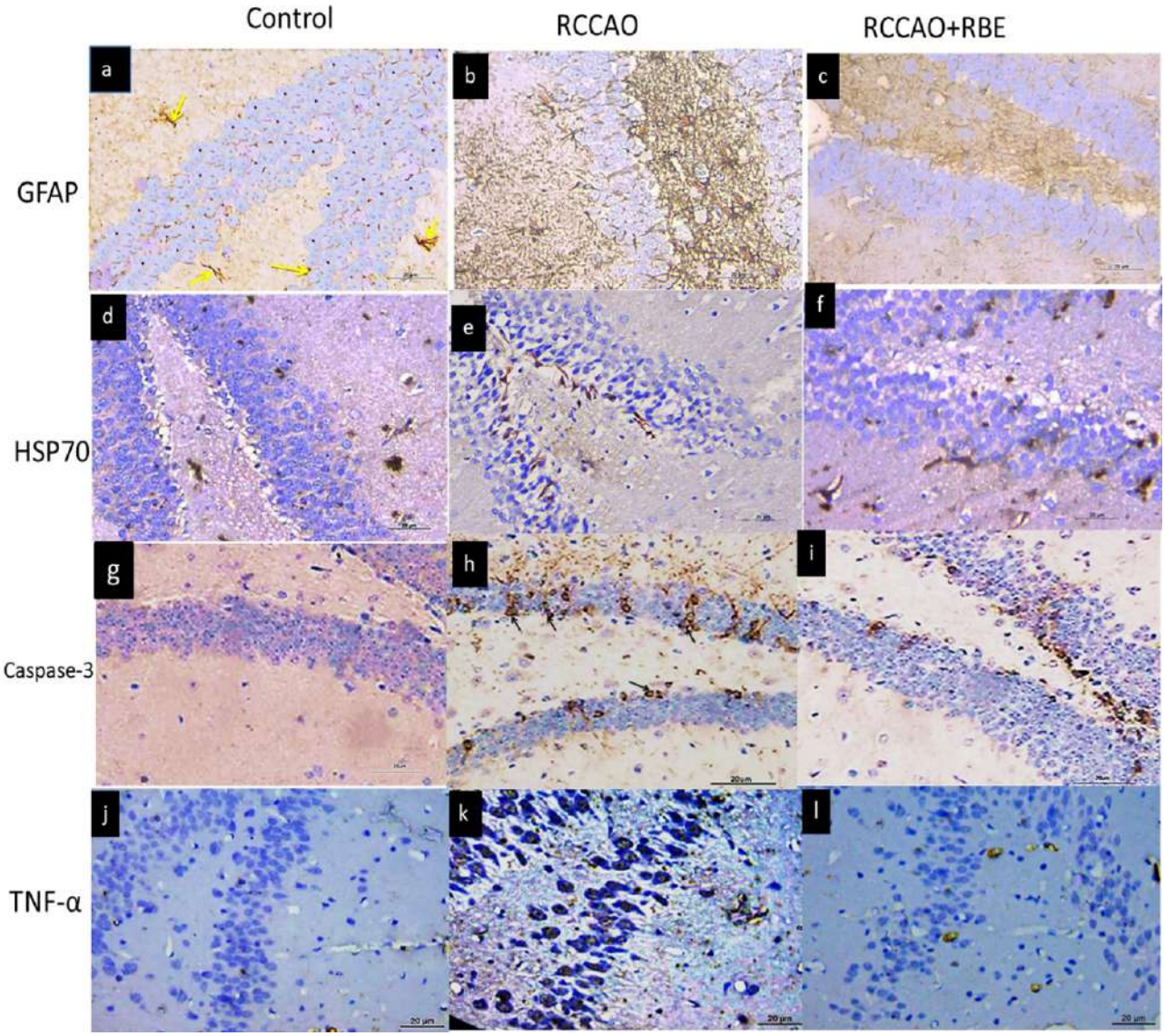

Fig. 3.- Representative micrographs of the different experimental groups showing significant upregulation of the GFAP **(a-c)**, Caspase-3 **(g-i)**, and TNF-α **(j-l)** immunoreaction in the RCCAO group and their downregulation in RCCAO+RBE group. HSP70 **(d-f)** shows significant slight upregulation in the RCCAO group and more upregulation in RCCAO+RBE group. Scale bars a-l = 20 µm, ×400).

et al., 2003) and increases the occurrence of apoptotic cell death in the brain (Chan, 2001; Choi-Kwon et al., 2004).

H&E-stained sections of the RCCAO group of our study reported numerous spindle-shaped cells in the subgranular zone (SGZ). These results were explained by Neuberger et al. (2017), who mentioned that after traumatic brain injury the hippocampal dentate gyrus acts as a focus of enhanced neurogenesis and excitability. This increment of neurogenesis has been proposed to help repair the injured granular cells.

Nissl granules in toluidine blue staining were used as a morphological indicator of neuronal survival. This study revealed a significant reduction in toluidine blue color intensity in the dentate gyrus. The same results were obtained by Guo et al. (2016).

We used immunohistochemistry to detect expressions of HSP-70, GFAP, Caspase-3, and TNF-alpha. Caspase-3 assay was used in order to detect the neuronal apoptosis, which was upregulated in the dentate gyrus of the RCCAO group. This follows Liu et al. (2013), who explained that ischemia/reperfusion injury enhanced caspase-3 activity or induced its expression, promoting neuron apoptosis.

The number of active GFAP-positive cells significantly increased in the dentate gyrus of the RCCAO group, and this agrees with Erfani et al. (2019), who stated that cerebral ischemia causes neuroinflammation intermediary activity of astrocytes in the hippocampus. These findings were confirmed by Turturici et al. (2011), who stated that astrocytic response or gliosis was a recognized response to an insult, which is typically characterized by an increase of polymerized GFAP. They added that increase GFAP expression was the major hallmark of the astroglial response to brain injury.

HSP-70 and TNF-α immunohistochemistry showed a statistically significant increased expression in the dentate gyrus of the RCCAO group. The release of TNF-α inflammatory molecules with other substances aggravates cell injury during ischemia (Gilmore, 2006). This agrees with previous studies in rat models. HSP-70 is a 70-kDa heat-shock protein stress-induced molecule that up-regulated in response to various types of CNS injuries, including stroke, trauma, or neurodegenerative disorders. Marked increase of HSP-70 in brain tissue of ischemic group induced by oxidative stress (Yasuda et al., 2011; Robinson et al., 2005).

Oxidative stress plays a major role in cerebral ischemic-reperfusion injury (Granger and Kvietys, 2015). In this study, oxidative stress in RCCAO rats, as indicated by significantly higher MDA and NO and significantly lower SOD in the RCCAO group than in the Control group, coincides with a previous study (Guven et al., 2015). MDA is the ultimate product and is one of the most sensitive indicators of lipid peroxidation (Gutteridge, 1995). Increased lipid peroxidation may result in the release of mitochondrial matrix enzymes and lysosomal proteolytic enzymes in the cytoplasm. So, intracellular proteolysis and cellular destruction increase (White et al., 1993). As a result, the immune system including SOD as an antioxidant enzyme involves a wide range of cellular activity to protect neuronal cells from ROS-induced cell death (Bosca and Hortelano, 1999). SOD detoxifies O_2 to H_2O_2, which is then scavenged by peroxisomal catalase. In brief, H_2O_2 cannot be easily scavenged during ischemia

Table 2. Biochemical results.

Group Parameter	Control Mean±SD	RCCAO Mean±SD	RCCAO+RBE Mean±SD
Tissue MDA UM. 100 mg	2.47±0.35	6.69±0.23***	4.02±0.03#
Tissue NO Mm. 100 mg	10.60±0.92	19.85±1.21***	15.34±1.32#
Tissue SOD U/100 mg	2.65±0.32	0.97±0.09 ***	1.62±.22#

RCCAO; right common carotid artery occlusion, RCCAO+RBE; right common carotid artery occlusion + Red beetroot extract, MDA: Malondialdehyde, NO: Nitric oxide, SOD: *Superoxide dismutase.* ***p<0.001 comparison between RCCAO and control, # P < 0.05 comparison between RCCAO+RBE and RCCAO.

due to the lower activity of SOD (Bosca and Hortelano, 1999). NO generated from neuronal NO synthase nitrosylates protein, which leads to cell dysfunction (Liu et al., 2008).

H&E-stained sections of the dentate gyrus of group III revealed that some of the granule cells regain their normal appearance (with rounded vesicular nuclei), while other cells had small dark nuclei. Vacuolation of the neuropil is still present in a small dose. These changes were also obtained by Bailey et al. (2009). Consuming beetroot juice as part of a high nitrate diet can improve the blood flow and oxygenation to the brain areas, so mediating inflammatory response and a less expressed and less overproduction of reactive oxygen species (ROS) protein, inflammation, and oxidative stress. This leads to less neuronal injury and decreases the occurrence of apoptotic cell death in the brain.

Less spindle-shaped cells were detected in SGZ. The same results obtained by Presley et al. (2003) added that red beetroot augmented neurogenesis in the ischemic brain and improved functional outcomes (Burdette et al., 2011). It attenuates neuroblast apoptosis and can enhance dentate gyrus neurogenesis by augmenting the survival and proliferation of the hippocampal neural progenitor cells (Toledano et al.,2012; Rockenstein et al., 2007). Thus, it plays a major role in promoting neurogenesis and gliogenesis (Nixdorf-Bergewiler et al.,1994).

In this study, a significant increase in toluidine blue color intensity in dentate gyrus was detected. The same results were obtained by Guo et al. (2016).

In immunohistochemistry of this group to detect Caspase-3 assay was downregulated in the dentate gyrus of the RCCAO+RBE group.

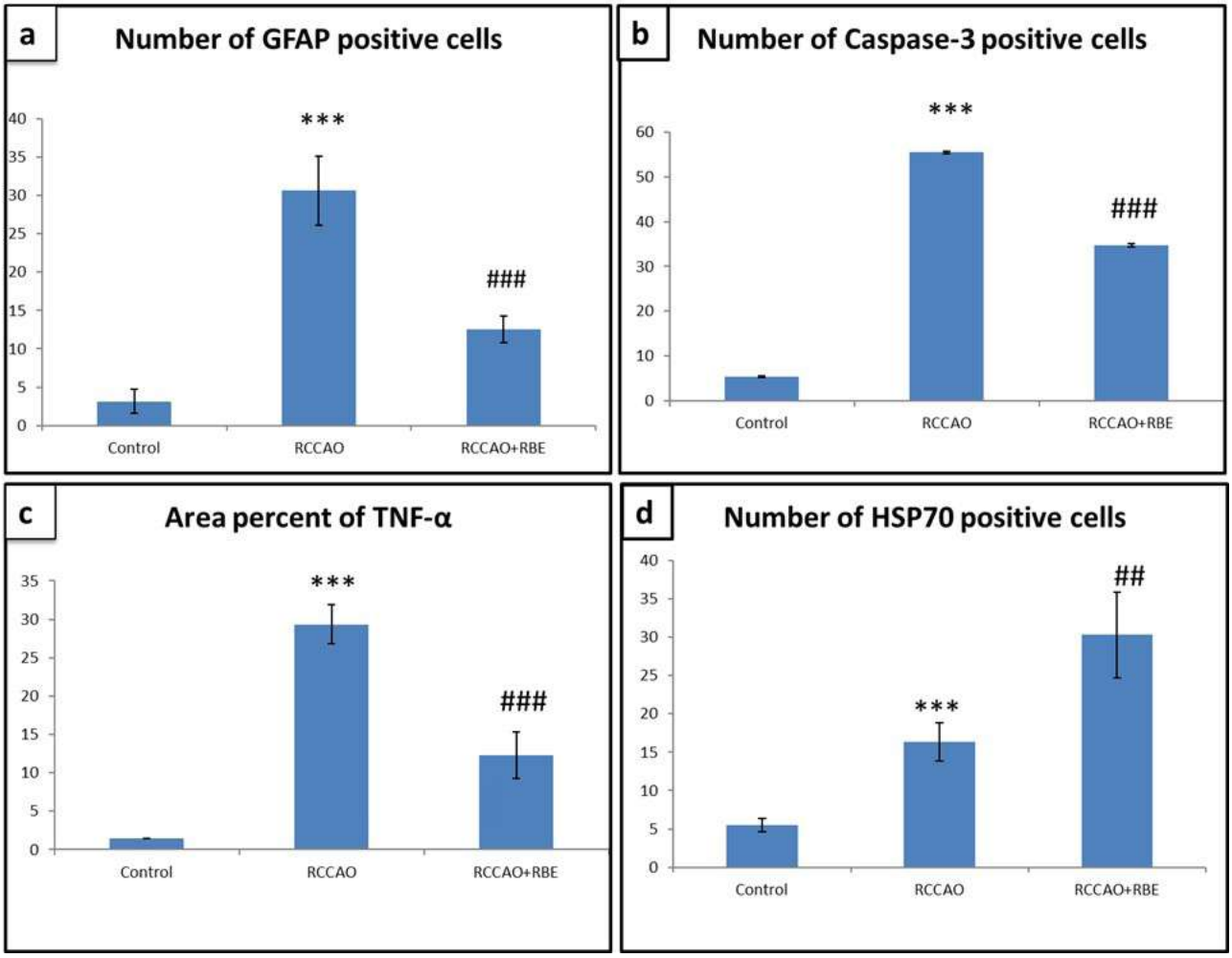

Fig. 4.- Histogram represent **(a)** Number of GFAP positive cells, **(b)** Number of Caspase-3 positive cells, **(c)** Area percent of TNF alpha immunoreaction and **(d)** Number of HSP 70 positive cells, *** $p < 0.001$ comparison between RCCAO and control groups; ## $P < 0.01$, ### $P < 0.001$ comparison between RCCAO+RBE and RCCAO groups.

This follows Liu et al. (2013), who explained that red beetroot contains nitrate, which makes vasodilatation, and so increases blood flow and inhibits ischemia/reperfusion injury by less expression of caspase-3.

TNF-α showed a significant decrease. Jin et al. (2013) stated that choline in beetroot helps to maintain the structure of cellular membranes, aids in the transmission of nerve impulses, assists in the absorption of fat, thus reducing inflammation.

Immunohistochemical results for GFAP-stained sections of group III revealed positive expression of GFAP in astrocytes. The same results were obtained by Yao et al. (2014), who stated that beetroot has a neurotrophic effect that might reduce the neurodegenerative alterations in Alzheimer's disease (AD). On the other hand, Jin et al. (2013) stated that beetroot did not significantly increase the number of GFAP positive cells, but beetroot in a dose-dependently way enhances neurogenesis.

However, HSP-70 showed significantly more increase than the RCCAO group. The same results obtained by Robinson et al. (2005) concluded that HSP-70 may have anti-inflammatory, cytoprotective, and anti-apoptotic actions. Beetroot has an anti-inflammatory effect (Gilchrist et al., 2014).

Also, the same group showed a statistically significant decrease in MDA and NO and a significant increase in antioxidant SOD. The same findings were founded by Fulford et al. (2013). Gilchrist et al. (2014) suggest adaptive mechanisms to fight against neurodegeneration and added that beets contain an antioxidant known as alpha-lipoic acid, which may help prevention of oxidative stress-induced changes.

CONCLUSION

The results of this study confirm the neurodegenerative effects of cerebral ischemia-reperfusion on the rat dentate gyrus, add new information to the known neuroprotective effects of beetroot extract, and provide new insight into the possible use of beetroot extract to enhance these effects after ischemia.

REFERENCES

ABD-ALLAH F, MOUSTAFA RR (2014) Burden of stroke in Egypt: current status and opportunities. *Int J Stroke*, 9(8): 1105-1108.

BAILEY SJ, WINYARD P, VANHATALO A, BLACKWELL JR, DIMENNA FJ, WILKERSON DP, TARR J, BENJAMIN N, JONES AM (2009) Dietary nitrate supplementation reduces the O_2 cost of low-intensity exercise and enhances tolerance to high-intensity exercise in humans. *J Appl Physiol*, 107(4): 1144-1155.

BENAMER HT, GROSSET D (2009) Stroke in Arab countries: a systematic literature review. *J Neurol Sci*, 284(1-2): 18-23.

BOSCA L, HORTELANO S (1999) Mechanisms of nitric oxide-dependent apoptosis: involvement of mitochondrial mediators. *Cell Signal*, 11: 239-244.

CHAN PH (2001) Reactive oxygen radicals in signaling and damage in the ischemic brain. *J Cereb Blood Flow Metab*, 21: 2-14.

CHOI-KWON S, PARK KA, LEE HJ, PARK MS, LEE JH, JEON, SE, CHOE MA, PARK KC (2004) Temporal changes in cerebral antioxidant enzyme activities after ischemia and reperfusion in a rat focal brain ischemia model: effect of dietary fish oil. *Dev Brain Res*, 152(1): 11-18.

CLIFFORD T, HOWATSON G, WEST DJ, STEVENSON EJ (2015) The potential benefits of red beetroot supplementation in health and disease. *Nutrients*, 7(4): 2801-2822.

EL GAMAL AA, ALSAID MS, RAISH M, AL-SOHAIBANI M, AL-MASSARANI SM, AJAZ A, HEFNAWY M, AL-YAHYA M, OMER A, BASOUDAN OA, RAFATULLAH S (2014) Beetroot (*Beta vulgaris L.*) extract ameliorates gentamicin-induced nephrotoxicity associated oxidative stress, inflammation, and apoptosis in rodent model. *Mediators Inflamm*, 22(1): 938-952.

ERFANI S, MOGHIMI A, ABOUTALEB N, KHAKSARI M (2019) Protective effects of nucleobinding-2 after cerebral ischemia via modulating Bcl-2/Bax ratio and reducing glial fibrillary acid protein expression. *Basic Clin Neurosci*, 10(5): 451-460.

EVENSON KR, ROSAMOND WD, CAI J, TOOLE JF, HUTCHINSON RG, SHAHAR E, FOLSOM AR (1999) Physical activity and ischemic stroke risk. The atherosclerosis risk in communities study. *Stroke*, 30(7): 1333-1339.

FULFORD J, WINYARD PG, VANHATALO A, BAILEY SJ, BLACKWELL JR, JONES AM (2013) Influence of dietary nitrate supplementation on human skeletal muscle metabolism and force production during maximum voluntary contractions. *Pflügers Arch*, 465(4): 517-528.

GILCHRIST M, WINYARD PG, FULFORD J, ANNING C, SHORE AC, BENJAMIN N (2014) Dietary nitrate supplementation improves reaction time in type 2 diabetes: development and application of a novel nitrate-depleted beetroot juice placebo. *Nitric Oxide*, 40: 67-74.

GILMORE TD (2006) Introduction to NF-κB: players, pathways, perspectives. *Oncogene*, 25(51): 6680-6684.

GOLDSTEIN LB (2007): Acute ischemic stroke treatment in 2007. *Circulation*, 116: 1504-1514.

GRANGER DN, KVIETYS PR (2015) Reperfusion injury and reactive oxygen species: The evolution of a concept. *Redox Biol*, 6: 524-551.

GUO K, YIN G, ZI X, YAN W (2016) Activation of STAT3 is involved in neuronal apoptosis in focal cerebral ischemia/reperfusion rats via Bcl2/Fas pathway. *Int J Clin Exp Pathol*, 9(2): 2660-2669.

GUTTERIDGE JM (1995) Lipid peroxidation and antioxidants as biomarkers of tissue damage. *Clin Chem*, 41: 1819-1828.

GUVEN M, ARAS AB, AKMAN T (2015) Neuroprotective effect of p-coumaric acid in rat model of embolic cerebral ischemia. *Iran J Basic Med Sci*, 18(4): 356-363.

IRMAK MK, FADILLIOGLU E, SOGUT S, ERDOQAN H, GULEC M, OZER M (2003) Effects of caffeic acid phenethyl ester and alpha-tocopherol on reperfusion injury in rat brain. *Cell Biochem Funct*, 21: 283-289.

JIN R, LIU L, ZHANG S, NANDA A, LI G (2013) Role of inflammation and its mediators in acute ischemic stroke. *J Cardiovasc Transl Res*, 6(5): 834-851.

KIM AS, JOHNSTON SC (2011) Global variation in the relative burden of stroke and ischemic heart disease. *Circulation*, 124(3): 314-323.

LEE H, NAM YS, LEE KM (2015) Development-assistance strategies for stroke in low- and middle-income countries. *J Korean Med Sci*, Suppl 2: S139-142.

LIU G, WANG T, WANG T, SONG J, ZHOU Z (2013) Effects of apoptosis-related proteins caspase-3, Bax and Bcl-2 on cerebral ischemia rats. *Biomed Rep*, 1(6): 861-867.

LIU R, GAO M, YANG ZH, DU GH (2008) Pinocembrin protects rat brain against oxidation and apoptosis induced by ischemia–reperfusion both in vivo and in vitro. *Brain Res*, 1216: 104-115.

LOZANO R, NAGHAVI M, FOREMAN K, LIM S, SHIBUYA K, ABOYANS V, ABRAHAM J, ADAIR T, AGGARWAL R, AHN SY, ALVARADO M, ANDERSON HR, ANDERSON LM, ANDREWS KG, ATKINSON C, BADDOUR LM, BARKER-COLLO S, BARTELS DH, BELL ML, BENJAMIN EJ, BENNETT D (2013) Global and regional mortality from 235 causes of death for 20 age groups in 1990 and 2010: a systematic analysis for the Global Burden of Disease Study 2010. *Lancet*, 380(9859): 2095-2128.

MENTARI IA, NAUFALINA R, RAHMADI M, KHOTIB J (2018) Development ischemic stroke model by right unilateral common carotid artery occlusion (RUCCAO) method. *Folia Medica Indonesiana*, 54(3): 200.

MOZAFFARIAN D, BENJAMIN EJ, GO AS, ARNETT DK, BLAHA MJ, CUSHMAN M, DAS SR, DE FERRANTI S, DESPRÉS JP, FULLERTON HJ, HOWARD VJ, HUFFMAN MD, ISASI CR, JIMÉNEZ MC, JUDD SE, KISSELA BM, LICHTMAN JH, LISABETH LD, LIU S, MACKEY RH, MAGID DJ, MCGUIRE DK, MOHLER ER 3RD, MOY CS, MUNTNER P, MUSSOLINO ME, NASIR K, NEUMAR RW, NICHOL G, PALANIAPPAN L, PANDEY DK, REEVES MJ, RODRIGUEZ CJ, ROSAMOND W, SORLIE PD, STEIN J, TOWFIGHI A, TURAN TN, VIRANI SS, WOO D, YEH RW, TURNER MB, et al. (2016) American Heart Association Statistics Committee: A report from the American Heart Association. *Circulation*, 133(4): 447-454.

NEUBERGER EJ, SWIETEK B, CORRUBIA L, PRASANNA A, SANTHAKUMAR V (2017) Enhanced dentate neurogenesis after brain injury undermines long-term neurogenic potential and promotes seizure susceptibility. *Stem Cell Reports*, 9(3): 972-984.

NIXDORF-BERGEWILER BE, ALBRECHT D, HEINEMANN U (1994) Developmental changes in the number, size and orientation of GFAP-positive cells in CA1 region of rat hippocampus. *Glia*, 12: 180-195.

PANELKEVIN M, MULLANE R, KRAEMER BS (1985) Myeloperoxidase activity as a quantitative assessment of neutrophil infiltration into ischemie myocardium. *J Pharmacol Meth*, 14(3): 157-167.

PRESLEY TD, MORGAN AR, BECHTOLD E, CLODFELTER W, DOVE RW, JENNINGS JM, KRAFT RA, KING SB, LAURIENTI PJ, REJESKI WJ, BURDETTE JH, KIM-SHAPIRO DB, MILLER GD (2011) Acute effect of a high nitrate diet on brain perfusion in older adults. *Nitric Oxide*, 24(1): 34-42.

ROBINSON MB, TIDWELL JL, GOULD T, TAYLOR AR, NEWBERN JM, GRAVES J, MILLIGAN CE (2005) Extracellular heat shock protein 70: a critical component for motor neuron survival. *J Neurosci*, 25(42): 9735-9745.

TATEBAYASHI Y, LEE MH, LI L, IQBAL K, GRUNDKE-IQBAL I (2003) The dentate gyrus neurogenesis: a therapeutic target for Alzheimer's disease. *Acta Neuropathol*, 105(3): 225-232.

TOLEDANO A, ALVAREZ MI, MONLEÓN E, TOLEDANO-DÍAZ A, BADIOLA JJ, MONZÓN M (2012) Changes induced by natural scrapie in the calretinin-immunopositive cells and fibres of the sheep cerebellar cortex. *Cerebellum*, 11(2): 593-604.

TURTURICI G, SCONZO G, GERACI F (2011) Hsp70 and its molecular role in nervous system diseases. *Biochem Res Int*, 2011: 618127.

VIRANI SS, ALONSO A, BENJAMIN EJ, BITTENCOURT MS, CALLAWAY CW, CARSON AP, CHAMBERLAIN AM, CHANG AR, CHENG S, DELLING FN, DJOUSSE L, ELKIND MSV, FERGUSON JF, FORNAGE M, KHAN SS, KISSELA BM, KNUTSON KL, KWAN TW, LACKLAND DT, LEWIS TT, LICHTMAN JH, LONGENECKER CT, LOOP MS, LUTSEY PL, MARTIN SS, MATSUSHITA K, MORAN AE, MUSSOLINO ME, PERAK AM, ROSAMOND WD, ROTH GA, SAMPSON UKA, SATOU GM, SCHROEDER EB, SHAH SH, SHAY CM, SPARTANO NL, STOKES A, TIRSCHWELL DL, VANWAGNER LB, TSAO CW, et al. (2020) American Heart Association Council on Epidemiology and Prevention Statistics Committee and Stroke Statistics Subcommittee. Heart Disease and Stroke Statistics-2020 update: A report from the American Heart Association. *Circulation*, 141(9): e139-e596.

WHITE BC, GROSSMAN LI, KRAUSE GS (1993) Brain injury by global ischemia and reperfusion: a theoretical perspective on membrane damage and repair. *Neurology*, 43: 1656-1665.

YAO Y, CHEN ZL, NORRIS EH, STRICKLAND S (2014) Astrocytic laminin regulates pericyte differentiation and maintains blood brain barrier integrity. *Nat Commun*, 5: 3413.

YASUDA Y, SHIMODA T, UNO K, TATEISHI N, FURUYA S, TSUCHIHASHI Y, FUJITA S (2011) Temporal and sequential changes of glial cells and cytokine expression during neuronal degeneration after transient global ischemia in rats. *J Neuroinflamm*, 8(1): 70.

Right-sided aortic arch and an aberrant left subclavian artery: a case report

Alexander Mrochek[1], Sergey Kabak[2], Hanna Model[3], Yuliya Melnichenko[2], Tamara Kalenchic[4], Nataliia Didenko[5]

[1] Republican Scientific and Practical Centre "Cardiology", Cardiologist of the Ministry of Health of the Republic of Belarus, Academician of National Academy of Science of Belarus

[2] Human Morphology Department, Belarusian State Medical University, Minsk, Belarus

[3] Radiologist of the Republican Scientific and Practical Centre "Cardiology", Minsk, Belarus

[4] Medical Rehabilitation and Physiotherapy Department, Belarusian State Medical University, Minsk, Belarus

[5] Center of Diagnostic and Rehabilitation of Gazprom transgaz, Moskow, Russian Federation

SUMMARY

A right-sided aortic arch is a rare congenital defect of the aorta. A 56-year-old Caucasian male patient was hospitalized with coronary artery disease (stable angina CCS II, postinfarction cardiosclerosis), stage II hypertension, impaired glucose tolerance and congestive heart failure NYHA class II. Contrast-enhanced ECG-gated multi-slice computed tomography was performed on Siemens SOMATOM Force Germany and revealed right-sided aortic arch, aberrant left subclavian artery with Kommerell's diverticulum and kinking of the thoracic aorta. This case is an example of the great advantages of knowing human anatomy and embryology in clinical practice. Modern diagnostic modalities give an accurate information on congenital variants and anomalies of the aortic arch and its branch that is vital for vascular surgery in the thorax, head and neck region.

Key words: Aorta – Aberrant left subclavian artery – Congenital heart disease – Kommerell's diverticulum – Right-sided aortic arch – Multi-slice computed tomography

INTRODUCTION

A left- or right-sided aortic arch (RSAA) refers to the position of the aortic arch in relation to the trachea (Miranda et al., 2014). The normal left aortic arch lies on the left of the trachea and courses over the left main bronchus. A RSAA refers to an aortic arch that courses and descends to the right side of the trachea.

A right-sided aortic arch is a rare congenital defect of the aorta and occurs in 0.05% to 0.1% of radiology series and in 0.04%-0.1% of autopsy series (Arazinska et al., 2017; Priya et al., 2018; Popieluszko et al., 2018). The real incidence of RSAA in the general population is unknown, but a rate of 1/1000 has been suggested by Achiron et al. (2002). The recent progress in perinatal medicine and imaging techniques had facilitated the prenatal diagnosis of this cardiovascular anomaly (Muraoka et al., 2018). RSAA was detected in 0.6% of all fetal

Corresponding author:
Yuliya Michailovna Melnichenko. Human Morphology Department, Belarusian State Medical University, 220116, Dzerzhinskogo Avenue 83, Minsk, Belarus. Phone: +375291637867. E-mail: mjm1980@yandex.ru - Orcid.org/0000-0002-8742-6973.

Submitted: July 14, 2020. **Accepted:** February 21, 2021
Not final proof's revision by the authors

cardiac examinations and to 5.0% of all cardiac abnormalities (Miranda et al., 2014). Abnormalities of aortic arch orientation are often associated with a variety of congenital heart defects (Tetralogy of Fallot and truncus arteriosus), as well as chromosomal abnormalities, such as DiGeorge syndrome (22q11 deletion) (Law and Mohan, 2019).

There are three main subtypes of RSAA according to Edwards' model: type I – RSAA with mirror image branching; type II – RSAA with aberrant left subclavian artery (ALSA); and type III – RSAA with isolated subclavian artery. The most common subtype is type II, when the right common artery arises as the first branch and is followed by the right subclavian artery and the left common carotid artery while the left subclavian artery is the last branch and takes a retroesophageal course to reach on the left side (García-Guereta et al., 2016; Priya et al., 2018. The aberrant left subclavian artery has a variable descending: posterior to the esophagus in 80% of cases, anterior to the trachea in 5% of cases and just between the trachea and esophagus in 15% of cases (Tong et al., 2015). Edwards' type II reveals cardiac anomalies only in 5-10% of cases, which are commonly diagnosed in newborns and young children and rarely become symptomatic in adults (Ebner et al., 2013). About half of the patients with right-sided aortic arch have an aberrant left subclavian artery, which may arise either directly from the aorta or from the Kommerell's diverticulum (Tong et al., 2015). The complete vascular ring is formed by the segment of the ascending aorta anteriorly, Kommerell's diverticulum posteriorly and the ligamentum arteriosum coursing on the left side of the trachea. Any symptoms, which result from an aberrant left subclavian artery, are associated with compression of the esophagus or trachea and are most likely to occur if its origin is dilated (Kakaria et al., 2008; Yang et al., 2009).

In this article, we report an asymptomatic patient with right-sided aortic arch in whom an aneurysm of the aberrant left subclavian artery was detected.

CASE REPORT

A 56-year-old Caucasian male patient was hospitalized in the Belarusian State Institution «Republican Scientific and Practical Centre «Cardiology» in 2018 for typical angina combined with shortness of breath upon walking about 1000 m and climbing stairs to the 4th floor. He had a history of an acute myocardial infarction in 2017. The patient provided the informed consent regarding radiological images, clinical assessment and publication of patient's data.

He was diagnosed with chronic coronary artery disease (stable angina CCS II, postinfarction cardiosclerosis) based on typical clinical presentation, hypertension stage III, impaired glucose tolerance and congestive heart failure NYHA class II. Contrast-enhanced ECG-gated multi-slice computed tomography, performed on Siemens SOMATOM Force (Germany), revealed:

The right-sided aortic arch (Fig. 1) crossing the midline at the level of the Th4-Th5 vertebral bodies, following a retroesophageal path and continuing to the descending part of the aorta, which was situated on the left side of the vertebral column.

Kommerell's diverticulum (Fig. 1), a bulbous formation at the point of origin of the aberrant left subclavian artery with a diameter of 36 mm.

Kinking of the thoracic aorta at the level of the arch (Fig. 1). The diameter of the aorta fell within the normal range: 26 mm at the level of the valve's annulus; 36 mm at the level of the aortic sinuses; 25 mm at the level of the sinotubular junction and proximal ascending aorta was measured at 27 mm. The diameter of the thoracic region of the descending part of the aorta was expanded to 49 mm.

The branches of the aortic arch – the right subclavian artery, the right and left common carotid arteries – did not show any stenosis. The pulmonary trunk was not expanded. Our patient did not have any cardiac and vascular congenital abnormalities associated with RAA and aberrant LSCA.

COMMENTS

The aberrant right subclavian artery accounts for 0.5-1.8% of the population as the most frequently encountered aortic arch anomaly

(Polguj et al., 2013; Naqvi et al., 2017), while right-sided aortic arch and an aberrant origin of the left subclavian artery with Kommerell's diverticulum is a rare congenital anatomical condition most often observed in adults (Silveira et al., 2019). In the current report, we presented a classic case of this malformation diagnosed accidentally in which the aberrant left subclavian artery arises from the retroesophageal diverticulum located behind the esophagus. The complete vascular ring encircling of trachea and esophagus was not formed, and therefore there were no clinical signs of esophageal compression. The approach to asymptomatic patients with vascular ring

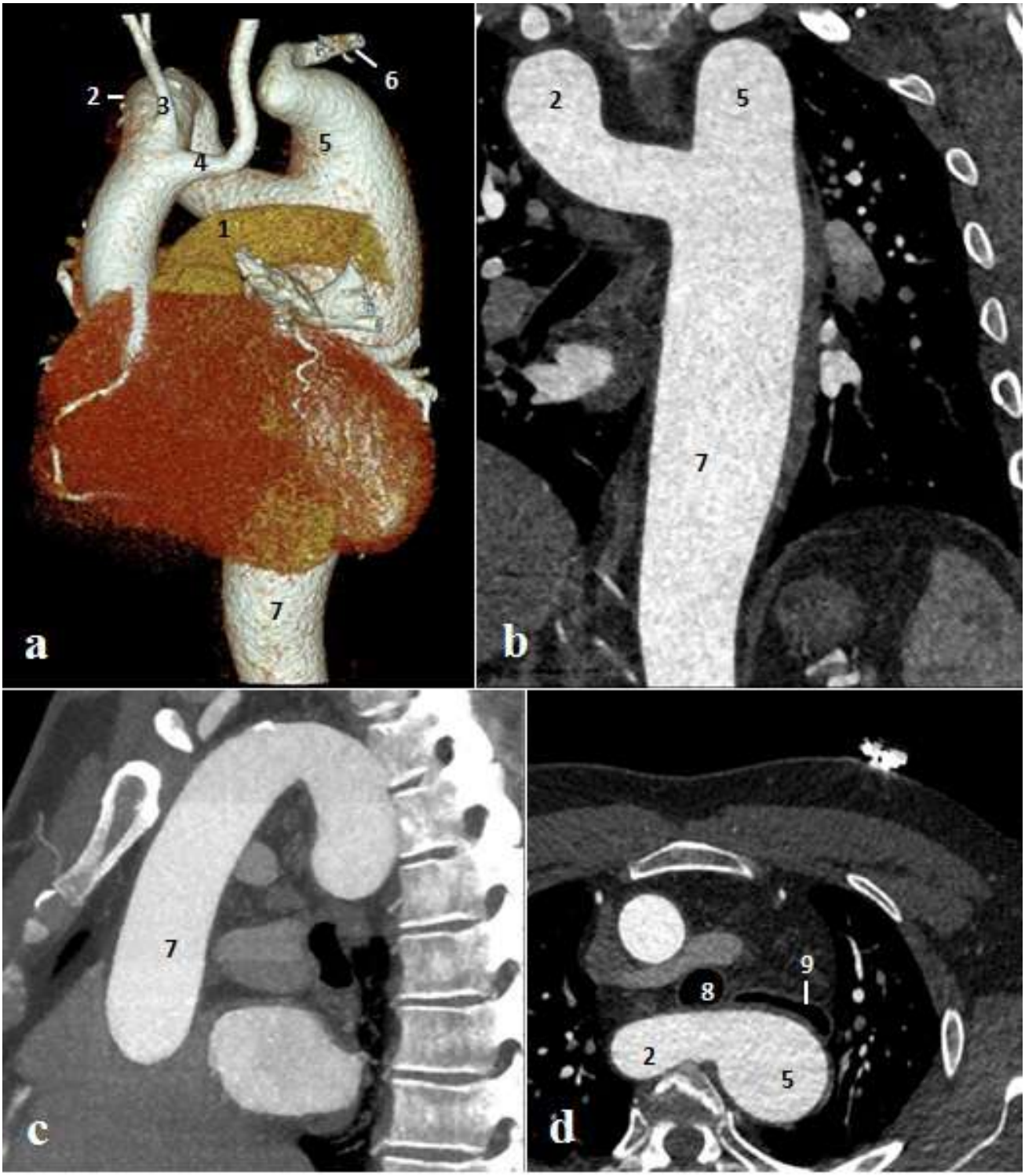

Fig. 1.- Right-sided aorta and its branches: **a** – CTA VRT image, front view; **b** – CTA MIP image, coronal section; **c** – CTA MIP image, sagittal section; **d** – CTA MIP image, axial section. 1. Pulmonary trunk. 2. Right-side aortic arch. 3. Brachiocephalic trunk. 4. Left common carotid artery. 5. Kommerell's diverticulum. 6. Aberrant left subclavian artery. 7. Descending thoracic aorta. 8. Trachea. 9. Esophagus.

(VR) is controversial because this condition is usually diagnosed during pregnancy and affected individuals can remain asymptomatic for a long period of time (García-Guereta et al., 2016). Most centers perform some type of postnatal confirmatory tests of the VR, particularly echocardiography, but due to the limitations of echocardiography magnetic resonance imaging has been proposed.

Aneurysmal diverticulum itself can cause the compression of the esophagus or may rupture spontaneously (Priya et al., 2018). The diverticulum is usually resected in symptomatic patients and followed by the aortopexy of the arch. Alternatively, after the resection of diverticulum, the left subclavian artery can be re-anastomosed to the left carotid artery.

The embryological origin of the various anomalies of the aortic arch is based on the theory of the hypothetic double aortic arch, which was described by Edwards (Yoo et al., 2003; Hsu et al., 2011). The ascending (ventral) aorta is divided into two aortic arches, which surround each side of the trachea and esophagus and connect to form the descending (dorsal) aorta. A common carotid artery and subclavian artery are derived from each aortic arch. Normally, the regression occurs between the origin of right subclavian artery and descending aorta in the right ascending aorta. Thus, the normal aortic arch is formed. If the interruption presents between the left carotid artery and the left subclavian artery in the left aortic arch, it will form a right-sided aortic arch with the aberrant left subclavian artery. There can be a dilated segment at the proximal part of the ALSA. The proximal part of the aberrant artery carries the blood flow from the ductus arteriosus into the descending aorta; and, therefore, the proximal part of the aberrant artery is as wide as the ductus and descending aorta (Hsu et al., 2011).

This case is a clear example of the helpfulness of the human anatomy and embryology knowledge in clinical practice. Accurate information about congenital variants and anomalies of the aortic arch and its branch obtained with modern diagnostic imaging modalities is vital for vascular surgery in the thorax, head and neck region.

REFERENCES

ACHIRON R, ROTSTEIN Z, HEGGESH J, BRONSHTEIN M, ZIMAND S, LIPITZ S, YAGEL S (2002) Anomalies of the fetal aortic arch: a novel sonographic approach to in-utero diagnosis. *Ultrasound Obstet Gynecol*, 20(6): 553-557.

ARAZIŃSKA A, POLGUJ M, SZYMCZYK K, KACZMARSKA M, TRĘBIŃSKI Ł, STEFAŃCZYK L (2017) Right aortic arch analysis – Anatomical variant or serious vascular defect? *BMC Cardiovasc Disord*, 17: 102.

EBNER L, HUBER A, CHRISTE A (2013) Right aortic arch and Kommerell's diverticulum associated with acute aortic dissection and pericardial tamponade. *Acta Radiol Short Rep*, 2(1): 2047981613476283.

GARCÍA-GUERETA L, GARCÍA-CERRO E, BRET-ZURITA M (2016) Multidetector computed tomography for congenital anomalies of the aortic arch: vascular rings. *Rev Esp Cardiol (Engl Ed)*, 69(7): 681-693.

HSU KC, TSUNG-CHE HSIEH C, CHEN M, TSAI HD (2011) Right aortic arch with aberrant left subclavian artery--prenatal diagnosis and evaluation of postnatal outcomes: Report of three cases. *Taiw J Obstet Gynecol*, 50: 353-358.

KAKARIA AK, SAWHNEY S, JAIN R (2008) Right aortic arch with aberrant left subclavian artery. *Sultan Qaboos Univ Med J*, 8(3): 356-357.

LAW MA, MOHAN J (2019) Right aortic arches. In: StatPearls. StatPearls Publishing, Treasure Island (FL).

MIRANDA JO, CALLAGHAN N, MILLER O, SIMPSON J, SHARLAND G (2014) Right aortic arch diagnosed antenatally: associations and outcome in 98 fetuses. *Heart*, 100 (1): 54-59.

MURAOKA M, NAGATA H, HIRATA Y, UIKE K, TERASHI E,MORIHANA E, OCHIAI M, FUJITA Y, KATO K, YAMAMURA K, OHGA S (2018) High incidence of progressive stenosis in aberrant left subclavian artery with right aortic arch. *Heart Vessels*, 33(3): 309-315.

NAQVI SEH, BEG MH, THINGAM SKS, ALI E (2017) Aberrant right subclavian artery presenting as tracheoesophagial fistula in a 50-year-old lady: Case report of a rare presentation of a common arch anomaly. *Ann Pediatr Cardiol*, 10(2): 190-193.

POLGUJ M, CHRZANOWSKI Ł, KASPRZAK JD, STEFAŃCZYK L, TOPOL M, MAJOS A (2014) The aberrant right subclavian artery (arteria lusoria): the morphological and clinical aspects of one of the most important variations – a systematic study of 141 reports. *Sci World J*, 2014: 292734.

POPIELUSZKO P, HENRY BM, SANNA B, HSIEH WC, SAGANIAK K, PĘKALA PA, WALOCHA JA, TOMASZEWSKI KA (2018) A systematic review and meta-analysis of variations in branching patterns of the adult aortic arch. *J Vasc Surg*, 68(1): 298-306.

PRIYA S, THOMAS R, NAGPAL P, SHARMA A, STEIGNER M (2018) Congenital anomalies of the aortic arch. *Cardiovasc Diagn Ther*, 8(Suppl 1): S26-S44.

SILVEIRA JV, JUNQUEIRA FP, SILVEIRA CG, CONSOLIM-COLOMBO FM (2019) Kommerell diverticulum: right aortic arch with anomalous origin of left subclavian artery and duplicity of right vertebral artery in a 16-year-old girl. *Am J Case Rep*, 20: 228-232.

TONG E, RIZVI T, HAGSPIEL KD (2015) Complex aortic arch anomaly: Right aortic arch with aberrant left subclavian artery, fenestrated proximal right and duplicated proximal left vertebral arteries – CT angiography findings and review of the literature. *Neuroradiol J*, 28(4): 396-403.

YANG MH, WENG ZC, WENG YG, CHANG H-H (2009) A right-sided aortic arch with Kommerell's diverticulum of the aberrant left subclavian artery presenting with syncope. *J Chin Med Assoc*, 72: 275-277.

YOO SJ, MIN JY, LEE YH, ROMAN K, JAEGGI E, SMALLHORN J (2003) Fetal sonographic diagnosis of aortic arch anomalies. *Ultrasound Obstet Gynecol*, 22(5): 535-546.

Case report of an anatomic variation of the buccal nerve (branch of Trigeminal Nerve - V3)

Beatriz C. Ferreira[1], Alexandre R. Freire[1], José A.G. Junqueira[2], Paulo R. Botacin[2], Felippe B. Prado[1], Ana C. Rossi[1]

[1] Department of Biosciences, Anatomy Division, Piracicaba Dental School, University of Campinas, Piracicaba, São Paulo, Brazil
[2] Department Basic Sciences, Araçatuba Dental School, Paulista State University, Araçatuba, São Paulo, Brazil

SUMMARY

One of the branches of the mandibular nerve is the buccal nerve. It is responsible for sensory innervating of the buccal gingiva of the lower teeth and the buccal mucosa of the cheek. The aim of this study was to report a case of a cadaver with an anatomic variation of the buccal nerve (branch of Trigeminal Nerve - V3). During a routine Anatomy class, from the observation of a 43-year-old female cadaver head, a unilateral (left side) communicating branch between the buccal branch of the trigeminal nerve and the inferior alveolar nerve was found. The knowledge of anatomical variations is essential to avoid errors and to give the patient adequate clinical management during specific dental and surgical procedures in each case.

Key words: Anatomic variation – Buccal nerve – Clinical Anatomy – Macroscopic human anatomy

INTRODUCTION

The trigeminal nerve is the fifth pair of cranial nerve (V) and its primary function is to give sensory and especially motor innervation to the masticatory musculature. The mandibular nerve (V3) is the third division of the trigeminal nerve (Standring, 2015). It is the only branch that carries afferent and efferent fibers. Its motor component is responsible for innervating the mandibular muscles, while the sensory component is divided to innervate the lower dental arcade, the buccal mucosa, the temporomandibular joint and the anterior two-thirds of the tongue (Standring, 2015; Huff and Daly, 2018; Ghatak and Ginglen, 2018).

One of the branches of the mandibular nerve is the buccal nerve. It is responsible for sensory innervating of the buccal gingiva of the lower dental arcade and the buccal mucosa of the cheek (Katori et al., 2012; Standring, 2015). After passing between the upper and lower heads of the lateral pterygoid muscle, it descends anteriorly in association with the maxillary artery, the temporalis muscle tendon, which is inserted into the anterior border of the mandibular ramus, and the buccal fat pad to go through the surface of the buccinator muscle (Mérida-Velasco et al., 2001; Takezawa et al., 2018). Katori et al. (2012) reported that the topographical relationship between the

Corresponding author:
Prof. Ana Cláudia Rossi. Department of Biosciences, Anatomy Division, Piracicaba Dental School, University of Campinas, 901 Limeira Avenue, 13414-903 Piracicaba, São Paulo, Brazil. E-mail: rossianac01@gmail.com.

Submitted: August 4, 2020. **Accepted:** February 28, 2021
Not final proof's revision by the authors

buccal nerve and the lateral pterygoid muscle seems to alter during fetal development, due to the delayed development of the upper head, which is much smaller than the lower head in young fetuses. The authors described that the postero-anterior nerve course seemed to be determined by a branch to the temporalis muscle (i.e., the anterior deep temporal nerve).

Descriptions regarding the distribution of the buccal nerve in Anatomy contents usually do not provide precise and detailed information about the plurality of nerve distribution variations between individuals (Takezawa et al., 2018). According to Voirol et al. (2016), the mandibular nerve, including its branches, present the most considerable anatomic variations when compared to the other cranial nerves. The buccal nerve, for example, may innervate the lower molar by reaching the alveolar bone through the retromolar foramen. It can be the reason of a failure in local anesthesia in dental procedures when doing the inferior alveolar nerve block (Ghatak and Ginglen, 2018).

The aim of this study was to report a case of a cadaver with an anatomic variation of the buccal nerve (branch of Trigeminal Nerve - V3).

CASE REPORT

During a routine Anatomy class, from the observation of a 43-years-old female cadaver head fixed in 10% formalin, in the Anatomy Laboratory of the Araçatuba Dental School, Paulista State University - UNESP of Araçatuba, SP, Brazil, a unilateral (left side) communicating branch between the buccal branch of the trigeminal nerve and the inferior alveolar nerve was found.

When the buccal nerve passes laterally to the heads of the lateral pterygoid muscle, a communicating branch was observed downward to the inferior alveolar nerve (Fig. 1). Then, this communicating branch penetrates the mandibular canal through the mandibular foramen (the mandibular ramus was removed to show the nerves) (Fig. 2). It can be observed that the inferior alveolar nerve has a loop (a branch that leaves the main trunk of the nerve and then returns to it). The origin of the loop is at the same level of the buccal nerve is passing between the superior and inferior heads of the lateral pterygoid muscle. Then, the communicating branch of the buccal nerve joins with this loop and both are incorporated into the main trunk of the inferior alveolar nerve inside the mandibular canal (Fig. 3).

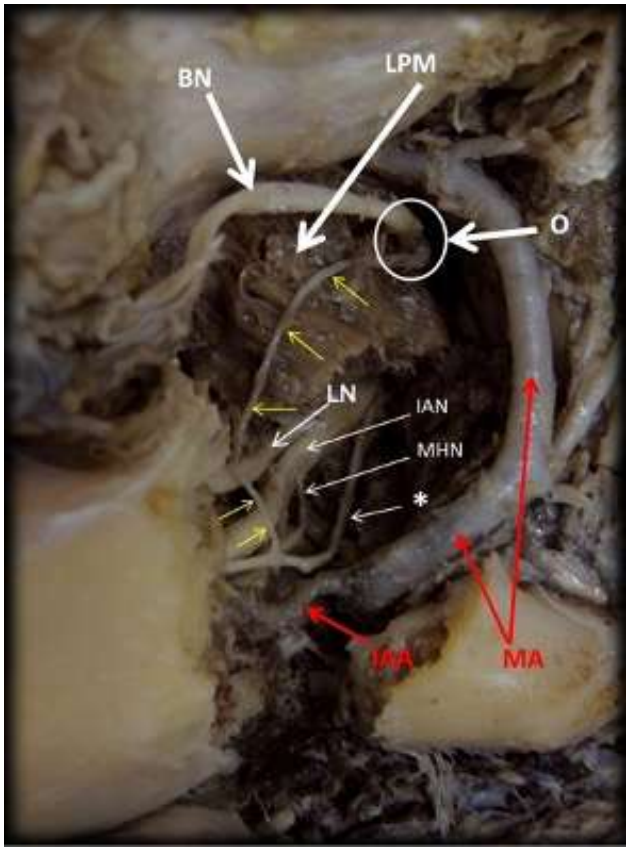

Fig. 1.- Lateral view of the mandible (left side), whose ramus was removed to expose the nerves. The communicating buccal nerve branch presented an origin (O) directly from the buccal nerve (BN), with a descendent way to join with an inferior alveolar nerve loop (*). BM: Buccinator muscle. LPM: Lateral Pterygoid Muscle. IAN: Inferior Alveolar Nerve. MHN: Milo-Hyoid Nerve. IAA: Inferior Alveolar Artery. MA: Maxillary Artery. LN: Lingual Nerve. Yellow arrows indicate the communicating buccal nerve branch.

DISCUSSION

Approximately 20% of the population has anatomical variations of the trigeminal nerve, and all of these are described to be related to the mandibular nerve and its branches (Ghatak and Ginglen, 2018). Comparing all the cranial nerves, the mandibular nerve, including its branches, present the most substantial anatomic variations (Voirol et al., 2016).

According to Yang et al. in 2014, when studying Korean cadavers, in all cases, the buccal nerve formed anastomosis with the lateral superior labial nerve (a branch of the infraorbital

nerve) in the angular area. Consequently, the supplementary sensory component by the buccal nerve may mask a paresthesia in the angular area originated by damage to the infraorbital nerve. Thus, a differential diagnosis may be required (Yang et al., 2014).

Furthermore, the buccal nerve was related to form anastomosis with some branches of the mental nerve, supplying sensation to the skin and the mucosa over the lateral region of the lower lip (Won et al., 2014).

The retromolar foramen is a small external orifice of the retromolar canal, located in the retromolar region of the mandible and is thought to occur in a significant percentage of the population. The accessory innervation can be the reason why failures in anesthesia techniques by regional block of the inferior alveolar and buccal nerves occur (DeSantis and Liebow, 1996; Rossi et al., 2012; Voirol et al., 2016). According to Ossenberg (1987), they may be possible due to the existence of accessory innervation to the

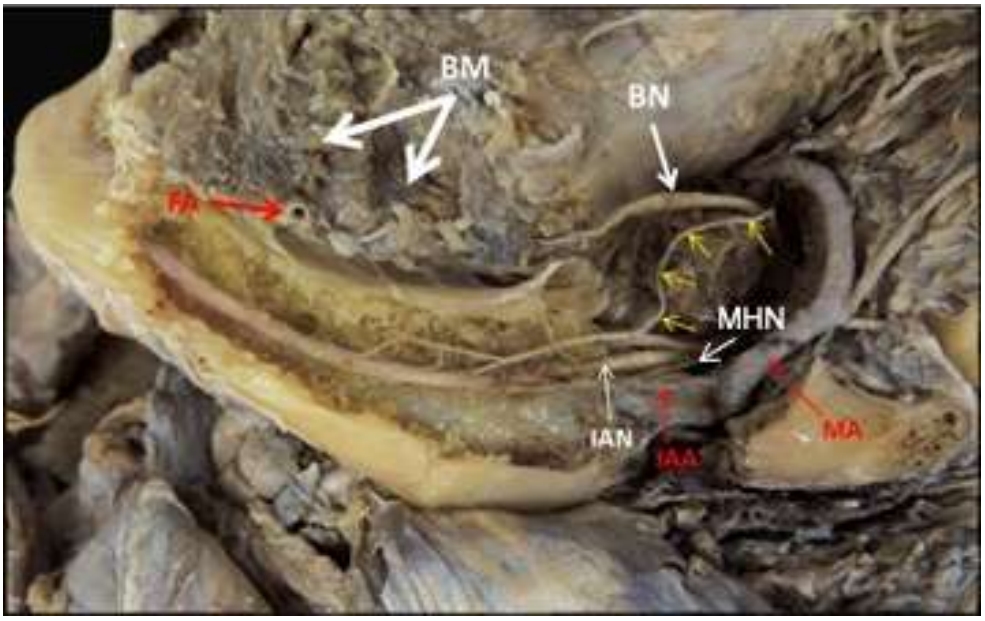

Fig. 2.- Lateral view of the mandible (left side) after removing the cortical bone to expose the internal region of the mandibular body and the branch formed by the communication of the buccal nerve (yellow arrows) and the inferior alveolar nerve loop. MA: Maxillary Artery. FA: Facial Artery. IAA: Inferior Alveolar Artery. BN: Buccal Nerve. IAN: Inferior Alveolar Nerve. MHN: Milo-Hyoid Nerve.

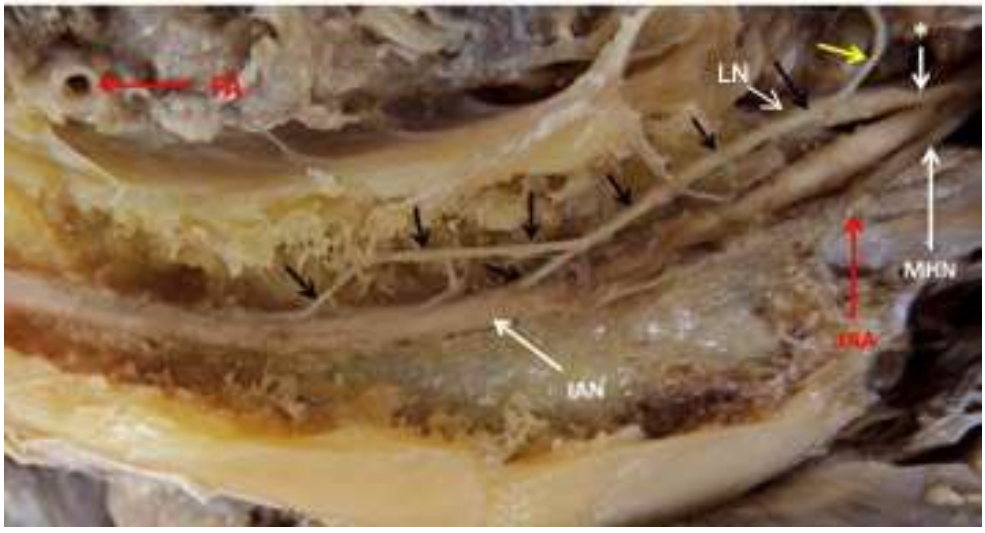

Fig. 3.- Close internal view of the mandibular body (left side) after removing the cortical bone. The figure shows the branch (black arrows) formed by the communication of the buccal nerve (yellow arrow) and inferior alveolar loop (*), which join the inferior alveolar nerve (IAN) by two sites. FA: Facial Artery. IAA: Inferior Alveolar Artery. MHN: Milo-Hyoid Nerve. LN: Lingual Nerve.

mandibular molars. Schejtman et al. (1967) performed a cadaveric study by dissections in twenty-three hemi-mandibles and by histological sections. They reported that the retromolar canal was not observed in all cases where the retromolar foramen was present, and when it occurred, its most frequent content was a myelinated nerve (observed in eight of the nine cases that were studied microscopically). There have been cases where they found blood vessels (one or more arterioles - six cases -, and one or more venules - four cases - were found) passing through the retromolar canal, accompanied or not by a myelinated nerve. Yet, there were some cases where the retromolar canal was present and they could not observe any content in it.

Shah and Mehta (2020) reviewed the literature and reported different studies of morphometric analysis of the retromolar foramen and retromolar canal in different populations. These authors verified that when the frequency of the retromolar foramen is evaluated by the cone beam computed tomography (CBCT), studies range from 5.4% to 75.4%; when the retromolar foramen is analyzed by human dry mandible, the studies showed the frequency ranging from 3.2% to 72%. And in panoramic studies the retromolar foramen frequency ranges from 3.06% to 8.8%.

Routinely, the retromolar accessory innervation occurs as a branch of the inferior alveolar nerve. One study has found that loss of sensation in the distribution of the buccal nerve happens probably because of the presence of the retromolar foramen (Singh, 1981). In this case report a retromolar foramen was not found, but the buccal nerve reached the mandibular foramen, and this anatomical variation can be responsible for a local anesthesia failure. Because of that, when assessing local anesthesia failures, dentists must have a strong working knowledge of both normal and variant human anatomy (Gamieldien and Van Schoor, 2016).

In a literature search for publications, it was found that Jablonski et al. (1985) reported an anatomic variation of the buccal nerve in which it is possible to note a unilateral origin that comes from the inferior alveolar nerve within the mandibular ramus. Besides that, no case report of an anatomical variation such as this—i.e., having a communicating branch between the buccal branch of trigeminal and the inferior alveolar nerve—was found.

In view of the anatomical variation described in the present case report, there are some factors that must be considered: which structures are innervated by the buccal nerve when passing through the mandibular canal? Is it collaborating in the innervation of structures that are normally innervated by the inferior alveolar nerve? Is the buccal nerve emitting intraosseous branches during its course through the mandibular canal? And yet, even knowing that the buccal nerve had its normal course, did the structures normally innervated by it have their innervation properly maintained?

According to Sicher and Du Brul (1970), some branches of the posterior superior alveolar nerve may innervate an area of the cheek, but they rarely substitute the normal distribution and innervation area of the buccal nerve. This corroborates, together with our findings that, despite a variant branch having emerged, the buccal nerve presented its normal path to innervate the buccal gingiva of the lower molar and the buccal mucosa of the cheek.

Thus, knowledge of anatomical variations is essential to avoid errors and to give the patient adequate clinical management during specific dental and surgical procedures in each case.

REFERENCES

DESANTIS JL, LIEBOW C (1996) Four common mandibular nerve anomalies that lead to local anesthesia failures. *J Am Dent Assoc*, 127(7): 1081-1086.

GAMIELDIEN MY, VAN SCHOOR A (2016) Retromolar foramen: an anatomical study with clinical considerations. *Br J Oral Maxillofac Surg*, 54(7): 784-787.

GHATAK RN, GINGLEN JG (2018) Anatomy, Head and Neck, Mandibular Nerve. StatPearls [Internet]. StatPearls Publishing, Treasure Island (FL).

HUFF T, DALY DT (2018) Neuroanatomy, Cranial Nerve 5 (Trigeminal). StatPearls [Internet]. StatPearls Publishing, Treasure Island (FL).

JABLONSKI NG, CHENG CM, CHENG LC, CHEUNG HM (1985) Unusual origins of the buccal and mylohyoid nerves. *Oral Surg Oral Med Oral Pathol*, 60: 487-488.

KATORI Y, YAMAMOTO M, ASAKAWA S, MAKI H, RODRÍGUEZ-VÁZQUEZ JF, MURAKAMI G, ABE S (2012) Fetal developmental change in topographical relationship between the human lateral pterygoid muscle and buccal nerve. *J Anat*, 220(4): 384-395.

MÉRIDA-VELASCO JR, RODRÍGUEZ-VÁZQUEZ JF, DE LA CUADRA C, MÉRIDA-VELASCO JA, JIMÉNEZ-COLLADO J (2001) The course of the buccal nerve: relationships with the temporalis muscle during the prenatal period. *J Anat*, 198(Pt 4): 423-429.

OSSENBERG NS (1987) Retromolar foramen of the human mandible. *Am J Phys Anthropol*, 73(1): 119-128.

ROSSI AC, FREIRE AR, PRADO BG, PRADO FB, BOTACIN PR, CARIA PHF (2012) Incidence of retromolar foramen in human mandibles: ethnic and clinical aspects. *Int J Morphol*, 30(3): 1074-1078.

SCHEJTMAN R, DEVOTO FC, ARIAS NH (1967) The origin and distribution of the elements of the human mandibular retromolar canal. *Arch Oral Biol*, 12(11): 1261-1268.

SHAH SP, MEHTA D (2020) Mandibular retromolar foramen and canal - a systematic review and meta-analysis. *Ann Maxillofacial Surg*, 10(2): 444-449.

SICHER H, DU BRUL EL (1970) Oral Anatomy. 5th ed. Ishiyaku EuroAmerica: Saint Louis.

SINGH S (1981) Aberrant buccal nerve encountered at third molar surgery. *Oral Surg Oral Med Oral Pathol*, 52(2): 142.

STANDRING S (2015) Gray's Anatomy: The Anatomical Basis of Clinical Practice. 41st edition. Elsevier.

TAKEZAWA K, GHABRIEL M, TOWNSEND G (2018) The course and distribution of the buccal nerve: clinical relevance in dentistry. *Aust Dent J*, 63(1): 66-71.

VOIROL JR, STROTHMANN KA, ZANDIAN A, VILENSKY JA (2016) Cranial Nerves N-VI. In: Tubbs RS, Shoja MM, Loukas M (eds). *Bergman's Comprehensive Encyclopedia of Human Anatomic Variation*.

WON SY, YANG HM, WOO HS, CHANG KY, YOUN KH, KIM HJ, HU KS (2014) Neuroanastomosis and the innervation territory of the mental nerve. *Clin Anat*, 27(4): 598-602.

YANG HM, WON SY, LEE YI, KIM HJ, HU KS (2014) The Sihler staining study of the infraorbital nerve and its clinical complication. *J Craniofac Surg*, 25(6): 2209-2213.

Ethics behind technology-enhanced medical education and the effects of the COVID-19 pandemic

Claudia Krebs[1β], Alejandro Quiroga-Garza[2β], Patrick Pennefather[3], Rodrigo E. Elizondo-Omaña[2]

[1] Department of Cellular and Physiological Sciences, Faculty of Medicine, University of British Columbia, Vancouver, British Columbia, Canada

[2] Human Anatomy Department, School of Medicine, Universidad Autonoma de Nuevo Leon, Monterrey, Mexico

[3] Digital Media Program, School of Theatre and Film, University of British Columbia, Vancouver, British Columbia, Canada

SUMMARY

This century has been marked by an ever-growing technology-dependent society. Medical education has not been exempt from this, with the integration of technological advancements into the classroom and laboratory. Research has been focused primarily on the impact of students' learning and perception, with limited data oriented towards the impact it will cause on future pedagogics and healthcare providers, as well as the ethical implications behind its integration in education. Although the benefits are evident, a bridge between technology-enhanced medicine and education with basic humanity should always be present. The human-centered educational experience cannot be lost. Educators must remain committed and be persistent in learning how to engage new technologies in order to prevent the loss of ethical principles and professionalism, as well as interpersonal relationships and mentoring, thus avoiding isolation, the production of incompetent healthcare professionals and unfit pedagogics. The COVID-19 pandemic forced remote teaching worldwide and will have a lasting effect on medical education. However, educational strategies need to constantly evolve alongside the integration of emerging technologies, and educators must be instructed and adequately trained for their use. As much as technology affords us enriched mediated interactions, face-to-face teaching is an important and ongoing necessity in the evolution of anatomy and medical education. Technology must be integrated purposefully in the design of learning and should complement and support the persistent need for interpersonal interaction, teamwork, and communication skills.

Key words: Medical education – Ethics – Technology – Technological advancements – COVID-19 – Anatomy

Corresponding author:
Rodrigo E. Elizondo-Omaña, M.D., Ph.D. Departamento de Anatomía Humana, Facultad de Medicina, Universidad Autonoma de Nuevo Leon. Ave. Madero y Calle Dr. Eduardo Aguirre Pequeño s/n. Colonia Mitras Centro, Monterrey, Nuevo Leon, Mexico CP 64460. E-mail: rod_omana@yahoo.com

β The authors Claudia Krebs and Alejandro Quiroga-Garza participated equally in the communication and are both in position as first author, listed in alphabetical order by last name.

Submitted: January 1, 2021. **Accepted:** February 9, 2021

LIST OF ABBREVIATIONS:

AI: artificial intelligence

TEL: technology-enhanced learning

INTRODUCTION

Technology has taken a strong foothold in all post-secondary classrooms —a reflection of an increasingly technology-savvy and technology-dependent society (Payne et al. 2012; Barry et al., 2016a; Stigmar, 2016; Altınay-Gazi and Altınay-Aksal, 2017; Salinas-Alvarez et al., 2020). The question now focuses on how technology is changing students' perceptions of the role of educators, the role of peer-to-peer interactions, and their own role as developing professionals (Koehler et al., 2012; George et al., 2013; Boruff and Storie 2014; Brooks and Pomerantz, 2017; Masters, 2017; Khamis et al., 2018). A proactive approach to the integration of technology, aware of the benefits and risks of technology, can build the pedagogical foundation to support a new generation that will have to bridge technology-enhanced medicine and education with the basic humanity of healthcare interactions (Granger, 2004; Alexander et al., 2009; Sugand et al., 2010; Cook et al., 2011; Barry et al., 2016b; Delgaty et al., 2017; Hennessy et al., 2019; Hildenbrandt, 2019).

The motivations to integrate technology into medical education are manifold and are at times at odds with more traditional approaches to the delivery of essential anatomy course content such as dissection. Whereas there has been ample discussion around the ethics of dissection and its role in professional identity formation (Sugand et al., 2010; Hasan, 2011; Miller and Lewis, 2016; Jones, 2018; Quiroga-Garza et al., 2017; Hildebrandt, 2019), this same discussion has been limited around the use of technology in the anatomy classroom. Most papers evaluate the impact on student learning as measured in summative assessments —and indeed, by that metric, dissection is not superior to other teaching modalities (Sugand et al., 2010; Barry et al., 2016a,b; Holland and Pawlikoska, 2019). However, body-based instruction has survived the curricular reforms. It arguably fortifies anatomy education, as a basic constructional principle of professionalism and compassion —and indeed, by that metric, anatomists affirm their preference and its benefits in the formation of future physicians (Elizondo-Omaña et al., 2005; Korf et al., 2008; Estai and Bunt, 2016; Kumar Ghosh and Kumar, 2019; Salinas-Alvarez et al., 2020).

There are many success stories of those who have implemented technology to change their curriculum. These successes need to be used as a foundation (Sugand et al., 2010; Drake et al., 2014; Barry et al., 2016a; Darras et al., 2019; Holland and Pawlikowska, 2019; Salinas-Alvarez et al., 2020). Advances in technology can support educators to enhance and reimagine more traditional course content to properly prepare students for future clinical challenges. Online and mobile access to platforms with learning modules, activities, and videos provide students with the tools to attain, understand, review, and apply knowledge that complements traditional forms of lecture-based delivery. (George et al., 2013; Krebs et al., 2014; Masters et al., 2015; Student et al., 2015; Barry et al., 2016a; Mordhurst et al., 2017; Holland and Pawlikowska, 2019; Maudsley et al., 2019). Alongside the integration of new technological platforms, the role of the educators also needs to change and adapt. How can educators continue to balance an authentic, human-centered educational experience while adapting the curriculum to take advantage of new technological developments and at the same time maintain that unique human spark and creativity? (Fig. 1).

A PERSISTENT CHALLENGE IN MEDICAL EDUCATION

When interventions are well planned, technology can be integrated purposefully into achieving specific learning outcomes. The use of visual aids such as animations, can illustrate complex concepts and encourage innovation and creativity (Barry et al., 2016a,b; Miller and Lewis, 2016; Brooks and Pomerantz, 2017; Holland and Pawlikowska, 2019). These can be also controlled by the user/student for individual pacing and exploration of didactic content: by pausing a pre-recorded video, repeating any part of it, any day, any time, or fast-forwarding to support their own learning process. A direct access to remote content

removes the physical dependency of learning being contained to a classroom/laboratory (Alexander et al., 2009; Cook et al., 2011; Boruff and Storie, 2014; Altinay-Gazi and Altinay-Aksal, 2017; Brooks and Pomerantz, 2017). Purchasing larger volumes of a specific technology can reduce the overall cost for increased class sizes. Content can be distributed with other institutions, both locally and globally. Moderated forums allow easier participation, even for more introverted personalities. When technologies are evaluated by a multidisciplinary team, their integration can easily be improved from course to course (Elizondo-Omaña et al., 2005; Miller and Lewis, 2016; Mordhorst et al., 2017).

When not integrated within the learning ecosystem nor associated with specific learning outcomes, technology can be an impediment. The multitude of technological resources available and the lack of time result in educators' inability to keep a check on all content. This also makes it challenging to focus on what is critically important for students. Most learners build a personal relationship with their instructors, connecting the educator's passions and insights with the didactic content. This makes them care about what they are learning, which allows learners to remember the content better (Chopin, 2002; Gershenfeld, 2014; Vallée et al., 2020). Technology alone can be cold and lack human connection. These advantages can be easily ignored when technology is forced upon students and faculty, causing disengagement with the course. They can build social isolation/disconnection of the user by neglecting the need for interpersonal interactions (Huang, 2010; Rhim and Han, 2020). They can generate a social divide amongst those who lack the economic resources (Van Deursen and Helsper, 2015; Warschauer and Xu, 2018). The familiarity of accessing knowledge through various technologies may lead professionals to either overestimate or underestimate their competence (Kruger and Dunning, 1999; Abduallah, 2014). Without a commitment to persistently learning how to engage with new technologies, or when situated in a work environment that does not

Fig. 1.- Technology adaptations. (**A**) Balanced use of technology in anatomy education with interaction between educators, near-peers, and students in small groups. (**B**) Students in laboratory practice with face-to-face interaction. (**C**) Online teaching with video interaction and online material. (**D**) Online laboratory practice teaching students surgical knots.

have rapid access to technology, a professional's knowledge may soon be out of date. Excessive use of computers or smart-devices has also been correlated to ergonomic and health problems (Korpinen and Pääkkönen, 2011; Fuentes-Ramirez et al., 2020).

Current technological tools do not adapt in real-time or empathize with the user, although artificial intelligence (AI) may soon change that. AI will impact medical education with the application of adaptive learning, although evidence shows that it will primarily enhance the role of teachers, not replace them (Masters, 2017; Masters, 2019). The design of user experiences that respect universal design principles and are built on best practices for human-computer interactions is imperative in order to move the field forward. When not integrated, technology can increase a sense of alienation, exclude those with different abilities, and lead to social depersonalization and a loss of humanity in education.

ETHICAL IMPLICATIONS OF TECHNOLOGY OVERUSE

Educator identities are tied to teaching and inspire learning. Behaviors from the classroom and laboratory are mimicked by students and teaching assistants, as professors become role models. (Chopin, 2002; Pawlina, 2006; Lachman et al., 2012; Gershenfeld, 2014; Masters, 2019; Guerrero-Mendivil et al., 2020). Friendlier and more accessible educators promote better learning (George et al., 2013; Hennessy et al., 2019).

The student/teacher relationship is the foundation for the physician/patient relationship. Human interaction with educators, peers, donors, set off a cascade of professionalism and understanding of medical ethics (Dyer and Thorndike, 2000; Pawlina, 2006; Englander et al., 2013; Jones, 2016; Hildebrandt, 2018; Kumar Ghosh and Kumar, 2019). These human interactions cannot be easily simulated with technology —the most extensive experiment with artificial intelligence (AI) was by Jill Watson, as an online teaching assistant, who has demonstrated the limitations of AI to date (Eicher, 2018). The overuse of technology may even cause dependence on technology in a clinical environment due to a developed habit that ensues other ethical and legal issues (Goodman, 2010; Jones, 2016; Barry, et al., 2016b; Miller and Lewis, 2016).

There is, of course, an evident need for technology in medicine: task management, data processing, and collection are some of the tasks facilitated by these tools, but how this information is managed also raises some ethical concerns. (Goodman, 2010; Tavani, 2011; Hennessy et al., 2019).

There is no formal pedagogic link between health and information technology (Goodman, 2010, Barry et al., 2016b; Estai and Bunt, 2016). One concern is the exponential growth of online resources. Many resources are user-generated and user-regulated and lack both peer review and validation. Some materials bring up the ethical boundaries within which modern anatomy programs operate —and the question of whether and how to present images of cadaveric dissections (Philip et al., 2008; George et al., 2013; Barry et al., 2016b; Miller and Lewis, 2016; Cornwall and Hildebrandt 2019; Hildebrandt, 2019). With a constant increase in student to staff ratio, time demands for research, and reduced course hours, educators must depend on the use of technology-enhanced learning (TEL) to uphold content standards (McGaghie et al., 2010; Sugand et al., 2010; Bleakley et al., 2011; Guze, 2015; Green and Whitburn, 2016; Delgaty et al., 2017; Hildebrandt, 2018).

There are risks to the use of TEL resources. If not addressed by their developers, conflict will be inevitable. Grunwald mentioned two branches to orient technology policy: the philosophical ethics implicated and technology assessment (Grunwald, 1999). Research has been primarily focused on the assessment and effectiveness of new tools, disregarding the ethics and implications of these. Social isolation, technology dependency and a lack of the natural mentoring formed by the student-teacher interaction may lead us to incompetent healthcare professionals, incapable of teaching, of developing inter-personal relations and of mentoring. Depersonalization and commodification will cause clinical detachment

(Jones, 2018; Hildebrandt, 2019) —as Sungand et al. stated: "weak and unfit pedagogics" (Sugand et al., 2010)

So, how to reconcile the integration of technology in teaching and learning experiences? There is no simple solution for medical educators when asked whether or not to include the latest tech in the classrooms (Frenk et al. 2010; Jones, 2018; Vallée et al., 2020). Educational strategies need to constantly evolve alongside the integration of emerging technologies. Within set time limits that are often imposed by administrators (Sugand et al., 2010; Drake et al., 2014; Estai and Bunt, 2016; Hildebrandt, 2019), educators are challenged to constantly upgrade skills so that they can efficiently interact with students and take full advantage of resources. Program administrators also need to ensure that they offer resources and support in order to instruct and adequately train their faculty to teach with the technologies that they want faculty to use (Salinas-Alvarez et al., 2020). For example, a balance must be defined by all stakeholders for blended learning to maintain and achieve efficient student learning outcomes (Barry et al., 2016a,b; Green and Whitburn, 2016; Miller and Lewis, 2016; Brooks and Pomerantz, 2017). As much as technology affords us enriched mediated interactions, face-to-face teaching is an important and ongoing necessity in the evolution of anatomy and medical education.

SARS-COV-2 (COVID-19) PANDEMIC

Debating the overuse of technology was not an option for the year 2020. The outbreak of the SARS-COV-2 pandemic forced the closure of schools and the implementation of social distancing. This created a situation in which all educational programs had to transfer to a 100% remote and online education curriculum (Cheng et al., 2020; Gordon et al., 2020; Hodges et al., 2020; Pather et al., 2020). Schools with prior experience were able to migrate more easily to online platforms, with most challenges present in low- to middle-income countries (Cecilio-Fernandes et al., 2020; Muñoz-Leija et al., 2020). In many cases, educators were faced with a lack of technological resources, infrastructure and/or training, unclear instructions by administrations, blindness to student situation/capacity, and even complex home environments (Espino-Díaz et al., 2020; Rizun and Strzelecki, 2020). These created a stressful situation in which educators could have been exposed to anxiety and emotional exhaustion, in addition to the confinement imposed by the pandemic (Espino-Díaz et al., 2020).

Educators had to quickly adapt (Espino-Díaz et al., 2020; González-Calvo et al., 2020; Tejedor et al., 2020). Synchronous and asynchronous methods were implemented for remote learning (Gordon et al., 2020; Hilty et al., 2020). Once the lasting effects of the pandemic and undefined longevity of social distancing were assimilated, educators understood the need to innovate teaching methods to better engage students without face-to-face interaction (Gordon et al., 2020; Rhim and Han, 2020).

Several studies report student satisfaction and self-efficacy with online learning. The majority of students are comfortable with online and remote learning, however, the development of certain key competencies may be shown to be deficient in the future, with consequences for the professional development of physicians. In 2021 2nd-year medical students will continue their education and will not have been face-to-face with their professor, not have been in a classroom or laboratory, not encountered an anatomical donor for dissection (in case of anatomy), or have been physically exposed to different academic scenarios. In many countries, an introduction to clinical environments was restricted due to the increased risk of COVID-19 transmission. The effects of social isolation, lack of interpersonal relationships, the exposure to anatomical donors/patients (development of values such as professionalism, respect, integrity, empathy, and humanity), the psychological effects, the level of student confidence, academic output: all need to be addressed if educators are to continue with remote learning (Chytas et al., 2020; Espino-Díaz et al., 2020; Gordon et al., 2020; Lozano-Díaz et al., 2020; Muñoz-Leija et al., 2020; Tejedor et al., 2020). Universities are facing an increase in burnout and dropout rates, as well as variability in student enrollment (Rizun and Strzelecki, 2020;

Tejedor et al., 2020; Zhan et al., 2020). Student academic misconduct during class and exams may also be present, which is increasingly challenging to detect, especially in large groups (Clark et al., 2020; Elizondo-Omaña et al., 2020; Gamage et al., 2020; Hylton et al., 2016). Multitasking during online sessions may also leave in question the lasting effects of learning (Rhim and Han, 2020). These are all issues that need to be kept in mind and addressed in the design and implementation of online and mixed asynchronous/synchronous educational offerings.

There is no doubt that the changes implemented during the pandemic will leave a lasting effect in medical education. Currently, there is an abundance of publications regarding remote teaching methods that we can draw from historically (Lynch and Dembo, 2004; Puzziferro, 2008; Barnard et al., 2009; Broadbent, 2017; Hodges et al., 2020). However, current publications detailing the impact of teaching medical education remotely during the time of Covid-19 are limited to short-term studies, and assertions are not readily generalizable across different teaching contexts. Subsequent research will be needed to determine the impact of these methods in the student's professional formation (Gordon et al., 2020; Hilty et al., 2020; Rhim and Han, 2020).

CONCLUSIONS

The COVID-19 pandemic has caused a disruption in medical education and forced a transition of all courses to online platforms. Technology has been a fundamental solution to continue with academic curricula, with evident advantages and disadvantages. In order to have any lasting impact on the community of medical practitioners, technology must be integrated purposefully in the design of learning and should complement and support the persistent need for interpersonal interaction, teamwork and communication skills (Philips et al., 2008; Alexander et al., 2009; Englander et al., 2013; George et al., 2013; Barry et al., 2016b; Green and Whitburn, 2016; Jones, 2016; Miller and Lewis, 2016; Elizondo-Omaña et al., 2019). It must be organized, structured and curated to meet the objectives and competencies of the curriculum. Looking at the use of technology in terms of how it can enhance medical education and solve contemporary problems facing the community, educators are encouraged to resist the temptation to engage in a polar opinion as to whether technology is good or bad. Part of the research needs to continue to user-test technology in learning contexts. Disseminating those results will help others make more informed decisions as to the benefits of integrating emerging technologies and their impact on learning and the user.

REFERENCES

ABDULLAH JM (2014) The eight stages of trust and "Amanah" in medicine and the Dunning-Kruger effect. *Malay J Med Sci*, 21(4): 1.

ALEXANDER CJ, CRESCINI WM, JUSKEWITCH JE, LACHMAN N, PAWLINA W (2009) Assessing the integration of audience response system technology in teaching of anatomical sciences. *Anat Sci Educ*, 2(4): 160-166.

ALTINAY-GAZI Z, ALTINAY-AKSAL F (2017) Technology as mediation tool for improving teaching profession in higher education practices. *Eurasia J Math Sci Tech Educ*, 13(3): 803-813.

BARNARD L, LAN WY, TO YM, PATON VO, LAI SL (2009) Measuring self-regulation in online and blended learning environments. *Internet High Educ*, 12(1): 1-6.

BARRY DS, MARZOUK F, CHULAK-OGLU K, BENNETT D, TIERNEY P, O'KEEFFE GW (2016a) Anatomy education for the YouTube generation. *Anat Sci Educ*, 9(1): 90-96.

BARRY DS, TIERNEY P, O'KEEFFE GW (2016b) The need for ethical and pedagogical frameworks for developing online media in anatomy education. *Anat Sci Educ*, 9(5): 498-499.

BLEAKLEY A, BRENNAN N (2011) Does undergraduate curriculum design make a difference to readiness to practice as a junior doctor? *Med Teach*, 33(6): 459-467.

BORUFF JT, STORIE D (2014) Mobile devices in medicine: a survey of how medical students, residents, and faculty use smartphones and other mobile devices to find information. *J Med Libr Assoc*, 102: 22-30.

BROADBENT J (2017) Comparing online and blended learner's self-regulated learning strategies and academic performance. *Internet High Educ*, 33: 24-32.

BROOKS DC, POMERANTZ J (2017) ECAR study of undergraduate students and information technology, 2017. *Educause*, 4(3): 3.

CECILIO-FERNANDES D, PARISI MCR, SANTOS TM, SANDARS J (2020) The COVID-19 pandemic and the challenge of using technology for medical education in low and middle income countries. *Med Ed Publish*, 9: 74.

CHENG X, CHAN LK, PAN SQ, HONGMEI C, LI YQ, YANG X (2020) Gross Anatomy Education in China during the Covid-19 pandemic: a national survey. *Anat Sci Educ*,. 14(1): 8-18.

CHOPIN SF (2002) Undergraduate research experiences: The translation of science education from reading to doing. *Anat Rec*, 269(1): 3-10.

CHYTAS D, SALMAS M, PIAGKOU M, JOHNSON EO (2020) Decline of cadaveric dissection in anatomy education during the Covid-19 pandemic: Can it affect future surgeons' competency?. *Anat Sci Educ*, 14(2): 166-168.

CLARK TM, CALLAM CS, PAUL NM, STOLTZFUS MW, TURNER D (2020) Testing in the time of COVID-19: A sudden transition to unproctored online exams. *J Chem Educ*, 97: 3413-3417.

COOK DA, HATALA R, BRYDGES R, ZENDEJAS B, SZOSTEK JH, WANG AT, ERWIN PJ, HAMSTRA S (2011) Technology-enhanced simulation for health professions education: a systematic review and meta-analysis. *JAMA*, 306(9): 978-988.

CORNWALL J, HILDEBRANDT S (2019) Anatomy, education, and ethics in a changing world. *Anat Sci Educ*, 12(4): 329-331.

DARRAS KE, SPOUGE R, HATALA R, NICOLAOU S, HU J, WORTHINGTON A, KREBS C, FORSTER BB (2019) Integrated virtual and cadaveric dissection laboratories enhance first year medical students' anatomy experience: a pilot study. *BMC Med Educ*, 19(1): 366.

DELGATY L, FISHER J, THOMSON R (2017) The "Dark Side" of technology in medical education. *Med Ed Publish*, 6(2): 19.

DRAKE RL, MCBRIDE JM, PAWLINA W (2014) An update on the status of anatomical sciences education in United States medical schools. *Anat Sci Educ*, 7(4): 321-325.

DYER GS, THORNDIKE ME (2000) Quidne mortui vivos docent? The evolving purpose of human dissection in medical education. *Acad Med*, 75: 969-979.

ENGLANDER R, CAMERON T, BALLARD AJ, DODGE J, BULL J, ASCHENBRENNER CA (2013) Toward a common taxonomy of competency domains for the health professions and competencies for physicians. *Acad Med*, 88: 1088-1094.

EICHER B, POLEPEDDI L, GOEL AK (2018) Jill Watson doesn't care if you're pregnant: grounding at ethics in empirical studies. *AIES*, 88-94.

ELIZONDO-OMAÑA RE, GUZMÁN-LÓPEZ S, GARCÍA-RODRÍGUEZ MDLA (2005) Dissection as a teaching tool: past, present, and future. *Anat Rec Part B*, 285(1): 11-15.

ELIZONDO-OMAÑA RE, QUIROGA-GARZA A, SALINAS-ALVAREZ YE, GUZMAN-LOPEZ S (2020) Breaking down large anatomy groups. *FASEB J*, 34(S1): 1.

ELIZONDO-OMAÑA RE, ZARATE-GARZA PP, JACOBO-BACA G, SALINAS-ALVAREZ Y, FERNANDEZ-RODARTE BA, MARTINEZ-GARZA JH, QUIROGA-GARZA A, GUZMAN-LOPEZ S (2019) Collaborative mentoring for effective medical research groups. *Med Ed Publish*, 8.

ESPINO-DÍAZ L, FERNANDEZ-CAMINERO G, HERNANDEZ-LLORET CM, GONZALEZ-GONZALEZ H, ALVAREZ-CASTILLO JL (2020) Analyzing the impact of COVID-19 on education professionals. toward a paradigm shift: ICT and neuroeducation as a binomial of action. *Sustainability*, 12(14): 5646.

ESTAI M, BUNT S (2016) Best teaching practices in anatomy education: A critical review. *Ann Anat*, 208: 151-157.

FRENK J, CHEN L, BHUTTA ZA, COHEN J, CRISP N, EVANS T, FINEBERG H, GARCIA P, KE Y, KELLEY P, KISTNASAMY B, MELEIS A, NAYLOR D, PABLOS-MENDEZ A, REDDY S, SCRIMSHAW S, SEPULVEDA J, SERWADDA D, ZURAYK H (2010) Health professionals for a new century: transforming education to strengthen health systems in an interdependent world. *Lancet*, 376: 1923-1958.

FUENTES-RAMÍREZ LD, ALFARO-GOMEZ U, ESPINOSA-URIBE AG, TERAN-GARZA R, QUIROGA-GARZA A, GUTIÉRREZ-DE LA O J, VILCHEZ-CAVAZOS F, GUZMAN-LOPEZ S, ELIZONDO-OMAÑA RE (2020) Morphologic changes of the fifth phalange secondary to smartphone use. *Work*, 65(2): 429-433.

GAMAGE KA, SILVA EKD, GUNAWARDHANA N (2020) Online delivery and assessment during COVID-19: safeguarding academic integrity. *Educ Sci*, 10: 301.

GEORGE DR, ROVNIAK LS, KRASCHNEWSKI JL (2013) Dangers and opportunities for social media in medicine. *Clin Obstet Gynecol*, 56(3): 453-462.

GERSHENFELD S (2014) A review of undergraduate mentoring programs. *Rev Educ Res*, 84(3): 365-391.

GONZÁLEZ-CALVO G, BARBA-MARTÍN RA, BORES-GARCÍA D, GALLEGO-LEMA V (2020) Learning to be a teacher without being in the classroom: COVID-19 as a threat to the professional development of future teachers. *Int Multidiscip J Soc Sci*, 9(2): 152-177.

GOODMAN KW (2010) Ethics, information technology, and public health: new challenges for the clinician-patient relationship. *J Law Med Eth*, 38(1): 58-63.

GORDON M, PATRICIO M, HORNE L, MUSTON A, ALSTON SR, PAMMI M, THAMMASITBOON S, PARK S, PAWLIKOSKA T, REES EL, DOYLE AJ DANIEL M (2020) Developments in medical education in response to the COVID-19 pandemic: a rapid BEME systematic review: BEME Guide No. 63. *Med Teach*, 42(11): 1202-1215.

GRANGER NA (2004) Dissection laboratory is vital to medical gross anatomy education. *Anat Rec Part B*, 281(1): 6-8.

GREEN RA, WHITBURN LY (2016) Impact of introduction of blended learning in gross anatomy on student outcomes. *Anat Sci Educ*, 9(5) :422-430.

GRUNWALD A (2011) Responsible innovation: bringing together technology assessment, applied ethics, and STS research. *Enter Work Innov Stud*, 31: 10-19.

GUERRERO-MENDIVIL FD, MUÑOZ-LEIJA MA, QUIROGA-GARZA A, DE LA FUENTE-VILLARREAL D, JACOBO-BACA G, ZÁRATE-GARZA PP, ELIZONDO-OMAÑA RE, GUZMÁN-LÓPEZ S (2020) Training and education model for anatomy near-peer teachers. *Med Univ*, 22(4): 1-4.

GUZE PA (2015) Using technology to meet the challenges of medical education. *T Am Clin Clim*, 126: 260.

HASAN T (2011) Is dissection humane? *J Med Ethics H Med*, 4.

HENNESSY CM, SMITH CF, GREENER S, FERNS G (2019) Social media guidelines: a review for health professionals and faculty members. *Clin Teach*, 16(5): 442-447.

HILDEBRANDT S (2019) The role of history and ethics of anatomy in medical education. *Anat Scie Educ*, 12(4): 425-431.

HILTY DM, TOROUS J, PARISH MB, CHAN SR, XIONG G, SCHER L, YELLOWLEES PM (2020) A literature review comparing clinicians' approaches and skills to in-person, synchronous, and asynchronous care: moving toward competencies to ensure quality care. *Telemed J E Health*, 27(4): 356-373.

HODGES C, MOORE S, LOCKEE B, TRUST T, BOND A (2020) The difference between emergency remote teaching and online learning. *Educ Rev*, 27.

HOLLAND JC, PAWLIKOWSKA T (2019) Undergraduate medical students' usage and perceptions of anatomical case-based learning: comparison of facilitated small group discussions and elearning resources. *Anat Sci Educ*, 12(3): 245-256.

HUANG C (2010) Internet use and psychological well-being: A meta-analysis. *Cyberpsychol Behav Soc Netw*, 13(3): 241-249.

HYLTON K, LEVY Y, DRINGUS LP (2016) Utilizing webcam-based proctoring to deter misconduct in online exams. *Comp Educ*, 92: 53-63.

JONES DG (2016) Anatomy in ethical review. *Clin Anat*, 29(1): 2-3.

JONES DG (2018) Three-dimensional printing in Anatomy Education: assessing potential ethical dimensions. *Anat Sci Educ*, 12(4): 435-443.

KHAMIS N, ALJUMAIAH R, ALHUMAID A, ALRAHEEM H, ALKADI D, KOPPEL C, ABDULGHANI HM (2018) Undergraduate medical students' perspectives of skills, uses and preferences of information technology in medical education: A cross-sectional study in a Saudi Medical College. *Med Teach*, 40(sup1): S68-S76.

KOEHLER N, YAO K, VUJOVIC O, MCMENAMIN C (2012) Medical students' use of and attitudes towards medical applications. *JournalMTM*, 1: 16-21.

KORF HW, WICHT H, SNIPES RL, TIMMERMANS JP, PAULSEN F, RUNE G, BAUMGART-VOGT E (2008) The dissection course–necessary and indispensable for teaching anatomy to medical students. *Ann Anat*, 190(1): 16-22.

KORPINEN L, PÄÄKKÖNEN R (2011) Physical symptoms in young adults and their use of different computers and mobile phones. *Int J Occup Saf Ergon*, 17(4): 361-371.

KREBS C, HOLMAN P, BODNAR T, WEINBERG J, VOGL W (2014) Flipping the neuroanatomy labs: how the production of high quality video and interactive modules changed our approach to teaching (211.3). *FASEB J*, 28: S211.3.

KRUGER J, DUNNING D (1999) Unskilled and unaware of it: how difficulties in recognizing one's own incompetence lead to inflated self-assessments. *J Pers Soc Psychol*, 77(6): 1121.

KUMAR GHOSH S, KUMAR A (2019) Building professionalism in human dissection room as a component of hidden curriculum delivery: A systematic review of good practices. *Anat Sci Educ*, 12(2): 210-221.

LACHMAN N, CHRISTENSEN KN, PAWLINA W (2013) Anatomy teaching assistants: facilitating teaching skills for medical students through apprenticeship and mentoring. *Med Teach*, 35(1): e919-e925.

LYNCH R, DEMBO M (2004) The relationship between self-regulation and online learning in a blended learning context. *Int Rev Res Open Dis*, 5(2).

LOZANO-DÍAZ A, FERNÁNDEZ-PRADOS JS, CANOSA VF, MARTÍNEZ AMM (2020) Impactos del confinamiento por el COVID-19 entre universitarios: satisfacción vital, resiliencia y capital social online. *Int J Soc Educ*, Special Issue, 79-104.

MASTERS K (2017) Preparing medical students for the e-patient. *Med Teach*, 39(7): 681-685.

MASTERS K (2019) Artificial intelligence in medical education. *Med Teach*, 41(9): 976-980.

MASTERS K, ELLAWAY RH, TOPPS D, ARCHIBALD D, HOGUE RJ (2016) Mobile technologies in medical education: AMEE Guide no. 105. *Med Teach*, 38: 537-549.

MAUDSLEY G, TAYLOR D, ALLAM O, GARNER J, CALINICI T, LINKMAN K (2019) A Best Evidence Medical Education (BEME) systematic review of: What works best for health professions students using mobile (hand-held) devices for educational support on clinical placements? BEME Guide No. 52. *Med Teach*, 41(2): 125-140.

MCGAGHIE WC, ISSENBERG SB, PETRUSA ER, SCALESE RJ (2010) A critical review of simulation-based medical education research: 2003-2009. *Med Edu*, 44(1): 50-63.

MILLER GW, LEWIS TL (2016) Anatomy education for the YouTube generation: Technical, ethical, and educational considerations. Anat Sci Educ, 9(5): 496-497.

MORDHORST A, FEJTEK M, SIDDIQUI A, KREBS C (2017) The development of a globally accessible interactive anatomy web atlas. *FASEB J*, 31: S580.10.

MUÑOZ-LEIJA MA, ZARATE-GARZA PP, JACOBO-BACA G, QUIROGA-GARZA A, SALINAS-ALVAREZ Y, MARTINEZ-GARZA JH, ELIZONDO-OMAÑA RE, GUZMÁN-LÓPEZ S (2020) Modifications to the delivery of a gross anatomy course during the COVID-19 pandemic at a Mexican medical school. *Eur J Anat*, 24(6): 507-512.

PATHER N, BLYTH P, CHAPMAN JA, DAYAL MR, FLACK NA, FOGG QA, GREEN RA, HULME AK, JOHNSON IP, MEYER AJ, MORLEY JW, SHORTLAND PJ, ŠTRKALJ G, ŠTRKALJ M, VALTER K, WEBB AL, WOODLEY SJ, LAZARUS MD (2020) Forced disruption of anatomy education in Australia and New Zealand: an acute response to the Covid-19 pandemic. *Anat Sci Educ*, 13(3): 284-300.

PAWLINA W (2006) Professionalism and anatomy: How do these two terms define our role? *Clin Anat*, 19(5): 391-392.

PAYNE KB, WHARRAD H, WATTS K (2012) Smartphone and medical related App use among medical students and junior doctors in the United Kingdom (UK): a regional survey. *BMC Med Inform Decis Mak*, 12: 121.

PHILIP CT, UNRUH, KP, LACHMAN N, PAWLINA W (2008) An explorative learning approach to teaching clinical anatomy using student generated content. *Anat Sci Educ*, 1(3): 106-110.

PUZZIFERRO M (2008) Online technologies self-efficacy and self-regulated learning as predictors of final grade and satisfaction in college-level online courses. Amer J Distance Educ, 22(2): 72-89.

QUIROGA-GARZA A, REYES-HERNÁNDEZ CG, ZARATE-GARZA PP, ESPARZA-HERNÁNDEZ CN, GUTIERREZ-DE LA O J, DE LA FUENTE-VILLARREAL D, ELIZONDO-OMAÑA RE, GUZMAN-LOPEZ S (2017) Willingness toward organ and body donation among anatomy professors and students in Mexico. *Anat Sci Educ*, 10(6): 589-597.

RHIM HC, HAN H (2020) Teaching online: foundational concepts of online learning and practical guidelines. *Korean J Med Educ*, 32(3): 175.

RIZUN M, STRZELECKI A (2020) Students' acceptance of the Covid-19 impact on shifting higher education to distance learning in Poland. *Int J Env Res Pub He*, 17(18): 6468.

SALINAS-ALVAREZ Y, QUIROGA-GARZA A, MARTINEZ-GARZA JH, JACOBO-BACA G, ZARATE-GARZA PP, RODRÍGUEZ-ALANÍS KV, GUZMAN-LOPEZ S, ELIZONDO-OMAÑA RE (2020) Mexican Educators Survey on Anatomical Sciences Education and a Review of World Tendencies. *Anat Sci Educ*, doi: 10.1002/ase.2017. Online ahead of print.

SHORE R, HALSEY J, SHAH K, CRIGGE BJ, DOUGLAS SP (2011) Report of the AMA Council on ethical and judicial affairs: professionalism in the use of social media. *J Clin Ethics*, 22(2): 165-172.

STIGMAR M (2016) Peer-to-peer teaching in higher education: A critical literature review. Mentoring & Tutoring: partnership in learning, 24(2): 124-136.

STUDENT J, ROTHMAN Z, KREBS C (2015) Flipping the Neuroanatomy labs: a creative approach to producing videos and multimedia for students. *Med Educ*, 49: 87.

SUGAND K, ABRAHAMS P, KHURANA A (2010) The anatomy of anatomy: a review for its modernization. *Anat Sci Educ*, 3(2): 83-93.

TEJEDOR S, CERVI L, TUSA F, PAROLA A (2020) Education in times of pandemic: reflections of students and teachers on virtual university education in Spain, Italy, and Ecuador. *Rev Lat Com Soc*, (78): 1-21.

VALLÉE A, BLACHER J, CARIOU A, SORBETS E (2020) Blended learning compared to traditional learning in medical education: systematic review and meta-analysis. *J Med Internet Res*, 22(8): e16504.

VAN DEURSEN AJ, HELSPER EJ (2015) The third-level digital divide: Who benefits most from being online? In: Robinson L, Cotten SR, Schulz J (Editors) Communication and information technologies annual, *Emerald*, 29-52.

WARSCHAUER M, XU Y (2018) Technology and Equity in Education. In: Voogt J, Knezek G, Christensen R, Lai KW (eds). Second Handbook of Information Technology in Primary and Secondary Education. *Cham*, Switzerland, chapter 71: 1063-1079.

ZHANG J, SHU T, XIANG M, FENG Z (2020) Learning burnout: evaluating the role of social support in medical students under the influence of Covid-19 epidemic. *Research Square*, doi: 10.21203/rs.3.rs-53416/v2.

European Journal of Anatomy